UNIVERSITÀ DI TRENTO

DIPARTIMENTO DI FISICA

Corso di Dottorato di Ricerca in Fisica - XXXVI ciclo

PH.D. THESIS

Cluster Effective Field Theory calculation of electromagnetic breakup reactions with the Lorentz Integral Transform method

Candidate:
Ylenia Capitani

Supervisor:
Prof. Winfried Leidemann

June, 17 2024

Abstract

Nuclear electromagnetic breakup processes at low energy are particularly relevant in the astrophysical context. In this Thesis we analyse the Beryllium–9 photodisintegration reaction, whose inverse process, under certain astrophysical conditions, is related to the Carbon–12 formation. A preliminary study of the Carbon–12 photodisintegration is also carried out. The interaction of these nuclei with a low–energy photon induces a transition to a state consisting of cluster sub–units, the α–particles, and possibly a neutron, n. The theoretical study of the cross section in the low–energy regime is conducted by using a three–body *ab initio* approach.

Beryllium–9 exhibits a clear separation of energy scales, since its $\alpha\alpha n$ three–body binding energy is shallow compared to the binding of the α–particle. Within this framework a halo/cluster Effective Field Theory (EFT) can be developed. The α–α and α–n effective interactions are defined in momentum space as a series of contact terms, regularized by a momentum–regulator function. The Low Energy Constants are expressed in terms of scattering observables, i.e. scattering length and effective range. A three–body potential is also introduced in the model. Carbon–12 is studied on the same footing.

By means of an integral transform approach, the problem of the transition to a state in the continuum can be advantageously reformulated in terms of a bound–state problem: in the calculations we use the Lorentz Integral Transform method, in conjunction with the Non–Symmetrized Hyperspherical Harmonics method.

In determining the low–energy photodisintegration cross section, the nuclear current matrix element is evaluated through the electric dipole, or quadrupole, transition operator (Siegert theorem). Since the continuity equation is used explicitly, the contribution of the one–body and the many–body current operators is implicitly included in the calculation. By comparing the results with those obtained by using a one–body convection current, the effect of the many–body terms can be quantified.

The dependence of the results on different EFT parameters is discussed, always in connection with the experimental data available in the literature. By following the power counting dictated by the EFT approach for Beryllium–9, the inclusion of different partial waves in the potential model is explored. In addition to a α–α S–wave, a α–n P–wave and a three–body effective interaction, a α–n S–wave term is also required to obtain results more consistent with the experimental data. The contribution of the many–body currents to the cross section is found to be non–negligible. Although at an early stage, Carbon–12 results show interesting features.

The formalism presented in this Thesis can be extended to study the photodisintegration of Oxygen–16 within a fully four–body *ab initio* approach.

A babbo, a mamma.

Contents

List of Figures

List of Tables

Chapter 1

Introduction

The formation of the elements, from the light to the heavy ones, is one of the principle subject in the field of nuclear astrophysics. The fundamental building blocks of nucleosynthesis are the single nucleons, protons and neutrons, as well as cluster structures, such as the α–particles. Understanding the processes in which these particles are involved is of primary importance. Within this framework, nuclear physics provides an essential input through the determination of nuclear structures and reactions [1].

The absence of stable elements at mass numbers $A = 5$ and $A = 8$ represents an obstacle to the formation of heavy elements starting from p, n and α. In the Helium–burning phase of stars, one reaction path capable of bridging these well–known gaps is the triple–α process, leading to the Carbon–12 nucleosynthesis [2]. However, in a neutron–rich environment, such as neutron star mergers or supernovae explosions, an alternative path to ^{12}C is represented by both direct and sequential reactions that combine two α–particles and a neutron into Beryllium–9. The whole process can be represented schematically as

$$^4\mathrm{He}(\alpha n, \gamma)^9\mathrm{Be}(\alpha, n)^{12}\mathrm{C}\,, \tag{1.1}$$

whereas in the case of sequential reactions, first ^{8}Be is formed from two α–particles, being a resonance located slightly above the two–α threshold, and then $^8\mathrm{Be}(n, \gamma)^9\mathrm{Be}$ takes place [3]. In this way, under certain astrophysical conditions, the production of heavier elements, turns out to be sensitive to the rate of ^{9}Be formation [4]. In order to construct models as accurate as possible, a theoretical study is therefore required. Due to the time reversal invariance, one can focus on the inverse process, which is the ^{9}Be photodisintegration reaction. For these reasons, in this work we present a theoretical study of the following reaction

$$\gamma + {}^9\mathrm{Be} \to \alpha + \alpha + n\,, \tag{1.2}$$

in a fully three–body *ab initio* approach and in the low–energy regime of astrophysical interest.

Since direct measurements of the three–body capture are not possible, several experiments have been conducted over the years to measure the ^{9}Be photodisintegration cross section by using different photon sources. One of the most recent ones is reported in Ref. [5], by Arnold, *et al.* (2012), carried out by employing a

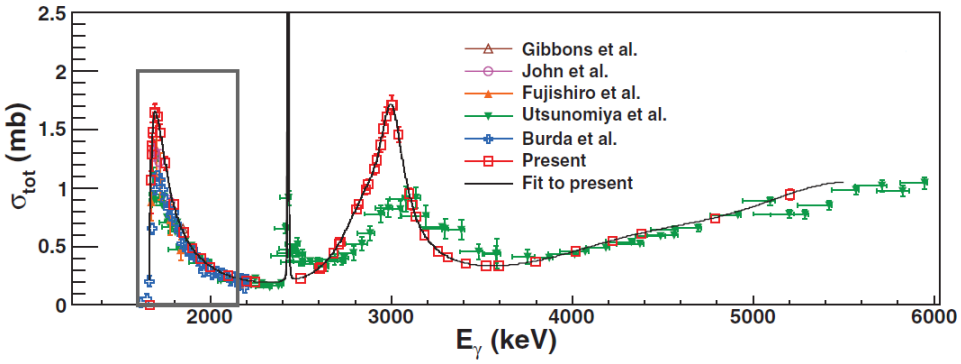

Figure 1.1: Data relative to the total $^{9}\mathrm{Be}(\gamma, n)^{8}\mathrm{Be}$ cross section collected by using different γ–ray sources such as real photons from both natural radioisotopes (Gibbons *et al.*, John *et al.*, Fujishiro, *et al.* [6]) and inverse Compton scattering (Utsunomiya, *et al.* [7]) as well as virtual photons from inelastic electron scattering (Burda, *et al.* [8]). The label "present" refers to the experiment conducted by Arnold, *et al.* with nearly monoenergetic photon beams and reported in Ref. [5], from which the figure is taken.

highly efficient neutron detector and nearly monoenergetic photon beams produced by the High Intensity γ–ray Source of Triangle Universities Nuclear Laboratory. In Fig. 1.1 the collected data are shown, where also a comparison with those from previous measurements is present. These include experiments performed with real photons from both natural radioisotopes [6] and laser–induced Compton backscattered γ–rays [7], and with virtual photons from inelastic electron scattering [8]. It can be noticed that the data collected by Arnold, *et al.* are larger than most of the measurements coming from earlier experiments, both in the region just above the two–body threshold, corresponding to energy $\approx 1.7\,\mathrm{MeV}$, and at energy $\approx 3\,\mathrm{MeV}$, where the difference is almost a factor of two. Another recent set of data regarding a broader range of energy, up to $\approx 16\,\mathrm{MeV}$, can be found in Ref. [9] by Utsunomiya, *et al.* (2015). They focused on the resonance peak just above the neutron threshold energy, due to the state $J^{\pi} = 1/2^{+}$, finding consistence with the previous 2001 data [7], and on the Cluster Dipole Resonance (CDR) below the Giant Dipole Resonance (GDR). Fig. 1.2 shows the experimental cross section obtained by using quasi–monochromatic γ–ray beams produced by means of the inverse Compton scattering of laser photons at the NewSUBARU synchrotron radiation facility.

The grouping of elementary constituents into sub–units is characteristic of a wide variety of physical systems, and it is commonly defined *clustering*. This can be seen as an effect due to the transition of such systems towards states characterized by a lower potential energy, leading also to a gain in stability [11]. Specifically, nuclear clustering structures are the result of a balance between different ingredients: the repulsive short–range interactions and the Pauli blocking effects, the attractive medium–range nuclear forces, and the long–range Coulomb interactions involving protons. A good candidate for such a structure is represented by the $^{4}\mathrm{He}$ nucleus, i.e. the α–particle, which is highly symmetric and stable. α–clustering is indeed a reality in light nuclei [12].

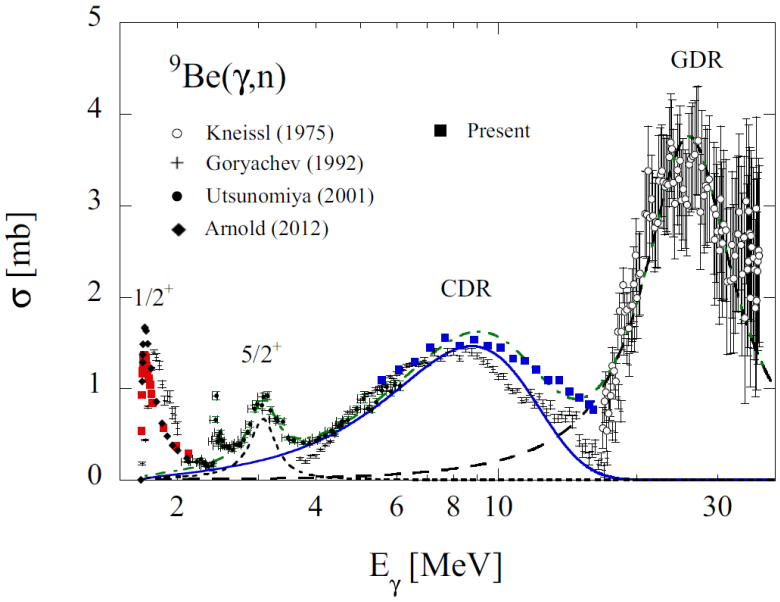

Figure 1.2: Figure taken from Ref. [9] by Utsunomiya, *et al.* (2015), to which the label "present" refers. The ^{9}Be(γ, n) cross section is shown, from the energy corresponding to the two–body $n + {}^8$Be threshold, and up to the Giant Dipole Resonance (GDR) region. For the state $J^\pi = 1/2^+$ also the bremsstrahlung data by Goryachev, *et al.* [10] and the data collected by Arnold, *et al.* [5] are reported. $J^\pi = 5/2^+$ 2001 data are from Ref. [7].

The origin of the cluster model for atomic nuclei dates back to the very early stages of nuclear physics (see [11] and References therein). After the discovery of α–radioactivity by Becquerel, and Marie and Pierre Curie, and after the identification of α–particles with ^{4}He nuclei by Rutherford, already in 1930, Gamow proposed a type of nuclear model in which nuclei are composed of α–particles. During the 30's Wefelmeier pointed out that the $N = Z$ even–even nuclei, such as ^{12}C and ^{16}O, show a great stability in terms of binding energy, and he suggested for these nuclei a structure of α–particles with a regular geometry. Together with other studies by Wheeler and Fano, this pioneered a strong development of the α–model of the nucleus in the late 30's, represented by the works of Hafstad and Teller, and Dennison. The success in describing the binding energy of the ground state of self–conjugate nuclei led also to a thorough investigation of the α–α interaction. The widely used phenomenological Ali–Bodmer potential [13] was developed in the 60's for the description of the α–α scattering. In those years, another step forward was represented by the publication of the so–called Ikeda diagram [14], developed by following the idea that clustered structures in light nuclei should occur close to the α–threshold energies, i.e. the energies required for the decay into the relevant sub–units. This also suggested that clustering could play a significant role in nuclear astrophysics, since states existing near the thresholds could influence the reaction rates relative to the processes occurring in the Helium–burning stage. An example of this kind is provided by the triple–α process and the Hoyle state [15]. Later, these concepts were somehow extended also to neutron–rich systems. In 1996, von

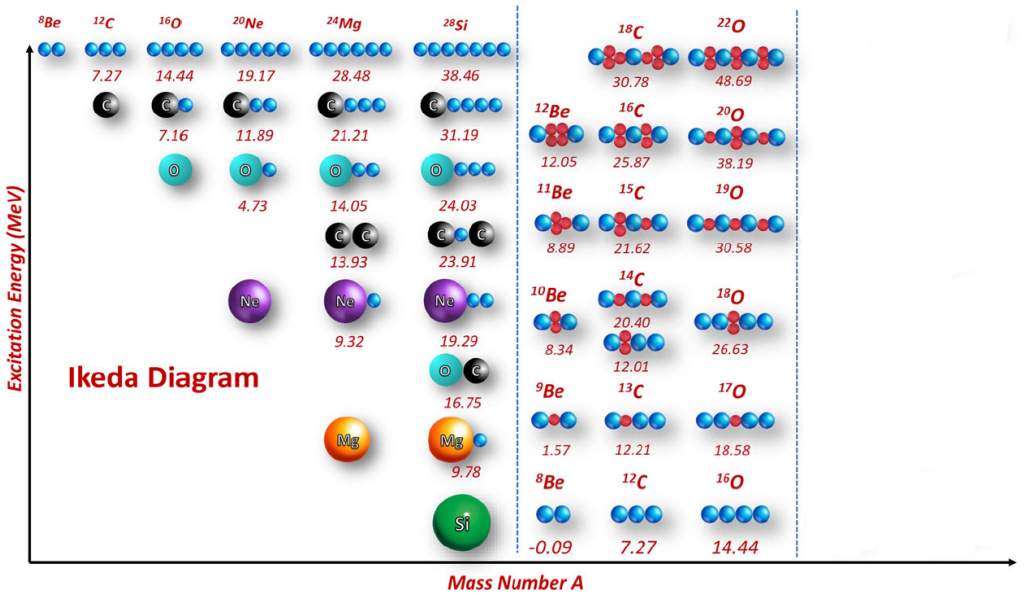

Figure 1.3: Re–elaboration of the Ikeda diagram taken from Ref. [11], where the threshold energy (MeV) for each decay mode is indicated. The threshold–rule is represented for different nuclei: self–conjugate nuclei (left–section) and neutron–rich light isotopes (section on the right). On the horizontal axis they are ordered by increasing mass number A. The α–particles are depicted in light blue, neutrons in red.

Oertzen [16] argued about the possible presence of dimeric structures in Beryllium isotopes, leading, among other things, to the full understanding of ^{9}Be structure concerning the ground state and the first excited states. In Fig. 1.3 the threshold–rule of the Ikeda diagram is represented for both self–conjugate nuclei and neutron–rich light isotopes. Among others, α–clustering of ^{9}Be and ^{12}C is visible.

^{9}Be nucleus provides a three–body effective clustering system with a Borromean structure: the whole nucleus is bound but each of the two–body subsystems, here α–n and α–α, is not bound. The threshold energy for the three–body $\alpha + \alpha + n$ breakup corresponds to $B_3 \approx 1.57$ MeV, while the proton separation energy relative to the α–particle is $S_p(^4\text{He}) = 19.81\,\text{MeV}$. The three–body binding of ^{9}Be is therefore shallow when compared to the α binding. This provides a clear separation of energy scales, which is an essential feature required for the use of an Effective Field Theory (EFT) approach. In the literature, theoretical calculations of the low–energy ^{9}Be photodisintegration can be found, where a three–body representation of the nucleus in its bound state is assumed, and two–body phenomenological potentials are employed. We mention here, for example, the work by Efros, *et al.* [17], as well as that by Casal, *et al.* [18], or Kikuchi, *et al.* [19], in which also a three–body potential is included in the model in order to adjust the energy of the system. In the latter a wider range of energies, up to 16 MeV, is also considered. Instead of using phenomenological potentials, in this work the aforementioned separation of scales is exploited, leading to a description of ^{9}Be by means of interactions derived from a halo/cluster EFT [20], and therefore based on a more solid theoretical background.

Since their introduction into nuclear physics [21], EFTs have had a huge impact in this field. Nowadays a large part of *ab initio* calculations, consisting mainly in solving the Schrödinger equation relative to the chosen degrees of freedom, are performed by using interactions from EFTs. An EFT provides a general framework for studying the low–energy behaviour of a physical system consistently with some assumed symmetries. By taking the known symmetries of Quantum Chromodynamics (QCD), an EFT essentially provides a realisation of QCD in terms of hadrons instead of quarks and gluons [22]. Once the energies of interest have been identified, the most general Lagrangian is constructed by means of a set of fields corresponding to the relevant degrees of freedom, and each term is constrained only by the symmetries of the underlying theory. The long–distance physics is treated explicitly. All the details about the short–distance dynamics that cannot be resolved at low energy are implicitly included in the interaction strengths, commonly known as Low Energy Constants (LECs). This also provides a "controlled" framework, where the physical quantities are given by means of an expansion in powers of the small ratio M_{lo}/M_{hi}; M_{lo} is the typical scale of the effective theory to be constructed while M_{hi} represents the scale at which the EFT breaks down ($M_{lo} \ll M_{hi}$). By considering processes characterized by a typical momentum $Q \sim M_{lo}$, if calculations are carried out at a certain order ν of the expansion, then the errors can be quantified as $(M_{lo}/M_{hi})^{\nu+1}$ [20]. In this sense an EFT is renormalizable, since at each order in the expansion the sensitivity to the unaccounted short–distance physics is small, being of relative size $\mathcal{O}(M_{lo}/M_{hi})$ [22].

Historically, the first nuclear effective theory to be developed was the chiral EFT [21], which includes as degrees of freedom nucleons and pions, and it is designed for momenta of the order $Q \sim m_\pi \ll 1\,\mathrm{GeV}$. Despite its success in terms of phenomenology, renormalization has proven to be challenging [22]. A different effective theory is the so–called pionless EFT (see [22] and References therein), working for momenta well below the pion mass. The degrees of freedom are represented by the nucleons, since the pions can be treated as short–range interactions. In this case, renormalization is relatively better understood. A variant of the pionless (or contact) EFT is represented by the halo/cluster EFT [20, 23–25]. Within this framework, halo and cluster nuclei can be studied. In some processes involving these nuclear systems the typical energies are so low that not only nucleons but also clusters of nucleons, such as α–particles, can be treated as elementary degrees of freedom. This is the effective theory of interest to us, from which our α–n and α–α effective potentials, as well as a possible three–body interaction, are inspired.

Photodisintegration reactions of light nuclei are processes in which a real photon interacts with the single nucleus, as diagrammatically represented in Fig. 1.4. Basically, the photon with energy ω causes a transition from an initial nuclear state $|\psi_i\rangle$ to a final state in the continuum $|\psi_f\rangle$, where the nucleus breaks into sub–units. In this work we are interested in the low–energy regime of astrophysical relevance, and therefore, by taking the initial state as the ground state of the nucleus under study, the sub–units in the final configuration are represented by nucleons and α–particles.

The calculation of the photodisintegration cross section involves the evaluation of the so–called Nuclear Current matrix element (NCme). In its more general form, it explicitly depends on the Fourier transform of the nuclear current, $\tilde{\boldsymbol{J}}(\boldsymbol{q})$, and on the spherical component of the photon polarization vector, $\hat{\boldsymbol{\varepsilon}}_{\boldsymbol{q},\lambda}$. The NCme is

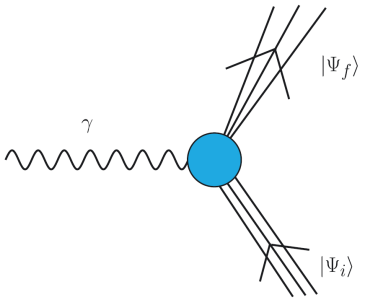

Figure 1.4: Figure taken from Ref. [26]. The diagram of the interaction between a single real photon and a nucleus is represented.

commonly denoted as [26]

$$\mathcal{N}_{fi} = \left\langle \psi_f \left| \hat{\boldsymbol{\varepsilon}}_{\boldsymbol{q},\lambda} \cdot \tilde{\boldsymbol{J}}(\boldsymbol{q}) \right| \psi_i \right\rangle . \tag{1.3}$$

Since the photon is real, it must be $\lambda = \pm 1$. Moreover, the momentum $\boldsymbol{q}$ transferred by the photon is such that $\omega = |\boldsymbol{q}|$. Essentially, $\mathcal{N}_{fi}$ encodes all the necessary information about the nuclear structure. From a theoretical point of view, the calculation of the final states $|\psi_f\rangle$ belonging to the continuum is not an easy task. To overcome this difficulty, in this work, we adopt an integral transform approach [27] in conjunction with the Non–Symmetrized Hyperspherical Harmonics (NSHH) method [28], where the interactions derived from a halo/cluster EFT are given as an input.

Since the nuclear current $\tilde{\boldsymbol{J}}(\boldsymbol{q})$ can be formally expressed as a sum of a one–body and many–body terms, one way to proceed is to evaluate $\mathcal{N}_{fi}$ by taking into account only the one–body term, i.e. the nuclear convection current. This calculation has already been performed by Filandri in Ref. [29]. With respect to this computation, here we want to make a step further. Due to the condition of Gauge invariance of the electromagnetic interaction, i.e. the continuity equation, the transverse electric multipoles of the nuclear current operator can be related to the Coulomb multipoles of the nuclear charge of the same order. This can be demonstrated rather easily by restricting to low energies. As a consequence, if we focus on the electric transitions, then an explicit expression of the nuclear current is not required anymore, since the NCme is completely determined by the nuclear charge [30]. For electric $E1$ transitions, this corresponds to the formulation of the Siegert theorem [31]. In this case, in the low–energy limit, the calculation of the cross section entirely depends on the matrix element of the dipole operator. Since the continuity equation has been used explicitly, this turns out to be a powerful mechanism that allows to implicitly include in the calculation the contribution of the one–body current as well as that of the many–body terms. From a direct comparison with the cross section obtained by using only the one–body current, the contribution due to the many–body currents can be quantified.

The models and the methods presented so far can be employed to study also other processes of astrophysical relevance. Among others, the nuclear system provided by ^{12}C nucleus can be analysed. In the regime of low energies, ^{12}C can be considered as an effective three–body system. This nucleus is Borromean, since it is

bound, with a three–body binding energy corresponding to $B_3 = 7.275\,\mathrm{MeV}$, while each two–body α–α subsystem is unbound. The EFT approach is still legitimate, if one takes into account the energy scales given by the binding energy of each α–particle and the proton separation energy $S_p(^4\mathrm{He})$.

As already mentioned, the triple–α process

$$^4\mathrm{He}(2\alpha,\gamma)^{12}\mathrm{C}\,, \tag{1.4}$$

assumes a key role in bridging the mass gaps at $A = 5$ and $A = 8$, leading to the production of ^{12}C in the Helium–burning stage of red giant stars [2]. The importance of this element in understanding the origin of organic life is well–known. The reaction that proceeds through the formation of ^{8}Be from two α, and the subsequent capture of another α–particle by the unstable ^{8}Be, has a very low rate, not being able to explain the observed abundance of Carbon in the Universe. In 1953, Hoyle proposed the existence of a $J^\pi = 0^+$ resonance, the $^{12}\mathrm{C}(0_2^+)$ state, very close to the $^8\mathrm{Be} + \alpha$ decay threshold, which is capable of strongly enhancing the process (1.4) [32]. This was later confirmed experimentally.

When the stellar temperature $T \sim 10^9$ K is reached, approximately corresponding to energies $\approx 0.1\,\mathrm{MeV}$, the triple–$\alpha$ process is dominated by the *sequential* picture: first ^{8}Be resonance is formed, and then the Hoyle state plays an essential role in the reaction (1.4), where the bound state $^{12}\mathrm{C}(2_1^+)$ is formed through γ–decay of $^{12}\mathrm{C}(0_2^+)$. By the emission of another γ, also the ground state $^{12}\mathrm{C}(0_1^+)$ can be reached. On the other hand, at lower temperatures $T \sim 10^7$ K, since the formation of the intermediate resonances is not possible, the process should be considered as a *direct* three–body reaction. In this very–low–energy regime measurements are not feasible, and therefore a theoretical study is essential.

The computation of the triple–α reaction rate is still a subject of discussion [33]. Among calculations performed by assuming the sequential picture, we mention the approach by Angulo *et al.* [34], who also carried out an extrapolation of the sequential model to very–low energies. In the most recent works, in order to carry out a proper computation, the importance of adopting the non–sequential picture at very–low energies was pointed out [35]. Since Ogata *et al.* [35], a large literature has been produced on this subject, the results of which can be summarised by saying that the computed reaction rates are essentially in agreement at higher temperatures; however, the calculation in the low–temperature regime remains controversial. It is worth mentioning, among the others, the works by Garrido, *et al.* [36], Nguyen, *et al.* [37], Ishikawa [38] and Suno, *et al.* [33] (and the References therein), where thorough studies of the triple–α process can be found, by using different techniques.

A full treatment of this subject is beyond the scope of this work. For the moment, our aim is to see to what extent our models and methods can be used to analyse the inverse triple–α process, which is represented by the ^{12}C photodisintegration reaction, leaving other possible in–depth studies for the future. In this work, we will therefore study the following process

$$\gamma + {}^{12}\mathrm{C} \to \alpha + \alpha + \alpha\,, \tag{1.5}$$

at low energies, proceeding through the $E2$ transition $2_1^+ \to 0_2^+$, by adopting a three–body *ab initio* approach. In line with what is done with ^{9}Be photodisintegration,

the cross section of the reaction in Eq. (1.5) is calculated by employing potential models derived from a halo/cluster EFT, in conjunction with the NSHH method and an integral transform approach.

Outline

This Thesis is organized according to the scheme below.

In Chapter 2 we introduce the observable of interest, the cross section of nuclear photodisintegration processes, whose calculation in terms of the NCme is derived in detail. Starting from the multipole decomposition of the nuclear current operator, by exploiting the continuity equation, the definition of the so–called Siegert operator is given.

Chapter 3 is entirely devoted to the description of the integral transform approach used to calculate the reaction cross section. Essentially, one of the main advantages in using this approach is that the problem of the transition to the continuum is reformulated as a typical bound–state–like problem. The response function relative to the reaction under study can be computed by means of the Lorentz Integral Transform (LIT) method: first an integral transform with a Lorentzian kernel is calculated, then an inversion procedure is required. A discussion about both these steps is presented.

After a brief description of the α–n and α–α systems from the point of view of EFTs, including the power counting procedure, Chapter 4 contains the explicit derivation of the two–body effective potentials employed in this work. A three–body potential is also introduced.

In Chapter 5 we construct a Non–Symmetrized Hyperspherical Harmonics basis, both in coordinate and in momentum space. The bound–state problem is then solved by means of a variational procedure. These are the key ingredients of the so–called NSHH method. The procedure of defining bases that allow to switch from momentum to coordinate space (and vice versa) when computing matrix elements is also particularly emphasised.

Our results of the calculated cross section relative to ^{9}Be and ^{12}C photodisintegration reactions are collected in Chapter 6 and Chapter 7, respectively.

Driven by the results obtained, the conclusions and the possible outlooks are reported in Chapter 8.

Chapter 2

Nuclear photodisintegration reactions

In this Chapter we study photodisintegration processes involving nuclear systems. The observable of interest is the reaction cross section, whose expression in terms of the nuclear current matrix element is derived in Section 2.1. In Section 2.2 an expansion of the nuclear current operator by means of electric and magnetic multipoles is performed. By focussing on the electric terms, the definition of the Siegert operator is given in Section 2.3, where also the long–wavelength limit approximation is analysed. Finally, Section 2.4 highlights the main advantages of using the Siegert operator, in connection with the continuity equation.

Photonuclear reactions, together with electron–scattering processes, have been analysed in several works, from Ref. [39] to the more recent and comprehensive review by Bacca and Pastore [26] about electromagnetic reactions on light nuclei. Explicit calculations of the various quantities can also be found, among others, in Refs. [40, 41].

2.1 The reaction cross section

Our aim is to study the interaction of the nucleus with the electromagnetic field. Since we are interested in photoabsorption processes, we start from the relevant term of the interaction Hamiltonian [42]

$$H_{\text{int}}(t) = -\int d^3\boldsymbol{x}\, \boldsymbol{J}(x) \cdot \boldsymbol{A}(x)\,, \tag{2.1}$$

which is linear in the vector potential field $\boldsymbol{A}(x)$. The assumption here is the existence of a charge $\rho(x)$ and a current operator $\boldsymbol{J}(x)$ that describe the nucleus, with x the spacetime vector $x^\mu = (t, \boldsymbol{x})$. We need to calculate the matrix element $\langle f|S|i\rangle \equiv S_{fi}$ between the initial $|i\rangle$ and the final state $|f\rangle$, with S defined at the lowest order as

$$S \cong I - i\int dt\, H_{\text{int}}(t)\,. \tag{2.2}$$

In the photodisintegration reaction $\gamma + Y \to Y'$, the single photon γ, with quadrimomentum $q^\mu = (\omega_{\boldsymbol{q}}, \boldsymbol{q})$ and polarization λ, is absorbed by the nucleus Y, inducing

a transition between two states. Since the photon is real, its energy is fixed by the relation $\omega_{\boldsymbol{q}} = |\boldsymbol{q}| = q$. We write the initial and final states of the process as $|i\rangle = |\boldsymbol{q}, \lambda\rangle\,|Y\rangle$ and $|f\rangle = |0\rangle\,|Y'\rangle$, respectively, where $|0\rangle$ denotes the vacuum state relative to the photon space. We also introduce the quadrimomentum relative to the nucleus in its initial state $P_i^\mu = (E_i, \boldsymbol{P}_i)$, and the quadrimomentum of the final state of the system $P_f^\mu = (E_f, \boldsymbol{P}_f)$. For the matrix element S_{fi}, with $f \neq i$, we can write

$$S_{fi} = -i \int d^4x \,\langle Y'|\boldsymbol{J}(x)|Y\rangle\,\langle 0|\boldsymbol{A}(x)|\boldsymbol{q}, \lambda\rangle \ , \tag{2.3}$$

where the matrix element of the photon and the one relative to the nucleus factorize.

First of all we focus on $\langle 0|\boldsymbol{A}(x)|\boldsymbol{q}, \lambda\rangle$. The vector potential field $\boldsymbol{A}(x)$ relative to the photon is defined as

$$\boldsymbol{A}(x) = \sum_{\lambda=\pm1} \Omega \int \frac{d^3\boldsymbol{k}}{(2\pi)^3} \frac{1}{\sqrt{2\Omega\omega_{\boldsymbol{k}}}} \left(\hat{\boldsymbol{\varepsilon}}_{\boldsymbol{k},\lambda} a_{\boldsymbol{k},\lambda} e^{-ikx} + \hat{\boldsymbol{\varepsilon}}^*_{\boldsymbol{k},\lambda} a^\dagger_{\boldsymbol{k},\lambda} e^{ikx}\right) , \tag{2.4}$$

where $k^\mu = (\omega_{\boldsymbol{k}}, \boldsymbol{k})$ and the unit vectors $\hat{\boldsymbol{\varepsilon}}_{\boldsymbol{k},\lambda}$ are the photon polarization vectors defined on a spherical basis as

$$\hat{\boldsymbol{\varepsilon}}_{\boldsymbol{k},\pm1} = \mp\frac{1}{\sqrt{2}}(\hat{\boldsymbol{\varepsilon}}_{\boldsymbol{k},x} \pm i\hat{\boldsymbol{\varepsilon}}_{\boldsymbol{k},y}) \, . \tag{2.5}$$

The creation and annihilation operators $a^\dagger_{\boldsymbol{k}',\lambda'}$ and $a_{\boldsymbol{k},\lambda}$ satisfy the following anti-commutation relation

$$\left[a_{\boldsymbol{k},\lambda}, a^\dagger_{\boldsymbol{k}',\lambda'}\right] = \frac{(2\pi)^3}{\Omega}\delta^3(\boldsymbol{k} - \boldsymbol{k}')\delta_{\lambda,\lambda'} \, , \tag{2.6}$$

Ω being a normalization volume. The initial state of the photon can be rewritten by using the creation operator as $|\boldsymbol{q}, \lambda\rangle = a^\dagger_{\boldsymbol{q},\lambda}\,|0\rangle$. With the help of the anticommutator (2.6), it is not difficult to demonstrate that the photon matrix element in Eq. (2.3) reduces to the following expression

$$\langle 0|\boldsymbol{A}(x)|\boldsymbol{q}, \lambda\rangle = \frac{1}{\sqrt{2\Omega\omega_{\boldsymbol{q}}}} \hat{\boldsymbol{\varepsilon}}_{\boldsymbol{q},\lambda} e^{-iqx} \, . \tag{2.7}$$

Now we move on to consider the nuclear matrix element that appears in Eq. (2.3). The nuclear current is Lorentz invariant and we can use the operator $T(x) = e^{-iPx}$ to rewrite $\boldsymbol{J}(x)$. P is defined as the momentum operator. We have that $\boldsymbol{J}(x) = e^{iPx}\boldsymbol{J}(0)e^{-iPx}$, and therefore we can write

$$\langle Y'|\boldsymbol{J}(x)|Y\rangle = e^{i(P_f - P_i)x}\,\langle Y'|\boldsymbol{J}(0)|Y\rangle \ . \tag{2.8}$$

By using the expressions of the matrix elements in Eqs. (2.7) and (2.8), we can rewrite S_{fi} in Eq. (2.3) as

$$S_{fi} = -i(2\pi)^4\delta^4(P_f - P_i - q)\frac{\hat{\boldsymbol{\varepsilon}}_{\boldsymbol{q},\lambda}}{\sqrt{2\Omega\omega_{\boldsymbol{q}}}}\,\langle Y'|\boldsymbol{J}(0)|Y\rangle \ , \tag{2.9}$$

where the delta function relative to the conservation of the quadrimomenta is the result of the integration. In the equation above, the matrix element of the nuclear

current can be further manipulated. We project the nuclear states $|Y\rangle$ and $|Y'\rangle$ on the space of the position coordinates $\boldsymbol{r}_j$ relative to each component of the nucleus. By assuming a system composed of A particles, we have $j = 1, \ldots, A$, and we define

$$\langle \boldsymbol{r}_1, \ldots, \boldsymbol{r}_A | Y \rangle = \Psi_A^i(\boldsymbol{r}_1, \ldots, \boldsymbol{r}_A) \,, \quad \langle \boldsymbol{r}_1, \ldots, \boldsymbol{r}_A | Y' \rangle = \Psi_A^f(\boldsymbol{r}_1, \ldots, \boldsymbol{r}_A) \,, \tag{2.10}$$

in which the part dependent on the center–of–mass coordinate $\boldsymbol{R}_{\rm cm}$ can be separated from the internal degrees of freedom as follows

$$\Psi_A^i(\boldsymbol{r}_1, \ldots, \boldsymbol{r}_A) = \psi^i(\boldsymbol{R}_{\rm cm})\, \Psi_N^i(\boldsymbol{r}'_1, \ldots, \boldsymbol{r}'_A) \,, \tag{2.11a}$$

$$\Psi_A^f(\boldsymbol{r}_1, \ldots, \boldsymbol{r}_A) = \psi^f(\boldsymbol{R}_{\rm cm})\, \Psi_N^f(\boldsymbol{r}'_1, \ldots, \boldsymbol{r}'_A) \,. \tag{2.11b}$$

The functions $\psi^i(\boldsymbol{R}_{\rm cm})$ and $\psi^f(\boldsymbol{R}_{\rm cm})$ are written in the form of plane waves as

$$\psi^i(\boldsymbol{R}_{\rm cm}) = \frac{1}{\sqrt{\Omega}} e^{i\boldsymbol{P}_i \boldsymbol{R}_{\rm cm}} \,, \qquad \psi^f(\boldsymbol{R}_{\rm cm}) = \frac{1}{\sqrt{\Omega}} e^{i\boldsymbol{P}_f \boldsymbol{R}_{\rm cm}} \,, \tag{2.12}$$

where Ω is a normalization volume. Each new position coordinate $\boldsymbol{r}'_j$ is defined as $\boldsymbol{r}'_j = \boldsymbol{r}_j - \boldsymbol{R}_{\rm cm}$, $j = 1, \ldots, A$. Since the set $\{\, \boldsymbol{r}'_1, \ldots, \boldsymbol{r}'_A \,\}$ can be easily related to the $N \equiv A - 1$ internal coordinates that describe the nuclear system, the states $|\Psi_N^i\rangle$ and $|\Psi_N^f\rangle$ are the so–called intrinsic nuclear states. By using Eqs. (2.10) and (2.11), the matrix element of the nuclear current operator, assumes the form

$$\langle Y' | \boldsymbol{J}(0) | Y \rangle = \frac{1}{\Omega} \int d^3\boldsymbol{R}_{\rm cm}\, e^{-i\boldsymbol{R}_{\rm cm}(\boldsymbol{P}_f - \boldsymbol{P}_i)}\, \langle \Psi_N^f | \boldsymbol{J}(0) | \Psi_N^i \rangle \,. \tag{2.13}$$

In the center–of–mass frame we have

$$\langle Y' | \boldsymbol{J}(\boldsymbol{0}) | Y \rangle = \frac{1}{\Omega}\, \langle \Psi_N^f | \tilde{\boldsymbol{J}}(\boldsymbol{P}_f - \boldsymbol{P}_i) | \Psi_N^i \rangle \,, \tag{2.14}$$

where $\tilde{\boldsymbol{J}}(\boldsymbol{P}_f - \boldsymbol{P}_i)$ is the Fourier transform of the nuclear current with respect to the center–of–mass coordinate. This yields to the following expression for S_{fi}

$$\begin{aligned} S_{fi} = {} & -i(2\pi)\, \delta(E_f - E_i - \omega_{\boldsymbol{q}})\, (2\pi)^3\, \delta^3(\boldsymbol{P}_f - \boldsymbol{P}_i - \boldsymbol{q}) \\ & \times \frac{1}{\sqrt{2\Omega\omega_{\boldsymbol{q}}}} \frac{1}{\Omega}\, \langle \Psi_N^f | \hat{\boldsymbol{\varepsilon}}_{\boldsymbol{q},\lambda} \cdot \tilde{\boldsymbol{J}}(\boldsymbol{P}_f - \boldsymbol{P}_i) | \Psi_N^i \rangle \,. \end{aligned} \tag{2.15}$$

At this point, it is important to note that, by considering the nucleus initially at rest in the laboratory frame, we have $\boldsymbol{P}_i = 0$, and from the momentum conservation $\boldsymbol{P}_f = \boldsymbol{q}$. Typically, E_i is the energy of the nucleus in its ground state, $E_i = E_0$, while E_f is explicitly $E_f \simeq E' + \frac{q^2}{2M_A}$, where E' is the energy of the final nuclear state, and M_A is the mass of the A–body nucleus. It follows that, if we neglect the recoil of the nucleus, we can identify $E_f \simeq E'$. This is the case that we will consider here and henceforth.

The matrix element S_{fi} enters in the calculation of the differential photodisintegration cross section, which is, according to the Fermi's Golden Rule,

$$d\sigma(\omega) = \frac{1}{2(2J_i + 1)} \sum_{\lambda = \pm 1} \sum_{M_i} \sum_f \frac{1}{|\boldsymbol{j}_{\rm in}| \rho_t} \frac{|S_{fi}|^2}{\Omega T}\, \Omega \frac{d^3\boldsymbol{P}_f}{(2\pi)^3} \,. \tag{2.16}$$

In this expression, we sum over the final states of the nuclear system and we average over the initial states, which are characterized by the angular momentum quantum number J_i. We also average over the two polarizations λ relative to the real photon. The differential cross section explicitly depends also on $\boldsymbol{j}_{\text{in}}$ and ρ_t, the incoming flux and the density of the target, respectively. By considering a single incoming photon we have $\boldsymbol{j}_{\text{in}} = 1/\Omega$, and for a single target nucleus the density is $\rho_t = 1/\Omega$. Moreover, the factor $\Omega\, d^3\boldsymbol{P}_f\,/(2\pi)^3$ represents the phase space volume of the final configuration. By inserting the calculated matrix element S_{fi} (2.15) in the expression of the differential cross section (2.16), if we make use of the following identities for a squared delta function

$$[(2\pi)\,\delta(E_f - E_i - \omega_{\boldsymbol{q}})]^2 = T(2\pi)\,\delta(E_f - E_i - \omega_{\boldsymbol{q}})\,, \tag{2.17a}$$

$$[(2\pi)^3\,\delta^3(\boldsymbol{P}_f - \boldsymbol{P}_i - \boldsymbol{q})]^2 = \Omega(2\pi)^3\,\delta^3(\boldsymbol{P}_f - \boldsymbol{P}_i - \boldsymbol{q})\,, \tag{2.17b}$$

where ΩT is the space–time volume element, we obtain the final result

$$\sigma(\omega_{\boldsymbol{q}}) = \frac{\pi}{2(2J_i+1)\omega_{\boldsymbol{q}}} \sum_{\lambda=\pm1} \sum_{M_i} \sum_{f} \left|\langle \Psi_N^f | \hat{\boldsymbol{\varepsilon}}_{\boldsymbol{q},\lambda} \cdot \tilde{\boldsymbol{J}}(\boldsymbol{q}) | \Psi_N^i \rangle\right|^2 \delta(E_f - E_i - \omega_{\boldsymbol{q}})\,. \tag{2.18}$$

By extracting the unit electric charge e from the nuclear current operator $\tilde{\boldsymbol{J}}(\boldsymbol{q})$, the cross section turns out to depend explicitly on e^2, and therefore we can rewrite $\sigma(\omega_{\boldsymbol{q}})$ in terms of the fine structure constant $\alpha = e^2/(4\pi)$ as [26]

$$\sigma(\omega_{\boldsymbol{q}}) = \frac{4\pi^2\alpha}{\omega_{\boldsymbol{q}}} R(\omega_{\boldsymbol{q}})\,. \tag{2.19}$$

The so–called response function $R(\omega_{\boldsymbol{q}})$ contains the energy–conserving delta function as well as the nuclear current matrix element, which encodes all the necessary information about the internal dynamics of the nuclear system:

$$R(\omega_{\boldsymbol{q}}) = \frac{1}{2(2J_i+1)} \sum_{\lambda=\pm1} \sum_{M_i} \sum\!\!\!\!\!\!\int_f \left|\langle \Psi_N^f | J_\lambda(q) | \Psi_N^i \rangle\right|^2 \delta(E_f - E_i - \omega_{\boldsymbol{q}})\,. \tag{2.20}$$

In the definition above, we have introduced the symbol $\sum\!\!\!\!\!\!\int_f$, denoting the sum over all the final states belonging to the discrete and the continuum spectrum as well as the sum over M_f. Moreover, the operator $J_\lambda(q)$, defined as $J_\lambda(q) \equiv \hat{\boldsymbol{\varepsilon}}_{\boldsymbol{q},\lambda} \cdot \tilde{\boldsymbol{J}}(\boldsymbol{q})$, represents the spherical component of the vector nuclear current operator $\tilde{\boldsymbol{J}}(\boldsymbol{q})$.

2.2 The nuclear current operator: multipole decomposition

Since the nuclear intrinsic states on which we evaluate the matrix element in the response function of Eq. (2.20) are typically eigenstates of the total angular momentum of the nucleus, the most convenient way to proceed is to perform a multipole decomposition of the current operator $\tilde{\boldsymbol{J}}(\boldsymbol{q})$. With this aim, we follow here the notation of Ref. [43], where the multipole decomposition is formulated in momentum space. An alternative derivation can be carried out entirely in configuration space,

as reported for example in Ref. [42]. Of course both approaches lead to the same final results.

We start by introducing the vector spherical harmonics. These functions are defined in terms of the standard spherical harmonics as [44]

$$\boldsymbol{Y}^{(\ell)}_{JM}(\hat{q}) = \sum_{m\lambda} C^{JM}_{\ell m,1\lambda} Y_{\ell m}(\hat{q}) \hat{\boldsymbol{\varepsilon}}_\lambda \,, \tag{2.21}$$

where $\hat{q}$ denotes the pair of spherical polar angles $\hat{q} = (\theta_q, \phi_q)$ and the coefficients $C^{JM}_{\ell m,1\lambda}$ are the Clebsch–Gordan coefficients. The unit vectors $\hat{\boldsymbol{\varepsilon}}_\lambda$, with $\lambda = 0, \pm 1$, are defined on a spherical basis as in Eq. (A.2). More details about the vector spherical harmonics functions can be found in Appendix A. Here we mention the following important orthonormality property:

$$\int d\hat{x}\, \boldsymbol{Y}^{(\ell)*}_{JM}(\hat{x})\, \boldsymbol{Y}^{(\ell')}_{J'M'}(\hat{x}) = \delta_{JJ'}\delta_{MM'}\delta_{\ell\ell'} \,. \tag{2.22}$$

Being a vector quantity, the nuclear current operator can be expanded in terms of the vector spherical harmonics. In momentum space we write

$$\tilde{\boldsymbol{J}}(\boldsymbol{q}) = \sum_{\ell JM} J^\ell_{JM}(q) \boldsymbol{Y}^{(\ell)*}_{JM}(\hat{q}) \,, \tag{2.23}$$

where the coefficients of the expansion depend only on $|\boldsymbol{q}| = q$, and they are formally defined as

$$J^\ell_{JM}(q) = \int d\hat{q}'\, \tilde{\boldsymbol{J}}(\boldsymbol{q}') \cdot \boldsymbol{Y}^{(\ell)}_{JM}(\hat{q}') \,. \tag{2.24}$$

The vectors $\boldsymbol{q}$ and $\boldsymbol{q}'$ have the same modulus, $|\boldsymbol{q}'| = |\boldsymbol{q}| = q$, but they differ in the orientation. Due to the properties of the Clebsch–Gordan coefficients in the definition of the vector spherical harmonics (2.21), for given quantum numbers J and M, with $J \geq 1$, there exist only three kinds of functions $\boldsymbol{Y}^{(\ell)}_{JM}(\hat{q})$, and they correspond to the orbital momentum values $\ell = J, J \pm 1$. As a consequence, they can be grouped according to their behaviour under the parity operator [44]. For this reason, we split the nuclear current operator as follows:

$$\tilde{\boldsymbol{J}}(\boldsymbol{q}) = \sum_{JM} \left(\tilde{\boldsymbol{J}}^{el}_{JM}(\boldsymbol{q}) + \tilde{\boldsymbol{J}}^{mag}_{JM}(\boldsymbol{q}) \right) . \tag{2.25}$$

The electric and magnetic currents $\tilde{\boldsymbol{J}}^{el}_{JM}(\boldsymbol{q})$ and $\tilde{\boldsymbol{J}}^{mag}_{JM}(\boldsymbol{q})$ are written in terms of the vector spherical harmonics as

$$\tilde{\boldsymbol{J}}^{el}_{JM}(\boldsymbol{q}) = J^{J-1}_{JM}(q) \boldsymbol{Y}^{(J-1)*}_{JM}(\hat{q}) + J^{J+1}_{JM}(q) \boldsymbol{Y}^{(J+1)*}_{JM}(\hat{q}) \,, \tag{2.26}$$

$$\tilde{\boldsymbol{J}}^{mag}_{JM}(\boldsymbol{q}) = J^{J}_{JM}(q) \boldsymbol{Y}^{(J)*}_{JM}(\hat{q}) \,, \tag{2.27}$$

and the parity of each operator is $(-1)^J$ and $(-1)^{J+1}$, respectively. Due to the properties of the vector spherical harmonics functions, it can be demonstrated that the explicit form of the electric and magnetic current operators is the following:

$$\begin{aligned} \tilde{\boldsymbol{J}}^{el}_{JM}(\boldsymbol{q}) = {} & \hat{\boldsymbol{q}}\, Y^*_{JM}(\hat{q}) \int d\hat{q}'\; \hat{\boldsymbol{q}}' \cdot \tilde{\boldsymbol{J}}(\boldsymbol{q}')\, Y_{JM}(\hat{q}') \\ & + \hat{\boldsymbol{q}} \times \boldsymbol{Y}^{(J)*}_{JM}(\hat{q}) \int d\hat{q}' \left(\hat{\boldsymbol{q}}' \times \boldsymbol{Y}^{(J)}_{JM}(\hat{q}') \right) \cdot \tilde{\boldsymbol{J}}(\boldsymbol{q}') \,, \end{aligned} \tag{2.28}$$

$$\tilde{\boldsymbol{J}}^{mag}_{JM}(\boldsymbol{q}) = \boldsymbol{Y}^{(J)*}_{JM}(\hat{q}) \int d\hat{q}'\, \tilde{\boldsymbol{J}}(\boldsymbol{q}') \cdot \boldsymbol{Y}^{(J)}_{JM}(\hat{q}') \,. \tag{2.29}$$

A detailed derivation of the expressions above is reported in Appendix A. If we now proceed by introducing the longitudinal and the transverse electric multipoles, $L^{el}_{JM}(q)$ and $T^{el}_{JM}(q)$, as well as the transverse magnetic multipole, $T^{mag}_{JM}(q)$,

$$L^{el}_{JM}(q) = \frac{1}{4\pi}\int d\hat{q}'\ \hat{\boldsymbol{q}}'\cdot\tilde{\boldsymbol{J}}(\boldsymbol{q}')\,Y_{JM}(\hat{q}')\,, \tag{2.30}$$

$$T^{el}_{JM}(q) = \frac{i}{4\pi}\int d\hat{q}'\left(\hat{\boldsymbol{q}}'\times\boldsymbol{Y}^{(J)}_{JM}(\hat{q}')\right)\cdot\tilde{\boldsymbol{J}}(\boldsymbol{q}')\,, \tag{2.31}$$

$$T^{mag}_{JM}(q) = \frac{1}{4\pi}\int d\hat{q}'\,\tilde{\boldsymbol{J}}(\boldsymbol{q}')\cdot\boldsymbol{Y}^{(J)}_{JM}(\hat{q}')\,, \tag{2.32}$$

then Eqs. (2.28) and (2.29) become

$$\tilde{\boldsymbol{J}}^{el}_{JM}(\boldsymbol{q}) = 4\pi\Big(L^{el}_{JM}(q)\,\hat{\boldsymbol{q}}\,Y^{*}_{JM}(\hat{q}) - iT^{el}_{JM}(q)\,\hat{\boldsymbol{q}}\times\boldsymbol{Y}^{(J)*}_{JM}(\hat{q})\Big)\,, \tag{2.33}$$

$$\tilde{\boldsymbol{J}}^{mag}_{JM}(\boldsymbol{q}) = 4\pi\,T^{mag}_{JM}(q)\,\boldsymbol{Y}^{(J)*}_{JM}(\hat{q})\,. \tag{2.34}$$

By summing these two terms, it is straightforward to derive the new complete expression for the nuclear current operator already defined in Eq. (2.25), which is

$$\tilde{\boldsymbol{J}}(\boldsymbol{q}) = 4\pi\sum_{JM}\left(L^{el}_{JM}(q)\,\hat{\boldsymbol{q}}\,Y^{*}_{JM}(\hat{q}) - iT^{el}_{JM}(q)\,\hat{\boldsymbol{q}}\times\boldsymbol{Y}^{(J)*}_{JM}(\hat{q}) + T^{mag}_{JM}(q)\,\boldsymbol{Y}^{(J)*}_{JM}(\hat{q})\right)\,. \tag{2.35}$$

By making the assumption that the momentum of the photon is oriented along the z–axis, $\boldsymbol{q} = q\hat{\boldsymbol{\varepsilon}}_z = q\hat{\boldsymbol{\varepsilon}}_0$, the equation above can be further simplified. If we use the explicit expressions for $\hat{\boldsymbol{q}}\,Y^{*}_{JM}(\hat{q})$, $\hat{\boldsymbol{q}}\times\boldsymbol{Y}^{(J)*}_{JM}(\hat{q})$ and $\boldsymbol{Y}^{(J)*}_{JM}(\hat{q})$ derived in Appendix A [see Eqs. (A.9), (A.10) and (A.11)], then we are able to write the nuclear current operator as

$$\tilde{\boldsymbol{J}}(\boldsymbol{q}) = \sqrt{2\pi}\sum_{JM}\sqrt{2J+1}\left(\sqrt{2}L^{el}_{JM}(q)\hat{\boldsymbol{\varepsilon}}_0 - M^2T^{el}_{JM}(q)\hat{\boldsymbol{\varepsilon}}^{*}_{M} - MT^{mag}_{JM}(q)\hat{\boldsymbol{\varepsilon}}^{*}_{M}\right)\,. \tag{2.36}$$

As a consequence, the spherical components $J_\lambda(q)\equiv\hat{\boldsymbol{\varepsilon}}_\lambda\cdot\tilde{\boldsymbol{J}}(\boldsymbol{q})$, written in terms of the electric and magnetic multipoles defined in Eqs. (2.30), (2.31) and (2.32), are

$$J_\lambda(q) = \sqrt{2\pi}\sum_{J}\sqrt{2J+1}\left[\sqrt{2}L^{el}_{J\lambda}(q)\delta_{\lambda 0} + (-1)^\lambda\left(T^{el}_{J\lambda}(q) + \lambda T^{mag}_{J\lambda}(q)\right)\delta_{|\lambda|1}\right]\,. \tag{2.37}$$

When dealing with real photons, as in the photodisintegration processes, the possible spherical polarization are characterized by $\lambda=\pm1$, and in this case the current operator in Eq. (2.37) reduces to

$$J_\lambda(q) = -\sqrt{2\pi}\sum_{J}\sqrt{2J+1}\left(T^{el}_{J\lambda}(q) + \lambda T^{mag}_{J\lambda}(q)\right)\,,\qquad \lambda=\pm1\,. \tag{2.38}$$

In the following Section we will see in detail how these nuclear electric and magnetic multipole operators can be constructed.

2.3 The transverse electric and the transverse magnetic multipole operators

As shown in the last Section, when we calculate the operator $J_\lambda(q)$ for photodisintegration reactions, we must take into account only the transverse electric $T^{el}_{J\lambda}(q)$ and transverse magnetic $T^{mag}_{J\lambda}(q)$ multipoles. Their definition is given in Eqs. (2.31) and (2.32), respectively. In this Section we will mainly focus on the electric multipole, with a brief mention of the magnetic term at the end.

We rewrite the cross product $\hat{\boldsymbol{q}} \times \boldsymbol{Y}^{(J)}_{JM}(\hat{q})$ that enters in the definition of Eq. (2.31) by using the following equivalence

$$\hat{\boldsymbol{q}} \times \boldsymbol{Y}^{(J)}_{JM}(\hat{q}) = i\sqrt{\frac{J+1}{J}}\hat{\boldsymbol{q}}\, Y_{JM}(\hat{q}) + i\sqrt{\frac{2J+1}{J}}\boldsymbol{Y}^{(J+1)}_{JM}(\hat{q})\,, \tag{2.39}$$

which follows from the relation (A.8b) derived in Appendix A. In this way the transverse electric multipole $T^{el}_{J\lambda}(q)$ results to be the sum of two terms

$$T^{el}_{JM}(q) = T^{el,I}_{JM}(q) + T^{el,II}_{JM}(q)\,, \tag{2.40}$$

which are

$$T^{el,I}_{JM}(q) = -\frac{1}{4\pi}\sqrt{\frac{J+1}{J}}\int d\hat{q}'\, \hat{\boldsymbol{q}}' \cdot \tilde{\boldsymbol{J}}(\boldsymbol{q}')\, Y_{JM}(\hat{q}')\,, \tag{2.41}$$

$$T^{el,II}_{JM}(q) = -\frac{1}{4\pi}\sqrt{\frac{2J+1}{J}}\int d\hat{q}'\, \tilde{\boldsymbol{J}}(\boldsymbol{q}') \cdot \boldsymbol{Y}^{(J+1)}_{JM}(\hat{q}')\,. \tag{2.42}$$

Both terms depend explicitly on the nuclear current $\tilde{\boldsymbol{J}}(\boldsymbol{q})$ but the important property of the first one, $T^{el,I}_{JM}(q)$, is that it can be rewritten by using the continuity equation. In momentum space the continuity equation reads

$$\omega_{\boldsymbol{q}}\tilde{\rho}(\boldsymbol{q}) - \boldsymbol{q} \cdot \tilde{\boldsymbol{J}}(\boldsymbol{q}) = 0\,, \tag{2.43}$$

and therefore it relates $\tilde{\boldsymbol{J}}(\boldsymbol{q})$ to the Fourier transform of the nuclear charge operator, denoted as $\tilde{\rho}(\boldsymbol{q})$. As a consequence, we can make use of the equivalence

$$\hat{\boldsymbol{q}} \cdot \tilde{\boldsymbol{J}}(\boldsymbol{q}) = \frac{\omega_{\boldsymbol{q}}}{q}\tilde{\rho}(\boldsymbol{q})\,, \tag{2.44}$$

to rewrite the electric multipole in Eq. (2.41), obtaining the so–called Siegert operator

$$T^{el,S}_{JM}(q) = -\frac{1}{4\pi}\sqrt{\frac{J+1}{J}}\frac{\omega_{\boldsymbol{q}}}{q}\int d\hat{q}'\, \tilde{\rho}(\boldsymbol{q}')Y_{JM}(\hat{q}')\,. \tag{2.45}$$

Clearly, the advantage of doing calculations with the Siegert operator is that the explicit form of the nuclear current $\tilde{\boldsymbol{J}}(\boldsymbol{q})$ is no longer needed. This point will be discussed in more detail later in Section 2.4. The "residual" multipole term in Eq. (2.42), under certain conditions, represents a correction to the Siegert operator, and the reason will become clear later.

Now we will see how the expression of the Siegert operator given in Eq. (2.45) can be reformulated in terms of the multipole operators relative to the nuclear charge. In fact, as already done with the nuclear current, we can also calculate the multipoles of the operator $\tilde{\rho}(\boldsymbol{q})$. In momentum space, the expansion of the charge in terms of the spherical harmonics functions is the following

$$\tilde{\rho}(\boldsymbol{q}) = 4\pi \sum_{JM} (-i)^J C_{JM}(q) Y^*_{JM}(\hat{q}) \,, \tag{2.46}$$

where the coefficients $C_{JM}(q)$ are the so–called Coulomb multipoles, and they are formally defined as

$$C_{JM}(q) = \frac{i^J}{4\pi} \int d\hat{q}' \, \tilde{\rho}(\boldsymbol{q}') Y_{JM}(\hat{q}') \,. \tag{2.47}$$

Note that the nuclear charge has been expanded in terms of the scalar spherical harmonics, following from the fact that it is a scalar quantity. We proceed by writing $\tilde{\rho}(\boldsymbol{q})$ as a Fourier transform

$$\tilde{\rho}(\boldsymbol{q}) = \int d^3\boldsymbol{x} \, e^{-i\boldsymbol{q}\boldsymbol{x}} \rho(\boldsymbol{x}) \,, \tag{2.48}$$

and then we replace the plane wave with its well–know expansion in terms of the spherical Bessel functions $j_\ell(qx)$ [44]

$$e^{-i\boldsymbol{q}\boldsymbol{x}} = 4\pi \sum_{\ell m} (-i)^\ell j_\ell(qx) Y^*_{\ell m}(\hat{q}) Y_{\ell m}(\hat{x}) \,. \tag{2.49}$$

In this way we obtain for the nuclear charge, in momentum space,

$$\tilde{\rho}(\boldsymbol{q}) = 4\pi \sum_{JM} (-i)^J Y^*_{JM}(\hat{q}) \int d^3\boldsymbol{x} \, j_J(qx) \rho(\boldsymbol{x}) Y_{JM}(\hat{x}) \,. \tag{2.50}$$

From the equation above, it is straightforward that the Coulomb multipoles can be identified as

$$C_{JM}(q) = \int d^3\boldsymbol{x} \, j_J(qx) \rho(\boldsymbol{x}) Y_{JM}(\hat{x}) \,. \tag{2.51}$$

The Siegert operator in Eq. (2.45) is easily rewritten in terms of the Coulomb multipoles as follows:

$$\begin{aligned} T^{el,S}_{JM}(q) &= -(-i)^J \sqrt{\frac{J+1}{J}} \frac{\omega_{\boldsymbol{q}}}{q} \, C_{JM}(q) \\ &= -(-i)^J \sqrt{\frac{J+1}{J}} \frac{\omega_{\boldsymbol{q}}}{q} \int d^3\boldsymbol{x} \, j_J(qx) \rho(\boldsymbol{x}) Y_{JM}(\hat{x}) \,. \end{aligned} \tag{2.52}$$

By following a similar procedure, we can also rewrite the operator $T^{el,II}_{JM}(q)$ defined in Eq. (2.42). One can start from the expression of the nuclear current as a Fourier transform $\tilde{\boldsymbol{J}}(\boldsymbol{q}) = \int d^3\boldsymbol{x} \, e^{-i\boldsymbol{q}\boldsymbol{x}} \boldsymbol{J}(\boldsymbol{x})$, and then use the plane wave expansion in Eq. (2.49). This leads to the result

$$T^{el,II}_{JM}(q) = -(-i)^{J+1} \sqrt{\frac{2J+1}{J}} \int d^3\boldsymbol{x} \; j_{J+1}(qx) \, \boldsymbol{J}(\boldsymbol{x}) \cdot \boldsymbol{Y}^{(J+1)}_{JM}(\hat{x}) \,. \tag{2.53}$$

If we now proceed to consider the limit of low–momentum transfer by the photon, the expressions of the electric multipoles $T^{el,S}_{JM}(q)$ and $T^{el,II}_{JM}(q)$ can be further simplified. The integrals in Eqs. (2.52) and (2.53) contain spherical Bessel functions of different orders. By taking $qR \ll 1$, where R represents the spatial extension of the system, the spherical Bessel functions behave as [45]

$$j_\ell(qR) \to \frac{(qR)^\ell}{(2\ell+1)!!}\,. \tag{2.54}$$

In this limit, which is also called long–wavelength limit, the Siegert operator $T^{el,S}_{JM}(q)$ in Eq. (2.52) becomes

$$T^{el,S}_{JM}(q) \simeq -(-i)^J \sqrt{\frac{J+1}{J}}\frac{q^{J-1}\omega_{\boldsymbol{q}}}{(2J+1)!!}\int d^3\boldsymbol{x}\, x^J \rho(\boldsymbol{x}) Y_{JM}(\hat{x})\,, \tag{2.55}$$

while for the multipole $T^{el,II}_{JM}(q)$ in Eq. (2.53) we have

$$T^{el,II}_{JM}(q) \simeq -(-i)^{J+1} \sqrt{\frac{2J+1}{J}}\frac{q^{J+1}}{(2J+3)!!}\int d^3\boldsymbol{x}\, x^{J+1} \boldsymbol{J}(\boldsymbol{x})\cdot \boldsymbol{Y}^{(J+1)}_{JM}(\hat{x})\,. \tag{2.56}$$

In the case of real photons, the dependence of the Siegert term in Eq. (2.55) on the transferred momentum is $T^{el,S}_{JM}(q) \sim q^J$, while the operator in Eq. (2.56) behaves as $T^{el,II}_{JM}(q) \sim q^{J+1}$. This means that, in the low–energy regime, calculations performed by using the Siegert operator are quite accurate and the term $T^{el,II}_{JM}(q)$ represents a correction that can be neglected in first approximation.

We underline that the expression of the Siegert operator in Eq. (2.55) for $J = 1$ represents the the so–called unretarded $E1$ approximation. We remark that this long–wavelength approximation is reliable only when dealing with low–momentum transfer, and therefore it is well suited for our calculations concerning reactions of astrophysical relevance. With increasing energies approaching $\sim$100 MeV [46], retardation effects should be taken into account, i.e. the operator in Eq. (2.52) should be considered, as well as the contribution due to term $T^{el,II}_{JM}(q)$ in (2.53).

We conclude this Section by briefly analyse the transverse magnetic multipole $T^{mag}_{JM}(q)$ defined in Eq. (2.32). Similarly to the expression given in Eq. (2.53), also the magnetic multipole can be written explicitly in terms of the spherical Bessel functions:

$$T^{mag}_{JM}(q) = (-i)^J \int d^3\boldsymbol{x}\, j_J(qx)\, \boldsymbol{J}(\boldsymbol{x})\cdot \boldsymbol{Y}^{(J)}_{JM}(\boldsymbol{x})\,. \tag{2.57}$$

In the low–energy regime, when we are allowed to apply the limit (2.54) for $j_J(qx)$, this operator behaves as $T^{mag}_{JM}(q) \sim q^J$. As a consequence, in principle, when carrying out photodisintegration reactions calculations, this contribution should not be neglected in first approximation.

2.4 The continuity equation and the Siegert theorem

In the last Section we have used the continuity equation of the electromagnetic current operator $J^\mu(x) = (\rho(x), \boldsymbol{J}(x))$ expressed in momentum space, Eq. (2.43), to rewrite the term $T^{el,I}_{JM}(q)$ in Eq. (2.41). In this way we have obtained the Siegert operator $T^{el,S}_{JM}(q)$ in (2.55), which represents the dominant contribution for electric transitions in the limit of low–momentum transfer. In other words, by means of the condition of Gauge invariance of the electromagnetic interaction, i.e. the continuity equation, the transverse electric multipoles are easily related to the Coulomb multipoles of the nuclear charge of the same order. As a consequence, the electric transition matrix elements, in the low–energy regime, are completely determined by the charge density operator, without knowing the explicit expression of the nuclear currents [30].

In the specific case of an electric $J = 1$ transition, in the low–energy regime, the evaluation of the current matrix elements is done by means of the charge dipole operator, as also emerges from Eq. (2.55). Schematically, if we write the continuity equation in momentum space in the alternative form

$$\boldsymbol{q} \cdot \tilde{\boldsymbol{J}}(\boldsymbol{q}) = [H, \tilde{\rho}(\boldsymbol{q})]\,, \tag{2.58}$$

by taking the matrix elements of the operators between initial and final states, we have, in the low–energy limit $\boldsymbol{q} \to 0$ [46, 47]

$$\tilde{\boldsymbol{J}}_{fi}(0) = i(E_f - E_i)\boldsymbol{D}_{fi}\,, \tag{2.59}$$

where the energy difference $E_f - E_i$ is equal to the photon energy, previously denoted as $\omega_{\boldsymbol{q}}$, and the dipole operator is defined as $\boldsymbol{D} = \int d^3\boldsymbol{x}\, \boldsymbol{x}\rho(\boldsymbol{x})$. This is a formulation of what is better known as the Siegert theorem [31]. This powerful theorem can be exploited in low–energy calculations, and in the rest of this Section we will briefly explain why.

The nuclear charge and nuclear current densities can be formally written as a sum of one– and many–body operators as follows [48]

$$\tilde{\rho}(\boldsymbol{q}) = \sum_i \tilde{\rho}^{[1]}_i(\boldsymbol{q}) + \sum_{i<j} \tilde{\rho}^{[2]}_{ij}(\boldsymbol{q}) + \sum_{i<j<k} \tilde{\rho}^{[3]}_{ijk}(\boldsymbol{q}) + \dots\,, \tag{2.60}$$

$$\tilde{\boldsymbol{J}}(\boldsymbol{q}) = \sum_i \tilde{\boldsymbol{J}}^{[1]}_i(\boldsymbol{q}) + \sum_{i<j} \tilde{\boldsymbol{J}}^{[2]}_{ij}(\boldsymbol{q}) + \sum_{i<j<k} \tilde{\boldsymbol{J}}^{[3]}_{ijk}(\boldsymbol{q}) + \dots\,. \tag{2.61}$$

By retaining only the non relativistic contributions, i.e. at the leading order in the expansion in powers of $1/m$, the one–body charge operator is explicitly

$$\tilde{\rho}^{[1]}_i(\boldsymbol{q}) = eZ_i e^{i\boldsymbol{q}\boldsymbol{r}_i}\,. \tag{2.62}$$

Regarding the one–body current, we can express this operator as the sum of a convection and a spin term

$$\tilde{\boldsymbol{J}}^{[1]}_i(\boldsymbol{q}) = \tilde{\boldsymbol{J}}^{[1],c}_i(\boldsymbol{q}) + \tilde{\boldsymbol{J}}^{[1],s}_i(\boldsymbol{q})\,, \tag{2.63}$$

whose explicit form is the following

$$\tilde{\boldsymbol{J}}_i^{[1],c}(\boldsymbol{q}) = \frac{eZ_i}{2m}\left\{\boldsymbol{p}_i, e^{i\boldsymbol{q}\boldsymbol{r}_i}\right\}, \tag{2.64}$$

$$\tilde{\boldsymbol{J}}_i^{[1],s}(\boldsymbol{q}) = i\frac{eZ_i}{2m}\mu_i\boldsymbol{\sigma}_i \times \left[\boldsymbol{p}_i, e^{i\boldsymbol{q}\boldsymbol{r}_i}\right], \tag{2.65}$$

where square and curl brackets denote the commutator and the anticommutator, respectively. In the equations above eZ_i is the electric charge of the particle i, whose position and momentum is given by the pair of vectors $\boldsymbol{r}_i$ and $\boldsymbol{p}_i$. $\boldsymbol{\sigma}_i$ and μ_i represent the Pauli spin operator and the magnetic moment of the particle, respectively. By taking the operators in Eqs. (2.60) and (2.61) at the lowest order in $1/m$, if we impose that they satisfy the Gauge condition (2.58) with the most general nuclear Hamiltonian defined as

$$H = \sum_i T_i + \sum_{i<j} V_{ij} + \sum_{i<j<k} V_{ijk}\,, \tag{2.66}$$

then we obtain different continuity equations for each n–body current operator. The first equation involves the one–body kinetic term operator $T_i = \frac{\boldsymbol{p}_i^2}{2m_i}$, being explicitly

$$\boldsymbol{q}\cdot\tilde{\boldsymbol{J}}_i^{[1]}(\boldsymbol{q}) = \left[T_i, \tilde{\rho}_i^{[1]}(\boldsymbol{q})\right]. \tag{2.67}$$

With the nuclear one–body current defined as in (2.63), it can be demonstrated that the equation above is always satisfied. The other conditions involve the two– and the three–body interaction terms of the Hamiltonian in (2.66), and they are

$$\boldsymbol{q}\cdot\tilde{\boldsymbol{J}}_{ij}^{[2]}(\boldsymbol{q}) = \left[V_{ij}, \tilde{\rho}_i^{[1]}(\boldsymbol{q}) + \tilde{\rho}_j^{[1]}(\boldsymbol{q})\right], \tag{2.68}$$

$$\boldsymbol{q}\cdot\tilde{\boldsymbol{J}}_{ijk}^{[3]}(\boldsymbol{q}) = \left[V_{ijk}, \tilde{\rho}_i^{[1]}(\boldsymbol{q}) + \tilde{\rho}_j^{[1]}(\boldsymbol{q}) + \tilde{\rho}_k^{[1]}(\boldsymbol{q})\right]. \tag{2.69}$$

When the interaction potential is such that the commutator terms on the right–hand–side of the equations above are non–vanishing, then, to maintain consistency, we must also postulate the existence of non–vanishing two– and three–body nuclear current operators $\tilde{\boldsymbol{J}}^{[2]}$ and $\tilde{\boldsymbol{J}}^{[3]}$, respectively. Since they are required by Gauge invariance, these many–body currents are referred to as "model independent" currents. Their longitudinal part is in fact constrained by the continuity equation and it is directly related to the nuclear interaction potential, as explicitly shown in Eqs. (2.68) and (2.69).

In the photodisintegration reactions that we want to study at low–momentum transfer conditions, as already shown, the nuclear current enters in the calculation of the transverse electric multipole as

$$T_{JM}^{el}(q;\tilde{\boldsymbol{J}}) \simeq T_{JM}^{el,I}(q;\tilde{\boldsymbol{J}}) = T_{JM}^{el,S}(q;\tilde{\rho})\,, \tag{2.70}$$

where in the last equivalence the continuity equation has been used. The multipole $T_{JM}^{el,I}$ and the Siegert term $T_{JM}^{el,S}$ have been already defined in Eqs. (2.41) and (2.45) and here we have highlighted also their operator dependence. At this point, the advantage of the application of the Siegert theorem is manifest. When we evaluate the Siegert operator by making use of the one–body non–relativistic charge density $\tilde{\rho}^{[1]}$,

since the continuity equation (2.58) has been employed, we are implicitly including in the calculation the main contribution due to the one–body current operator $\tilde{\boldsymbol{J}}^{[1]}$, as well as that of the two– and three–body currents $\tilde{\boldsymbol{J}}^{[2]}$ and $\tilde{\boldsymbol{J}}^{[3]}$. Schematically, this can be summarized as follows [49]

$$T^{el,S}_{JM}(q;\tilde{\rho}^{[1]}) = T^{el,I}_{JM}(q;\tilde{\boldsymbol{J}}^{[1]} + \tilde{\boldsymbol{J}}^{[2]} + \tilde{\boldsymbol{J}}^{[3]})\,. \tag{2.71}$$

Chapter 3

The Lorentz Integral Transform method

The Lorentz Integral Transform (LIT) method [50, 51] is a well–established tool that is included in the more general context of calculating reactions cross sections by using integral transforms [52]. This method can be applied to any perturbation–induced reaction of inclusive as well as exclusive type. A complete review of the topic and its applications is the one by Efros, *et al.* [27], which is also the main reference for the discussion and the formalism presented in this Chapter.

Instead of trying to solve the Schrödinger equation directly, if one focuses on the transition matrix elements, then it turns out that their calculation can be reduced to the evaluation of an integral transform and its subsequent inversion. As we will show in this Chapter, within this approach, the closure property of the eigenstates of the Hamiltonian plays a central role. Another very important point is the choice of the kernel that is used in the definition of the integral transform itself.

The main advantage of using such a method is that formal calculations involving explicit wave functions in the continuum are avoided, and the problem is reformulated as a typical bound–state–like problem. In this work we will deal with systems composed of $A = 3$ constituents and even in this case, where one could also use a Faddeev–Yakubovsky approach [53, 54], this reformulation in terms of bound–state wave functions allows an easier implementation of the problem with respect to the initial one.

After a brief introduction to the subject and a presentation of the main motivations that lead us to use the LIT method, Section 3.1, we will introduce the formalism for inclusive processes in Section 3.2. More details about the practical implementation of the method can be found in Section 3.3. Finally, in Section 3.4 we discuss about the inversion of the integral transform, which enables us to calculate indirectly the response function, and thus to evaluate the cross section of the reactions that we want to study.

3.1 Introduction and motivations

The LIT method allows to perform *ab initio* calculations of cross sections of light nuclei. When all the degrees of freedom of the many–body system are explicitly taken into account in the nuclear Hamiltonian, the solution of the quantum mechanical problem can be demanding, especially in the continuum. If we look at the response function defined in Eq. (2.20), we see that the knowledge of the explicit wave functions belonging to the full spectrum of the nuclear system is required. Unfortunately, when we have to find a solution of the problem in the continuum, various difficulties arise. In configuration space, for example, one of the main issues is the implementation of the proper boundary conditions. In addition to this, at a given energy, more than one final configuration becomes accessible to the system, corresponding to the different breakup channels of the nucleus under study. In principle, in performing exact calculations, all of these configurations should be taken into account in the final state but this is not an easy task. At this point it is possible to introduce some approximations, which eventually have to be validated by the experiment. However, this approach is rather inadequate especially for studying reactions of astrophysical interest, because in some cases experiments could not be performed. An *ab initio* calculation is therefore required.

By using an integral transform approach, the direct calculation of a generic response function $R(\omega)$, as the one defined in Eq. (2.20), can be bypassed. Starting from $R(\omega)$, one can define an integral transform as follows

$$L(\sigma) = \int d\omega \, K(\sigma, \omega) \, R(\omega) \, . \tag{3.1}$$

If one chooses a suitable kernel function $K(\sigma, \omega)$, then it can be demonstrated that the direct calculation of the transform $L(\sigma)$ is reduced to the task of finding the solutions of a Schrödinger–like equation with a source term. In this sense, one can say that the calculation in the continuum, which involves the response function $R(\omega)$, is "shifted" to a bound–state–like calculation in terms of the function $L(\sigma)$. At the end, the response function is recovered by performing an inversion of the transform $L(\sigma)$. In the next Sections, we will go into the details of this procedure.

Although in this work we will only make use of a kernel of Lorentzian type, the choice of the function $K(\sigma, \omega)$ is not unique [55]. Due to the fact that $L(\sigma)$ is calculated numerically and therefore it may contain inaccuracies, the inversion of this function could be somehow problematic and affected by errors [56]. In order to minimise these errors, a "clever" kernel should be chosen. In addition to leading to a transform $L(\sigma)$ that has to exist and has to be finite, the kernel function should also be of finite range and should preserve the information contained inside the response function. From the point of view of the latter requirement, the ideal kernel to use could be a delta function, $K(\sigma, \omega) = \delta(\sigma - \omega)$. However, in this case, there is no improvement in the calculation, since the defining integral in Eq. (3.1) would lead to the response function $R(\sigma)$ itself, whose direct calculation we want to avoid, as already explained. This is the reason why the choice of the kernel should fall on a function that is a representation of the delta function. In this sense the Lorentz function is a suitable kernel to use in the calculations.

Before going any further, it is worth clarifying another aspect. In this work we are studying photodisintegration reactions in which the nuclei involved break into

clusters of nucleons, i.e. α–particles, and possibly only one neutron is present

$$\gamma + {}^{9}\mathrm{Be} \to \alpha + \alpha + n\,, \qquad \gamma + {}^{12}\mathrm{C} \to \alpha + \alpha + \alpha\,. \tag{3.2}$$

Since actually we are choosing a specific breakup channel among all the possible final states, these processes seem to be of exclusive type. This is no longer the case, if we also specify that we are studying the photodisintegration reactions in the low–energy regime. Under this condition, the breakup channel that we consider is the only accessible final configuration, and therefore we can use the LIT method in its formulation for inclusive processes.

3.2 LIT for inclusive processes

In the most general case of an inclusive process the quantity of main interest is [27]

$$R(E) = \sum\!\!\!\!\!\!\int_f \langle Q|\Psi_f\rangle \, \langle \Psi_f|Q'\rangle \, \delta(E_f - E)\,, \tag{3.3}$$

where with the symbol $\sum\!\!\!\!\!\!\int_f$ we denote the summation and the integration over the discrete and continuum spectrum of the states $|\Psi_f\rangle$. The states $|\Psi_f\rangle$ are the solutions of the Schrödinger equation $(\hat{H} - E_f)\,|\Psi_f\rangle = 0$, where $\hat{H}$ is the nuclear Hamiltonian operator. Since the set $|\Psi_f\rangle$ is complete and orthonormal, the following relation holds

$$\sum\!\!\!\!\!\!\int_f |\Psi_f\rangle \, \langle \Psi_f| = 1\,. \tag{3.4}$$

Both norms $\langle Q|Q\rangle$ and $\langle Q'|Q'\rangle$ are assumed to be finite. If we specialise to the case of perturbation–induced reactions, then the states $|Q\rangle$ ($|Q'\rangle$) are the result of the application of a transition operator, denoted as $\hat{\mathcal{O}}$ ($\hat{\mathcal{O}}'$), to the initial state $|\Psi_i\rangle$, which is typically chosen as the ground state of the nuclear system. This means that we can write $|Q\rangle = \hat{\mathcal{O}}\,|\Psi_0\rangle$ ($|Q'\rangle = \hat{\mathcal{O}}'\,|\Psi_0\rangle$) and, as a consequence, Eq. (3.3) assumes the form

$$R(E) = \sum\!\!\!\!\!\!\int_f \langle \Psi_0|\,\hat{\mathcal{O}}^{\dagger}\,|\Psi_f\rangle \, \langle \Psi_f|\,\hat{\mathcal{O}}'\,|\Psi_0\rangle \, \delta(E_f - E)\,. \tag{3.5}$$

When the identity $\hat{\mathcal{O}} = \hat{\mathcal{O}}'$ holds, the function $R(E)$ can be identified with the so–called response function of the system. Essentially, it encodes the response of the nucleus to a perturbative probe when the energy E is transferred to the system. Due to the fact that a summation and an integration over the full spectrum of the final states $|\Psi_f\rangle$ is involved, the direct calculation of the response function is difficult. To overcome this problem, we define an integral transform of the response function as follows

$$L(\sigma) = \int\!\!\!\!\!\!\int dE\, K(\sigma, E)\, R(E)\,, \tag{3.6}$$

where the kernel function $K(\sigma, E)$ is assumed to be of Lorentzian type [50]

$$K(\sigma, E) = \frac{1}{(E - \sigma^*)(E - \sigma)}\,. \tag{3.7}$$

This functional form makes both the evaluation and the subsequent inversion of $L(\sigma)$ feasible. With σ we denote a complex energy parameter, which is defined as $\sigma = E_0 + \sigma_R + i\sigma_I$, E_0 being the initial ground–state energy of the nuclear system. This yields to the following explicit form for the kernel

$$K(\sigma_R, \sigma_I, E) = \frac{1}{(E - E_0 - \sigma_R)^2 + \sigma_I^2} \,, \tag{3.8}$$

which is in fact a Lorentzian function centered in the point $E_0 + \sigma_R$ with a width equal to $2\sigma_I$. With this choice, the integral transform (3.6) becomes

$$L(\sigma_R, \sigma_I) = \sum\!\!\!\!\!\!\int dE \, \frac{R(E)}{(E - E_0 - \sigma_R)^2 + \sigma_I^2} \,. \tag{3.9}$$

Starting from the more general transform in Eq. (3.6), if we insert directly the definition of the response function (3.5) and we perform the integral in dE, then we obtain the following result

$$L(\sigma) = \sum\!\!\!\!\!\!\int_f \langle \Psi_0 | \, \hat{\mathcal{O}}^\dagger \, | \Psi_f \rangle \, K(\sigma, E_f) \, \langle \Psi_f | \, \hat{\mathcal{O}}' \, | \Psi_0 \rangle \ , \tag{3.10}$$

where we have taken into account the presence of the energy–conserving delta function. This expression can be rewritten in the equivalent operator form

$$L(\sigma) = \sum\!\!\!\!\!\!\int_f \langle \Psi_0 | \, \hat{\mathcal{O}}^\dagger \, K(\sigma, \hat{H}) | \Psi_f \rangle \, \langle \Psi_f | \, \hat{\mathcal{O}}' \, | \Psi_0 \rangle \ . \tag{3.11}$$

At this point we exploit the closure property of the final states $|\Psi_f\rangle$, which assumes a fundamental role here. Following from Eq. (3.4), we are able to express the integral transform $L(\sigma)$ as

$$L(\sigma) = \langle \Psi_0 | \, \hat{\mathcal{O}}^\dagger \, K(\sigma, \hat{H}) \, \hat{\mathcal{O}}' \, | \Psi_0 \rangle \ . \tag{3.12}$$

If we make again the explicit choice of using a Lorentzian kernel function in the form of Eq. (3.7), it is not difficult to demonstrate that the function $L(\sigma)$ can be represented in the compact form

$$L(\sigma_R, \sigma_I) = \langle \widetilde{\Psi} | \widetilde{\Psi}' \rangle \ , \tag{3.13}$$

where $|\widetilde{\Psi}\rangle$ and $|\widetilde{\Psi}'\rangle$ are the so–called "LIT states" and their formal definition is

$$|\widetilde{\Psi}\rangle \equiv \left(\hat{H} - E_0 - \sigma_R - i\sigma_I \right)^{-1} \hat{\mathcal{O}} \, | \Psi_0 \rangle \ , \tag{3.14a}$$

$$|\widetilde{\Psi}'\rangle \equiv \left(\hat{H} - E_0 - \sigma_R - i\sigma_I \right)^{-1} \hat{\mathcal{O}}' \, | \Psi_0 \rangle \ . \tag{3.14b}$$

From the expressions above, it is straightforward that each LIT state satisfies a Schrödinger–like inhomogeneous equation

$$\left(\hat{H} - E_0 - \sigma_R - i\sigma_I \right) |\widetilde{\Psi}\rangle = \hat{\mathcal{O}} \, | \Psi_0 \rangle \ , \tag{3.15a}$$

$$\left(\hat{H} - E_0 - \sigma_R - i\sigma_I \right) |\widetilde{\Psi}'\rangle = \hat{\mathcal{O}}' \, | \Psi_0 \rangle \ , \tag{3.15b}$$

with a source term $\hat{\mathcal{O}}\,|\Psi_0\rangle$ ($\hat{\mathcal{O}}'\,|\Psi_0\rangle$) that depends on the transition operator $\hat{\mathcal{O}}$ ($\hat{\mathcal{O}}'$). The "LIT equations" above are essentially the same for all the reactions with the exception of the term on the right–hand–side, since the transition operator is characteristic of the process that we are studying.

Without loosing generality, we can consider the identity $\hat{\mathcal{O}} = \hat{\mathcal{O}}'$ and restrict the discussion to the case in which the transform (3.13) reduces to $L(\sigma_R, \sigma_I) = \langle\widetilde{\Psi}|\widetilde{\Psi}\rangle$. Since we have chosen a kernel function for which the defining integral in Eq. (3.9) does not diverge for $\sigma_I \neq 0$, the function $L(\sigma_R, \sigma_I)$ does exist. As a consequence, the norm $\langle\widetilde{\Psi}|\widetilde{\Psi}\rangle$ must be finite, and therefore the LIT states $|\widetilde{\Psi}\rangle$ result to be localized functions. This also implies that one can find unique solutions of Eq. (3.15a) by using bound–state methods. This can be achieved by employing different techniques, working either in coordinate or in momentum space. The LIT functions are therefore constructed as bound–state wave functions, whose asymptotic behaviour is not as complicated as in the continuum.

We proceed by performing an explicit separation between the discrete and the continuum spectrum of the final states. We introduce the discrete excitation energies, $e_n = E_n - E_0$, as well as the excitation energy in the continuum, $e = E - E_0$, with the relation $e_n < e_{\rm th} < e$, where $e_{\rm th}$ is the continuum threshold energy. The response function already defined in Eq. (3.5) may then be written as the sum of the following two contributions

$$R_n = \langle\Psi_0|\,\hat{\mathcal{O}}^\dagger\,|\Psi_n\rangle\,\langle\Psi_n|\,\hat{\mathcal{O}}'\,|\Psi_0\rangle\ , \tag{3.16}$$

$$R(e) = \int_{e_{\rm th}}^{\infty} dE_l\,\langle\Psi_0|\,\hat{\mathcal{O}}^\dagger\,|\Psi_l\rangle\,\langle\Psi_l|\,\hat{\mathcal{O}}'\,|\Psi_0\rangle\,\delta(E_l - E_0 - e)\,. \tag{3.17}$$

An analogue separation can be done for the integral transform. We write $L(\sigma_R, \sigma_I)$ as a sum of two terms

$$L(\sigma_R, \sigma_I) = L_d(\sigma_R, \sigma_I) + L_c(\sigma_R, \sigma_I)\,, \tag{3.18}$$

where the discrete and continuum contributions are now defined as

$$L_d(\sigma_R, \sigma_I) = \sum_n \frac{R_n}{(e_n - \sigma_R)^2 + \sigma_I^2}\,, \tag{3.19}$$

$$L_c(\sigma_R, \sigma_I) = \int_{e_{\rm th}}^{\infty} de\,\frac{R(e)}{(e - \sigma_R)^2 + \sigma_I^2}\,, \tag{3.20}$$

with the corresponding response functions R_n and $R(e)$ already defined in Eqs. (3.16) and (3.17), respectively. Essentially, our aim is to first determine $L(\sigma_R, \sigma_I) = \langle\widetilde{\Psi}|\widetilde{\Psi}\rangle$ for σ_R belonging to a certain energy range, while keeping the parameter σ_I fixed. Then, by using this calculated transform as an input, we want to obtain the terms R_n and $R(e)$. If one finds the discrete levels explicitly, i.e. $|\Psi_n\rangle$ and e_n, then R_n could be calculated directly from the overlaps (3.16). At this point, the discrete contribution to the transform, $L_d(\sigma_R, \sigma_I)$, is known and this term can be subtracted from the computed $L(\sigma_R, \sigma_I)$. As a result, we are left with the contribution $L_c(\sigma_R, \sigma_I)$ in Eq. (3.20), an integral equation that should be solved for $R(e)$. Later in this work, we will deal only with the continuum part of the integral transform and we will often refer to the function $L_c(\sigma_R, \sigma_I)$ by omitting the subscript and the σ_I dependence in the argument.

A few comments are here in order about the choice of the real positive parameters σ_R and σ_I relative to the Lorentzian kernel defined in Eq. (3.8) [27]. Due to the fact that σ_I is actually the half–width of the Lorentzian kernel function employed, a reasonable range of values for the parameter σ_R is $e_{\rm th} - \sigma_I \leq \sigma_R \leq e_{\rm max} + \sigma_I$, provided that $e_{\rm th} \leq e \leq e_{\rm max}$ is the spectrum relative to the response function. In this way the information contained in the response function $R(e)$ is fully exploited and encoded in the transform $L(\sigma_R)$. Concerning the parameter σ_I, the smaller is the width of the kernel function, the less is the "blurring" of the response function. Intuitively, for very small values of σ_I, the Lorentz function approaches the delta function, which is the ideal kernel to use, as we have already pointed out. Therefore, by following this reasoning, one would conclude that it is better to choose a very small σ_I value. This is partly true, because it is indeed preferable to do calculations with small σ_I, although this choice has some drawbacks. First of all, with $\sigma_I \to 0$ the LIT equations (3.15) approach the scattering regime, and under this condition it is more difficult to obtain the LIT states $|\tilde{\Psi}\rangle$ by using bound–state methods. Secondly, in practical implementations, the rate of converge of the transform $L(\sigma_R)$ depends on the value of σ_I. Typically, the smaller is σ_I, the later the convergence is reached. Based on this discussion, we conclude by saying that the chosen σ_I should be therefore small enough in order not to lose the information about the structure of the response function. At the same time, the computed $L(\sigma_R)$ should be fully convergent at the chosen σ_I, in order to get as good as possible results from the inversion procedure.

3.3 Procedures for practical implementation

In the last Section we have seen how the calculation of the LIT can be reduced to the evaluation of the overlap $\langle\widetilde{\Psi}|\widetilde{\Psi}'\rangle$, where the LIT states $|\widetilde{\Psi}\rangle$ and $|\widetilde{\Psi}'\rangle$ are the solutions of a Schrödinger–like equation with a source term that depends on the specific reaction. Moreover, we have deduced that these states are localized functions, and therefore they can be calculated by employing bound–state techniques. One possible strategy to proceed is to start by assuming an expansion of these LIT states over a basis of localized functions. This approach is valid even when the number of particles of the system increases, and it has been used in a large number of applications. Then, one can directly solve the LIT equations (3.15) for different values of the parameter σ_R. However, the disadvantage of this approach is that, in order to have a good reconstruction of the transform $L(\sigma_R, \sigma_I)$ at fixed σ_I, one may need a large number of σ_R values, and this corresponds to solve the LIT equations each time. In this Section we will present two better strategies to calculate $L(\sigma_R, \sigma_I)$, namely the eigenvalue method and the Lanczos method.

3.3.1 The eigenvalue method

The eigenvalue method entails the full diagonalization of the nuclear Hamiltonian represented on a basis set of localized functions. By assuming a basis with finite dimension N_Λ, the resulting eigenvectors and eigenvalues are $|\Psi_l\rangle$ and E_l, respectively, with $\hat{H}\,|\Psi_l\rangle = E_l\,|\Psi_l\rangle$, $l = 1, \ldots, N_\Lambda$. The LIT states in Eq. (3.14) can then

be expanded as

$$|\widetilde{\Psi}\rangle = \sum_{l=1}^{N_\Lambda} \frac{\langle\Psi_l|\,\hat{\mathcal{O}}\,|\Psi_0\rangle}{E_l - E_0 - \sigma_R - i\sigma_I}\,|\Psi_l\rangle\ , \tag{3.21a}$$

$$|\widetilde{\Psi}'\rangle = \sum_{l=1}^{N_\Lambda} \frac{\langle\Psi_l|\,\hat{\mathcal{O}}'\,|\Psi_0\rangle}{E_l - E_0 - \sigma_R - i\sigma_I}\,|\Psi_l\rangle\ , \tag{3.21b}$$

and, as a consequence, the overlap in Eq. (3.13) assumes the form

$$L(\sigma_R, \sigma_I) = \sum_{l=1}^{N_\Lambda} \frac{\langle\Psi_0|\,\hat{\mathcal{O}}^\dagger\,|\Psi_l\rangle\,\langle\Psi_l|\,\hat{\mathcal{O}}'\,|\Psi_0\rangle}{(E_l - E_0 - \sigma_R)^2 + \sigma_I^2}\,. \tag{3.22}$$

It is clear that the contribution to the continuum part of the integral transform, $L_c(\sigma_R, \sigma_I)$, comes from the eigenvalues such that $E_l > E_{\text{th}}$, with E_{th} defined as the energy threshold to the continuum. Then, from the inversion, the continuum part of the response function (3.17) can be recovered. When $\hat{\mathcal{O}} = \hat{\mathcal{O}}'$, which is our case of study, the LIT reduces to

$$L(\sigma_R, \sigma_I) = \sum_{l=1}^{N_\Lambda} \frac{\left|\langle\Psi_l|\,\hat{\mathcal{O}}\,|\Psi_0\rangle\right|^2}{(E_l - E_0 - \sigma_R)^2 + \sigma_I^2}\,. \tag{3.23}$$

The equation above shows that, essentially, the LIT can be reconstructed as a sum of Lorentz functions with half–width σ_I, whose center depends on each eigenvalue E_l. Moreover, this sum is weighted with the overlap factors $\left|\langle\Psi_l|\,\hat{\mathcal{O}}\,|\Psi_0\rangle\right|^2$, which depend on the transition operator $\hat{\mathcal{O}}$ [57]. We conclude the discussion about this method with a remark. The spacing between the eigenvalues E_l located above the energy threshold to the continuum depends on N_Λ, the dimension of the basis employed in the calculation. If the density of such eigenvalues is sufficiently high within the extension of the Lorentzian function, i.e. within σ_I, then the inversion procedure can be said to be reliable.

3.3.2 The Lanczos method

The Lanczos method is a procedure used to calculate the LIT, which is essentially based on the Lanczos algorithm [58]. More details about this technique can be found in Appendix B. As seen in the last Section, when we use the eigenvalue method, it is necessary to perform a full diagonalization of the nuclear Hamiltonian. This calculation can be computationally demanding, especially with an increasing number of particles, as the number of basis functions rapidly increases as well. The reformulation of the LIT method via the Lanczos algorithm seems to overcome these difficulties [59]. In fact, by applying this technique, the computational time decreases. Moreover, it allows to obtain accurate results that are in excellent agreement with the calculations carried out with other methods.

It is not difficult to demonstrate that the LIT in Eq. (3.13), with the LIT states expressed as in (3.14), can be rewritten in the following form

$$L(\sigma_R, \sigma_I) = -\frac{1}{\sigma_I}\,\text{Im}\left\{\left\langle \Psi_0 \,\middle|\, \hat{\mathcal{O}}^\dagger\,\frac{1}{-\hat{H} + z}\,\hat{\mathcal{O}} \,\middle|\, \Psi_0 \right\rangle\right\}, \tag{3.24}$$

where we have restricted the case to $\hat{\mathcal{O}} = \hat{\mathcal{O}}'$, and we have defined $z = E_0 + \sigma_R + i\sigma_I$. We start by introducing the following normalized vector

$$|\phi_0\rangle = \frac{\hat{\mathcal{O}}\,|\Psi_0\rangle}{\sqrt{\langle\Psi_0|\,\hat{\mathcal{O}}^\dagger\,\hat{\mathcal{O}}\,|\Psi_0\rangle}}\,, \tag{3.25}$$

which can be used as a pivot for the Lanczos basis of vectors $|\phi_i\rangle$, with $i = 0, \ldots, N_{\text{Lanc}}$. This yields to a new expression for the LIT

$$L(\sigma_R, \sigma_I) = -\frac{1}{\sigma_I}\,\langle\Psi_0|\,\hat{\mathcal{O}}^\dagger\,\hat{\mathcal{O}}\,|\Psi_0\rangle\,\mathrm{Im}\{x_{00}\}\,, \tag{3.26}$$

where the matrix element x_{00} is defined as

$$x_{00} = \left\{ \left\langle \phi_0 \left| \frac{1}{-\hat{H} + z} \right| \phi_0 \right\rangle \right\}. \tag{3.27}$$

In the following we will demonstrate how the calculation of the matrix element x_{00} can be reduced to the evaluation of a continued fraction written in terms of the so–called Lanczos coefficients $\{\, a_i, b_i \,\}$ (see Appendix B). The operator identity $(-\hat{H} + z)(-\hat{H} + z)^{-1} = 1$ written in matrix form on the Lanczos basis is

$$\sum_n (-\hat{H} + z)_{ij}\, x_{j0} = \delta_{i0}\,, \tag{3.28}$$

and x_{00} can be calculated by applying the Cramer's rule to this linear system [59]. Therefore the following relation is valid

$$x_{00} = \frac{\det(M_{00})}{\det(M)}\,, \tag{3.29}$$

where the matrices M and M_{00} are explicitly

$$M = \begin{pmatrix} -a_0 + z & -b_1 & 0 & \ldots \\ -b_1 & -a_1 + z & -b_2 & \ldots \\ 0 & -b_2 & -a_2 + z & \ldots \\ \vdots & \vdots & \vdots & \ddots \end{pmatrix}, \quad M_{00} = \begin{pmatrix} 1 & -b_1 & 0 & \ldots \\ 0 & -a_1 + z & -b_2 & \ldots \\ 0 & -b_2 & -a_2 + z & \ldots \\ \vdots & \vdots & \vdots & \ddots \end{pmatrix}. \tag{3.30}$$

If we proceed by defining D_i as the matrix obtained by removing the first i rows and i columns from the matrix M, then it can be demonstrated that the following recursive relation between determinants is valid [27]

$$\det(D_i) = (-a_i + z)\det(D_{i+1}) - b_{i+1}^2 \det(D_{i+2})\,. \tag{3.31}$$

As a consequence, by exploiting the following results for the determinant of the matrices D_0 and D_1

$$\det(D_0) = (-a_0 + z)\det(D_1) - b_1^2 \det(D_2)\,, \qquad \det(D_1) = \det(M_{00})\,, \tag{3.32}$$

since $D_0 = M$, x_{00} in Eq. (3.29) becomes

$$x_{00} = \frac{1}{-a_0 + z - b_1^2 \frac{\det(D_2)}{\det(D_1)}}\,. \tag{3.33}$$

At this point the recursive relation (3.31) can be repeatedly used to calculate first the determinant $\det(D_1)$, and so on. Finally, the whole procedure leads to the following expression for x_{00}

$$x_{00} = \cfrac{1}{-a_0 + z - \cfrac{b_1^2}{-a_1 + z - \cfrac{b_2^2}{-a_2 + z - \cfrac{b_3^2}{\cdots}}}} \,. \tag{3.34}$$

In this way we have completely determined the LIT in Eq. (3.26). The main advantage of using this reformulation is that the continued fraction above converges after a certain number of steps of the Lanczos algorithm, let's say $N_{\rm Lanc}$, and this number is always lower than the full dimension of the Hamiltonian matrix, i.e. $N_{\rm Lanc} \ll N_\Lambda - 1$.

3.4 Inversion of the LIT

As repeatedly stated, the last step to be done in order to recover the continuum part of the response function, Eq. (3.17), is to perform the inversion of the integral transform. As a consequence, this step is somehow crucial. The problem of inverting the LIT represents one of the so–called *ill–posed* problems, whose main mathematical aspects are thoroughly analysed in Ref. [60]. However, as also discussed in Ref. [56], the term *ill–posed* could be misleading and its origin is mainly historical. In fact there is no relation between this expression and the accuracy of the results, and the approaches used are *well–founded* instead. In the following we will expose one "standard" technique used to perform the inversion of the LIT [27].

We start by assuming that the response function can be written as a linear combination of $N_{\rm max}$ functions $\chi_n(x, \alpha_i)$ that depend on some non–linear parameters $\{\,\alpha_i\,\}$. Typically, this basis set of functions is defined in the following form

$$\chi_n(x, \alpha_i) = x^{\alpha_1} \exp\left\{-\frac{\alpha_2 x}{n}\right\}, \tag{3.35}$$

and therefore the ansatz for the response function is

$$R(e') = \sum_{n=1}^{N_{\rm max}} c_n \chi_n(e', \alpha_i) \,. \tag{3.36}$$

In the definition above we have used the variable $e' = e - e_{\rm th}$, with $e_{\rm th}$ the energy threshold to the continuum, and the coefficients c_n have to be determined. By inserting the linear combination (3.36) in the continuum part of the integral transform already defined in Eq. (3.20), we easily obtain

$$L_c(\sigma_R, \sigma_I) = \sum_{n=1}^{N_{\rm max}} c_n \widetilde{\chi}_n(\sigma_R, \sigma_I, \alpha_i) \,, \tag{3.37}$$

where the new set of functions $\widetilde{\chi}_n(\sigma_R, \sigma_I, \alpha_i)$ is formally defined as

$$\widetilde{\chi}_n(\sigma_R, \sigma_I, \alpha_i) = \int_0^\infty de' \, \frac{\chi(e', \alpha_i)}{(e' - \sigma_R)^2 + \sigma_I^2} \,. \tag{3.38}$$

For every fixed set of non–linear parameters $\{\alpha_1, \alpha_2\}$, the coefficients c_n of the expansion in Eq. (3.37) are determined by performing a least–square fit to the computed LIT $L_c(\sigma_R, \sigma_I)$. The chosen value of the parameter α_1 has to do with the energy dependence of the response function in the vicinity of the energy threshold, and therefore it is somehow constrained by the characteristics of the nuclear system and of the reaction under study. Conversely, the parameter α_2 typically varies over a wide range of values. Once the best fit has been computed for $N_{\max}$, the procedure is repeated for $N_{\max}+1$ and so on, each time increasing the dimension of the basis by one unit. This is done for a certain number of steps, until the converge of the computed response function (3.36) is achieved. We point out that the parameter $N_{\max}$ is always kept inside a range that is characterized by the stability of the results. A further increase of $N_{\max}$ outside this range would lead to an unstable result for the response function, in which random oscillations appear. Typically, it is not difficult to find the aforementioned range of stability for the resulting response function. However, it is also possible that the inversion procedure does not lead to stable results. In this case, one could try either to calculate the LIT with more accuracy or to work with a basis of functions that is more flexible [27]. For instance, when a narrow resonance structure is present in the response function, an additional function should be included in the basis set of Eq. (3.35) [61]. The new basis element could be of the form [62]

$$\chi_1(x,\alpha_i) = \frac{1}{(x-\alpha_1)^2+\alpha_2^2}\left[\left(1+e^{-1}\right)^{-1} - \left(1+e^{\frac{x-\alpha_3}{\alpha_3}}\right)^{-1}\right], \tag{3.39}$$

where an explicit resonance structure with center $E_{\rm res}$ and half–width Γ has been introduced explicitly through the non–linear parameters $\alpha_1 \equiv E_{\rm res}$ and $\alpha_2 \equiv \Gamma$. The other basis functions are now

$$\chi_n(x,\alpha_i) = x^{\alpha_4}\exp\left\{-\frac{\alpha_5 x}{n-1}\right\}, \qquad n \geq 2\,. \tag{3.40}$$

If the LIT is computed with a sufficiently small value of σ_I, then, by using this new basis of functions, the position, width, and strength of the resonance can be better determined in the inversion process.

Chapter 4

Cluster Effective Field Theory

This Chapter is devoted to the explicit derivation of the interactions between our effective degrees of freedom, neutrons and α–particles. In Section 4.1 the general form of the two–body potentials is derived within a halo/cluster EFT framework. The power counting procedure relative to each two–body system α–n and α–α is described in Section 4.2. The effective potentials are defined in momentum space as a series of contact terms parametrized by the Low Energy Constants (LECs). A momentum–regulator function is also introduced, which depends on a cut–off parameter. In this work we use an implicit renormalization procedure, by keeping the cut–off finite [63] and expressing the LECs in terms of observable quantities. In Sections 4.3 and 4.4 this procedure is shown explicitly, by focussing first on the α–n and then on the α–α system. Finally, a three–body potential is also introduced in Section 4.5.

4.1 Potentials from Effective Field Theory

We write the effective Langrangian $\mathcal{L}$ as a sum of terms

$$\mathcal{L} = \mathcal{L}_1 + \mathcal{L}_2 + \mathcal{L}_3 \,, \tag{4.1}$$

where $\mathcal{L}_1$ is the free Lagrangian, while $\mathcal{L}_2$ and $\mathcal{L}_3$ represent the two–body and three–body interaction terms, respectively. We will first focus on the term $\mathcal{L}_2$, leaving the discussion about the three–body term to Section 4.5.

If we start by considering the simple system composed of two spinless particles of one species, represented by the non–relativistic field operator ψ, then the relative low–energy theory can be described by the following effective Lagrangian [64, 65]

$$\mathcal{L}_2 = \tilde{a}_0 (\psi\psi)^\dagger (\psi\psi) + \tilde{a}_1 \left[(\psi\psi)^\dagger (\psi \overleftrightarrow{\nabla}^2 \psi) + \text{H.c.} \right] + \dots \,, \tag{4.2}$$

where $\overleftrightarrow{\nabla}$ is the Galilean invariant derivative defined as $\overleftrightarrow{\nabla} \equiv \overleftarrow{\nabla} - \overrightarrow{\nabla}$, and H.c. stands for Hermitian conjugate. In writing the term $\mathcal{L}_2$ above, the EFT "paradigm" has been followed: the most general effective Lagrangian should contain all the contact interactions constrained by the symmetries of the strong interaction at low–energies, which are Galilean invariance and the discrete symmetries of parity and time reversal. Other terms in the expansion (4.2) include operators with a different

combination of field derivatives as well as derivatives of higher order. Relativistic corrections will not be taken into account. The set $\{\,\tilde{a}_n\,\}$ in (4.2) is the set of the Low Energy Constants (LECs), which depend on the details of the short–range physics. In the literature different parametrization can be found to express these constants. Feynman rules from the Lagrangian (4.2) lead to the following interaction potential defined in momentum space [64, 66]

$$V(\boldsymbol{p},\boldsymbol{p}') = a_0 + a_1(\boldsymbol{p}^2 + \boldsymbol{p}'^2) + \dots\,, \tag{4.3}$$

where $\boldsymbol{p}$ ($\boldsymbol{p}'$) is the relative momentum between the two particles in the center–of–mass frame before (after) the interaction. Furthermore, the explicit expression of the constants $\{\,a_n\,\}$ depends on the specific parametrization adopted, and they are equal or at most proportional to the corresponding $\{\,\tilde{a}_n\,\}$ appearing in the Lagrangian (4.2). Specifically, the potential in Eq. (4.3) represents a S–wave interaction. Possible corrections as well as terms related to higher partial waves can be derived from the terms omitted in the expansion (4.2). In coordinate space, the potential $V(\boldsymbol{p},\boldsymbol{p}')$ in (4.3) corresponds to a sum of delta functions and their derivatives [67].

The approach that we have described so far, which is also characteristic of a pionless EFT involving nucleons, can be generalized to include other particles as well. Under certain energy conditions, for example, also clusters of nucleons, such as α–particles, can be considered as effective degrees of freedom. In this case, a so–called halo/cluster EFT can be constructed by following the same formalism. Since in this work we will study ^{9}Be and ^{12}C nuclei in a three–body approach and in the low–energy regime, we are interested in analysing the α–n and α–α subsystems. If now n and ψ are the non–relativistic field operators relative to the neutron and the α–particle, respectively, then the relevant low–energy α–n Lagrangian terms are [29]

$$\mathcal{L}^S_{n\alpha} = \tilde{\lambda}^S_{0,n\alpha}(\psi n)^\dagger(\psi n) + \tilde{\lambda}^S_{1,n\alpha}\left[(\psi n)^\dagger(\psi \overleftrightarrow{\nabla}^2 n) + \text{H.c.}\right] + \dots\,, \tag{4.4}$$

$$\mathcal{L}^P_{n\alpha} = \tilde{\lambda}^P_{0,n\alpha}(\psi \overleftrightarrow{\nabla} n)^\dagger(\psi \overleftrightarrow{\nabla} n) + \tilde{\lambda}^P_{1,n\alpha}\left[(\psi \overleftrightarrow{\nabla} n)^\dagger(\psi \overleftrightarrow{\nabla}^2 \overleftrightarrow{\nabla} n) + \text{H.c.}\right] + \dots\,, \tag{4.5}$$

where we have written explicitly the lowest S– and P–wave contributions, which are parametrized by the LECs $\tilde{\lambda}^S_{0,n\alpha}$, $\tilde{\lambda}^S_{1,n\alpha}$ and $\tilde{\lambda}^P_{0,n\alpha}$, $\tilde{\lambda}^P_{1,n\alpha}$, respectively. Here the left and right derivative is defined as $\overleftrightarrow{\nabla} \equiv (\overrightarrow{m}\overleftarrow{\nabla} - \overleftarrow{m}\overrightarrow{\nabla})/(\overleftarrow{m} + \overrightarrow{m})$, where $\overleftarrow{m}$ ($\overrightarrow{m}$) is the mass of the field on which $\overleftarrow{\nabla}$ ($\overrightarrow{\nabla}$) operates. For the α–α case we have

$$\mathcal{L}^S_{\alpha\alpha} = \tilde{\lambda}^S_{0,\alpha\alpha}(\psi\psi)^\dagger(\psi\psi) + \tilde{\lambda}^S_{1,\alpha\alpha}\left[(\psi\psi)^\dagger(\psi \overleftrightarrow{\nabla}^2 \psi) + \text{H.c.}\right] + \dots\,. \tag{4.6}$$

whose characteristic LECs are $\tilde{\lambda}^S_{0,\alpha\alpha}$, $\tilde{\lambda}^S_{1,\alpha\alpha}$. The term above includes only the strong component of the α–α interaction, whose long–range part is driven by the Coulomb interaction. More details about low–energy α–n and α–α theories can be found in Refs. [23, 25]. In these works the effective two–body Lagrangians are also reformulated in terms of the dimeron, an auxiliary operator field describing the two–particle state [68].

Following from Eqs. (4.4) and (4.5) or (4.6), as a generalization of the expression already given in (4.3), we write the most general non–relativistic two–body effective

potential in momentum space in the following compact form

$$V(\boldsymbol{p},\boldsymbol{p}') = \sum_{\ell=0}^{\infty}(2\ell+1)P_\ell(\hat{\boldsymbol{p}}\cdot\hat{\boldsymbol{p}}')V_\ell(p,p')\,, \tag{4.7}$$

which is valid for both α–n and α–α systems. P_ℓ is the Legendre polynomial of degree ℓ due to the partial wave expansion, for which we have the definition

$$V_\ell(p,p') = \frac{1}{2}\int d(\hat{\boldsymbol{p}}\cdot\hat{\boldsymbol{p}}')\,P_\ell(\hat{\boldsymbol{p}}\cdot\hat{\boldsymbol{p}}')V(\boldsymbol{p},\boldsymbol{p}')\,. \tag{4.8}$$

Moreover, the ℓ–component of the interaction can be written explicitly as follows

$$V_\ell(p,p') = \left[\lambda_0^{(\ell)} + \lambda_1^{(\ell)}(p^2+p'^2) + \dots\right]p^\ell p'^\ell\,. \tag{4.9}$$

Here we adopt the standard notation in which $\ell = 0$ refers to S–wave while $\ell = 1$ denotes the P–wave. In order to avoid divergences due to the contact terms, the effective potential (4.9) is regularized by introducing a momentum–regulator function $g(p)$. This function "regulates" the short–distance behaviour of the interaction by introducing a cut–off parameter Λ on the momenta. The regulator satisfies

$$g(p=0) = 1\,, \qquad\qquad g(p) \xrightarrow{p\to\infty} 0\,. \tag{4.10}$$

In this work, the following expression for the ℓ–component of the potential will be used

$$V_\ell(p,p') = \left[\sum_{i,j=0}^{1} p^{2i}\lambda_{ij}^{(\ell)}p'^{2j}\right]p^\ell p'^\ell g(p)g(p')\,, \qquad \boldsymbol{\lambda}^{(\ell)} = \begin{pmatrix}\lambda_0^{(\ell)} & \lambda_1^{(\ell)}\\ \lambda_1^{(\ell)} & 0\end{pmatrix}\,, \tag{4.11}$$

where we have also included the regulator functions. $\boldsymbol{\lambda}^{(\ell)}$ is the matrix of the LECs, which will be determined through renormalization conditions, by relating them to the Effective Range Expansion (ERE) scattering parameters [69]. By keeping the cut–off Λ finite, we will in fact perform an implicit renormalization by expressing the constants in terms of some observable quantities. In principle, in the most general case, additional higher–order two–body interaction terms with higher powers of momentum could have been included in the theory, corresponding to an upper limit for the indices i, j greater than 1. Since here, as we will see, we need to reproduce the ERE of the low–energy on–shell T–matrix up to the effective range parameter term, we only need $i, j = 0, 1$.

4.2 Power counting

Separation of scales is an essential feature required for an EFT approach. It also allows to select the relevant degrees of freedom, which is a necessary step to develop the effective theory. Here we will work in the low–energy regime, where also clusters of nucleons can be taken as elementary degrees of freedom. In this case, the high momentum scale M_{hi} can be thought of as related to the energy necessary to separate the cluster structures. M_{hi} is also considered as the breakdown scale of the theory. On the contrary, the low momentum scale M_{low} is such that

$M_{low} \ll M_{hi}$ and can be associated to the energy required to remove the effective particles, i.e. nucleons and α–particles. In this framework, observables can be expanded in a series of powers $(M_{low}/M_{hi})^{\nu}$, whose truncation introduces an error that is characterised by a power of a small ratio.

In order to give a physical meaning to the effective Lagrangian and its truncation, it is also essential to formulate a power counting scheme for each different interaction involved in the theory. As already mentioned, the LECs will be determined upon the experimental values of the scattering parameters, which appear in the low–energy ERE of the on–shell T–matrix.

α–n system

We start by considering the case of the α–n interaction. With our effective theory we want to reproduce [23]

$$T_{\ell}^{on}(k) = -\frac{2\pi}{\mu}\frac{1}{k\cot\delta_{\ell} - ik} = -\frac{2\pi}{\mu}k^{2\ell}\left[-\frac{1}{a_{\ell}} + \frac{r_{\ell}}{2}k^2 - \frac{\mathcal{P}_{\ell}}{4}k^4 + \mathcal{O}(k^6) - ik^{2\ell+1}\right]^{-1}, \tag{4.12}$$

where μ is the reduced mass of the system, k is the on–shell momentum and δ_{ℓ} is the phase–shift. By adopting for $\ell > 0$ the same notation used in the $\ell = 0$ case, a_{ℓ} is the scattering length, r_{ℓ} is the effective range and $\mathcal{P}_{\ell}$ the shape parameter. The relevant partial waves to be considered in the α–n scattering at low energies are the S–wave $S_{1/2}$, and the two P–waves $P_{3/2}$, $P_{1/2}$. The experimental scattering parameters are collected in Tab. 4.1, where we have written explicitly also the relative dimensions. At low energy, the $P_{3/2}$ partial wave exhibits a resonant behaviour. The enhancement of a partial wave of higher order between a nucleon and a cluster or between clusters is rather common in halo/cluster EFTs [22]. From physical considerations one would expect the following relevant momentum scales

$$M_{hi} = \sqrt{2\mu S_p(^4\mathrm{He})} \approx 170\,\mathrm{MeV}\,, \qquad M_{lo} = \sqrt{2\mu E_R} \approx 30\,\mathrm{MeV} \ll M_{hi}\,, \tag{4.13}$$

where $S_p(^4\mathrm{He}) = 19.81\,\mathrm{MeV}$ is the proton separation energy of ^{4}He while E_R is the resonance energy of ^{5}He, $E_R = Q_{\alpha\text{-decay}}(^5\mathrm{He}) = 0.798\,\mathrm{MeV}$ [71]. Unlike M_{hi}, the low momentum scale M_{lo} arises from a fine–tuning. This means that the parameters of the underlying theory have to combine in a specific way in order to realize this *unnatural* scenario. This can be discussed also by looking at the $P_{3/2}$ scattering

	α–n			
ℓ_j	a_{ℓ}^{exp}	$[\mathrm{fm}^{2\ell+1}]$	r_{ℓ}^{exp}	$[\mathrm{fm}^{-2\ell+1}]$
$S_{1/2}$	2.4641	fm	1.385	fm
$P_{3/2}$	−62.951	fm^3	−0.8819	fm^{-1}
$P_{1/2}$	−13.821	fm^3	−0.419	fm^{-1}

Table 4.1: Scattering observables (scattering length and effective range) related to the α–n system in the partial waves $\ell = 0$ and $\ell = 1$. The experimental values are from Ref. [70].

length. In general, the simplest case is the one in which only a single scale M_{hi} is present. This is commonly called a *natural* scenario, where the scaling of all the parameters is associated to M_{hi}, according to their mass dimension, i.e. on the basis of a naive dimensional analysis. In this case we would expect $1/a_1 \sim M_{hi}^3$, which is in contrast with the large experimental value of a_1. As a consequence, a different power counting must be adopted in order to account for the existing shallow P–wave resonance. In principle different choices can be made. One is the power counting presented by Bertulani, *et al.* in Ref. [23], in which $1/a_1 \sim M_{lo}^3$ and $r_1 \sim M_{lo}$ while the higher effective range parameters scale with M_{hi} in a natural way. Here, we adopt instead the power counting suggested in Ref. [24] by Bedaque, *et al.* which is

$$\frac{1}{a_1} \sim M_{lo}^2 M_{hi}\,, \qquad\qquad r_1 \sim M_{hi}\,. \tag{4.14}$$

The successive parameters naively depend on M_{hi} with the appropriate power. In contrast to the former, where two fine–tunings are present, the latter power counting requires only one fine–tuning, and it also supports a narrower resonance. In the framework (4.14), the first two terms in (4.12), related to the scattering length a_1 and the effective range r_1, give rise to a contribution of the same order for low momentum $k \sim M_{lo}$. As a consequence, they must be retained at Leading Order (LO) calculations. This justifies the terms of the effective potential taken into account in Eq. (4.11). Contributions due to the successive terms in (4.12) are of higher order. As an example, the shape parameter term $\mathcal{P}_1$, scaling as $\mathcal{P}_1 \sim 1/M_{hi}$, enters at Next–to–Next–to Leading Order ($\mathrm{N^2LO}$). By using the experimental values a_1^{exp} and r_1^{exp} in Tab. 4.1, from (4.14), we obtain $M_{hi} \approx 170\,\mathrm{MeV}$ and $M_{lo} \approx 30\,\mathrm{MeV}$. The remaining partial waves, $S_{1/2}$ and $P_{1/2}$, can be treated by following the naive power counting based on dimensional analysis

$$\frac{1}{a_0} \sim M_{hi}\,, \qquad r_0 \sim \frac{1}{M_{hi}}\,, \qquad \frac{1}{a_1} \sim M_{hi}^3\,, \qquad r_1 \sim M_{hi}\,. \tag{4.15}$$

Among these non–enhanced partial waves, for momenta $k \sim M_{lo}$, the main contribution is due to the a_0 term, while r_0 and a_1 enter at $\mathrm{N^2LO}$. Notice that, although formally the a_0 term enters at LO, in this work we will retain as "LO" only the enhanced $P_{3/2}$ partial wave [20, 72], treating the contributions due to the non–enhanced $S_{1/2}$ and $P_{1/2}$ partial waves as "NLO". By using the experimental values, the lowest M_{hi} obtained from (4.15) is $\approx 80\,\mathrm{MeV}$. The expansion parameter can therefore be represented by the ratio $M_{lo}/M_{hi} \approx 0.3$, which is also an estimate for the order of the errors at LO.

When a natural scenario is assumed, a perturbative approach to calculate the T–matrix is implied [64]. The description of low–energy scattering data can be improved in a systematic way by including in the effective Lagrangian additional terms with derivatives of higher order. These are in fact in correspondence with the k/M_{hi} expansion terms of the T–matrix. An EFT of this kind can only describe scattering, since possible bound–states are outside the range of validity of the expansion, their typical momenta being $\sim M_{hi}$. The situation is different when a fine–tuning of the underlying theory is present, inducing inside the theory a second scale $M_{lo} \ll M_{hi}$. For momenta $k \sim M_{lo}$ a perturbative approach is not suitable anymore, and a resummation of the diagrams is needed. In this way a real or virtual

bound–state can arise at threshold as a pole of the T–matrix. In Section 4.3, we will derive the effective α–n potentials in the partial waves $\ell = 1$ and $\ell = 0$. For the enhanced $P_{3/2}$ wave the non–perturbative treatment of both a_1 and r_1 is required, and we will proceed by solving the Lippmann–Schwinger equation. Although not necessary, we will calculate the other subleading potentials by following the same non–perturbative approach. This is due to the fact that, given the effective potentials as an input, we will calculate observables, such as binding energies and cross sections, in an *ab initio* approach by solving the Schrödinger equation, and therefore in a non–perturbative way.

α–α system

Now we focus on the α–α interaction. This deserves a different treatment, since also the Coulomb interaction between the two α–particles must be taken into account. The Coulomb–modified ERE for the low–energy on–shell matrix $T_\ell^{\rm SC}$ in the partial wave $\ell = 0$ is the following [25]

$$\begin{aligned} T_{\ell=0}^{{\rm SC},on}(k) &= -\frac{2\pi}{\mu}\frac{e^{2i\sigma_0}}{k\cot\delta_0 - ik}\,, \\ &= -\frac{2\pi}{\mu}C_\eta^2 e^{2i\sigma_0}\left[-\frac{1}{a_0} + \frac{r_0}{2}k^2 - \frac{\mathcal{P}_0}{4}k^4 + \mathcal{O}(k^6) - 2k_C H(\eta)\right]^{-1}\,, \end{aligned} \tag{4.16}$$

where σ_0 is the Coulomb phase–shift and δ_0 are the Coulomb–corrected phase–shifts. The definitions of the Sommerfeld parameter η, the Sommerfeld factor C_η, and the function $H(\eta)$ will be given later in Section 4.4. The quantity k_C is defined as $k_C = Z_\alpha^2 \alpha_{\rm em}\mu$, and therefore we have $k_C \approx 60\,\text{MeV}$. The relevant momentum scales arising from physical considerations are now

$$M_{hi} = \sqrt{2\mu S_p(^4\text{He})} \approx 270\,\text{MeV}\,, \qquad M_{lo} = \sqrt{2\mu E_R} \approx 20\,\text{MeV} \ll M_{hi}\,, \tag{4.17}$$

where μ is the reduced mass of the α–α system. $S_p(^4\text{He}) = 19.81\,\text{MeV}$ is the proton separation energy of ^{4}He and E_R is the ^{8}Be resonance energy taken as $E_R = Q_{\alpha\text{-decay}}(^8\text{Be}) = 91.8\,\text{keV}$ [73]. The lower momentum scale M_{lo} set by the ^{8}Be resonance is due to a fine–tuning mechanism of the underlying theory. Basically, the α–α interaction consists of the attractive short–range strong part and the repulsive long–range Coulomb interaction, whose interplay facilitates quantum tunnelling and sustains the extremely shallow resonance between the two α–particles. In the low–energy regime, the former can be represented by contact terms, the latter is non–perturbative in the momentum range below k_C, and the central issue is represented by the relative importance of the two contributions [25]. In fact, in addition to M_{hi} and M_{lo} also k_C is a relevant scale of the theory. The power counting is associated to the way in which the parameters scale with M_{hi} and M_{lo}. In this case we have, by following Higa *et al.* [25],

$$\frac{1}{a_0} \sim \frac{M_{lo}^3}{M_{hi}^2}\,, \qquad\qquad r_0 \sim \frac{1}{M_{hi}} \quad (M_{hi} \sim 3k_C)\,. \tag{4.18}$$

The a_0 and r_0 terms in (4.16) enters at LO. By using the relations in Eq. (4.18), the experimental values $a_0^{\rm exp}$ and $r_0^{\rm exp}$, which we have also listed in Tab. 4.2, give

	α–α			
ℓ_j	$a_\ell^{\rm exp}$	$[\mathrm{fm}^{2\ell+1}]$	$r_\ell^{\rm exp}$	$[\mathrm{fm}^{-2\ell+1}]$
S_0	-1920	fm	1.099	fm

Table 4.2: Scattering observables (scattering length and effective range) relative to the α–α system in the partial wave $\ell = 0$. The values are taken from Ref. [25], being an ERE fit of the experimental data from Table II of Ref. [74].

approximately $M_{hi} \approx 180\,\mathrm{MeV}$ and $M_{lo} \approx 20\,\mathrm{MeV}$. The expansion parameter is now $M_{lo}/M_{hi} \approx 0.1$. The LO α–α potential in the partial wave $\ell = 0$ will be derived in Section 4.4 by following a non–perturbative approach.

4.3 Two–body α–n effective potential

In order to derive the LECs of the effective potentials given in Eq. (4.11), we adopt a non–perturbative approach, and therefore our aim is to calculate the T–matrix by solving the Lippmann–Schwinger equation. Here we follow the derivation already carried out in Refs. [75, 76].

For the α–n system, interacting only through the strong force, we start from the relation $\hat{T} = \hat{V} + \hat{V}\hat{G}_0^{(+)}\hat{T}$, where $\hat{G}_0^{(+)}$ is the free Green's function. In its projected form, it reads

$$T(\boldsymbol{p},\boldsymbol{p}';E) = V(\boldsymbol{p},\boldsymbol{p}') + \int \frac{d^3\boldsymbol{q}}{(2\pi)^3} V(\boldsymbol{p},\boldsymbol{q}) \frac{1}{E - \frac{\boldsymbol{q}^2}{2\mu} + i\varepsilon} T(\boldsymbol{q},\boldsymbol{p}';E)\,. \tag{4.19}$$

This equation is derived in Appendix C [see (C.10)], where also more details about the formalism are introduced. In this Section, we will use the symbol μ to denote the reduced mass of the α–n system, i.e. $\mu = \mu_{\alpha n}$. By analogy with the expansion of the potential given in Eq. (4.7), we make the following ansatz for the T–matrix

$$T(\boldsymbol{p},\boldsymbol{p}') = \sum_{\ell=0}^{\infty} (2\ell+1) P_\ell(\hat{\boldsymbol{p}}\cdot\hat{\boldsymbol{p}}') T_\ell(p,p')\,, \tag{4.20}$$

where P_ℓ is a Legendre polynomial. The partial–wave components $T_\ell(p,p')$ are formally defined as

$$T_\ell(p,p') = \frac{1}{2}\int d(\hat{\boldsymbol{p}}\cdot\hat{\boldsymbol{p}}')\, P_\ell(\hat{\boldsymbol{p}}\cdot\hat{\boldsymbol{p}}') T(\boldsymbol{p},\boldsymbol{p}')\,, \tag{4.21}$$

and they are parametrized as follows

$$T_\ell(p,p';E) = \left[\sum_{i,j=0}^{1} p^{2i} \tau_{ij}^{(\ell)}(E) p'^{2j}\right] p^\ell p'^\ell g(p) g(p')\,, \quad \boldsymbol{\tau}^{(\ell)} = \begin{pmatrix} \tau_{00}^{(\ell)} & \tau_{01}^{(\ell)} \\ \tau_{10}^{(\ell)} & \tau_{11}^{(\ell)} \end{pmatrix}. \tag{4.22}$$

In the equation above, $\boldsymbol{\tau}^{(\ell)}$ is the matrix of the parameters $\tau_{ij}^{\ell}(E)$, and $g(p)$ is a momentum–regulator function, whose properties have been already given in (4.10). By inserting in the Lippmann–Schwinger equation (4.19) the potential in the form of

Eqs. (4.7) and (4.11) and the T–matrix as in (4.20) and (4.22), we get the following relation between the parameters $\tau_{ij}^{(\ell)}(E)$ and $\lambda_{ij}^{(\ell)}$:

$$\tau_{ij}^{(\ell)}(E) = \lambda_{ij}^{(\ell)} + \sum_{n,m=0}^{1} \lambda_{im}^{(\ell)} \int \frac{d^3\boldsymbol{q}}{(2\pi)^3} \frac{q^{2n+2m+2\ell}}{E - \frac{q^2}{2\mu} + i\varepsilon} g^2(q) \tau_{nj}^{(\ell)}(E)\,. \tag{4.23}$$

This relation can be rewritten in matrix form by making use of the 2×2 matrices of the parameters defined in Eqs. (4.11) and (4.22). Solving for $\boldsymbol{\tau}^{(\ell)}$ we obtain

$$\boldsymbol{\tau}^{(\ell)}(E) = \left[\mathbf{1} - \boldsymbol{\lambda}^{(\ell)} \boldsymbol{\phi}^{(\ell)}(E)\right]^{-1} \boldsymbol{\lambda}^{(\ell)}\,, \tag{4.24}$$

where we have also rearranged the loop integrals in (4.23) with an additional 2×2 matrix, $\boldsymbol{\phi}^{(\ell)}$, whose elements are defined as

$$\phi_{2n}^{(\ell)} = \int \frac{d^3\boldsymbol{q}}{(2\pi)^3} \frac{q^{2n+2\ell}}{E - \frac{q^2}{2\mu} + i\varepsilon} g^2(q)\,, \qquad \boldsymbol{\phi}^{(\ell)} = \begin{pmatrix} \phi_0^{(\ell)} & \phi_2^{(\ell)} \\ \phi_2^{(\ell)} & \phi_4^{(\ell)} \end{pmatrix}. \tag{4.25}$$

The formal solution of Eq. (4.24) is the following

$$\boldsymbol{\tau}^{(\ell)} = \frac{1}{\phi_0^{(\ell)}\phi_4^{(\ell)} + \frac{\lambda_0}{\lambda_1^2}\phi_0^{(\ell)} - \left(\phi_2^{(\ell)} - \frac{1}{\lambda_1}\right)^2} \begin{pmatrix} -\frac{\lambda_0}{\lambda_1^2} - \phi_4^{(\ell)} & -\frac{1}{\lambda_1} + \phi_2^{(\ell)} \\ -\frac{1}{\lambda_1} + \phi_2^{(\ell)} & -\phi_0^{(\ell)} \end{pmatrix}, \tag{4.26}$$

which allows us to write a first expression for the on–shell T–matrix $T_\ell^{\rm on}(k)$

$$\frac{k^{2\ell}}{T_\ell^{\rm on}(k)} = \frac{1}{g^2(k)} \left[\frac{\phi_0^{(\ell)}\phi_4^{(\ell)} + \frac{\lambda_0}{\lambda_1^2}\phi_0^{(\ell)} - \left(\phi_2^{(\ell)} - \frac{1}{\lambda_1}\right)^2}{-\frac{\lambda_0}{\lambda_1^2} - \phi_4^{(\ell)} + 2k^2\left(-\frac{1}{\lambda_1} + \phi_2^{(\ell)}\right) - k^4\phi_0^{(\ell)}} \right], \tag{4.27}$$

where $\boldsymbol{k}$ is the on–shell momentum, $\boldsymbol{k} = \boldsymbol{p} = \boldsymbol{p}'$, and the energy is $E = \frac{k^2}{2\mu}$. To make the notation easier, we have dropped the superscript (ℓ) relative to the LECs. Before making a direct comparison between the calculated low–energy T–matrix and its ERE, the expression (4.27) needs to be manipulated further.

The integrals in Eq. (4.25) satisfy the following recursive relation

$$\phi_{2n}^{(\ell)} = I_{2n+2\ell+1} + k^2 \phi_{2n-2}^{(\ell)}\,, \tag{4.28}$$

I_n being defined as

$$I_n = -\frac{\mu}{\pi^2} \int_0^\infty dq\, q^{n-1} g^2(q)\,. \tag{4.29}$$

The recursive relation (4.28) can be employed to rewrite the integrals $\phi_0^{(\ell)}$, $\phi_2^{(\ell)}$ and $\phi_4^{(\ell)}$ as a sum of terms

$$\phi_4^{(\ell)} = I_{2\ell+5} + k^2 I_{2\ell+3} + k^4 \phi_0^{(\ell)}\,, \tag{4.30a}$$

$$\phi_2^{(\ell)} = I_{2\ell+3} + k^2 \phi_0^{(\ell)}\,, \tag{4.30b}$$

$$\phi_0^{(\ell)} = I_{2\ell+1} + k^2 I_{2\ell-1} + \cdots + k^{2\ell} I_1 + k^{2\ell+2} \phi_{-2\ell-2}^{(\ell)}\,, \tag{4.30c}$$

where $\phi^{(\ell)}_{-2\ell-2}$ denotes

$$\phi^{(\ell)}_{-2\ell-2} = -\frac{\mu}{\pi^2}\int_0^\infty dq\,\frac{g^2(q)}{q^2-k^2-i\varepsilon}\,, \tag{4.31}$$

which does not actually depend on the value of ℓ. Finally, by using the expressions in (4.30), Eq. (4.27) can be rewritten as

$$\frac{k^{2\ell}}{T^{\rm on}_\ell(k)} = \frac{1}{g^2(k)}\left[-\phi^{(\ell)}_0 + \frac{\left(I_{2\ell+3}-\frac{1}{\lambda_1}\right)^2}{I_{2\ell+5}+\frac{\lambda_0}{\lambda_1^2}-k^2\left(I_{2\ell+3}-\frac{2}{\lambda_1}\right)}\right]. \tag{4.32}$$

We assume a cut–off dependence of the LECs that preserves renormalizability, meaning that the contribution of higher–order loops is at most equal to the tree–diagram one [75]. A natural choice is therefore $\lambda_{ij}\sim\Lambda^{-2i-2j-2\ell-1}$, from which we have the following scaling

$$\lambda_0 \sim \frac{1}{\Lambda^{2\ell+1}}\,, \qquad\qquad \lambda_1 \sim \frac{1}{\Lambda^{2\ell+3}}\,. \tag{4.33}$$

This is also consistent with a naive dimensional analysis of Eq. (4.32). At this point, an expansion of Eq. (4.32) in powers of k/Λ can be carried out, leading to

$$\frac{k^{2\ell}}{T^{\rm on}_\ell(k)} = \frac{1}{g^2(k)}\left[-\phi^{(\ell)}_0+\frac{\left(I_{2\ell+3}-\frac{1}{\lambda_1}\right)^2}{I_{2\ell+5}+\frac{\lambda_0}{\lambda_1^2}}+k^2\frac{\left(I_{2\ell+3}-\frac{1}{\lambda_1}\right)^2\left(I_{2\ell+3}-\frac{2}{\lambda_1}\right)}{\left(I_{2\ell+5}+\frac{\lambda_0}{\lambda_1^2}\right)^2}+\mathcal{O}(k^4)\right]. \tag{4.34}$$

It is useful to extract the cut–off dependence from the integrals I_n and from the LECs $\lambda_{0,1}$. We start by studying the divergence pattern of I_n, already defined in Eq. (4.29). To this purpose we introduce the following quantity

$$f_{n,m} = \frac{n}{\Lambda^n}\int_0^\infty dq\,q^{n-1}g^2(q)\,, \qquad\qquad g(q) = e^{-\left(\frac{q}{\Lambda}\right)^{2m}}\,, \tag{4.35}$$

where we have chosen to use a momentum–regulator function of Gaussian form. A regulator of this kind behaves as a sharp cut–off in the limit $m\to\infty$. In fact, we have that $g(q)\xrightarrow{m\to\infty}\theta(\Lambda-q)$, where $\theta(x)$ is the Heaviside step function. Furthermore, by looking at Eq. (4.34), it can be noticed that, in order to suppress the effect of the regulator function in the expansion up to k^2, $g(k)$ must satisfy $g(k)\sim 1-(k/\Lambda)^{2m}$ in the limit $k\to 0$, with the condition $m\geq 2$. The quantity $f_{n,m}$ in (4.35) is of natural size $\mathcal{O}(1)$, it is finite and it can be expressed in terms of the Gamma function as follows

$$f_{n,m} = \left(\frac{1}{2}\right)^{\frac{n}{2m}}\Gamma\left(\frac{n}{2m}+1\right). \tag{4.36}$$

As a consequence, we can write the integral I_n as

$$I_n = -\frac{\mu}{\pi^2}\frac{\Lambda^n}{n}f_{n,m}\,. \tag{4.37}$$

By expressing the LECs in terms of the dimensionless coefficients c_0 and c_1, we have

$$\lambda_0 = -\frac{\pi^2}{\mu}\frac{c_0}{\Lambda^{2\ell+1}}\,, \qquad\qquad \lambda_1 = -\frac{\pi^2}{\mu}\frac{c_1}{\Lambda^{2\ell+3}}\,. \tag{4.38}$$

These last three relations allows to rewrite Eq. (4.34) in the alternative form

$$\begin{aligned}\frac{k^{2\ell}}{T_\ell^{\rm on}(k)} = \frac{1}{g^2(k)}\Bigg\{ &- \phi_0^{(\ell)} - \frac{\mu}{\pi^2}\Lambda^{2\ell+1}\Bigg[\frac{\left(\dfrac{f_{2\ell+3,m}}{2\ell+3} - \dfrac{1}{c_1}\right)^2}{\dfrac{f_{2\ell+5,m}}{2\ell+5} + \dfrac{c_0}{c_1^2}} \\ &- \frac{k^2}{\Lambda^2}\frac{\left(\dfrac{f_{2\ell+3,m}}{2\ell+3} - \dfrac{1}{c_1}\right)^2\left(\dfrac{f_{2\ell+3,m}}{2\ell+3} - \dfrac{2}{c_1}\right)}{\left(\dfrac{f_{2\ell+5,m}}{2\ell+5} + \dfrac{c_0}{c_1^2}\right)^2} + \mathcal{O}\left(\frac{k^4}{\Lambda^4}\right)\Bigg]\Bigg\}\,,\end{aligned} \tag{4.39}$$

whose terms up to order $\mathcal{O}(k^2)$ can be matched directly with the following ERE [23]

$$\frac{k^{2\ell}}{T_\ell^{on}(k)} = -\frac{\mu}{2\pi}\left[-\frac{1}{a_\ell} + \frac{r_\ell}{2}k^2 + \mathcal{O}(k^4) - ik^{2\ell+1}\right]\,. \tag{4.40}$$

a_ℓ denotes the scattering "length", while r_ℓ is the effective range.

Before specializing the calculation to $\ell = 0$ and $\ell = 1$, which are the relevant partial waves involved in the α–n interaction, we remark that, by assuming $m \geq 2$, we can take $g^2(k) \sim 1$ in the expansion (4.39), if terms beyond r_ℓ are omitted in (4.40). Moreover, we write here the integral $\phi^{(\ell)}_{-2\ell-2}$, already defined in Eq. (4.31), in the form [67]

$$\phi^{(\ell)}_{-2\ell-2} = I_{\mathcal{P}} - i\frac{\mu}{2\pi k}g^2(k) \qquad I_{\mathcal{P}} = -\frac{\mu}{\pi^2}\,\mathcal{P}\int_0^\infty dq\,\frac{g^2(q)}{q^2-k^2} \tag{4.41}$$

where the term $I_{\mathcal{P}}$ contains a principal value integral denoted as $\mathcal{P}$. For later purposes, by using the definition (4.35), we also notice that $I_{\mathcal{P}}$ can be expressed as an expansion:

$$I_{\mathcal{P}} = \frac{\mu}{\pi^2}\frac{1}{\Lambda}f_{-1,m} + \mathcal{O}(k^2)\,. \tag{4.42}$$

4.3.1 P–wave interaction

In this Subsection we focus on the derivation of the LECs relative to the α–n effective potential in the partial wave $\ell = 1$. To this purpose, each term of the low–energy result derived in Eq. (4.39) must be compared with the ERE (4.40) specialized to the case $\ell = 1$:

$$\frac{k^2}{T_1^{on}(k)} = -\frac{\mu}{2\pi}\left[-\frac{1}{a_1} + \frac{r_1}{2}k^2 + \mathcal{O}(k^4) - ik^3\right]\,. \tag{4.43}$$

First, by restricting Eq. (4.30c) to the value $\ell = 1$, the term $\phi_0^{(1)}$ in (4.39) assumes the form

$$\begin{aligned}\phi_0^{(1)} &= I_3 + k^2 I_1 + k^4\phi_{-4}^{(1)} \\ &= -\frac{\mu}{\pi^2}\Lambda^3\left(\frac{f_{3,m}}{3} + \frac{k^2}{\Lambda^2}f_{1,m}\right) - i\frac{\mu}{2\pi}k^3 g^2(k) + \mathcal{O}(k^4)\,,\end{aligned} \tag{4.44}$$

where we have also used the definitions (4.37) and (4.41). Notice that the term in $\phi_0^{(1)}$ proportional to ik^3, reproduces the pole term in the expansion (4.43), and therefore they cancel out. Then, by directly matching Eq. (4.39) with (4.43) we obtain the following relations between the dimensionless coefficients c_0, c_1 and the observables a_1, r_1:

$$\frac{\mu}{2\pi a_1} = \frac{\mu}{\pi^2}\Lambda^3 \left[\frac{f_{3,m}}{3} - \frac{\left(\frac{f_{5,m}}{5} - \frac{1}{c_1}\right)^2}{\frac{f_{7,m}}{7} + \frac{c_0}{c_1^2}} \right], \tag{4.45}$$

$$\frac{\mu}{4\pi} r_1 = \frac{\mu}{\pi^2}\Lambda \left[-f_{1,m} + \frac{\left(\frac{f_{5,m}}{5} - \frac{1}{c_1}\right)^2 \left(\frac{f_{5,m}}{5} - \frac{2}{c_1}\right)}{\left(\frac{f_{7,m}}{7} + \frac{c_0}{c_1^2}\right)^2} \right]. \tag{4.46}$$

We now focus on the equation involving the effective range r_1. By making use of (4.45), it can be rewritten as

$$r_1 = -\frac{4\Lambda}{\pi} f_{1,m} + \frac{4\Lambda}{\pi}\left(\frac{f_{3,m}}{3} - \frac{\pi}{2\Lambda^3 a_1}\right)^2 \frac{5}{f_{5,m}} \left[1 - \left(c_1 \frac{f_{5,m}}{5} - 1\right)^{-2}\right]. \tag{4.47}$$

By taking the limit for high cut–off $\Lambda \to \infty$, we obtain

$$r_1 \leq \frac{4}{\pi}\left(\frac{5}{9}\frac{f_{3,m}^2}{f_{5,m}} - f_{1,m}\right)\Lambda \equiv w_1 \Lambda\,, \tag{4.48}$$

with $w_1 < 0$, which is an effective range that goes to negative infinity. Therefore, we deduce that in order to have r_1 finite, the cut–off must be kept finite as well. This is the implicit renormalization procedure. If we use for the effective range an experimental value, say $r_1^{\rm exp}$, and we take into account the sign, then Eq. (4.48) can be inverted, leading to the following maximum value for the cut–off

$$\Lambda \leq \Lambda^{\rm max} = \frac{r_1^{\rm exp}}{w_1}\,, \tag{4.49}$$

where in the limit $m \to \infty$, the constant w_1 assumes the value $w_1 = -\frac{16}{9\pi}$. This is an expression of the so–called Wigner bound [77], which is a constraint on the effective range parameter due to the range of the interaction, relying on causality and unitarity. Originally defined for $\ell = 0$, it can be generalized also to higher partial waves [78]. Given Eqs. (4.45) and (4.46), we can solve for the dimensionless quantities c_0 and c_1, obtaining

$$c_0 = c_1^2 \left[-\frac{f_{7,m}}{7} + \frac{\left(\frac{f_{5,m}}{5} - \frac{1}{c_1}\right)^2}{\frac{f_{3,m}}{3} - \frac{\pi}{2\Lambda^3 a_1}} \right], \tag{4.50}$$

$$c_1 = \frac{5}{f_{5,m}} \pm \frac{5}{f_{5,m}} \left[1 - \frac{f_{5,m}}{5} \frac{\frac{\pi r_1}{4\Lambda} + f_{1,m}}{\left(\frac{f_{3,m}}{3} - \frac{\pi}{2\Lambda^3 a_1}\right)^2} \right]^{-1/2}. \tag{4.51}$$

By imposing a reality condition on c_0 and c_1, the Wigner bound already expressed in Eq. (4.48) is recovered.

From now on, we will fix $m = 2$ for the Gaussian momentum–regulator function (4.35). By following Eq. (4.11), we write here the explicit form of the α–n P–wave effective potential

$$V_{\ell=1}(p,p') = \left[\lambda_0 + \lambda_1(p^2+p'^2)\right] p\,p'\, e^{-\left(\frac{p}{\Lambda}\right)^4} e^{-\left(\frac{p'}{\Lambda}\right)^4}\,, \tag{4.52}$$

where the LECs are related to the dimensionless coefficients c_0 and c_1 by Eqs. (4.38). Their explicit expression as a function of the scattering length, the effective range and the cut–off, i.e. $c_{0,1} = c_{0,1}(a_1, r_1, \Lambda)$, is given in Eqs. (4.50) and (4.51). Basically, they can be entirely determined by using the experimental values $a_1^{\rm exp}$ and $r_1^{\rm exp}$ and by fixing the cut–off parameter Λ, such that $\Lambda \leq \Lambda^{\rm max}$, thus allowed by the Wigner bound (4.49). The experimental values of the scattering observables used throughout this work are listed in Tab. 4.1.

By specializing the calculation to the α–n $P_{3/2}$ partial wave, we show the variation of c_0 and c_1 as a function of the cut–off Λ in Fig. 4.1a. In this case, the limit set by the Wigner bound is $\Lambda^{\rm max} \approx 330\,\text{MeV}$. In Fig. 4.1a, the superscript $(\pm)$ denotes the pairs of coefficients $c_{0,1}^{(+)}$ and $c_{0,1}^{(-)}$ corresponding to the $\pm$ solutions in Eqs. (4.50) and (4.51). In principle, both pairs are valid solutions, since they are able to reproduce the low–energy T-matrix expansion. Here we choose to use the one with most natural size, which is the minus–solution $c_{0,1}^{(-)}$, providing also a weakly attractive potential at large distance. By following Ref. [79], we can also provide another argument in support of this choice. If one looks at the equation for c_1 (4.51), being $f_{5,m=2} > 0$, then we can say that the $c_1^{(-)}$ branch is the only one that contains the zero. As a consequence, only the minus–solution would be compatible with a theory in which only the LEC λ_0 is present in the ansatz of the effective potential (4.52), i.e. with a theory in which $c_1 = 0$. This can be visualized by plotting $c_1^{(\pm)}$ as a function of r_1, as done in Fig. 4.1b, for a fixed value of the cut-off. It can be noticed that, when $\Lambda = 300\,\text{MeV}$, only the "physical" branch $c_1^{(-)}$ crosses zero at $r_1 = -1.475\,\text{fm}^{-1}$. This numerical value corresponds to $r_1 = -4 f_{1,m}\Lambda/\pi$. It can be demonstrated that this relation can be obtained by assuming a theory in which the effective potential is parametrized with only one LEC: $V_{\ell=1}(p,p') = \lambda_0\, p\,p' g(p) g(p')$, with $g(p)$ the Gaussian momentum–regulator function in (4.35) with $m = 2$. The potential $V_{\ell=1}(p,p')$ in Eq. (4.52) constructed from the solutions $c_{0,1}^{(-)}$ is plotted in Fig. 4.2 with $p' = p$, for three fixed values of the cut–off Λ. Finally, in Fig. 4.3 we show the results of the calculated low–energy α–n phase–shifts. With a cut–off $\Lambda = 90\,\text{MeV}$ the range in which the results agree with the experimental data [80] is very small. By increasing Λ, the agreement is better. When $\Lambda = 200 - 300\,\text{MeV}$ almost all the experimental data are reproduced up to laboratory energies $\approx 3\,\text{MeV}$, corresponding to a relative momentum in the center–of–mass frame of about $\approx 60\,\text{MeV}$.

The α–n interaction in the partial wave $P_{1/2}$ has the same form as the one shown in Eq. (4.52). The associated LECs can be calculated through the relative dimensionless coefficients c_0 and c_1 with the same procedure explained above. The experimental values of the scattering observables to be inserted in the relations $c_{0,1} = c_{0,1}(a_1, r_1, \Lambda)$ of Eqs. (4.50) and (4.51) are those relative to the partial wave

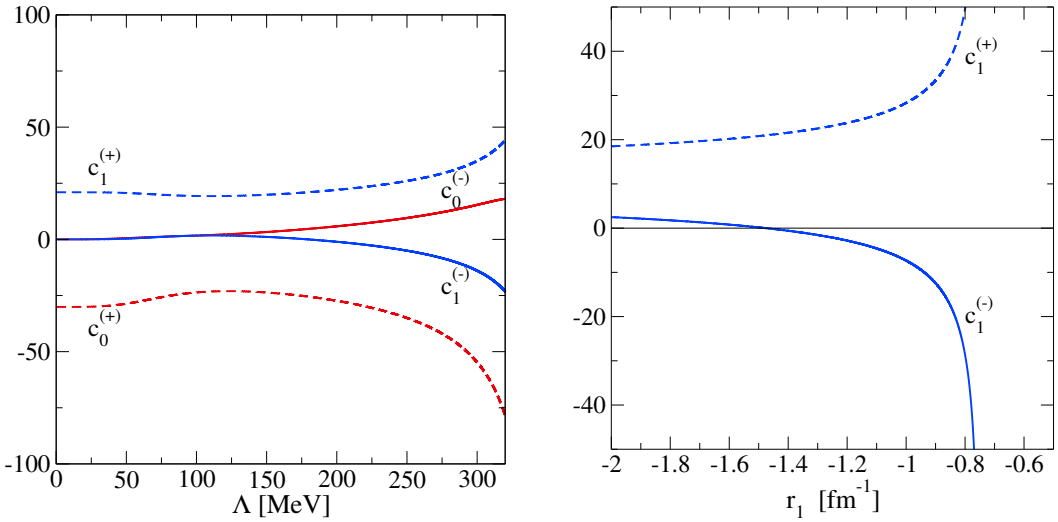

(a) (b)

Figure 4.1: (a) Dimensionless coefficients $c_{0,1}^{(+)}$ and $c_{0,1}^{(-)}$ relative to the α–n $P_{3/2}$–wave effective interaction as a function of the cut–off Λ. The superscript refers to the plus– or minus–solution of Eqs. (4.50) and (4.51). (b) Dimensionless coefficients $c_1^{(+)}$ and $c_1^{(-)}$ calculated with $\Lambda_3 = 300\,\mathrm{MeV}$ as a function of the effective range r_1. Only the $c_1^{(-)}$ branch crosses zero in the point $r_1 = -1.475\,\mathrm{fm}^{-1}$.

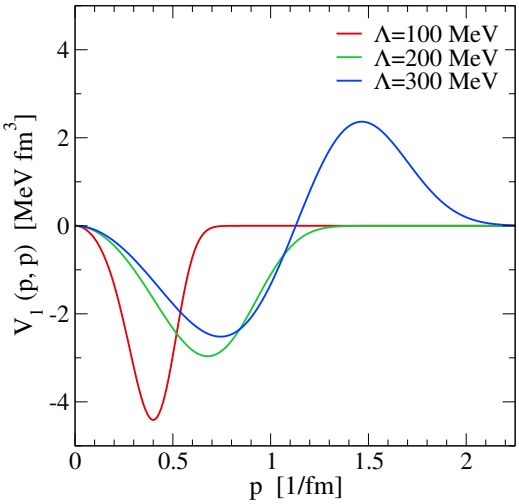

Figure 4.2: α–n effective "diagonal" potential in the partial wave $P_{3/2}$ as a function of the relative momentum p, for three different values of the cut–off parameter Λ. The parameter of the Gaussian momentum–regulator function (4.35) is fixed to $m = 2$. The LECs are calculated from the minus–solution of the dimensionless coefficients $c_{0,1}^{(-)}$.

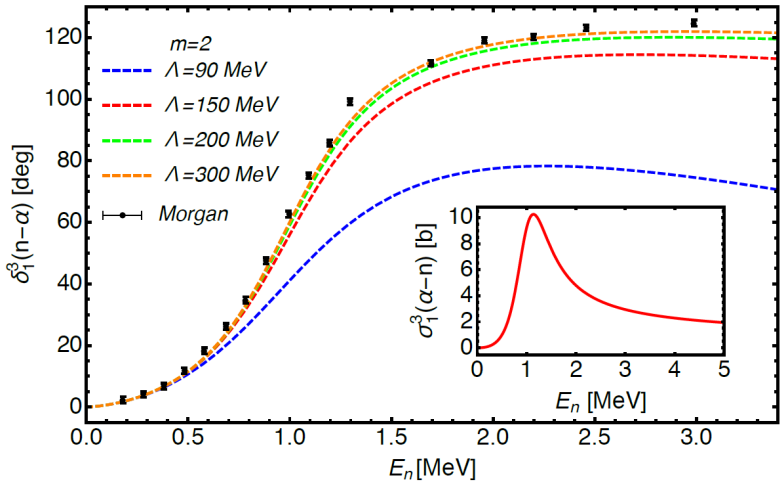

Figure 4.3: Figure taken from Ref. [76] showing the calculated α–n low–energy phase–shifts $\delta_\ell^{2j} = \delta_1^3$, relative to the partial wave $P_{3/2}$, calculated as a function of the neutron energy E_n, and for different values of the cut–off parameter Λ. The experimental data are from Ref. [80]. By fixing $\Lambda = 300\,\text{MeV}$, the cross section $\sigma_1^3(E_n)$ is calculated in the inset, where the ^{5}He resonance is visible.

$P_{1/2}$, and they are listed in Tab. 4.1. The estimated $\Lambda^{\max}$ from Eq. (4.49) results to be $\approx 150\,\text{MeV}$. However, the coefficients c_0 and c_1 satisfy the reality condition for cut–off values up to $\approx 270\,\text{MeV}$. The calculated low–energy phase–shifts are plotted in Fig. 4.5 as a function of the neutron energy in the laboratory frame, for different values of the cut–off. Already at $\Lambda = 150\,\text{MeV}$, we notice a good agreement with the experimental data [80] up to relative momenta in the center–of–mass frame $\approx 50\,\text{MeV}$.

4.3.2 S–wave interaction

Here we focus on the calculation of the LECs relative to the α–n effective potential in the partial wave $\ell = 0$, which assumes the form

$$V_{\ell=0}(p,p') = \left[\lambda_0 + \lambda_1(p^2+p'^2)\right] e^{-\left(\frac{p}{\Lambda}\right)^4} e^{-\left(\frac{p'}{\Lambda}\right)^4} . \tag{4.53}$$

As done in the $\ell = 1$ case, we start by writing an explicit expression for the term $\phi_0^{(0)}$ in Eq. (4.39). From the relations (4.30), (4.37) and (4.41), we obtain

$$\begin{aligned} \phi_0^{(0)} &= I_1 + k^2 \phi_{-2}^{(0)} \\ &= -\frac{\mu}{\pi^2}\Lambda\left(f_{1,m} - \frac{k^2}{\Lambda^2} f_{-1,m}\right) - i\frac{\mu}{2\pi} k g^2(k) + \mathcal{O}(k^4) . \end{aligned} \tag{4.54}$$

Notice that, unlike the $\ell = 1$ case, here the integral $\phi_{-2}^{(0)}$ enters at order k^2, and therefore we have also inserted the first term in the expansion of Eq. (4.42). Moreover, the term $\propto ik$ cancels out with its counterpart in the T–matrix ERE

$$\frac{1}{T_0^{on}(k)} = -\frac{\mu}{2\pi}\left[-\frac{1}{a_0} + \frac{r_0}{2}k^2 + \mathcal{O}(k^4) - ik\right] . \tag{4.55}$$

By matching the terms up to order k^2 with the corresponding ones in Eq. (4.39), we obtain, for $\ell = 0$, the following relations involving the scattering length a_0 and the effective range r_0:

$$\frac{\mu}{2\pi a_0} = \frac{\mu}{\pi^2}\Lambda\left[f_{1,m} - \frac{\left(\frac{f_{3,m}}{3} - \frac{1}{c_1}\right)^2}{\frac{f_{5,m}}{5} + \frac{c_0}{c_1^2}}\right], \tag{4.56}$$

$$\frac{\mu}{4\pi} r_0 = \frac{\mu}{\pi^2}\frac{1}{\Lambda}\left[f_{-1,m} + \frac{\left(\frac{f_{3,m}}{3} - \frac{1}{c_1}\right)^2\left(\frac{f_{3,m}}{3} - \frac{2}{c_1}\right)}{\left(\frac{f_{5,m}}{5} + \frac{c_0}{c_1^2}\right)^2}\right]. \tag{4.57}$$

Finally, solving for the dimensionless coefficients, we get the following expressions

$$c_0 = c_1^2\left[-\frac{f_{5,m}}{5} + \frac{\left(\frac{f_{3,m}}{3} - \frac{1}{c_1}\right)^2}{f_{1,m} - \frac{\pi}{2\Lambda a_0}}\right], \tag{4.58}$$

$$c_1 = \frac{3}{f_{3,m}} \pm \frac{3}{f_{3,m}}\left[1 - \frac{f_{3,m}}{3}\frac{\frac{\pi\Lambda r_0}{4} - f_{-1,m}}{\left(f_{1,m} - \frac{\pi}{2\Lambda a_0}\right)^2}\right]^{-1/2}. \tag{4.59}$$

The values assumed by the coefficients above, taking into account both the plus– and minus–solutions, are plotted in Fig. 4.4a as a function of the cut–off Λ. The Wigner bound [77] in this case can be expressed through the relation [79]

$$r_0 \leq \frac{w_0}{\Lambda}, \qquad w_0 = \frac{4}{\pi}\left(3\frac{f_{1,m}^2}{f_{3,m}} + f_{-1,m}\right), \tag{4.60}$$

with w_0 a positive–definite constant. In this case the high cut–off limit $\Lambda \to \infty$ leads to the result $r_0 \leq 0$ [67, 81], which is in contrast with the experimental data (see Tab. 4.1). By keeping Λ finite, the expression above also sets a limit on the maximum value allowed for the cut–off, which is $\approx 840\,\text{MeV}$. However, by using a_0^{exp} and r_0^{exp} in Eqs. (4.58) and (4.59), the upper bound turns out to be $\approx 540\,\text{MeV}$. Also in this case, we choose to use in the calculations the LECs obtained from the pair of solutions $c_{0,1}^{(-)}$. The corresponding effective α–n S–wave potential can be seen in Fig. 4.4b, for three different values of the cut–off Λ. Notice that a repulsive core is present only for $\Lambda = 100\,\text{MeV}$, the effective potential associated with $\Lambda = 200 - 300\,\text{MeV}$ being attractive. The calculated low–energy phase–shifts are reported in Fig. 4.5. By choosing $\Lambda = 100\,\text{MeV}$, the results are in agreement with the experimental data points [82] up to laboratory energies $\approx 1\,\text{MeV}$. However, above these values the calculated phase–shifts start to rise. Also in this case, by increasing the cut–off Λ to the values $200 - 300\,\text{MeV}$ the results are in complete agreement with all the experimental data inside the showed range of energies.

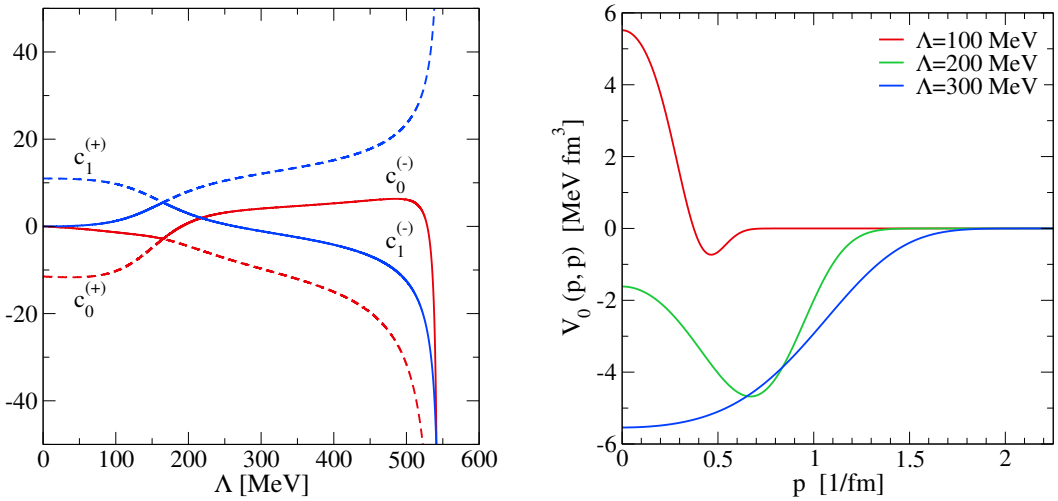

Figure 4.4: (a) Dimensionless coefficients $c_{0,1}^{(+)}$ and $c_{0,1}^{(-)}$ relative to the α–n $S_{1/2}$–wave effective interaction as a function of the cut–off Λ. The superscript refers to the plus– or minus–solution of Eqs. (4.58) and (4.59). (b) α–n effective "diagonal" potential in the partial wave $S_{1/2}$ as a function of the momentum p, for different values of the cut–off Λ. The LECs are calculated from the minus–solution of the dimensionless coefficients $c_{0,1}^{(-)}$.

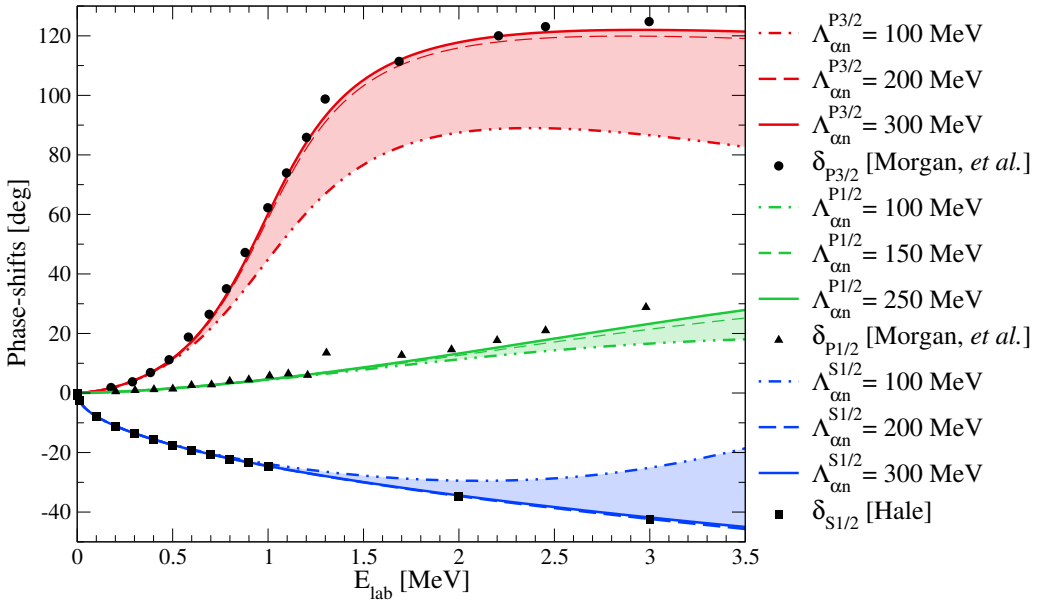

Figure 4.5: Low energy α–n phase–shifts in the partial waves $P_{3/2}$, $P_{1/2}$ and $S_{1/2}$ as a function of the neutron energy $E_{\rm lab}$ computed with the α–n effective potential for different values of the cut–off Λ. The experimental data points are taken from Refs. [80, 82].

4.4 Two–body α–α effective potential

When we study the system composed of two α–particles with electromagnetic charge Z_α, we must take into account the Coulomb force in addition to the short–range strong interaction. The derivation presented here has been already developed in Ref. [75]. By using a procedure similar to the one employed in Section 4.3, we start from the following Lippmann–Schwinger equation

$$T_{\rm SC}(\boldsymbol{p},\boldsymbol{p}';E) = \langle\psi^{(-)}_{\boldsymbol{p}}|\,V\,|\psi^{(+)}_{\boldsymbol{p}'}\rangle - 2\mu\int\frac{d^3\boldsymbol{q}}{(2\pi)^3}\,\langle\psi^{(-)}_{\boldsymbol{p}}|\,V\,|\psi^{(-)}_{\boldsymbol{q}}\rangle\,\frac{T_{\rm SC}(\boldsymbol{q},\boldsymbol{p}';E)}{\boldsymbol{q}^2-2\mu E-i\varepsilon}\,, \tag{4.61}$$

where $T_{\rm SC}(\boldsymbol{p},\boldsymbol{p}';E)$ represents the Coulomb–distorted strong term of the T–matrix, and V is the strong potential acting between the two α–particles. Here the reduced mass is defined as $\mu \equiv \mu_{\alpha\alpha}$. The states $|\psi^{(\pm)}_{\boldsymbol{p}}\rangle$ in Eq. (4.61), i.e. the Coulomb wave functions, are solutions of the Schrödinger equation $(\hat{H}-E)\,|\psi\rangle = 0$, where the Hamiltonian $\hat{H}$ is the sum of the free Hamiltonian and the Coulomb potential, $\hat{H} = \hat{H}_0 + \hat{V}_{\rm C}$. They can be formally constructed as follows

$$|\psi^{(\pm)}_{\boldsymbol{p}}\rangle = \left(1+\hat{G}^{(\pm)}_C\hat{V}_C\right)|\boldsymbol{p}\rangle\,, \tag{4.62}$$

where the Coulomb Green's function $\hat{G}^{(\pm)}_C$ is

$$\hat{G}^{(\pm)}_C(E) = \frac{1}{E-\hat{H}\pm i\varepsilon}\,. \tag{4.63}$$

More details about the formalism as well as the derivation of Eq. (4.61) can be found in Appendix C.

First we focus on the matrix elements $\langle\psi^{(-)}_{\boldsymbol{p}}|\,V\,|\psi^{(\pm)}_{\boldsymbol{p}'}\rangle$. In our case, the strong potential V is the α–α effective interaction taken in the form of Eqs. (4.7) and (4.11) for the partial wave $\ell = 0$, which reads

$$V_{\ell=0}(p,p') = \left[\sum_{i,j=0}^{1} p^{2i}\lambda_{ij}p'^{2j}\right]g(p)g(p')\,, \tag{4.64}$$

$g(p)$ being a momentum–regulator function. Throughout this Section, we will use a regulator in the Gaussian form $g(q) = e^{-\left(\frac{q}{\Lambda}\right)^{2m}}$, with $m = 1$. When we consider the S–wave Coulomb functions, the solutions denoted with $(\pm)$ differ by the phase factor $e^{\pm i\sigma_0}$ [see Eq. (C.20) and Ref. [83]]. This property allows us to write, for the $\ell = 0$ case,

$$\langle\psi^{(-)}_{\boldsymbol{p}}|\,V\,|\psi^{(+)}_{\boldsymbol{p}'}\rangle = e^{2i\sigma_0(p)}\,\langle\psi^{(+)}_{\boldsymbol{p}}|\,V\,|\psi^{(+)}_{\boldsymbol{p}'}\rangle\,, \tag{4.65a}$$

$$\langle\psi^{(-)}_{\boldsymbol{p}}|\,V\,|\psi^{(-)}_{\boldsymbol{p}'}\rangle = e^{2i\sigma_0(p)}\,\langle\psi^{(+)}_{\boldsymbol{p}}|\,V\,|\psi^{(+)}_{\boldsymbol{p}'}\rangle\,e^{-2i\sigma_0(p')}\,, \tag{4.65b}$$

In the relations above, $\sigma_0 = \sigma_0(p)$ is the Coulomb phase–shift. From the general definition (C.18), it can be written as

$$e^{2i\sigma_0} = \frac{\Gamma(1+i\eta)}{\Gamma(1-i\eta)}\,, \tag{4.66}$$

where $\eta = \eta(p)$ is the Sommerfeld parameter

$$\eta = Z_\alpha^2 \frac{\alpha_{\rm em}\mu}{p}\,, \tag{4.67}$$

and $\alpha_{\rm em} = \frac{e^2}{4\pi}$ is the fine–structure constant. In the present calculation, we use the Coulomb scattering wave functions $\psi_{\boldsymbol{p}}^{(+)}(\boldsymbol{q})$ defined in momentum space and in the partial wave representation [84]

$$\psi_{\boldsymbol{p}}^{(+)}(\boldsymbol{q}) = \sum_{\ell=0}^{\infty}(2\ell+1)P_\ell(\hat{\boldsymbol{q}}\cdot\hat{\boldsymbol{p}})\psi_{p,\ell}^{(+)}(q)\,. \tag{4.68}$$

The ℓ–component is expressed through the Legendre polynomials $P_\ell(\hat{\boldsymbol{q}}\cdot\hat{\boldsymbol{p}})$ as follows

$$\psi_{p,\ell}^{(+)}(q) = \frac{1}{2}\int d(\hat{\boldsymbol{q}}\cdot\hat{\boldsymbol{p}})\, P_\ell(\hat{\boldsymbol{q}}\cdot\hat{\boldsymbol{p}})\psi_{\boldsymbol{p}}^{(+)}(\boldsymbol{q})\,. \tag{4.69}$$

Moreover, it can be written in the following general form

$$\psi_{p,\ell}^{(+)}(q) = -\frac{2\pi e^{\frac{\pi\eta}{2}}}{qp}\lim_{\gamma\to 0^+}\frac{d}{d\gamma}\left\{\left[\frac{q^2-(p+i\gamma)^2}{2qp}\right]^{i\eta}(\zeta^2-1)^{-\frac{i\eta}{2}}\,Q_\ell^{i\eta}(\zeta)\right\}\,, \tag{4.70}$$

where $\zeta = \frac{q^2+p^2+\gamma^2}{2qp}$, and the functions $Q_\ell^{i\eta}(\zeta)$ are associated Legendre functions of second kind. Following Ref. [84], after some steps, the Coulomb wave functions for the partial wave $\ell = 0$ reduce to

$$\psi_{p,\ell=0}^{(+)}(q) = -\frac{4\pi}{q}e^{i\sigma_0(p)}C_{\eta(p)}\frac{1}{q^2-p^2}\lim_{\gamma\to 0^+}{\rm Im}\left\{\left(\frac{q+p}{q-p+i\gamma}\right)^{i\eta}\right\}\,, \tag{4.71}$$

where the Sommerfeld factor $C_\eta = C_{\eta(p)}$ has been introduced. Its definition is given by

$$C_\eta^2 = \frac{2\pi\eta}{e^{2\pi\eta}-1}\,. \tag{4.72}$$

The expression of the S–wave effective potential in Eq. (4.64) and the functions (4.71) can be used to rewrite the matrix element on the r.h.s of Eqs. (4.65), obtaining

$$\langle\psi_{p,0}^{(+)}|\,V_{\ell=0}\,|\psi_{p',0}^{(+)}\rangle = \sum_{i,j=0}^{1}X_{2i}^*(p)\lambda_{ij}X_{2j}(p')\,. \tag{4.73}$$

In the equation above, λ_{ij} are the LECs relative to the contact interaction, while the integrals $X_{2i}(p)$ are defined as follows

$$X_{2i}(p) = \frac{1}{2\pi^2}\int dq\, q^{2i+2}g(q)\psi_{p,0}^{(+)}(q)\,. \tag{4.74}$$

Since both indices i, j assume the values 0 or 1, explicitly we can have

$$X_0(p) = \gamma_0(p)e^{i\sigma_0(p)}C_{\eta(p)}\,, \tag{4.75a}$$

$$X_2(p) = [-\gamma_1(p)+\gamma_2(p)]e^{i\sigma_0(p)}C_{\eta(p)}\,, \tag{4.75b}$$

where we have introduced the following set of definitions for $\gamma_0(p)$, $\gamma_1(p)$ and $\gamma_2(p)$:

$$\gamma_0(p) = \frac{2}{\pi}\int dq\,\frac{q}{p^2-q^2}\,g(q)\lim_{\gamma\to 0^+}\mathrm{Im}\left\{\left(\frac{q+p}{q-p+i\gamma}\right)^{i\eta}\right\}, \tag{4.76a}$$

$$\gamma_1(p) = \frac{2}{\pi}\int dq\,q\,g(q)\lim_{\gamma\to 0^+}\mathrm{Im}\left\{\left(\frac{q+p}{q-p+i\gamma}\right)^{i\eta}\right\}, \tag{4.76b}$$

$$\gamma_2(p) = p^2\gamma_0(p)\,. \tag{4.76c}$$

The factor $e^{i\sigma_0(p)}C_{\eta(p)}$ in Eqs. (4.75) will often appear in our calculations, and therefore it is convenient to use the rescaled quantities

$$\widetilde{X}_{2i}(p) = \frac{X_{2i}(p)}{e^{i\sigma_0(p)}C_{\eta(p)}}\,. \tag{4.77}$$

We now make the following ansatz for the $\ell = 0$ component of the Coulomb–corrected T–matrix element:

$$T^{\mathrm{SC}}_{\ell=0}(p,p';E) = e^{i\sigma_0(p)}C_{\eta(p)}\left[\sum_{i,j=0}^{2}\gamma_i(p)\tau_{ij}(E)\gamma_j(p')\right]e^{i\sigma_0(p')}C_{\eta(p')}\,, \tag{4.78}$$

where $\gamma_i(p)$, $i = 0,1,2$, is the set of integrals already given in (4.76). The rescaled Coulomb–corrected T–matrix is

$$\widetilde{T}^{\mathrm{SC}}_{\ell=0}(p,p';E) = \sum_{i,j=0}^{2}\gamma_i(p)\tau_{ij}(E)\gamma_j(p')\,. \tag{4.79}$$

At this point we are able to rewrite the Lippmann–Schwinger equation (4.61) by making explicitly use of the relations in (4.65), (4.73) and (4.74). In terms of the rescaled quantities in Eqs. (4.77) and (4.79), we obtain

$$\begin{aligned}\widetilde{T}^{\mathrm{SC}}_{\ell=0}(p,p';E) = &\left[\sum_{i,j=0}^{1}\widetilde{X}^{*}_{2i}(p)\lambda_{ij}\widetilde{X}_{2j}(p')\right]\\ &-2\mu\int\frac{d^3\boldsymbol{q}}{(2\pi)^3}\left[\sum_{i,j=0}^{1}\widetilde{X}^{*}_{2i}(p)\lambda_{ij}\widetilde{X}_{2j}(q)\right]C^2_{\eta(q)}\frac{\widetilde{T}^{\mathrm{SC}}_{\ell=0}(q,p';E)}{\boldsymbol{q}^2-2\mu E-i\varepsilon}\,.\end{aligned} \tag{4.80}$$

By analogy with what done in the α–n case, we employ also here a matrix formalism. In order to solve Eq. (4.80) for the coefficients τ_{ij} relative to the matrix $\widetilde{T}^{\mathrm{SC}}_{\ell=0}$, we use the relation

$$\boldsymbol{T} = (\mathbf{1}-\boldsymbol{\Lambda}\boldsymbol{\Phi})^{-1}\boldsymbol{\Lambda}\,, \tag{4.81}$$

in which all the matrices have dimension 3×3. The matrix $\mathbf{T}$ is explicitly $\mathbf{T} = [\tau_{ij}(E)]$, while $\boldsymbol{\Phi} = [\Phi_{ij}(E))]$ is the matrix of the integrals

$$\Phi_{ij}(E) = -\frac{\mu}{\pi^2}\int dq\,q^2\gamma_i(q)\frac{C^2_{\eta(q)}}{q^2-2\mu E-i\varepsilon}\gamma_j(q) \equiv -\frac{\mu}{\pi^2}\widetilde{\Phi}_{ij}\,. \tag{4.82}$$

Moreover, $\mathbf{\Lambda}$ contains the LECs of the two–body effective potential

$$\mathbf{\Lambda} = \begin{pmatrix} \lambda_0 & -\lambda_1 & \lambda_1 \\ -\lambda_1 & 0 & 0 \\ \lambda_1 & 0 & 0 \end{pmatrix} \equiv -\frac{\pi^2}{\mu} \begin{pmatrix} \widetilde{\lambda}_0 & -\widetilde{\lambda}_1 & \widetilde{\lambda}_1 \\ -\widetilde{\lambda}_1 & 0 & 0 \\ \widetilde{\lambda}_1 & 0 & 0 \end{pmatrix} . \tag{4.83}$$

If $\boldsymbol{k}$ is the on–shell momentum, i.e. $\boldsymbol{p} = \boldsymbol{p}' = \boldsymbol{k}$, and therefore $2\mu E = k^2$, then each coefficient $\tau_{ij}(k)$ can be expressed in terms of the quantities $\widetilde{\lambda}_{0,1}$ and $\widetilde{\Phi}_{ij}(k)$ defined in Eqs. (4.83) and (4.82), respectively. We remark that in deriving $\widetilde{\Phi}_{ij}(k)$, when one of the two indices is equal to 2, the integral can be related to $\widetilde{\Phi}_{00}(k)$ as follows

$$\widetilde{\Phi}_{02} = I_3 + k^2 \widetilde{\Phi}_{00} \,, \tag{4.84a}$$

$$\widetilde{\Phi}_{12} = J_3 + k^2 \widetilde{\Phi}_{00} \,, \tag{4.84b}$$

$$\widetilde{\Phi}_{22} = I_5 + k^2 I_3 + k^4 \widetilde{\Phi}_{00} \,, \tag{4.84c}$$

where I_{2n+1} and J_{2n+1} have been defined as

$$I_{2n+1} = \int_0^\infty dq\, q^{2n} C^2_{\eta(q)} \gamma_0^2(q) \,, \tag{4.85}$$

$$J_{2n+1} = \int_0^\infty dq\, q^{2n} C^2_{\eta(q)} \gamma_0(q) \gamma_1(q) \,. \tag{4.86}$$

The complete calculation is omitted here, and we give only the final result for the on–shell Coulomb–corrected strong T–matrix in the partial wave $\ell = 0$:

$$\frac{1}{\widetilde{T}^{\rm SC}_{\ell=0}(k)} = -\frac{\mu}{\pi^2} \frac{1}{\gamma_0^2(k)} \left[-\widetilde{\Phi}_{00} + \frac{\widetilde{\lambda}_1^2 \left(\dfrac{1}{\widetilde{\lambda}_1} - I_3 + \widetilde{\Phi}_{01} - \dfrac{\gamma_1(k)}{\gamma_0(k)} \widetilde{\Phi}_{00} \right)^2}{\mathcal{U}(k)} \right] . \tag{4.87}$$

The symbol $\mathcal{U}(k)$ has been used to denote the quantity

$$\begin{aligned} \mathcal{U}(k) = \widetilde{\lambda}_1^2 \Bigg[& I_5 - 2J_3 + \frac{\widetilde{\lambda}_0}{\widetilde{\lambda}_1^2} + 2\frac{\gamma_1(k)}{\gamma_0(k)} \left(-\frac{1}{\widetilde{\lambda}_1} + I_3 - \widetilde{\Phi}_{01} + \frac{\gamma_1(k)}{\gamma_0(k)} \widetilde{\Phi}_{00} \right) \\ & + \left(\widetilde{\Phi}_{11} - \frac{\gamma_1^2(k)}{\gamma_0^2(k)} \widetilde{\Phi}_{00} \right) - k^2 \left(I_3 - \frac{2}{\widetilde{\lambda}_1} \right) \Bigg] . \end{aligned} \tag{4.88}$$

In order to easily match each term of $1/\widetilde{T}^{\rm SC}_{\ell=0}(k)$ with the ERE modified by the presence of the Coulomb potential, we need to work further on Eq. (4.87). We start by assuming that the functions $\gamma_i(k)$, with $i = 0, 1, 2$, already defined in Eq. (4.76), have the following form

$$\gamma_0(k) \approx \gamma_0(0) e^{\theta_0 \frac{k^2}{\Lambda^2}} \approx \gamma_0(0) \left(1 + \theta_0 \frac{k^2}{\Lambda^2} \right) , \tag{4.89a}$$

$$\gamma_1(k) \approx \gamma_1(0) e^{\theta_1 \frac{k^2}{\Lambda^2}} \approx \gamma_1(0) \left(1 + \theta_1 \frac{k^2}{\Lambda^2} \right) . \tag{4.89b}$$

In this way the terms in Eq. (4.87) containing Φ_{ij} can be expressed as expansions in powers of the on–shell momentum k

$$\widetilde{\Phi}_{01} - \frac{\gamma_1(k)}{\gamma_0(k)}\widetilde{\Phi}_{00} = u_1 + k^2\left(u_{-1} - \frac{\gamma_1(0)}{\gamma_0(0)}\frac{\theta_1-\theta_0}{\Lambda^2}I_1\right), \tag{4.90a}$$

$$\widetilde{\Phi}_{11} - \frac{\gamma_1^2(k)}{\gamma_0^2(k)}\widetilde{\Phi}_{00} = s_1 + k^2\left(s_{-1} - 2\frac{\gamma_1^2(0)}{\gamma_0^2(0)}\frac{\theta_1-\theta_0}{\Lambda^2}I_1\right), \tag{4.90b}$$

with I_{2n+1} given in Eq. (4.85), and with the following definitions for u_n and s_n

$$u_n = \int_0^\infty dq\, q^{n-1}\left[\frac{\gamma_1(q)}{\gamma_0(q)} - \frac{\gamma_1(0)}{\gamma_0(0)}\right]C^2_{\eta(q)}\gamma_0^2(q)\,, \tag{4.91}$$

$$s_n = \int_0^\infty dq\, q^{n-1}\left[\frac{\gamma_1^2(q)}{\gamma_0^2(q)} - \frac{\gamma_1^2(0)}{\gamma_0^2(0)}\right]C^2_{\eta(q)}\gamma_0^2(q)\,. \tag{4.92}$$

Moreover, the explicit expression of the integral $\widetilde{\Phi}_{00}$ is

$$\widetilde{\Phi}_{00} = I_1 + k^2 g_{-1} + k^2\gamma_0^2(k)\int_0^\infty dq\,\frac{C^2_{\eta(q)}}{q^2-k^2}\,. \tag{4.93}$$

In the equation above g_{-1} is defined as

$$g_n = \int_0^\infty dq\, q^{n-1}[\gamma_0^2(q) - \gamma_0^2(0)]C^2_{\eta(q)}\,, \tag{4.94}$$

and the integral in last term can be expressed by means of the function $H(\eta)$:

$$\int_0^\infty dq\,\frac{C^2_{\eta(q)}}{q^2-k^2} = \frac{\pi}{k^2}k_C H(\eta)\,. \tag{4.95}$$

$H(\eta)$ is commonly defined in terms of the digamma function $\psi(z)$, i.e. the logarithmic derivative of the Gamma function, as $H(\eta) = \psi(i\eta) + \frac{1}{2i\eta} - \ln(i\eta)$ [83]. Moreover, the definition of k_C is $k_C = Z_\alpha^2\alpha_{\rm em}\mu = k\eta(k)$. The combination $k_C H(\eta)$ is an expression that also appears in the Coulomb–modified ERE of the T–matrix. At this point, by using the expansions introduced in Eqs. (4.89) and (4.90) we can rewrite (4.87) as follows

$$\frac{1}{\widetilde{T}^{\rm SC}_{\ell=0}(k)} = -\frac{\mu}{\pi^2}\frac{1}{\gamma_0^2(k)}\left[-I_1 - k^2 g_{-1} + \frac{(\mathcal{A}-k^2\mathcal{B})^2}{\mathcal{C}-k^2\mathcal{D}}\right] + \frac{\mu}{\pi}k_C H(\eta) \tag{4.96}$$

where, to simplify the notation, we have introduced the quantities $\mathcal{A}$, $\mathcal{B}$, $\mathcal{C}$ and $\mathcal{D}$:

$$\mathcal{A} = -\frac{1}{\widetilde{\lambda}_1} + I_3 - u_1\,, \tag{4.97}$$

$$\mathcal{B} = u_{-1} - \frac{\gamma_1(0)}{\gamma_0(0)}\frac{\theta_1-\theta_0}{\Lambda^2}I_1\,, \tag{4.98}$$

$$\mathcal{C} = \frac{\widetilde{\lambda}_0}{\widetilde{\lambda}_1^2} + I_5 - 2J_3 + s_1 + 2\frac{\gamma_1(0)}{\gamma_0(0)}\mathcal{A}\,, \tag{4.99}$$

$$\mathcal{D} = 2\left(1 - \frac{\gamma_1(0)}{\gamma_0(0)}\frac{\theta_1-\theta_0}{\Lambda^2}\right)\mathcal{A} - I_3 + 2u_1 + 2\frac{\gamma_1(0)}{\gamma_0(0)}u_{-1} - s_{-1}\,. \tag{4.100}$$

Finally, an EFT expansion of Eq. (4.96) leads to the expression

$$\frac{1}{\widetilde{T}^{\mathrm{SC}}_{\ell=0}(k)} = -\frac{\mu}{\pi^2}\frac{1}{\gamma_0^2(0)}\Bigg\{ -I_1 + \frac{\mathcal{A}^2}{\mathcal{C}} - k^2\left[g_{-1} + 2\frac{\mathcal{A}\mathcal{B}}{\mathcal{C}} - \frac{\mathcal{A}^2\mathcal{D}}{\mathcal{C}^2} + 2\frac{\theta_0}{\Lambda^2}\left(-I_1 + \frac{\mathcal{A}^2}{\mathcal{C}}\right)\right] + \mathcal{O}(k^4)\Bigg\} + \frac{\mu}{\pi}k_C H(\eta)\,, \tag{4.101}$$

with which we can perform a direct match with the following Coulomb–modified ERE [25, 83] up to terms $\propto k^2$

$$\frac{1}{\widetilde{T}^{\mathrm{SC}}_{\ell=0}(k)} = -\frac{\mu}{2\pi}\left[-\frac{1}{a_0} + \frac{r_0}{2}k^2 + \mathcal{O}(k^4) - 2k_C H(\eta)\right]. \tag{4.102}$$

The implicit relations obtained between the LECs $\widetilde{\lambda}_0$, $\widetilde{\lambda}_1$ and the observable scattering parameters a_0, r_0 are the following:

$$-\frac{\pi}{2a_0}\gamma^2(0) = \frac{\mathcal{A}^2}{\mathcal{C}} - I_1\,, \tag{4.103}$$

$$-\frac{\pi r_0}{4}\gamma^2(0) = g_{-1} + 2\frac{\mathcal{A}\mathcal{B}}{\mathcal{C}} - \frac{\mathcal{A}^2\mathcal{D}}{\mathcal{C}^2} + 2\frac{\theta_0}{\Lambda^2}\left(\frac{\mathcal{A}^2}{\mathcal{C}} - I_1\right). \tag{4.104}$$

We conclude this Section by briefly describing the procedure adopted to fully determine $\widetilde{\lambda}_0$ and $\widetilde{\lambda}_1$. First we notice that the equation for the effective range (4.104) can be rewritten in terms of a_0 and $\mathcal{A}$ as follows

$$\begin{aligned} &\mathcal{A}^2\left[g_{-1} + \frac{\pi}{4}\gamma_0^2(0)\left(r_0 - \frac{4\theta_0}{a_0\Lambda^2}\right)\right] + \\ &+2\mathcal{A}\left(I_1 - \frac{\pi}{2a_0}\gamma^2(0)\right)\left[u_{-1} - I_1 + \frac{\pi}{2a_0}\gamma^2(0)\left(1 - \frac{\gamma_1(0)}{\gamma_0(0)}\frac{\theta_1 - \theta_0}{\Lambda^2}\right)\right] + \\ &-\left(I_1 - \frac{\pi}{2a_0}\gamma^2(0)\right)^2\left(-I_3 + 2u_1 - s_{-1} + 2\frac{\gamma_1(0)}{\gamma_0(0)}u_{-1}\right) = 0 \end{aligned} \tag{4.105}$$

This equation is quadratic in $\mathcal{A}$, and therefore, by inserting the experimental values of the scattering parameters a_0^{exp}, r_0^{exp}, we obtain a pair of solutions for $\mathcal{A}$, say $\mathcal{A}^{(\pm)}$. With these two solutions, we can calculate $\widetilde{\lambda}_1$ directly from Eq. (4.97):

$$\widetilde{\lambda}_1 = \frac{1}{I_3 - u_1 - \mathcal{A}}\,. \tag{4.106}$$

At this point, the calculation of $\widetilde{\lambda}_0$ is rather straightforward: by using (4.99), the equation for the scattering length (4.103) leads to

$$\widetilde{\lambda}_0 = \widetilde{\lambda}_1^2\left[-I_5 + 2J_3 - s_1 - 2\frac{\gamma_1(0)}{\gamma_0(0)}\mathcal{A} + \left(I_1 - \frac{\pi}{2a_0}\gamma_0^2(0)\right)^{-1}\mathcal{A}^2\right]. \tag{4.107}$$

By inserting a_0^{exp}, since $\widetilde{\lambda}_1$ and $\mathcal{A}$ are known, the r.h.s. is completely determined.

In this work we use the experimental values of the scattering parameters listed in Tab. 4.2. The calculated values of the LECs λ_0 and λ_1 are plotted in Fig. 4.6a

as a function of the cut–off Λ, where we have taken into account both plus– and minus–solutions of Eq. (4.105). The resulting α–α two–body effective "diagonal" potential is shown in Fig. 4.6b, for two values of the cut–off, $\Lambda = 100\,\text{MeV}$ and $\Lambda = 190\,\text{MeV}$. These potentials have been calculated by using Eq. (4.64) and the pair of coefficients $\lambda_{0,1}^{(-)}$, the one of most natural size, which will be used throughout this work, as also done in Ref. [29]. The low–energy phase–shifts calculated by using the α–α effective potential are represented in Fig. 4.7, as a function of the laboratory energy and for different values of the cut–off Λ. Due to the Wigner bound [77], the maximum value allowed for Λ is $\approx 230\,\text{MeV}$. By inspecting Fig. 4.7, it can be noted that the phase–shifts reproduced by the effective potential with $\Lambda = 100\,\text{MeV}$ or $\Lambda = 190 - 210\,\text{MeV}$ are in close agreement with the experimental data [74] up to laboratory energies $E_{\text{lab}} \approx 12\,\text{MeV}$, corresponding to a quite large center–of–mass relative momentum $\approx 150\,\text{MeV}$. In Fig. 4.7 a close up of the same phase–shifts is given, showing better the agreement up to energies corresponding to a relative momentum $\approx 80\,\text{MeV}$. Finally, in Fig. 4.8, by fixing the cut–off at $\Lambda = 100\,\text{MeV}$, we show a comparison of our results with the work by Higa, *et al.* [25], where a different approach has been used in the calculation involving an expansion up to NLO in k/k_C, with $k_C \approx 60\,\text{MeV}$. However, in comparison with their LO calculation, which is based on a_0 and r_0, our results align more closely with the experimental data.

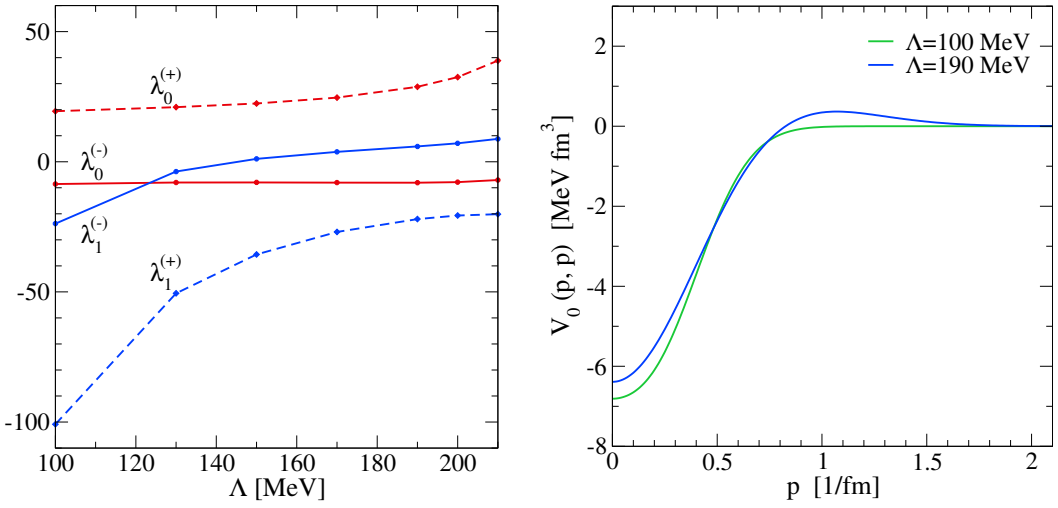

(a) (b)

Figure 4.6: (a) LECs $\lambda_{0,1}^{(+)}$ and $\lambda_{0,1}^{(-)}$ relative to the α–α effective interaction in the partial wave $\ell = 0$ as a function of the cut–off Λ. The superscript refers to the plus– or minus–solution of Eq. (4.105). (b) α–α effective "diagonal" S–wave potential as a function of the relative momentum p, for two different values of the cut–off Λ. It is calculated by using the minus–solution LECs $\lambda_{0,1}^{(-)}$.

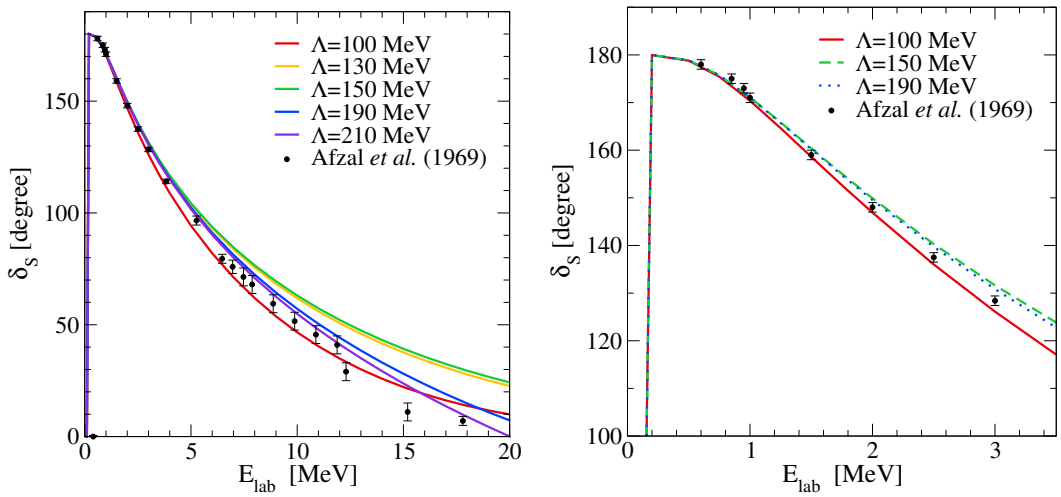

Figure 4.7: α–α phase–shifts in the partial wave $\ell = 0$ as a function of the laboratory energy $E_{\rm lab}$ calculated by using the α–α effective potential for different values of the cut–off Λ (a), and the same low–energy phase–shifts calculated in the energy range up to 3.5 MeV for $\Lambda = 100, 150, 190$ MeV (b). The experimental points are taken from Ref. [74].

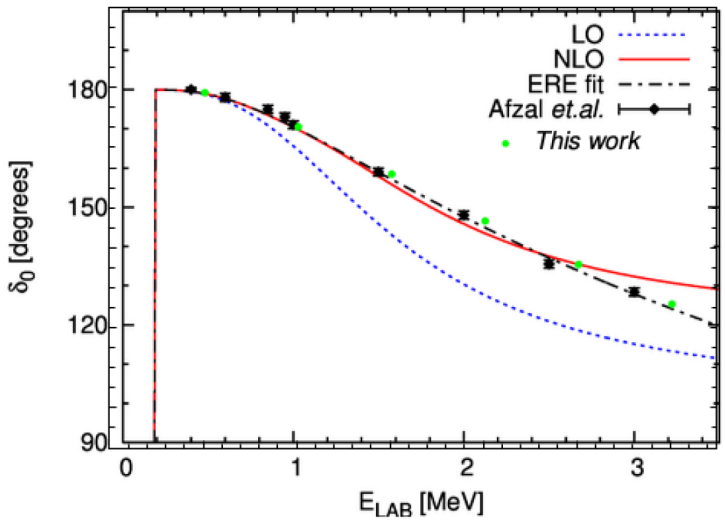

Figure 4.8: Figure taken from Ref. [85] showing the α–α scattering phase–shifts δ_0 ($\ell = 0$) calculated by using the α–α effective potential with fixed cut–off $\Lambda = 100$ MeV, in comparison with the experimental data from Ref. [74] and with another Halo EFT calculation [25] at Leading Order (LO) and Next–to–Leading Order (NLO). The fit to the experimental data (ERE fit) is also shown.

4.5 Three–body potential

The EFTs constructed in this Chapter are capable of reproducing the T–matrix ERE relative to the two–body α–n and α–α systems. However, since we are dealing here with effective three–body nuclei, i.e. ^{9}Be and ^{12}C, a much richer physics emerges compared to the physics of the two–body subsystems. An example is provided by the Efimov effect [86].

In a description at LO, the three–body system is not completely determined by including only two–body potentials. This can be seen from the fact that the three–body observables show a mild dependence on the cut–off associated to the two–body interactions. This dependence can be cured by including a three–body force in the model. This situation often occurs in pionless EFTs, where a contact three–body interaction is added at LO [87].

In our effective theory, we consider a three–body interaction Lagrangian term given by

$$\mathcal{L}_3 = \tilde{\lambda}_{3,\alpha\alpha n}(\psi^\dagger\psi)(\psi^\dagger\psi)(n^\dagger n)\,, \tag{4.108}$$

in case of ^{9}Be, or by

$$\mathcal{L}_3 = \tilde{\lambda}_{3,\alpha\alpha\alpha}(\psi^\dagger\psi)(\psi^\dagger\psi)(\psi^\dagger\psi)\,, \tag{4.109}$$

for the ^{12}C system, where the field operators are defined as in Section 4.1. The three–body potential defined in momentum space is therefore

$$V(Q,Q') = \tilde{\lambda}_3\, e^{-\left(\frac{Q}{\Lambda_3}\right)^2} e^{-\left(\frac{Q'}{\Lambda_3}\right)^2}\,. \tag{4.110}$$

The quantity Q (Q') is defined in terms of the momenta $\boldsymbol{p}_{12}$, $\boldsymbol{p}_{13}$ and $\boldsymbol{p}_{23}$ ($\boldsymbol{p}'_{12}$, $\boldsymbol{p}'_{13}$ and $\boldsymbol{p}'_{23}$), which are the two–particle relative momenta before (after) the interaction. Explicitly we have

$$Q = \sum_{i<j=1}^{3} \frac{m_\mathrm{r}}{M}\frac{(m_i+m_j)^2}{m_i m_j}\boldsymbol{p}_{ij}^2\,, \tag{4.111}$$

and Q' is defined accordingly. In the equation above, m_i is the mass of the particle i, with $i = 1,2,3$, M is the total mass of the system, while m_r is a reference mass. Q is commonly known as the hypermomentum of the three–body system. The interaction in Eq. (4.110) is parametrized by a new LEC. For every value of the cut–off parameter Λ_3, $\tilde{\lambda}_3$ can be fixed on a three–body observable, such as the three–body binding energy.

Chapter 5

The Hyperspherical Harmonics basis and the Non–Symmetrized Hyperspherical Harmonics method for the A–body system

In this Chapter the Non–Symmetrized Hyperspherical Harmonics method is introduced both in coordinate space and in momentum space.

We consider a system composed of A interacting particles of mass m_i, which is described by the position vectors $\boldsymbol{r}_i$ and the momenta $\boldsymbol{p}_i$, with $i = 1, \ldots, A$. The Hamiltonian operator is the sum of the kinetic energy and the potential [88]

$$\hat{H} = \hat{T} + \hat{V} = \sum_{i=1}^{A} \frac{\boldsymbol{p}_i^2}{2m_i} + \sum_{i<j}^{A} V_{ij} + \sum_{i<j<k}^{A} V_{ijk}\,, \tag{5.1}$$

where we have inserted explicitly the two–body and three–body contributions to the interaction.

5.1 The basis in coordinate space

Our aim is to solve the Schrödinger equation

$$\hat{H}\,|\Phi_A\rangle = E_{\rm tot}\,|\Phi_A\rangle\ , \tag{5.2}$$

by finding a solution for the A–body wave function in coordinate space, which we write as $\langle \boldsymbol{r}_1, \ldots, \boldsymbol{r}_A | \Phi_A \rangle = \Phi_A(\boldsymbol{r}_1, \ldots, \boldsymbol{r}_A)$. The most important result of Section 5.1.1 is the complete separation of the kinetic energy operator between the center–of–mass and the internal degrees of freedom. This will allow us to focus only on the internal motion, and to construct a proper basis to expand the internal wave function. This will be done in Sections 5.1.2 and 5.1.3.

5.1.1 Jacobi and Hyperspherical coordinates

We start by introducing the following set of $N \equiv A-1$ mass–weighted Jacobi coordinates in the reverse order convention, as in Ref. [89],

$$\boldsymbol{\eta}_{N+1-j} = \sqrt{\frac{M_j m_{j+1}}{m_{\rm r} M_{j+1}}}\left(\boldsymbol{r}_{j+1} - \frac{1}{M_j}\sum_{i=1}^{j} m_i \boldsymbol{r}_i\right), \qquad j = 1, \ldots, N\,, \tag{5.3}$$

where $m_{\rm r}$ is a reference mass. Although in the text we will maintain the notation $m_{\rm r}$, in practical calculations we will always set the reference mass equal to the nucleon mass. In the definition above, M_j is the total mass of the subsystem composed of the first j particles, whose center–of–mass is represented by $\frac{1}{M_j}\sum_{i=1}^{j} m_i \boldsymbol{r}_i$. We add to this set of coordinates also the following vector

$$\boldsymbol{\eta}_0 = \sqrt{\frac{M}{m_{\rm r}}}\boldsymbol{R}_{\rm cm}\,, \tag{5.4}$$

which is a rescaled center–of–mass coordinate relative to the whole A–body system. $\boldsymbol{R}_{\rm cm}$ is explicitly $\boldsymbol{R}_{\rm cm} = \frac{1}{M}\sum_{i=1}^{A} m_i \boldsymbol{r}_i$, where M is the total mass $M = \sum_{i=1}^{A} m_i$. The set of Jacobi coordinates, together with $\boldsymbol{\eta}_0$, will allow us separate the internal from the center–of–mass degrees of freedom in the kinetic energy operator.

In addition to the vector of the Jacobi coordinates $\vec{\boldsymbol{\eta}} = (\boldsymbol{\eta}_N, \ldots, \boldsymbol{\eta}_1, \boldsymbol{\eta}_0)$ and the vector of the position coordinates $\vec{\boldsymbol{r}} = (\boldsymbol{r}_1, \ldots, \boldsymbol{r}_A)$, we also introduce the rescaled position coordinates $\vec{\boldsymbol{y}} = (\boldsymbol{y}_1, \ldots, \boldsymbol{y}_A)$. The following relations hold

$$\vec{\boldsymbol{y}} = \mathcal{M}\vec{\boldsymbol{r}}\,, \qquad\qquad \vec{\boldsymbol{\eta}} = \frac{1}{\sqrt{m_{\rm r}}}\,\mathcal{B}\,\vec{\boldsymbol{y}}\,. \tag{5.5}$$

$\mathcal{M}$ is the diagonal matrix of the square root of the masses, whose elements are explicitly [90]

$$\mathcal{M}_{ij} = \sqrt{m_i}\delta_{ij}\,, \tag{5.6}$$

while $\mathcal{B}$ is an orthogonal matrix, $\mathcal{B}\mathcal{B}^{\rm t} = \mathcal{B}^{\rm t}\mathcal{B} = 1$, of dimension $A \times A$. The latter can be also separated into the product

$$\mathcal{B} = \mathcal{A}\mathcal{M}\,, \tag{5.7}$$

where $\mathcal{A}$ is the following matrix

$$\mathcal{A} = \begin{pmatrix} -\sqrt{\frac{m_2}{M_2 m_1}} & \sqrt{\frac{m_1}{M_2 m_2}} & 0 & \cdots & 0 \\ -\sqrt{\frac{m_3}{M_3 M_2}} & -\sqrt{\frac{m_3}{M_3 M_2}} & \sqrt{\frac{M_2}{M_3 m_3}} & \ddots & 0 \\ \vdots & \vdots & \ddots & \ddots & 0 \\ -\sqrt{\frac{m_{N+1}}{M_{N+1} M_N}} & \cdots & \cdots & -\sqrt{\frac{m_{N+1}}{M_{N+1} M_N}} & \sqrt{\frac{M_N}{M_{N+1} m_{N+1}}} \\ \frac{1}{\sqrt{M}} & \frac{1}{\sqrt{M}} & \frac{1}{\sqrt{M}} & \frac{1}{\sqrt{M}} & \frac{1}{\sqrt{M}} \end{pmatrix}. \tag{5.8}$$

The kinetic energy term in Eq. (5.1) can be rewritten first by using the definition of the rescaled coordinates $\vec{\boldsymbol{y}}$ given in (5.5), and then by exploiting the relation between

the vectors of the gradients $\vec{\boldsymbol{\nabla}}_{\boldsymbol{y}} = (\boldsymbol{\nabla}_{\boldsymbol{y}_1}, \ldots, \boldsymbol{\nabla}_{\boldsymbol{y}_A})$ and $\vec{\boldsymbol{\nabla}}_{\boldsymbol{\eta}} = (\boldsymbol{\nabla}_{\boldsymbol{\eta}_N}, \ldots, \boldsymbol{\nabla}_{\boldsymbol{\eta}_1}, \boldsymbol{\nabla}_{\boldsymbol{\eta}_0})$. We have

$$\vec{\boldsymbol{\nabla}}_{\boldsymbol{y}} = \frac{1}{\sqrt{m_{\mathrm{r}}}} \mathcal{B}^{\mathrm{t}} \vec{\boldsymbol{\nabla}}_{\boldsymbol{\eta}} \,, \tag{5.9}$$

and therefore the kinetic energy (5.1) reads

$$T = -\hbar^2 \sum_{i=1}^{A} \frac{\nabla^2_{\boldsymbol{r}_i}}{2m_i} \tag{5.10a}$$

$$= -\frac{\hbar^2}{2} \vec{\boldsymbol{\nabla}}_{\boldsymbol{y}}^{\mathrm{t}} \vec{\boldsymbol{\nabla}}_{\boldsymbol{y}} = -\frac{\hbar^2}{2m_{\mathrm{r}}} \vec{\boldsymbol{\nabla}}_{\boldsymbol{\eta}}^{\mathrm{t}} \, \mathcal{B} \, \mathcal{B}^{\mathrm{t}} \, \vec{\boldsymbol{\nabla}}_{\boldsymbol{\eta}} = -\frac{\hbar^2}{2m_{\mathrm{r}}} \sum_{i=0}^{N} \nabla^2_{\boldsymbol{\eta}_i} \,, \tag{5.10b}$$

where we have used the orthogonality property of the matrix $\mathcal{B}$. If now one makes use of the definition of the Jacobi vector $\boldsymbol{\eta}_0$ given in Eq. (5.4), it is straightforward that the kinetic energy in Eq. (5.10b) reduces to the sum of two terms: the center–of–mass kinetic energy ($i = 0$) and the internal one

$$T = -\frac{\hbar^2}{2M} \nabla^2_{\boldsymbol{R}_{\mathrm{cm}}} - \frac{\hbar^2}{2m_{\mathrm{r}}} \sum_{i=1}^{N} \nabla^2_{\boldsymbol{\eta}_i} \,. \tag{5.11}$$

The $3N$–dimensional space of the internal Jacobi coordinates $\{ \boldsymbol{\eta}_1, \ldots, \boldsymbol{\eta}_N \}$ can alternatively be described by using another set: the hyperspherical coordinates $\{ \rho, \Omega_N \}$. The quantity ρ is called hyperradius, and it is defined by the squared modulus of the N Jacobi vectors

$$\rho_j = \sqrt{\eta_1^2 + \cdots + \eta_j^2} \,, \qquad\qquad \rho_N \equiv \rho \,. \tag{5.12}$$

The symbol Ω_N denotes collectively the remaining $3N - 1$ angular coordinates. It is in fact a shorthand notation for the set

$$\Omega_N = (\hat{\eta}_1, \ldots, \hat{\eta}_N, \varphi_2, \ldots, \varphi_N) \,, \tag{5.13}$$

where each $\hat{\eta}_i = (\theta_i, \phi_i)$, $i = 1, \ldots, N$, represents the pair of spherical polar angles related to the Jacobi vector $\boldsymbol{\eta}_i$ ($0 \leq \theta_i \leq \pi$ and $0 \leq \phi_i \leq 2\pi$), while φ_j are $N - 1$ hyperangles defined as

$$\varphi_j = \arcsin \frac{\eta_j}{\rho_j} \,, \qquad\qquad j = 2, \ldots, N \,, \tag{5.14}$$

with ρ_j as in (5.12) and $0 \leq \varphi_j \leq \frac{\pi}{2}$. The inverse transformation is explicitly:

$$\begin{cases} \eta_N = \rho \sin \varphi_N \,, \\ \quad \vdots \\ \eta_j = \rho \cos \varphi_N \ldots \cos \varphi_{j+1} \sin \varphi_j \,, \qquad j = 2, \ldots, N-1 \,, \\ \quad \vdots \\ \eta_1 = \rho \cos \varphi_N \ldots \cos \varphi_2 \,. \end{cases} \tag{5.15}$$

In the equations above we have defined the hyperspherical coordinates relative to the set of Jacobi vectors in Eq. (5.3). In principle, given a system of A particles, this

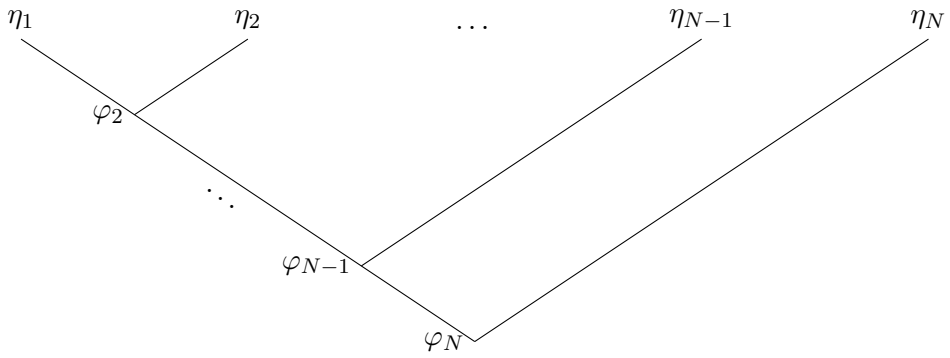

Figure 5.1: Tree diagram relative to the standard definition of the hyperspherical coordinates in Eq. (5.15).

choice is not unique. A useful tool that provides a visual representation of the chosen set is the so–called tree diagram, which was first introduced by Vilenkin, *et al.* [91]. In Fig. 5.1 we have represented the tree diagram relative to the coordinates defined in (5.15). Each hyperangle φ_j is associated to a node. If the segment joining the j–node to the upper one extends to the right (left), a factor $\sin\varphi_j$ ($\cos\varphi_j$) appears. Then, each η_j can be obtained by the product of ρ with the sine or cosine factors associated to each node, starting from the lowest vertex and following the path to the η_j termination. An example of an alternative scheme of coordinates can be found in Ref. [92].

Finally, the volume element relative to the Jacobi vectors written in terms of the hyperspherical coordinates is

$$d^3\boldsymbol{\eta}_1 \dots d^3\boldsymbol{\eta}_N = d\Omega_N \, d\rho \, \rho^{3N-1} \,, \tag{5.16}$$

where we have used the following definition

$$d\Omega_N = \left[\prod_{i=1}^{N} d\hat{\eta}_i \right] \left[\prod_{j=2}^{N} d\varphi_j \, (\cos\varphi_j)^{3j-4} (\sin\varphi_j)^2 \right] . \tag{5.17}$$

As a further step, we want to rewrite the internal kinetic energy in Eq. (5.11) in terms of the variables $\{\, \rho, \Omega_N \,\}$. If we first use the expression of the Laplace operator $\nabla^2_{\boldsymbol{\eta}_i}$ in spherical coordinates $(\eta_i, \hat{\eta}_i)$, and then we adopt the hyperspherical coordinates introduced above, we can write

$$-\frac{\hbar^2}{2m_{\rm r}} \sum_{i=1}^{N} \nabla^2_{\boldsymbol{\eta}_i} = -\frac{\hbar^2}{2m_{\rm r}} \sum_{i=1}^{N} \left[\frac{\partial^2}{\partial \eta_i^2} + \frac{2}{\eta_i} \frac{\partial}{\partial \eta_i} - \frac{\hat{\boldsymbol{\ell}}_i^2(\hat{\eta}_i)}{\eta_i^2} \right] , \tag{5.18a}$$

$$= -\frac{\hbar^2}{2m_{\rm r}} \left[\frac{\partial^2}{\partial \rho^2} + \frac{3N-1}{\rho} \frac{\partial}{\partial \rho} - \frac{\hat{\mathcal{K}}_N^2(\Omega_N)}{\rho^2} \right] , \tag{5.18b}$$

where $\hat{\boldsymbol{\ell}}_i(\hat{\eta}_i)$ is the angular momentum operator related to the Jacobi vector $\boldsymbol{\eta}_i$, and $\hat{\mathcal{K}}_N$ is the grand–angular momentum or generalized angular momentum operator. At fixed N, it can be demonstrated that the latter operator can be defined recursively, starting from the trivial case $j = 1$, for which $\hat{\mathcal{K}}_1^2(\Omega_1) = \hat{\boldsymbol{\ell}}_1^2(\hat{\eta}_1)$, and then

from $j = 2$ up to $j = N$ as follows [28]

$$\hat{\mathcal{K}}_j^2(\Omega_j) = -\frac{\partial^2}{\partial\varphi_j^2} + A_j\frac{\partial}{\partial\varphi_j} + \frac{\hat{\boldsymbol{\ell}}_j^2(\hat{\eta}_j)}{\sin^2\varphi_j} + \frac{\hat{\mathcal{K}}_{j-1}^2(\Omega_{j-1})}{\cos^2\varphi_j}\,, \qquad j = 2,\ldots,N\,, \tag{5.19}$$

where the coefficient A_j is explicitly $A_j = \frac{(3j-6)-(3j-2)\cos 2\varphi_j}{\sin 2\varphi_j}$.

5.1.2 The Hyperspherical Harmonics functions

As already stated, we want to solve the Schrödinger equation (5.2) by finding a solution for the A–body wave function in coordinate space, $\Phi_A(\boldsymbol{r}_1,\ldots,\boldsymbol{r}_A)$. Our starting point is the Hamiltonian operator in Eq. (5.1) with the kinetic energy term expressed as in (5.11), where we have separated explicitly the center–of–mass from the internal part. We write the total energy in (5.2) as $E_{\rm tot} = E_{\rm cm} + E$. Moreover, we separate the wave function relative to the center–of–mass from the one relative to the internal degrees of freedom by writing $\Phi_A(\boldsymbol{r}_1,\ldots,\boldsymbol{r}_A) = \phi(\boldsymbol{R}_{\rm cm})\Phi(\boldsymbol{\eta}_1,\ldots,\boldsymbol{\eta}_N)$. In this way the Schrödinger equation (5.2) splits into two distinct equations. The first one is the equation for $\phi(\boldsymbol{R}_{\rm cm})$

$$\left[-\frac{\hbar^2}{2M}\nabla^2_{\boldsymbol{R}_{\rm cm}}\right]\phi(\boldsymbol{R}_{\rm cm}) = E_{\rm cm}\phi(\boldsymbol{R}_{\rm cm})\,, \tag{5.20}$$

whose explicit solutions are essentially plane waves, $\phi(\boldsymbol{R}_{\rm cm}) \propto e^{\frac{i}{\hbar}\boldsymbol{P}_{\rm cm}\cdot\boldsymbol{R}_{\rm cm}}$ and the energy is explicitly $E_{\rm cm} = \frac{\boldsymbol{P}^2_{\rm cm}}{2M}$. The second equation is the following

$$\left[-\frac{\hbar^2}{2m_{\rm r}}\sum_{i=1}^{N}\nabla^2_{\boldsymbol{\eta}_i} + V\right]\Phi(\boldsymbol{\eta}_1,\ldots,\boldsymbol{\eta}_N) = E\,\Phi(\boldsymbol{\eta}_1,\ldots,\boldsymbol{\eta}_N)\,, \tag{5.21}$$

and it is the one of main interest to us. The function $\Phi(\boldsymbol{\eta}_1,\ldots,\boldsymbol{\eta}_N)$ is the wave function relative to the internal motion of the nuclear system and in the following we will rewrite this function in terms of the hyperspherical coordinates $\{\,\rho,\Omega_N\,\}$.

Having in mind the expression of the kinetic energy in Eq. (5.18b), we start by searching for the eigenfunctions of the grand–angular momentum operator $\hat{\mathcal{K}}^2_N(\Omega_N)$, which we have already defined recursively in Eq. (5.19). In practice, this is achieved by solving the following equation

$$\left[\hat{\mathcal{K}}^2_N(\Omega_N) - K(K+3N-2)\right]Y^K_{[K]}(\Omega_N) = 0\,. \tag{5.22}$$

$Y^K_{[K]}(\Omega_N)$ are the so–called Hyperspherical Harmonics (HH) functions, where $K \equiv K_N$ is the grand–angular momentum quantum number and the symbol $[K]$ denotes a set of quantum numbers that completely specifies the state.

Before proceeding, we say here very briefly how the relation in Eq. (5.22) can be derived [90]. We consider a homogeneous polynomial in the $3N$–cartesian coordinates relative to the N Jacobi vectors $\boldsymbol{\eta}_i$, say $h_{[K]}$, where K is the order of the polynomial. Due to the definition of homogeneous polynomial, the angular part can be completely separated, and the function $\rho^{-K}h_{[K]} \equiv Y_{[K]}(\Omega_N)$ does not depend on the hyperradius ρ. Since the polynomial is harmonic, we have $\Delta h_{[K]} = 0$, where

$\Delta = \sum_{i=1}^{N} \nabla^2_{\boldsymbol{\eta}_i}$. Finally, by making use of the equality in Eq. (5.18b), we can write the following relations

$$0 = \Delta h_{[K]} = \Delta \left(\rho^K Y_{[K]}(\Omega_N) \right) = \left[K(K+3N-2) - \hat{\mathcal{K}}^2_N(\Omega_N) \right] \rho^{K-2} Y_{[K]}(\Omega_N) \,, \tag{5.23}$$

from which we deduce the validity of Eq. (5.22).

We recall that the trivial case $N = 1$ corresponds to the two–body system. In this case, the grand–angular momentum operator is essentially the orbital angular momentum, $\hat{\mathcal{K}}^2_1(\Omega_1) = \hat{\boldsymbol{\ell}}^2_1(\hat{\eta}_1)$. From (5.22), it follows that

$$\hat{\mathcal{K}}^2_1(\Omega_1) Y^K_{[K]}(\Omega_1) = K(K+1) Y^K_{[K]}(\Omega_1) \,, \tag{5.24}$$

and the eigenfunctions $Y^K_{[K]}(\Omega_1)$ correspond to the standard spherical harmonics $Y_{\ell_1 m_1}(\hat{\eta}_1)$. In this specific case, K can be identified with the orbital angular momentum quantum number ℓ_1, and the set of quantum numbers that completely specifies the state is $[K] = [\ell_1, m_1]$.

Now we focus on the general case $N > 1$, where each eigenfunction $Y^{K_j}_{[K_j]}(\Omega_j)$, can be calculated recursively in terms of the previous $Y^{K_{j-1}}_{[K_{j-1}]}(\Omega_{j-1})$, $j = 2, \ldots, N$. Here we mainly follow Refs. [28, 90, 93] and the calculation also shown in Ref. [94]. We start by writing the HH functions in the following form

$$Y^{K_j}_{[K_j]}(\Omega_j) = F(\cos 2\varphi_j) (\sin\varphi_j)^{\ell_j} (\cos\varphi_j)^{K_{j-1}} Y_{\ell_j m_j}(\hat{\eta}_j) Y^{K_{j-1}}_{[K_{j-1}]}(\Omega_{j-1}) \,. \tag{5.25}$$

The function $F(\cos 2\varphi_j)$ can be determined by inserting the ansatz (5.25) in

$$\hat{\mathcal{K}}^2_j(\Omega_j) Y^{K_j}_{[K_j]}(\Omega_j) = K_j(K_j + 3j - 2) Y^{K_j}_{[K_j]}(\Omega_j) \,. \tag{5.26}$$

The above equation is essentially Eq. (5.22) written for a generic K_j. In order to obtain a differential equation for the function $F(\cos 2\varphi_j)$, we use the following relations: the recursive definition of $\hat{\mathcal{K}}^2_j(\Omega_j)$ in (5.19), the equation

$$\hat{\mathcal{K}}^2_{j-1}(\Omega_{j-1}) Y^{K_{j-1}}_{[K_{j-1}]}(\Omega_{j-1}) = K_{j-1}(K_{j-1} + 3j - 5) Y^{K_{j-1}}_{[K_{j-1}]}(\Omega_{j-1}) \,, \tag{5.27}$$

valid for $Y^{K_{j-1}}_{[K_{j-1}]}(\Omega_{j-1})$, and the well–known relation for the usual spherical harmonics functions $Y_{\ell_j m_j}(\hat{\eta}_j)$

$$\hat{\boldsymbol{\ell}}^2_j(\hat{\eta}_j) Y_{\ell_j m_j}(\hat{\eta}_j) = \ell_j(\ell_j + 1) Y_{\ell_j m_j}(\hat{\eta}_j) \,. \tag{5.28}$$

By putting together these ingredients, we finally obtain

$$(1 - z^2)\, F''(z) + (\alpha - z\beta)\, F'(z) + \gamma\, F(z) = 0 \,, \qquad z = \cos 2\varphi_j \,, \tag{5.29}$$

where the constants α, β and γ are defined in terms of the quantum numbers characterizing the state:

$$\alpha = K_{j-1} - \ell_j + \frac{3j}{2} - 3 \,, \tag{5.30a}$$

$$\beta = K_{j-1} + \ell_j + \frac{3j}{2} \,, \tag{5.30b}$$

$$\gamma = \frac{1}{4} K_j(K_j + 3j - 2) - \frac{1}{4}(\ell_j + K_{j-1})(\ell_j + K_{j-1} + 3j - 2) \,. \tag{5.30c}$$

Since Eq. (5.29) resembles the differential equation satisfied by the Jacobi Polynomials $P_n^{(a,b)}(z)$ of order n ($n = 0, 1, 2, \dots$, $-1 \leq z \leq 1$) with

$$b - a = \alpha\,, \qquad b + a + 2 = \beta\,, \qquad n(n + b + a + 1) = \gamma\,, \tag{5.31}$$

the function $F(z)$ can be expressed as

$$F(z) \propto P_{n_j}^{(\ell_j + \frac{1}{2}, K_{j-1} + \frac{3j-5}{2})}(z)\,, \qquad n_j = 0, 1, 2, \dots\,, \tag{5.32}$$

provided that $K_j = K_{j-1} + \ell_j + 2n_j$ with $K_1 = \ell_1$. More details about the Jacobi polynomials are reported in Appendix D.1.

Once the function $F(z)$ has been determined, the ansatz in Eq. (5.25) leads to the following complete expression for the HH functions

$$\begin{aligned} Y_{[K]}^K(\Omega_N) = &\left[\prod_{i=1}^N Y_{\ell_i m_i}(\hat{\eta}_i)\right]\left[\prod_{j=2}^N \mathcal{N}_{n_j}^{K_j;\ell_j,K_{j-1}}\right. \\ &\left.\times (\sin\varphi_j)^{\ell_j}(\cos\varphi_j)^{K_{j-1}} P_{n_j}^{(\ell_j+\frac{1}{2}, K_{j-1}+\frac{3j-5}{2})}(\cos 2\varphi_j)\right]. \end{aligned} \tag{5.33}$$

The coefficients $\mathcal{N}_{n_j}^{K_j;\ell_j,K_{j-1}}$ follow from the normalization of the Jacobi polynomials (see Appendix D.1), and they are given explicitly by

$$\mathcal{N}_{n_j}^{K_j;\ell_j,K_{j-1}} = \sqrt{\frac{n_j!(2K_j + 3j - 2)\,\Gamma\left(n_j + K_{j-1} + \ell_j + \frac{3j-2}{2}\right)}{\Gamma\left(n_j + \ell_j + \frac{3}{2}\right)\Gamma\left(n_j + K_{j-1} + \frac{3j-3}{2}\right)}}\,. \tag{5.34}$$

The HH functions constructed as in Eq. (5.33) are completely specified by the set of $3N - 1$ quantum numbers

$$[K] = [\ell_1, m_1, \dots, \ell_N, m_N, n_2, \dots, n_N]\,, \tag{5.35}$$

with the definition $K \equiv K_N$. Moreover, they represent a complete and orthonormal set of functions [93]

$$\sum_{[K]} \left[Y_{[K]}^K(\Omega'_N)\right]^* Y_{[K]}^K(\Omega_N) = \delta^{3N-1}(\Omega_N - \Omega'_N)\,, \tag{5.36}$$

$$\int d\Omega_N \left[Y_{[K]}^K(\Omega_N)\right]^* Y_{[K']}^{K'}(\Omega_N) = \delta_{[K][K']}\delta_{KK'}\,, \tag{5.37}$$

with the volume element $d\Omega_N$ already defined in Eq. (5.17). As a consequence, the HH functions represent a proper basis that can be used to expand a regular function of the hyperangular variables Ω_N. Specifically, as anticipated at the beginning of this Section, we will use this basis to expand a generic function of the Jacobi coordinates $\{\boldsymbol{\eta}_1, \dots, \boldsymbol{\eta}_N\}$, such as the internal wave function $\Phi(\boldsymbol{\eta}_1, \dots, \boldsymbol{\eta}_N)$ relative to the A–nucleon system

$$\Phi(\boldsymbol{\eta}_1, \dots, \boldsymbol{\eta}_N) = \sum_{[K]} a_{[K]}(\rho) Y_{[K]}^K(\Omega_N)\,, \tag{5.38}$$

where the coefficients depend uniquely on the hyperradius ρ.

5.1.3 The spatial, spin and isospin basis

To properly construct a basis that describes an A–body nuclear system, in addition to the spatial degrees of freedom, also the spin and the isospin of the constituents must be taken into account. If $\boldsymbol{s}_i$ and $\boldsymbol{t}_i$ are the spin and the isospin of the i–particle, respectively, then the total spin angular momentum operator is $\boldsymbol{S} = \boldsymbol{s}_1 + \cdots + \boldsymbol{s}_A$, and $\boldsymbol{T} = \boldsymbol{t}_1 + \cdots + \boldsymbol{t}_A$ is the total isospin. The total angular momentum operator is defined as $\boldsymbol{J} = \boldsymbol{L} + \boldsymbol{S}$. The operator $\boldsymbol{L}$ denotes the total orbital momentum $\boldsymbol{L} = \boldsymbol{\ell}_1 + \cdots + \boldsymbol{\ell}_N$, i.e. the sum of the orbital angular momenta operators relative to the N Jacobi coordinates. The definitions of the operators projected on the z–axis are easily understood.

In the most general case, the wave function of the nuclear many–body system is an eigenfunction of the operators $\boldsymbol{J}^2$, J_z and the parity Π. As a consequence, we need first to couple the angular momenta relative to the single particles, and then to recouple the total orbital momentum and the total spin. The particular case in which a central interaction potential acts between the particles is easier to implement, because the quantum numbers relative to $\boldsymbol{L}$ and $\boldsymbol{S}$ can be still considered good quantum numbers.

Focussing on the spin (isospin), we define the eigenfunctions of the operators $\hat{\boldsymbol{s}}_i^2$ and $\hat{s}_{iz}$ ($\hat{\boldsymbol{t}}_i^2$ and $\hat{t}_{iz}$) as $\chi_{s_i m_{s_i}}(i) = \langle \boldsymbol{\sigma}_i | s_i m_{s_i} \rangle$ ($\xi_{t_i m_{t_i}}(i) = \langle \boldsymbol{\tau}_i | t_i m_{t_i} \rangle$), $i = 1, \ldots, A$, satisfying the following eigenvalues equations

$$\hat{\boldsymbol{s}}_i^2 \chi_{s_i m_{s_i}}(i) = s_i(s_i+1)\chi_{s_i m_{s_i}}(i) \qquad \hat{s}_{zi}\chi_{s_i m_{s_i}}(i) = m_{s_i}\chi_{s_i m_{s_i}}(i)\,, \tag{5.39}$$

$$\hat{\boldsymbol{t}}_i^2 \xi_{t_i m_{t_i}}(i) = t_i(t_i+1)\xi_{t_i m_{t_i}}(i) \qquad \hat{t}_{zi}\xi_{t_i m_{t_i}}(i) = m_{t_i}\xi_{t_i m_{t_i}}(i)\,. \tag{5.40}$$

The eigenfunctions of the total spin are constructed by following the reverse order convention:

$$\chi_{[S]}^{SM_S} = \Big[\big[\ldots\big[\big[\chi_{s_A}(A)\,\chi_{s_{A-1}}(A-1)\big]_{S_2}\chi_{s_{A-2}}(A-2)\big]_{S_3}\ldots\big]_{S_N}\chi_{s_1}(1)\Big]_{SM_S}\,. \tag{5.41}$$

In the scheme above, the coupling starts from the last two particles, A and $A-1$, giving S_2. Then, the spin of each successive particle is added until the first particle is reached, and the last coupling gives $S_A \equiv S$. In fact the set of quantum numbers involved is

$$\{S\} \equiv [S]S = [S_2, \ldots, S_N]S\,. \tag{5.42}$$

These eigenfunctions satisfy the eigenvalues equations

$$\hat{\boldsymbol{S}}^2\,\chi_{[S]}^{SM_S} = S(S+1)\,\chi_{[S]}^{SM_S} \qquad \hat{S}_z\,\chi_{[S]}^{SM_S} = M_S\,\chi_{[S]}^{SM_S}\,. \tag{5.43}$$

The eigenfunctions of the total isospin are constructed by following the same reversed scheme

$$\xi_{[T]}^{TM_T} = \Big[\big[\ldots\big[\big[\xi_{t_A}(A)\,\xi_{t_{A-1}}(A-1)\big]_{T_2}\xi_{t_{A-2}}(A-2)\big]_{T_3}\ldots\big]_{T_N}\xi_{t_1}(1)\Big]_{TM_T}\,, \tag{5.44}$$

where $T_A \equiv T$, and they satisfy

$$\hat{\boldsymbol{T}}^2\,\xi_{[T]}^{TM_T} = T(T+1)\,\xi_{[T]}^{TM_T} \qquad \hat{T}_z\,\xi_{[T]}^{TM_T} = M_T\,\xi_{[T]}^{TM_T}\,, \tag{5.45}$$

with the definition

$$\{T\} \equiv [T]T = [T_2, \dots, T_N]T\,. \tag{5.46}$$

Based on the derivation carried out in the last Section, specifically Eq. (5.33), the HH functions $Y^K_{[K]}(\Omega_N)$, with $[K] \equiv [\ell_1, m_1, \dots, \ell_N, m_N, n_2, \dots, n_N]$, are constructed from a product of spherical harmonics $Y_{\ell_i m_i} (i = 1, \dots, N)$. As a consequence, they are eigenfunctions of the operators $\hat{\boldsymbol{\ell}}_i^2$ and $\hat{\ell}_{zi}$ with eigenvalues $\ell_i(\ell_i+1)$ and m_i, respectively. By applying the general rules of angular momentum recoupling, we can write [28]

$$\begin{aligned}\mathcal{Y}^{KLM_L}_{[K]}(\Omega_N) = &\Big[\big[\dots\big[[Y_{\ell_1}(\hat{\eta}_1)Y_{\ell_2}(\hat{\eta}_2)\big]_{L_2}Y_{\ell_3}(\hat{\eta}_3)\big]_{L_3}\dots\big]_{L_{N-1}}Y_{\ell_N}(\hat{\eta}_N)\Big]_{LM_L}\\ &\times\prod_{j=2}^{N} {}^j\mathcal{P}^{\ell_j,K_{j-1}}_{n_j}(\varphi_j)\,,\end{aligned} \tag{5.47}$$

where now $\mathcal{Y}^{KLM_L}_{[K]}(\Omega_N)$ are eigenfunctions of $\hat{\boldsymbol{L}}^2$ and $\hat{L}_z$. The symbol $[K]$ here denotes the new set of quantum numbers

$$[K] \equiv [\ell_1, \dots, \ell_N, L_2, \dots, L_{N-1}, n_2, \dots, n_N]\,, \tag{5.48}$$

with the definition $L_N \equiv L$ and

$$\{K\} \equiv [K]L\,, \tag{5.49}$$

Moreover, we have introduced the HH polynomial ${}^j\mathcal{P}^{\ell_j,K_{j-1}}_{n_j}(\varphi_j)$ as a compact notation for the expression

$${}^j\mathcal{P}^{\ell_j,K_{j-1}}_{n_j}(\varphi_j) = \mathcal{N}^{K_j;\ell_j,K_{j-1}}_{n_j}(\sin\varphi_j)^{\ell_j}(\cos\varphi_j)^{K_{j-1}}P^{(\ell_j+\frac{1}{2},K_{j-1}+\frac{3j-5}{2})}_{n_j}(\cos 2\varphi_j)\,, \tag{5.50}$$

where the normalization coefficients $\mathcal{N}^{K_j;\ell_j,K_{j-1}}_{n_j}$ are the same as in Eq. (5.34). We remark that the brackets notation used in Eq. (5.47) to represent the angular momenta recoupling [also used in the spin and isospin formalism (5.41) and (5.44)], is a compact form to denote the summation

$$\begin{aligned}\mathcal{Y}^{KLM_L}_{[K]}(\Omega_N) = \sum_{m_1\dots m_N} &(\ell_1 m_1 \ell_2 m_2|L_2M_2)\,(L_2M_2\ell_3m_3|L_3M_3)\dots\\ &\times\dots(L_{N-1}M_{N-1}\ell_N m_N|LM_L)\,Y^K_{[K]}(\Omega_N)\,,\end{aligned} \tag{5.51}$$

where the Clebsch–Gordan coefficients appear and the quantum number M_j is explicitly $M_j = \sum_{i=1}^{j} m_i$ for $j = 2, \dots, N-1$. The recoupled HH functions in (5.47) satisfy the following eigenvalues equations [88]

$$\hat{\mathcal{K}}^2_N(\Omega_N)\,\mathcal{Y}^{KLM_L}_{[K]}(\Omega_N) = K(K+3N-2)\,\mathcal{Y}^{KLM_L}_{[K]}(\Omega_N)\,, \tag{5.52}$$

$$\hat{\boldsymbol{L}}^2(\Omega_N)\,\mathcal{Y}^{KLM_L}_{[K]}(\Omega_N) = L(L+1)\,\mathcal{Y}^{KLM_L}_{[K]}(\Omega_N)\,, \tag{5.53}$$

$$\hat{L}_z(\Omega_N)\,\mathcal{Y}^{KLM_L}_{[K]}(\Omega_N) = M_L\,\mathcal{Y}^{KLM_L}_{[K]}(\Omega_N)\,. \tag{5.54}$$

In the most general case, a L–S recoupling is needed. By considering Eqs. (5.47) and (5.41), and the isospin dependence as in (5.44), we define the functions

$$\mathcal{Y}^{JM\pi}_{[K][S][T]KLST}(\Omega_N) = \Big[\mathcal{Y}^{KL}_{[K]}(\Omega_N)\chi^S_{[S]}\Big]_{JM}\xi^{TM_T}_{[T]}\,, \tag{5.55}$$

which are simultaneously eigenfunctions of the operators $\hat{\boldsymbol{J}}^2$ and $\hat{J}_z$ [88]

$$\hat{\boldsymbol{J}}^2\, \mathcal{Y}^{JM\pi}_{[K][S][T]KLST}(\Omega_N) = J(J+1)\, \mathcal{Y}^{JM\pi}_{[K][S][T]KLST}(\Omega_N)\,, \tag{5.56}$$

$$\hat{J}_z\, \mathcal{Y}^{JM\pi}_{[K][S][T]KLST}(\Omega_N) = M\, \mathcal{Y}^{JM\pi}_{[K][S][T]KLST}(\Omega_N)\,, \tag{5.57}$$

in addition to the parity operator $\hat{\Pi}$

$$\hat{\Pi}\, \mathcal{Y}^{JM\pi}_{[K][S][T]KLST}(\Omega_N) = (-1)^K\, \mathcal{Y}^{JM\pi}_{[K][S][T]KLST}(\Omega_N)\,. \tag{5.58}$$

From this last equation, it can be deduced that the parity $\pi = (-1)^K$ is entirely due to the value of the grand–angular momentum quantum number K.

If the total orbital momentum L and the total spin S are good quantum numbers, then the final expression of the basis is much less complicated. In fact, we can use the direct product of the HH functions, the spin and the isospin functions as constructed in Eqs. (5.47), (5.41) and (5.44), respectively. In this way, the functions in Eq. (5.55) reduce to

$$\mathcal{Y}^{JM\pi,KLST}_{[K][S][T]}(\Omega_N) = \mathcal{Y}^{KLM_L}_{[K]}(\Omega_N)\chi^{SM_S}_{[S]}\eta^{TM_T}_{[T]}\,. \tag{5.59}$$

In the process of constructing the basis, it is obvious that the quantum numbers K, L and S must always be compatible with a given total spin and parity J^π.

Finally, the complete basis in coordinate space

$$\langle \boldsymbol{\eta}_1, \ldots, \boldsymbol{\eta}_N | \Phi_\kappa \rangle = \langle \rho\, \Omega_N | \Phi_\kappa \rangle \equiv \Phi_\kappa(\rho, \Omega_N) \tag{5.60}$$

is the following

$$\Phi_\kappa(\rho, \Omega_N) = f_m(\rho)\, \mathcal{Y}^{JM\pi}_{\mu}(\Omega_N)\,, \qquad \kappa \equiv [m, \mu]\,. \tag{5.61}$$

It is often useful to employ the index κ to refer collectively to all the quantum numbers involved. In the formulation above, the HH, spin and isospin dependence is entirely contained in the functions $\mathcal{Y}^{JM\pi}_{\mu}(\Omega_N)$, defined either as in Eq. (5.55) or (5.59), which are characterized by the collective index $\mu = [K][S][T]KLST$. Conversely, the functions $f_m(\rho)$ depend completely on the hyperradius, and they can be written as follows

$$f_m(\rho) = \left(\frac{1}{\beta}\right)^{\frac{3N}{2}} \sqrt{\frac{m!}{(m+3N-1)!}}\, L_m^{(3N-1)}\left(\frac{\rho}{\beta}\right) \mathrm{e}^{-\frac{\rho}{2\beta}}\,. \tag{5.62}$$

In constructing $f_m(\rho)$, we use the generalized Laguerre polynomials $L_m^{(\alpha)}(x)$ of order $\alpha = 3N-1$, which are a orthonormal set (see Appendix D.2). Moreover, a decreasing exponential factor is present, regulating the asymptotic behaviour of $f_m(\rho)$ as follows: $f_m(\rho) \to 0$ for $\rho \to \infty$. β is a non–linear parameter. The normalization factor in Eq. (5.62) is such that the following orthonormality relation is valid [see also Eq. (D.5)]

$$\int_0^\infty d\rho\, \rho^{3N-1} f_m(\rho) f_{m'}(\rho) = \delta_{mm'}\,. \tag{5.63}$$

We would like to point out that in the following we will often use the term "HH basis" to refer to the complete spatial, spin and isospin basis, thus including also the hyperradial part.

The internal wave function relative to the A–body nuclear system can be written in terms of the basis constructed in Eq. (5.61) as follows

$$\Phi(\boldsymbol{\eta}_1, \ldots, \boldsymbol{\eta}_N) = \sum_{\kappa} c_\kappa \Phi_\kappa(\rho, \Omega_N) \,, \tag{5.64}$$

where the coefficients c_κ have to be determined. In the following Sections we will see how this can be achieved variationally and by means of the so–called Non-Symmetrized Hyperspherical Harmonics method.

5.2 The Non–Symmetrized Hyperspherical Harmonics method

5.2.1 The symmetry of the Hyperspherical Harmonics basis

The HH basis that we have constructed so far does not possess any particular symmetry under the permutations of the A particles. On the other hand, the wave function of a nuclear system must have a well–defined behaviour under the operation of particles permutation. As a consequence, a procedure to perform a proper symmetrization must be taken into account. This is one of the main difficulties that arise in using this method, since the symmetrization procedure becomes more and more sophisticated as the number of particles increases.

One approach to this problem is the following: the HH functions are constructed recursively by realizing irreducible representations not only of the orthogonal group $O(3N)$ but also of the group $O(N)$, accordingly to the chain $O(3N) \supset O(3) \otimes O(N)$ [95]

$$\begin{array}{ccccccccccc} O(3N-3) & \supset & O(3) & \otimes & O(N-1) & \supset & O(N-2) & \ldots & \supset & O(2) & \\ & & & & \cup & & \cup & & & \cup & \\ & & & & S_N & & S_{N-1} & \ldots & \supset & S_3 & \supset \; S_2 \,. \end{array} \tag{5.65}$$

Almost three decades ago, this has been developed by Barnea [96] through an efficient technique that allowed *ab initio* calculations for $A > 4$ nucleon systems [97] and up to $A = 7$ using semi–realistic potentials [98]. Once the wave functions are properly symmetrized, also due to the recursive construction of the basis functions, the evaluation of the matrix elements of a two–body operator such as the interaction potential

$$V = \sum_{i<j} V_{ij} \,, \tag{5.66}$$

is simplified. In fact the calculation can be reduced to that of a matrix element involving only one pair of particles

$$\langle \Phi'^{\mathcal{A}} | \sum_{i<j} V_{ij} | \Phi'^{\mathcal{A}} \rangle = \frac{A(A-1)}{2} \langle \Phi'^{\mathcal{A}} | V_{12} | \Phi'^{\mathcal{A}} \rangle \,, \tag{5.67}$$

where $\Phi'^{\mathcal{A}}$ is the antisymmetrized wavefunction. Other developments of this method are also due to the Pisa Group, whose calculations, performed by using a properly

symmetrized HH basis, have led to successful results up to $A = 6$ nucleons with the most recent interaction potentials [88, 93, 99].

The method mentioned above represents a powerful tool to study systems of A identical fermionic particles, such as the nucleons. However, in our cluster EFT framework, since we are studying effective nuclear systems made up of non–identical components, where the pairs of particles have different masses and different symmetries under permutations, this approach is rather difficult to implement. Instead, a suitable method to use is the one first introduced by Gattobigio, *et al.* in Ref. [100]. The basic idea is that the previous symmetrization procedure of the basis is not strictly necessary, and one can use in the calculation a basis that does not possess a well–defined behaviour under the permutations of the particles. In the following Sections we will analyse this so–called Non–Symmetrized Hyperspherical Harmonics (NSHH) method. In this work, in order to determine the physical bound state of the nuclear system, i.e. the lowest eigenvalue of the nuclear Hamiltonian with the correct symmetry, we will use a variation on the original NSHH method introduced in Ref. [28] by Deflorian, *et al.*. The same method has also been further developed in Refs. [92, 101] to study hypernuclear systems as well.

5.2.2 The rotation coefficients

The Jacobi coordinates defined in Section 5.1.1 depend on the ordering of the A particles of the system, as Eq. (5.3) explicitly shows. By taking the initial ordering $(1, \dots, A)$ as a reference, if we consider a generic permutation $p = (p_1, \dots, p_A)$ of the A particles, then the effect is a redefinition of the Jacobi coordinates in Eq. (5.3), where we must replace each pair $(m_i, \boldsymbol{r}_i)$ by the corresponding one in the specific permutation, i.e. $(m_{p_i}, \boldsymbol{r}_{p_i})$ [100]. This also affects the corresponding HH functions, for which we can write

$$\mathcal{Y}^{KLM_L}_{[K]}(\Omega_N^{(p)}) = \sum_{[K']} \mathcal{C}^{KL(p,\bar{p})}_{[K][K']} \mathcal{Y}^{KLM_L}_{[K']}(\Omega_N^{(\bar{p})}) \,. \tag{5.68}$$

This relation reflects the fact that any HH function in a given permutation p can be expressed as a linear combination of HH functions in the reference permutation $\bar{p}$. In the equation above the sum runs over the set of quantum numbers $[K']$ with the constraint $K' = K$, and LM_L are conserved. The coefficients in Eq. (5.68) are sometimes called Transformation Coefficients (TC). For $A = 3$ the TC coincide with the Raynal–Revai coefficients [102], and they are calculated by using recurrence relations. However, in the general case of A particles, their evaluation could be challenging (see for example [93] and other References therein).

For a less demanding computation of the matrix elements of the two–body potential operator V_{ij}, we exploit two facts: its dependence on the relative distance between the particles on which it acts, and the fact that the last Jacobi coordinate $\boldsymbol{\eta}_N$ is always proportional to a distance between two particles (1 and 2 in the reference ordering). For these reasons, in order to perform the calculation, the most advantageous choice is the set of Jacobi vectors such that $\boldsymbol{\eta}'_N \propto (\boldsymbol{r}_j - \boldsymbol{r}_i)$. If we take for example the case $A = 3$, then the interaction terms V_{12}, V_{23} and V_{13} should be calculated by using different sets of Jacobi vectors, in which $\boldsymbol{\eta}'_N \propto (\boldsymbol{r}_2 - \boldsymbol{r}_1)$, $\boldsymbol{\eta}'_N \propto (\boldsymbol{r}_3 - \boldsymbol{r}_2)$ and $\boldsymbol{\eta}'_N \propto (\boldsymbol{r}_3 - \boldsymbol{r}_1)$, respectively. The first set is exactly the

one defined in Eq. (5.3), corresponding to the particles ordering $(1,2,3)$, which we take as reference. The second and the third ones correspond to the particles orderings $(2,3,1)$ and $(1,3,2)$, respectively. Furthermore, it is not difficult to show that both orderings can be achieved by elementary transpositions between adjacent particles. Since this can be generalized to a number of particles $A > 3$, basically we are interested in combinations of transposition operators interchanging only adjacent particles: $(\boldsymbol{r}_1,\ldots,\boldsymbol{r}_A,\boldsymbol{r}_{A-1})$, $(\boldsymbol{r}_1,\ldots,\boldsymbol{r}_{A-1},\boldsymbol{r}_{A-2},\boldsymbol{r}_A)$ and so on [100]. These transpositions belong to the type of transformations that are called kinematic rotations [92, 103]. The interchange between the particles k and $k+1$, with $k = 2,\ldots,N$, involves a redefinition of the Jacobi vectors $\boldsymbol{\eta}_{N+1-k}$ and $\boldsymbol{\eta}_{N+1-k+1}$, while the others remain unchanged. As a consequence, the associated transformation matrix $p_{k,k+1}$ has a block structure made of identity matrices and the following block of dimension 2×2

$$\begin{pmatrix} \boldsymbol{\eta}'_{N+1-k} \\ \boldsymbol{\eta}'_{N+1-k+1} \end{pmatrix} = \begin{pmatrix} -\cos\beta_k & \sin\beta_k \\ \sin\beta_k & \cos\beta_k \end{pmatrix} \begin{pmatrix} \boldsymbol{\eta}_{N+1-k} \\ \boldsymbol{\eta}_{N+1-k+1} \end{pmatrix} , \tag{5.69}$$

with the definition of the kinematic angle β_k

$$\cos\beta_k = \sqrt{\frac{m_k m_{k+1}}{M_k(M_{k-1}+m_{k+1})}} . \tag{5.70}$$

The hyperradius ρ is invariant because these transformations have the following property: $\boldsymbol{\eta}'^2_{N+1-k}+\boldsymbol{\eta}'^2_{N+1-k+1} = \boldsymbol{\eta}^2_{N+1-k}+\boldsymbol{\eta}^2_{N+1-k+1}$. If $\mathcal{Y}^{KLM_L}_{[K]}(\Omega^{(k)}_N)$ are the HH functions associated to the transformed Jacobi set, then, by following the general relation in Eq. (5.68), we can also write

$$\mathcal{Y}^{KLM_L}_{[K]}(\Omega^{(k)}_N) = \sum_{[K']} \mathcal{P}^{KL(k)}_{[K][K']} \mathcal{Y}^{KLM_L}_{[K']}(\Omega_N) . \tag{5.71}$$

Essentially, the matrix of the coefficients $\mathcal{P}^{KL(k)}_{[K][K']}$ is the representation of the kinematic rotation $p_{k,k+1}$ on the HH basis. The HH functions are a complete and orthonormal set of functions, and therefore the coefficients can be calculated by means of the following relation

$$\mathcal{P}^{KL(k)}_{[K][K']} = \int d\Omega_N \left[\mathcal{Y}^{KLM_L}_{[K']}(\Omega_N)\right]^* \mathcal{Y}^{KLM_L}_{[K]}(\Omega^{(k)}_N) . \tag{5.72}$$

The operator $\mathcal{P}^{KL(k)}$, also denoted simply as $\mathcal{P}^{(k)}$, is unitary and it satisfies [92]

$$\mathcal{P}^{(k)}\mathcal{P}^{(k)} = 1 , \qquad \mathcal{P}^{(ab)} = \prod_{k=a}^{b-1} \mathcal{P}^{(k)} \prod_{k=b-2}^{a} \mathcal{P}^{(k)} , \quad a < b , \tag{5.73}$$

where $\mathcal{P}^{(ab)}$ is the transposition between the generic non–adjacent particles $(m_a,\boldsymbol{r}_a)$ and $(m_b,\boldsymbol{r}_b)$. As discussed above, in the practice we will only deal with transposition matrices of the type

$$\mathcal{P}^{(12,ij)} \equiv \mathcal{P}^{(2j)}\mathcal{P}^{(1i)} , \tag{5.74}$$

and we remark that they always correspond to the product of elementary transpositions $\mathcal{P}^{(k)}$ between adjacent particles. In this way $\mathcal{P}^{(12,ij)}$ is a product of block

diagonal matrices that can be calculated with no particular issues [28]. In a more extended notation we can write [100]

$$\mathcal{Y}^{KLM_L}_{[K]}(\Omega^{(ij)}_N) = \sum_{[K']} \mathcal{P}^{KL(ij,12)}_{[K][K']} \mathcal{Y}^{KLM_L}_{[K']}(\Omega^{(12)}_N)\,, \tag{5.75}$$

and it is straightforward that

$$\mathcal{P}^{KL(ij,12)}_{[K][K']} = \int d\Omega_N \left[\mathcal{Y}^{KLM}_{[K']}(\Omega^{(12)}_N)\right]^* \mathcal{Y}^{KLM}_{[K]}(\Omega^{(ij)}_N)\,, \tag{5.76}$$

where the HH functions denoted as $\mathcal{Y}^{KLM_L}_{[K]}(\Omega^{(12)}_N)$ and $\mathcal{Y}^{KLM_L}_{[K]}(\Omega^{(ij)}_N)$ are related to the set of Jacobi vectors in which $\boldsymbol{\eta}_N \propto (\boldsymbol{r}_2 - \boldsymbol{r}_1)$, i.e. the reference set, and $\boldsymbol{\eta}'_N \propto (\boldsymbol{r}_j - \boldsymbol{r}_i)$, respectively.

For completeness, following Refs. [92, 100], we report here the explicit form of the TC relative to the elementary transpositions. The trivial case $k = 1$ corresponds to the action of the operator $p_{1,2}$ and the result is a change of sign of the last Jacobi vector: $\boldsymbol{\eta}'_N = -\boldsymbol{\eta}_N$. This leads to a phase factor

$$\mathcal{P}^{KL(1)}_{[K][K']} = (-1)^{\ell_N} \delta_{[K][K']}\,. \tag{5.77}$$

The case $k = N$ involves the transformation of the Jacobi coordinates $\boldsymbol{\eta}_1$ and $\boldsymbol{\eta}_2$, which are already coupled in the grand–angular and angular space, and the coefficients $\mathcal{P}^{KL(N)}_{[K][K']}$ are the Raynal–Revai coefficients [102]

$$\mathcal{P}^{KL(N)}_{[K][K']} = \delta_{KK'} \left[\prod_{a=3}^{N} \delta_{\ell_a \ell'_a} \delta_{L_{a-1} L'_{a-1}} \delta_{K_{a-1} K'_{a-1}}\right] \mathcal{R}^{K_2, L_2}_{\ell_1 \ell_2, \ell'_1 \ell'_2}(\beta_N)\,, \tag{5.78}$$

where β_N is the kinematic angle defined in Eq. (5.70). Finally, in the general case $1 < k < N$, where the transformation involves the pair of vectors $\boldsymbol{\eta}_{N+1-k} \equiv \boldsymbol{\eta}_{i-1}$ and $\boldsymbol{\eta}_{N+1-k+1} \equiv \boldsymbol{\eta}_i$ with $3 \le i \le N$, the coefficients are

$$\begin{aligned} \mathcal{P}^{KL(k)}_{[K][K']} = &\left[\prod_{a=1}^{i-2} \delta_{\ell_a \ell'_a} \prod_{b=2}^{i-2} \delta_{L_b L'_b} \delta_{K_b K'_b}\right] \\ &\times {}^{(k)}\widetilde{\mathcal{P}}^{L_{i-2} K_{i-2},\, L_i K_i}_{\ell_{i-1} \ell'_{i-1},\, \ell_i \ell'_i,\, L_{i-1} K_{i-1},\, L'_{i-1} K'_{i-1}} \left[\prod_{a=i+1}^{N} \delta_{\ell_a \ell'_a} \prod_{b=i}^{N} \delta_{L_b L'_b} \delta_{K_b K'_b}\right] \end{aligned} \tag{5.79}$$

where the matrices ${}^{(k)}\widetilde{\mathcal{P}}$, after an angular and a hyperangular recoupling represented by the T– and $\mathcal{T}$–coefficients, respectively, can be written again in terms of the Raynal–Revai coefficients [102] as follows

$$\begin{aligned} {}^{(k)}\widetilde{\mathcal{P}}^{L_{i-2} K_{i-2},\, L_i K_i}_{\ell_{i-1} \ell'_{i-1},\, \ell_i \ell'_i,\, L_{i-1} K_{i-1},\, L'_{i-1} K'_{i-1}} = &\sum_{L_{i,i-1}} T^{L_{i-2} \ell_{i-1} \ell_i}_{L_{i-1} L_{i,i-1} L_i} T^{L_{i-2} \ell'_{i-1} \ell'_i}_{L'_{i-1} L_{i,i-1} L_i} \\ &\times \sum_{K_{i,i-1}} \mathcal{T}^{\alpha_{K_{i-2}} \alpha_{\ell_{i-1}} \alpha_{\ell_i}}_{K_{i-1} K_{i,i-1} K_i} \mathcal{T}^{\alpha_{K_{i-2}} \alpha_{\ell'_{i-1}} \alpha_{\ell'_i}}_{K'_{i-1} K_{i,i-1} K_i} \\ &\times \mathcal{R}^{K_{i,i-1}, L_{i,i-1}}_{\ell_{i-1} \ell_i, \ell'_{i-1} \ell'_i}(\beta_k)\,. \end{aligned} \tag{5.80}$$

In the relation above, the indices α_{ℓ_i} and α_{K_i} are explicitly $\alpha_{\ell_i} = \ell_i + \frac{1}{2}$ and $\alpha_{K_i} = K_i + \frac{3i}{2} - 1$. More details about the T– and $\mathcal{T}$– coefficients as well as their definition can be found in Refs. [92, 100, 104].

In order to generalize the formalism including also the spin and the isospin of the particles, we define the following operator [92]

$$\mathcal{Q}^{(12,ij)} = \mathcal{P}^{(12,ij)} \otimes \mathcal{S}^{(12,ij)} \otimes \mathcal{I}^{(12,ij)} , \tag{5.81}$$

where $\mathcal{P}^{(12,ij)}$ is the transposition matrix already defined in Eq. (5.74), while $\mathcal{S}^{(12,ij)}$ and $\mathcal{I}^{(12,ij)}$ are the operators relative to the spin and isospin spaces, respectively. In order to calculate the matrix elements of the most general potential operator $\hat{V}_{ij}$, also the total spin S_{ij}, the total isospin T_{ij} and the total J_{ij} of the ij–pair are needed. As one can see from Eqs. (5.41) and (5.44), the quantum numbers S_{ij} and T_{ij} do not appear in the spin and isospin reference coupling schemes, with the exception of the pair $i, j = A-1, A$. In this sense, the operator $\mathcal{S}^{(12,ij)}$ represents all the spin recouplings needed to change the reference scheme into a new one in which the single particle spins s_i and s_j, initially related to the positions i and j, are moved to 1 and 2 as follows

$$\begin{aligned} &\Big[\dots\big[\big[\dots\big[\dots\big]_{S_{A-j}}\chi_{s_j}(j)\big]_{S_{A-j+1}}\dots\big]_{S_{A-i}}\chi_{s_i}(i)\big]_{S_{A-i+1}}\dots\Big]_{SM_S} \\ &\to \Big[\big[\big[\dots\big]_{S'_{A-2}}\chi_{s_j}(2)\big]_{S'_{A-1}}\chi_{s_i}(1)\Big]_{SM_S} . \end{aligned} \tag{5.82}$$

Then the total spin of the pair S_{ij} can be extracted by using the Wigner $6j$ symbols

$$\Big[\big[\big[\dots\big]_{S'_{A-2}}\chi_{s_j}(2)\big]_{S'_{A-1}}\chi_{s_i}(1)\Big]_{SM_S} \to \Big[\big[\dots\big]_{S'_{A-2}}\big[\chi_{s_i}(1)\chi_{s_j}(2)\big]_{S_{ij}}\Big]_{SM_S} . \tag{5.83}$$

Of course, the same procedure can be used for the isospin basis to extract T_{ij}. Essentially, in the most general case, the operator $\mathcal{Q}^{(12,ij)}$ moves the two interacting particles in the first positions and changes the spin and the isospin bases so that S_{ij} and T_{ij} become good quantum numbers.

A few comments are here in order [92]. Since the spin (isospin) and the spatial basis are independent, one is free to choose a certain scheme for the initial spin (isospin) coupling, in order to reduce the number of recoupling operations needed to calculate a specific matrix element. This fact can also be exploited, for example, in an A–body system containing two particles of one species and $A-2$ particles of another species. Moreover, when the particles involved belong to the same species, the spatial part of the operator in Eq. (5.81) is a true spatial permutation that exchanges the particles i and j with 1 and 2. As a consequence, the fermionic or bosonic nature of the particles must be taken into account.

Notice that for the most general case of a non–central potential, an additional recoupling involving the Wigner $9j$ symbols must be applied in the construction of the correct spatial–spin basis:

$$\begin{aligned} &\Big[\Big[\mathcal{Y}^{K_{N-1}L_{N-1}}_{[K_{N-1}]}(\Omega_{N-1})\,Y_{\ell_N}(\hat{\eta}_N)\Big]_L\Big[\chi^{S_{A-2}}_{[S_{A-2}]}\,\chi_{S_{ij}}\Big]_S\Big]_{JM} \\ &\to \Big[\Big[\mathcal{Y}^{K_{N-1}L_{N-1}}_{[K_{N-1}]}(\Omega_{N-1})\,\chi^{S_{A-2}}_{[S_{A-2}]}\Big]_{J_{A-2}}\Big[Y_{\ell_N}(\hat{\eta}_N)\,\chi_{S_{ij}}\Big]_{J_{ij}}\Big]_{JM} , \end{aligned} \tag{5.84}$$

where the spin function $\chi_{S_{ij}M_{S_{ij}}}$ has been defined as $\chi_{S_{ij}M_{S_{ij}}} = \left[\chi_{s_i}\chi_{s_j}\right]_{S_{ij}M_{S_{ij}}}$ and the HH functions are those in Eq. (5.47).

We conclude with a few observations. The spin and isospin operators $\mathcal{S}^{(12,ij)}$ and $\mathcal{I}^{(12,ij)}$ can be constructed, just like the spatial one, as the product of the elementary operators $\mathcal{S}^{(k)}$ and $\mathcal{I}^{(k)}$, representing the permutations between two adjacent spin and isospin, respectively. $\mathcal{S}^{(k)}$ and $\mathcal{I}^{(k)}$ are defined in analogy to Eq. (5.71), and they are combinations of Wigner $6j$ symbols. We also point out that, for the most generic permutation p of particles, similarly to the general transformation defined in Eq. (5.68), the following relations are valid

$$\chi^{SM_S(p)}_{[S]} = \sum_{[S']} \mathcal{C}^{S(p,\bar{p})}_{[S][S']}\, \chi^{SM_S(\bar{p})}_{[S']}\,, \qquad \xi^{TM_T(p)}_{[T]} = \sum_{[T']} \mathcal{C}^{T(p,\bar{p})}_{[T][T']}\, \xi^{TM_T(\bar{p})}_{[T']}\,, \tag{5.85}$$

with the prescriptions $S' = S$ and $T' = T$, in which the spin and isospin functions in the reference permutation $\bar{p}$ are those defined in Eq. (5.41). More details about this can be found in Ref. [92].

Application: the two–body local potential

As already stated, the term of the two–body potential that enters in the Hamiltonian is of the form

$$V = \sum_{i<j}^{A} V_{ij}\,. \tag{5.86}$$

In order to see explicitly how the operators in Eq. (5.81) enter in the calculation of the two–body interaction, for simplicity we consider here a local potential of central type. Moreover, we focus first on the spatial part. If one takes the HH basis defined from the Jacobi vectors in the reference permutation, Eq. (5.3), then the matrix elements of the operator V_{ij} are

$$V^{ij}_{[K][K']}(\rho) = \left\langle \mathcal{Y}^{KLM_L}_{[K]}(\Omega^{(12)}_N) \,\middle|\, V(\boldsymbol{r}_{ij}) \,\middle|\, \mathcal{Y}^{KLM_L}_{[K']}(\Omega^{(12)}_N) \right\rangle\,, \tag{5.87}$$

where $\boldsymbol{r}_{ij} \equiv \boldsymbol{r}_j - \boldsymbol{r}_i$ and, specifically for $i, j = 1, 2$, we have

$$V^{12}_{[K][K']}(\rho) = \left\langle \mathcal{Y}^{KLM_L}_{[K]}(\Omega^{(12)}_N) \,\middle|\, V(\boldsymbol{r}_{12}) \,\middle|\, \mathcal{Y}^{KLM_L}_{[K']}(\Omega^{(12)}_N) \right\rangle\,. \tag{5.88}$$

If we rewrite Eq. (5.87) by making use of the TC defined in Eqs. (5.75), then we obtain [100]

$$V^{ij}_{[K][K']}(\rho) = \sum_{[K'']}\sum_{[K''']} \left\langle \mathcal{Y}^{KLM_L}_{[K'']}(\Omega^{(ij)}_N) \,\middle|\, \mathcal{P}^{KL(12,ij)\dagger}_{[K''][K]} V(\boldsymbol{r}_{ij}) \mathcal{P}^{KL(12,ij)}_{[K'][K''']} \,\middle|\, \mathcal{Y}^{KLM_L}_{[K''']}(\Omega^{(ij)}_N) \right\rangle. \tag{5.89}$$

Moreover, by using the expression in Eq. (5.88), together with the following equivalence

$$\begin{aligned} &\left\langle \mathcal{Y}^{KLM_L}_{[K'']}(\Omega^{(ij)}_N) \,\middle|\, V(\boldsymbol{r}_{ij}) \,\middle|\, \mathcal{Y}^{KLM_L}_{[K''']}(\Omega^{(ij)}_N) \right\rangle \\ &= \left\langle \mathcal{Y}^{KLM_L}_{[K'']}(\Omega^{(12)}_N) \,\middle|\, V(\boldsymbol{r}_{12}) \,\middle|\, \mathcal{Y}^{KLM_L}_{[K''']}(\Omega^{(12)}_N) \right\rangle\,, \end{aligned} \tag{5.90}$$

we can also write

$$V^{ij}_{[K][K']}(\rho) = \sum_{[K'']}\sum_{[K''']} \left\langle \mathcal{Y}^{KLM_L}_{[K'']}(\Omega^{(12)}_N) \,\middle|\, \mathcal{P}^{KL(12,ij)\dagger}_{[K''][K]} V(\boldsymbol{r}_{12}) \mathcal{P}^{KL(12,ij)}_{[K'][K''']} \,\middle|\, \mathcal{Y}^{KLM_L}_{[K''']}(\Omega^{(12)}_N) \right\rangle . \tag{5.91}$$

In a NSHH basis framework, when we work with a potential of a more general type, by taking into account also the spin and the isospin dependence, the equations above can be generalized to

$$\left\langle \Psi^{\mathrm{NSHH}} \,\middle|\, V_{ij} \,\middle|\, \Psi^{\mathrm{NSHH}} \right\rangle = \left\langle \Psi^{\mathrm{NSHH}} \,\middle|\, \mathcal{Q}^{(12,ij)\dagger}\, V_{12}\, \mathcal{Q}^{(12,ij)} \,\middle|\, \Psi^{\mathrm{NSHH}} \right\rangle \tag{5.92}$$

where we have used the operators $\mathcal{Q}^{(12,ij)}$ already introduced in Eq. (5.81).

5.2.3 Bound–state problem

The bound–state problem relative to the A–body nuclear system described by the Schrödinger equation (5.21) is solved by means of a variational method, and in conjunction with the NSHH basis constructed in Section 5.1.3. We use as trial wave function the truncated expansion over a basis in configuration space as in Eq. (5.64), whose coefficients are determined by solving $\delta \langle \Phi \,|\, T + V - E \,|\, \Phi \rangle = 0$. By performing explicitly the variation over the set of real expansion coefficients $\{\, c_\kappa \,\}$, we obtain

$$\sum_{\kappa'} \langle \Phi_\kappa \,|\, T + V - E \,|\, \Phi_{\kappa'} \rangle \, c_{\kappa'} = 0 \,, \tag{5.93}$$

with $\kappa \equiv [m\mu]$. By using this variational procedure, namely the Rayleigh–Ritz variational principle [105], the whole problem is essentially reduced to finding a solution to the above eigenvalues equation.

The fact that we do not impose any symmetry condition on the basis employed leads to the diagonalization of matrices with large dimension. As a consequence, also the number of eigenfunctions, whose symmetry have to be analysed, is large. In order to search for the true ground state with the correct symmetry, a method has been developed in Ref. [28], which uses the transposition class sum operator of the permutation group S_A, i.e. the Casimir operator. The advantage of using this approach is that, since the physical ground state is somehow shifted to coincide with the lowest eigenstate, the full diagonalization of the Hamiltonian matrix is not required, and one can use in the calculations, for instance, the Lanczos algorithm [58]. In this way the computational time is considerably reduced (see Appendix B).

If we start by considering a system of A identical particles, then the physical ground state with the desired symmetry can be selected by means of the Casimir operator $\hat{C}(A)$. This operator is defined as a summation of all the transposition operators between the particles i and j, as follows

$$\hat{C}(A) = \sum_{i<j=1}^{A} \hat{P}_{ij} \,. \tag{5.94}$$

Since it commutes with the Hamiltonian $\left[\hat{H}, \hat{C}(A)\right] = 0$, the two operators can be diagonalized simultaneously. More mathematical details about the Casimir operators can be found in Ref. [106]. Here we only mention the following important

property: given a generic symmetric $|\Phi^s\rangle$, mixed–symmetry $|\Phi^m\rangle$ and antisymmetric $|\Phi^a\rangle$ eigenstate, then we have

$$\hat{C}(A)\,|\Phi^s\rangle = \lambda^s\,|\Phi^s\rangle\,, \quad \hat{C}(A)\,|\Phi^m\rangle = \lambda^m\,|\Phi^m\rangle\,, \quad \hat{C}(A)\,|\Phi^a\rangle = \lambda^a\,|\Phi^a\rangle\,, \tag{5.95}$$

with $\lambda_s > \lambda_m > \lambda_a$, where the eigenvalues relative to the symmetric and the antisymmetric states assume the extreme values

$$\lambda^s = \frac{A(A-1)}{2}\,, \qquad\qquad \lambda^a = -\frac{A(A-1)}{2}\,. \tag{5.96}$$

We proceed by defining a pseudo–Hamiltonian $\hat{\mathcal{H}}$ as follows [28]

$$\hat{\mathcal{H}} = \hat{H} + \gamma\hat{C}(A)\,, \tag{5.97}$$

where γ is a real parameter. The corresponding eigenvalues are

$$\mathcal{E}^x_n = E^x_n + \gamma\lambda^x\,, \tag{5.98}$$

with E^x_n the eigenvalues of the Hamiltonian operator $\hat{H}$ with symmetry $x = s, m, a$. The index n runs from 0 to $n_{\max}(x)$, and $\sum_x n_{\max}(x)$ gives the total dimension of the basis. For instance, if our aim is to calculate E^a_0, which is the lowest antisymmetric eigenvalue of the Hamiltonian $\hat{H}$, then we must choose a value for the parameter γ such that $\mathcal{E}^a_0$ results to be, by far, the lowest eigenvalue of the pseudo–Hamiltonian $\hat{\mathcal{H}}$. This requirement corresponds to the following inequality

$$\mathcal{E}^a_0 = E^a_0 + \gamma\lambda^a < E^x_n + \gamma\lambda^x\,, \qquad n = 0, 1, \ldots, n_{\max}(x), \quad x = s, m\,, \tag{5.99}$$

from which a condition on the parameter γ follows

$$\gamma > \frac{E^a_0 - E^x_n}{\lambda^x - \lambda^a}\,. \tag{5.100}$$

If one now notes that $\lambda^x - \lambda^a \geq A$, by assuming $E^a_0 < 0$, it is sufficient to impose

$$\gamma > \frac{|E_{\min}|}{A}\,, \tag{5.101}$$

with $E_{\min}$ the lowest eigenvalue of the Hamiltonian, $E_{\min} = \min\{E^s_0, E^m_0, E^a_0\}$. This method allows to obtain the lowest physical antisymmetric state of the Hamiltonian in terms of the lowest state of the pseudo–Hamiltonian. At the end of the procedure, the eigenvalue E^a_0 can be recovered by subtraction: $\mathcal{E}^a_0 - \gamma\lambda^a$. With the same technique, one can also calculate the physical totally symmetric lowest state.

If we are studying a system composed of A non–identical particles, then the generalization of the method is quite straightforward [92]. The definition of the Casimir operator must be generalized to include different species of particles. In this case, $\hat{C}(A)$ is the sum of $\sigma_{\max}$ Casimir operators relative to each different subsystem of A_σ particles of the same species σ

$$\hat{C}(A) = \sum_{\sigma=1}^{\sigma_{\max}} b_{x_\sigma}\hat{C}_\sigma(A_\sigma)\,, \qquad\qquad \hat{C}_\sigma(A_\sigma) = \sum_{i<j=1}^{A_\sigma} \hat{P}_{ij}\,, \tag{5.102}$$

where the coefficients b_{x_σ} depend on the symmetry of each subsystem ($b_{x_\sigma} = 1$ for $x = a, m$ and $b_{x_\sigma} = -1$ for $x = s$) and $\sum_{\sigma=1}^{\sigma_{\max}} A_\sigma = A$. Moreover, $\hat{C}_\sigma(A_\sigma = 1) = 0$. The Casimir operator still commutes with the hamiltonian $\hat{H}$. The eigenvalues of the pseudo–Hamiltonian $\hat{\mathcal{H}}$ defined as in Eq. (5.97) are now

$$\mathcal{E}_n^x = E_n^x + \gamma \sum_{\sigma=1}^{\sigma_{\max}} b_{x_\sigma} \lambda^{x_\sigma} , \tag{5.103}$$

with $n = 0, 1, \ldots, n_{\max}(x)$. If we want to find the lowest eigenvalue $E_0^{\bar{x}}$ with symmetry $\bar{x} = s, a$, then γ must be chosen large enough so that $\mathcal{E}_0^{\bar{x}}$ is the lowest eigenvalue of the pseudo–Hamiltonian, and therefore we must have

$$\mathcal{E}_0^{\bar{x}} = E_0^{\bar{x}} + \gamma \sum_{\sigma=1}^{\sigma_{\max}} b_{\bar{x}_\sigma} \lambda^{\bar{x}_\sigma} < E_n^x + \gamma \sum_{\sigma=1}^{\sigma_{\max}} b_{x_\sigma} \lambda^{x_\sigma} , \quad n = 0, 1, \ldots, n_{\max}(x), \;\; x \neq \bar{x} . \tag{5.104}$$

From this relation, we obtain a condition for the parameter γ similar to Eq. (5.100)

$$\gamma > \frac{E_0^{\bar{x}} - E_n^x}{\sum_{\sigma=1}^{\sigma_{\max}} (b_{x_\sigma} \lambda^{x_\sigma} - b_{\bar{x}_\sigma} \lambda^{\bar{x}_\sigma})} , \tag{5.105}$$

as well as the following lower limit

$$\gamma > \frac{|E_{\min}|}{\sum_{\sigma=1}^{\sigma_{\max}} A_\sigma} , \tag{5.106}$$

where $A_\sigma \neq 1$.

In the rest of this Section, we will explicitly compute the matrix elements of the operators involved in the eigenvalues equation (5.93).

Norm and kinetic energy matrix elements

The norm and the internal kinetic energy matrix elements are defined as

$$\langle \Phi_{m\mu} | \Phi_{m'\mu'} \rangle = \delta_{mm'} \delta_{\mu\mu'} , \qquad \langle \Phi_{m\mu} | T | \Phi_{m'\mu'} \rangle = T_{mm'} \delta_{\mu\mu'} , \tag{5.107}$$

where the delta on the Laguerre basis indices, $\delta_{mm'}$, comes from the orthonormality relation (5.63) while the deltas on the HH, spin and isospin collective indices, $\delta_{\mu\mu'}$, are due to the orthonormality of the functions $\mathcal{Y}_\mu^{JM\pi}(\Omega_N)$ in Eq. (5.61). The matrix $T_{mm'}$ is explicitly

$$T_{mm'} = -\frac{\hbar^2}{2m_{\text{ref}}} \int d\rho \, \rho^{3N-1} f_m(\rho) \left[\frac{\partial^2}{\partial \rho^2} + \frac{3N-1}{\rho} \frac{\partial}{\partial \rho} - \frac{K(K+3N-2)}{\rho^2} \right] f_{m'}(\rho) . \tag{5.108}$$

The two–body local potential matrix elements

Concerning the calculation of the matrix elements of the two–body local potential operator V, first we apply the rotation operators $\mathcal{Q}^{(12,ij)}$ as in Eq. (5.92)

$$V = \sum_{i<j=1}^{A} V_{ij} = \sum_{i<j=1}^{A} \mathcal{Q}^{(12,ij)\dagger} \, V_{12} \, \mathcal{Q}^{(12,ij)} \tag{5.109}$$

then, we are left with the calculation of the matrix elements $\langle\Phi_{m\mu}|V_{12}|\Phi_{m'\mu'}\rangle$. The proper NSHH basis to use is the one in Eq. (5.55) but constructed with different coupling schemes. We define $\widetilde{\Phi}_{m\mu}(\rho,\Omega_N) = f_m(\rho)\widetilde{\mathcal{Y}}^{JM\pi}_{\mu}(\Omega_N)$, where the functions $\widetilde{\mathcal{Y}}^{JM\pi}_{\mu}(\Omega_N)$ follow the orbital–spin recoupling defined in Eq. (5.84), together with the isospin recoupling defined by analogy with Eq. (5.83). Notice that the new scheme is related to the old one by the Wigner $6j$ and $9j$ coefficients. Then, it can be demonstrated that the matrix elements of the potential operator of local type can be written as

$$\begin{aligned}\langle\widetilde{\Phi}_{m\mu}|V_{12}|\widetilde{\Phi}_{m'\mu'}\rangle &= \delta_{\{K_{N-1}\}\{K'_{N-1}\}}\delta_{\{S_{A-2}\}\{S'_{A-2}\}}\delta_{\{T_{A-2}\}\{T'_{A-2}\}} \\ &\times \int d\rho_{N-1}\,\rho_{N-1}^{3(N-1)-1}\int d\eta_N\,\eta_N^2\,{}^N\mathcal{P}^{\ell_N,K_{N-1}}_{n_N}(\varphi_N) f_m(\rho) \\ &\times V^{J_{12}}_{K_N\ell_N S_{12}T_{12},K'_N\ell'_N S'_{12}T'_{12}}(r_{12})\,{}^N\mathcal{P}^{\ell'_N,K_{N-1}}_{n'_N}(\varphi_N)\, f_{m'}(\rho)\,.\end{aligned} \tag{5.110}$$

In the equation above we have already performed the integration in the variables $d\Omega_{N-1}$, the HH polynomials are those defined in Eq. (5.50) and explicitly we have $\eta_N = \rho\sin\varphi_N$. Moreover, the matrix elements $V^{J_{12}}_{K_N\ell_N S_{12}T_{12},K'_N\ell'_N S'_{12}T'_{12}}(r_{12})$ are

$$V^{J_{12}}_{K_N\ell_N S_{12}T_{12},K'_N\ell'_N S'_{12}T'_{12}}(r_{12}) = \int d\hat{\eta}_N \left[Y_{\ell_N}(\hat{\eta}_N)\,\chi_{S_{12}}\right]^{\dagger}_{J_{12}} V(\boldsymbol{r}_{12})\left[Y_{\ell'_N}(\hat{\eta}_N)\,\chi_{S'_{12}}\right]_{J_{12}}. \tag{5.111}$$

Notice that $\boldsymbol{r}_{12}\equiv\boldsymbol{r}_2-\boldsymbol{r}_1$ and, from the definition of the Jacobi vectors in Eq. (5.3), we have

$$\boldsymbol{r}_2-\boldsymbol{r}_1 = \sqrt{\frac{m_{\rm r}M_2}{m_1m_2}}\boldsymbol{\eta}_N \equiv C^{\eta}_{12}\boldsymbol{\eta}_N\,, \tag{5.112}$$

from which we deduce that the proportionality factor C^{η}_{12} between the quantity $\boldsymbol{r}_{12}$ and the last Jacobi coordinate $\boldsymbol{\eta}_N$ depends entirely on the masses of the first two particles. Further details about the calculation of the potential matrix elements can be found in Ref. [92].

5.3 Momentum space

Here we want to study the nuclear problem of A interacting particles by finding a solution of the Schrödinger equation (5.1) in momentum space,

$$\hat{H}\,|\Psi_A\rangle = E_{\rm tot}\,|\Psi_A\rangle\,, \tag{5.113}$$

where the wave function is $\langle\boldsymbol{p}_1,\ldots,\boldsymbol{p}_A|\Psi_A\rangle = \Psi_A(\boldsymbol{p}_1,\ldots,\boldsymbol{p}_A)$. We will mainly follow the formalism already developed in Section 5.1 for the solution in coordinate space. In Section 5.3.1 we will introduce the Jacobi momenta and the corresponding set of hyperspherical coordinates, and we will perform a separation of the center–of–mass motion from the internal one. By taking into account only the internal degrees of freedom, in Section 5.3.2 we will construct a proper basis in momentum space to expand the wave function. The last Section 5.3.3 is dedicated to the solution of the bound–state problem, by means of the NSHH method already introduced in Section 5.2 for the configuration space case.

5.3.1 Jacobi and Hyperspherical coordinates

Starting from the set of Jacobi coordinates in Eq. (5.3), the Jacobi momenta are defined by means of the following relation

$$\boldsymbol{\pi}_{N+1-j} = -i\hbar\boldsymbol{\nabla}_{\boldsymbol{\eta}_{N+1-j}} = -i\hbar\sum_{i=1}^{N}\frac{\partial \boldsymbol{r}_i}{\partial \boldsymbol{\eta}_{N+1-j}}\frac{\partial}{\partial \boldsymbol{r}_i} = \sum_{i=1}^{N}\frac{\partial \boldsymbol{r}_i}{\partial \boldsymbol{\eta}_{N+1-j}}\boldsymbol{p}_i\,. \tag{5.114}$$

By making use of the vector–matrix notation already introduced in 5.1.1, the relation above can be written as $\vec{\boldsymbol{\pi}} = \sqrt{m_{\rm r}}\,\mathcal{A}\,\vec{\boldsymbol{p}}$, where $\vec{\boldsymbol{\pi}} = (\boldsymbol{\pi}_N, \ldots, \boldsymbol{\pi}_1, \boldsymbol{\pi}_0)$ is the vector of the Jacobi momenta, $\vec{\boldsymbol{p}} = (\boldsymbol{p}_1, \ldots, \boldsymbol{p}_A)$ is the vector of the momenta of the particles and the matrix $\mathcal{A}$ is the one defined in Eq. (5.8). The mass $m_{\rm r}$ is a reference mass, and in the practical calculations we will set it equal to the nucleon mass. With the construction procedure above, $\boldsymbol{\eta}_i$ and $\boldsymbol{\pi}_i$ are conjugate variables

$$\left[\eta^i_k, \pi^{i'}_{k'}\right] = i\hbar\delta_{kk'}\delta_{ii'}\,, \tag{5.115}$$

where the indices k and k' refer to the cartesian components, while $i, i' = 0, 1, \ldots, N$. In a more extended way we write

$$\boldsymbol{\pi}_{N+1-j} = \sqrt{\frac{m_{\rm r}M_j}{M_{j+1}m_{j+1}}}\left(\boldsymbol{p}_{j+1} - \frac{m_{j+1}}{M_j}\sum_{i=1}^{j}\boldsymbol{p}_i\right), \qquad j = 1, \ldots, N\,, \tag{5.116}$$

$$\boldsymbol{\pi}_0 = \sqrt{\frac{m_{\rm r}}{M}}\sum_{i=1}^{A}\boldsymbol{p}_i\,, \tag{5.117}$$

where M_j is the sum of the masses up to particle j, and M is the total mass. We underline that the Jacobi vector $\boldsymbol{\pi}_0$ is simply proportional to the center–of–mass momentum of the system $\boldsymbol{P}_{\rm cm}$. Within this formalism the total kinetic energy in Eq. (5.1) assumes the simple form

$$T = \frac{1}{2m_{\rm r}}\vec{\boldsymbol{\pi}}^t\vec{\boldsymbol{\pi}} = \frac{\boldsymbol{P}^2_{\rm cm}}{2M} + \frac{1}{2m_{\rm r}}\sum_{j=1}^{N}\boldsymbol{\pi}^2_{N+1-j}\,, \tag{5.118}$$

where we have used the definition of the vector $\boldsymbol{\pi}_0$ in (5.117). The last term corresponds to the internal kinetic energy, and it results to be completely separated from the kinetic energy of the center–of–mass.

If we focus on the internal Jacobi vectors, in order to describe the space of vectors $\{\,\boldsymbol{\pi}_1, \ldots, \boldsymbol{\pi}_N\,\}$ of dimension $3N$, we can use the alternative set of hyperspherical coordinates

$$\{\,Q, \Omega^{(Q)}_N\,\} = \{\,Q, \hat{\pi}_1, \ldots, \hat{\pi}_N, \varphi_2, \ldots, \varphi_N\,\}\,. \tag{5.119}$$

The hypermomentum Q is defined as

$$Q_i = \sqrt{\pi_1^2 + \cdots + \pi_i^2}\,, \qquad\qquad Q_N \equiv Q\,, \tag{5.120}$$

and the superscript (Q) on the angular and hyperangular part $\Omega^{(Q)}_N$ is a reminder that the hyperspherical coordinates are defined in momentum space. With $\hat{\pi}_i$ we denote the direction of each Jacobi vector $\boldsymbol{\pi}_i$, and φ_i are the $N-1$ hyperangles

$$\varphi_i = \arcsin\frac{\pi_i}{Q_i}\,, \qquad\qquad i = 2, \ldots, N\,, \tag{5.121}$$

with $0 \leq \varphi_i \leq \frac{\pi}{2}$. The modulus of each Jacobi momentum is related to the hyperspherical coordinates as follows

$$\begin{cases} \pi_N = Q \sin\varphi_N \,, \\ \quad \vdots \\ \pi_i = Q \cos\varphi_N \ldots \cos\varphi_{i+1} \sin\varphi_i \,, \qquad i = 2, \ldots, N-1 \,, \\ \quad \vdots \\ \pi_1 = Q \cos\varphi_N \ldots \cos\varphi_2 \,. \end{cases} \tag{5.122}$$

The volume element relative to the Jacobi vectors $d^3\boldsymbol{\pi}_1 \ldots d^3\boldsymbol{\pi}_N$ in the hyperspherical formalism is

$$d^3\boldsymbol{\pi}_1 \ldots d^3\boldsymbol{\pi}_N = d\Omega_N^{(Q)}\, dQ\, Q^{3N-1} \,, \tag{5.123}$$

with the definition

$$d\Omega_N^{(Q)} = \left[\prod_{i=1}^{N} d\hat{\pi}_i\right] \left[\prod_{j=2}^{N} d\varphi_j \,(\cos\varphi_j)^{3j-4} (\sin\varphi_j)^2\right] . \tag{5.124}$$

By using the definition of the hypermomentum Q given in Eq. (5.120), the internal kinetic energy of the system, already calculated in Eq. (5.118), assumes the very simple form

$$T_{\rm int} = \frac{1}{2m_{\rm r}} \sum_{i=1}^{N} \boldsymbol{\pi}_i^2 = \frac{Q^2}{2m_{\rm r}} \,. \tag{5.125}$$

As a consequence, the Schrödinger equation relative to the internal degrees of freedom of the A–body nuclear system, in momentum space, reads

$$\left[\frac{Q^2}{2m_{\rm r}} + V\right] \Psi(\boldsymbol{\pi}_1, \ldots, \boldsymbol{\pi}_N) = E\, \Psi(\boldsymbol{\pi}_1, \ldots, \boldsymbol{\pi}_N) \,. \tag{5.126}$$

In the following we will expand the internal wave function written above on a proper basis, including the spatial, the spin and the isospin degrees of freedom.

5.3.2 The p–spatial, spin and isospin basis

The formalism already developed in configuration space to construct the basis of the HH functions, including the spin and the isospin degrees of freedom, remains valid also in momentum space (see Sections 5.1.2 and 5.1.3).

We write the internal wave function of the system as

$$\Psi(\boldsymbol{\pi}_1, \ldots, \boldsymbol{\pi}_N) = \sum_{\kappa} c_\kappa \Psi_\kappa(Q, \Omega_N^{(Q)}) \,, \tag{5.127}$$

with the coefficients c_κ to be determined variationally. The basis that we use in momentum space is explicitly

$$\langle \boldsymbol{\pi}_1, \ldots, \boldsymbol{\pi}_N | \Psi_\kappa \rangle = \langle Q\, \Omega_N^{(Q)} | \Psi_\kappa \rangle \equiv \Psi_\kappa(Q, \Omega_N^{(Q)}) \,, \tag{5.128}$$

with the definition

$$\Psi_\kappa(Q,\Omega_N^{(Q)}) = \mathcal{N} f_m(Q)\, \mathcal{Y}_\mu^{JM\pi}(\Omega_N^{(Q)})\,, \qquad \kappa \equiv [m,\mu]\,, \tag{5.129}$$

where $\mathcal{N}$ is a normalization factor.

In the most general case, the functions $\mathcal{Y}_\mu^{JM\pi}(\Omega_N^{(Q)})$, with $\mu = [K][S][T]KLST$, are eigenfunctions of the total angular momentum operator $\hat{\boldsymbol{J}}$, $\hat{J}_z$ and of the parity operator $\hat{\Pi}$ [see Eq. (5.55)]. Due to the form of the interaction potentials employed, in this work we will use these basis functions in the form

$$\mathcal{Y}_{[K][S][T]}^{JM\pi,KLST}(\Omega_N^{(Q)}) = \mathcal{Y}_{[K]}^{KLM_L}(\Omega_N^{(Q)}) \chi_{[S]}^{SM_S} \xi_{[T]}^{TM_T}\,, \tag{5.130}$$

where also the total orbital angular momentum L and total spin S are good quantum numbers [see Eq. (5.59)].

The HH functions in momentum space are constructed as

$$\begin{aligned}\mathcal{Y}_{[K]}^{KLM_L}(\Omega_N^{(Q)}) = &\Big[\big[\dots\big[[Y_{\ell_1}(\hat{\pi}_1)Y_{\ell_2}(\hat{\pi}_2)]_{L_2} Y_{\ell_3}(\hat{\pi}_3)\big]_{L_3}\dots\big]_{L_{N-1}} Y_{\ell_N}(\hat{\pi}_N)\Big]_{LM_L} \\ &\times \prod_{j=2}^{N} {}^j\mathcal{P}_{n_j}^{K_{j-1},\ell_j}(\varphi_j)\,,\end{aligned} \tag{5.131}$$

with the HH polynomial ${}^j\mathcal{P}_{n_j}^{K_{j-1},\ell_j}(\varphi_j)$ defined as in Eq. (5.50). The spin and the isospin functions in (5.130) are the same as those reported in Eqs. (5.41) and (5.44), respectively.

Concerning the definition of the "hypermomental" functions $f_m(Q)$ that appear in Eq. (5.129), we follow the formalism developed in Ref. [107]. Although other choices are possible, we take these functions in the form

$$f_m(Q) = \left(\frac{1}{\beta}\right)^{\frac{3N}{2}} \sqrt{\frac{m!}{(m+3N-1)!}}\, L_m^{(3N-1)}\left(\frac{Q}{\beta}\right) \mathrm{e}^{-\frac{Q}{2\beta}}\,. \tag{5.132}$$

Essentially, by analogy with the definition in configuration space, Eq. (5.62), we use also here a Laguerre polynomials basis set $L_m^{(\alpha)}(x)$ to express $f_m(Q)$. The exponential decreasing factor regulates the behaviour of the functions at large Q, and β is a non–linear parameter. Due to the normalization factor inserted in the definition (5.132), we also have

$$\int_0^\infty dQ\, Q^{3N-1} f_m(Q) f_{m'}(Q) = \delta_{mm'}\,. \tag{5.133}$$

Further details about the Laguerre polynomials are reported in Appendix D.2.

5.3.3 Bound–state problem

By using the Rayleigh–Ritz variational principle [105], the bound–state problem is reduced to finding a solution of the following eigenvalues equation

$$\sum_{\kappa'} \langle \Psi_\kappa \,|\, T + V - E \,|\, \Psi_{\kappa'} \rangle\, c_{\kappa'} = 0\,, \tag{5.134}$$

with the collective index κ defined as $\kappa = [m, \mu]$.

As thoroughly discussed in Section 5.2, our approach is based on the use of a NSHH basis. The whole formalism of the pseudo–Hamiltonian, together with the procedure developed in 5.2.3, which is necessary to select the physical ground state, can be extended to the problem in momentum space with no particular issues. Therefore, in the rest of this Section, we will only focus on the detailed calculation of the matrix elements appearing in Eq. (5.134).

Norm and kinetic energy matrix elements

The matrix elements of the norm and the internal kinetic energy to be calculated are the following

$$\langle \Psi_{m\mu} | \Psi_{m'\mu'} \rangle = \delta_{mm'}\delta_{\mu\mu'} \,, \qquad \langle \Psi_{m\mu} | T | \Psi_{m'\mu'} \rangle = T_{mm'}\delta_{\mu\mu'} \,, \tag{5.135}$$

where the delta function $\delta_{mm'}$ on the Laguerre indices follows from the orthonormality of the basis functions defined in Eq. (5.132), as explicitly shown in Eq. (5.133); the delta functions $\delta_{\mu\mu'}$ comes from the orthonormality of the HH, spin and isospin functions $\mathcal{Y}^{JM\pi}_{\mu}(\Omega^{(Q)}_N)$, just as in the coordinate space case. The explicit expression of the matrix elements of the internal kinetic energy follows from Eq. (5.125), and they are simply given by

$$T_{mm'} = \frac{\hbar^2}{2m_{\mathrm{r}}} \int dQ\, Q^{3N+1} f_m(Q) f_{m'}(Q) \,. \tag{5.136}$$

To obtain these results, the normalization factor in Eq. (5.129) has been chosen as $\mathcal{N} = (2\pi)^{3N/2}$, following from the convention

$$\Omega^N \int \frac{d^3\boldsymbol{\pi}_1}{(2\pi)^3} \cdots \frac{d^3\boldsymbol{\pi}_N}{(2\pi)^3} \, |\boldsymbol{\pi}_1 \ldots \boldsymbol{\pi}_N\rangle \langle \boldsymbol{\pi}_1 \ldots \boldsymbol{\pi}_N| = 1 \,, \tag{5.137}$$

which will be used throughout this work, specifically with the normalization volume set to $\Omega = 1$.

The two–body potential matrix elements

The computation of the potential matrix elements is a little more involved. Here we will specialize the calculation to a central potential that does not depend on the spin or isospin of the particles involved. The effective potentials derived in Chapter 4 are in fact of this type. Moreover, they depend on the relative momenta between the two particles before and after the interaction. Specifically, we will follow the calculation entirely developed in Ref. [107].

First we apply the rotation coefficients as in Eq. (5.92)

$$V = \sum_{i<j=1}^{A} V_{ij} = \sum_{i<j=1}^{A} \mathcal{P}^{(12,ij)\dagger} \, V_{12} \, \mathcal{P}^{(12,ij)} \,, \tag{5.138}$$

and then we calculate the matrix elements $\langle \Psi_{m\mu} | V_{12} | \Psi_{m'\mu'} \rangle$ in momentum space by making use of the basis (5.130). By assuming that the potential does not depend

on the spin and the isospin of the particles, both spin and isospin parts of the basis give rise to delta functions, and therefore we can consider only

$$\Psi_{m\mu}(Q,\Omega_N^{(Q)}) = \mathcal{N} f_m(Q) \mathcal{Y}_{[K]}^{KLM_L}(\Omega_N^{(Q)})\,. \tag{5.139}$$

The HH functions are those defined in Eq. (5.131), which we rewrite here as

$$\mathcal{Y}_{[K]}^{KLM_L}(\Omega_N^{(Q)}) = \left[\mathcal{Y}_{[K_{N-1}]}^{K_{N-1}L_{N-1}}(\Omega_{N-1}^{(Q)})\, Y_{\ell_N}(\hat{\pi}_N)\right]_{LM_L}{}^N\mathcal{P}_{n_N}^{\ell_N,K_{N-1}}(\varphi_N)\,. \tag{5.140}$$

The two–body interaction operator V_{12} represented in momentum space assumes the form $V(\boldsymbol{p}_{12},\boldsymbol{p}'_{12})$, where the relative momentum between the particles 1 and 2 is explicitly

$$\boldsymbol{p}_{12} \equiv \frac{m_1\boldsymbol{p}_2 - m_2\boldsymbol{p}_1}{m_1+m_2}\,, \tag{5.141}$$

and we have the following proportionality relation between $\boldsymbol{p}_{12}$ and $\boldsymbol{\pi}_N$

$$\boldsymbol{p}_{12} = \sqrt{\frac{m_1 m_2}{m_{\rm r} M_2}}\boldsymbol{\pi}_N \equiv C_{12}^{\pi}\boldsymbol{\pi}_N\,. \tag{5.142}$$

The equation above follows from the definition of the Jacobi momentum $\boldsymbol{\pi}_N$ given in Eq. (5.116). The dependence of the potential on the quantity $\boldsymbol{p}'_{12}$ is taken into account by introducing a second set of Jacobi momenta $\{\boldsymbol{\pi}_1,\ldots,\boldsymbol{\pi}_{N-1},\boldsymbol{\pi}'_N\}$, in which only the last vector is changed. In this way, the matrix elements can be written explicitly as

$$\begin{aligned}\langle\Psi_{m\mu}|V_{12}|\Psi_{m'\mu'}\rangle = \frac{1}{(2\pi)^3}\int d^3\boldsymbol{\pi}_1\ldots d^3\boldsymbol{\pi}_{N-1}\, d^3\boldsymbol{\pi}_N\, d^3\boldsymbol{\pi}'_N \left[\mathcal{Y}_{[K]}^{KLM_L}(\Omega_N^{(Q)})\right]^\dagger \\ \times f_m(Q) V(\boldsymbol{p}_{12},\boldsymbol{p}'_{12}) f_{m'}(Q')\, \mathcal{Y}_{[K']}^{KLM_L}(\Omega_N^{\prime(Q)})\,.\end{aligned} \tag{5.143}$$

The set of hyperspherical coordinates $\{Q',\Omega_N^{\prime(Q)}\}$ is the one constructed from the new set of Jacobi momenta, hence we have that

$$Q' = \sqrt{\pi_1^2+\cdots+\pi_{N-1}^2+\pi_N'^2}\,, \qquad\qquad \pi'_N = Q'\sin\varphi'_N\,. \tag{5.144}$$

By making use of the relation

$$\cos^2\varphi'_N = \frac{Q^2}{Q'^2}\cos^2\varphi_N\,, \tag{5.145}$$

which follows from the identity $Q^2-\pi_N^2 = Q'^2-\pi_N'^2$, the volume element $d^3\boldsymbol{\pi}'_N$ can be written as

$$d^3\boldsymbol{\pi}'_N = d\hat{\pi}'_N\, d\pi'_N\, \pi_N'^2 = d\hat{\pi}'_N\, dQ' Q'^2 \sin\varphi'_N\,. \tag{5.146}$$

At the same time, from the expression of the volume element in Eq. (5.123) it can be deduced that

$$d^3\boldsymbol{\pi}_1\ldots d^3\boldsymbol{\pi}_{N-1}\, d^3\boldsymbol{\pi}_N = d\Omega_{N-1}^{(Q)}\, dQ_{N-1}\, Q_{N-1}^{3N-4}\, d\hat{\pi}_N\, d\pi_N\, \pi_N^2 \tag{5.147a}$$

$$= d\Omega_{N-1}^{(Q)}\, d\hat{\pi}_N\, d\varphi_N\, (\cos\varphi_N)^{3N-4}(\sin\varphi_N)^2\, dQ\, Q^{3N-1} \tag{5.147b}$$

Starting from Eq. (5.143), as a first step, we use the expression of the HH functions given in (5.140), and we perform the integration in $d\Omega^{(Q)}_{N-1}$, obtaining

$$
\begin{aligned}
I_1 &= \int d\Omega^{(Q)}_{N-1} \Big[\mathcal{Y}^{K_{N-1}L_{N-1}}_{[K_{N-1}]}(\Omega^{(Q)}_{N-1})\, Y_{\ell_N}(\hat{\pi}_N)\Big]^{\dagger}_{LM_L} \Big[\mathcal{Y}^{K'_{N-1}L'_{N-1}}_{[K'_{N-1}]}(\Omega^{(Q)}_{N-1})\, Y_{\ell'_N}(\hat{\pi}_N)\Big]_{LM_L} \\
&= \sum_{\substack{m_N M_{L_{N-1}} \\ m'_N M'_{L_{N-1}}}} (\ell_N m_N L_{N-1} M_{L_{N-1}} | L M_L)\, (\ell'_N m'_N L'_{N-1} M'_{N-1} | L M_L) \\
&\quad \times Y^*_{\ell_N m_N}(\hat{\pi}_N) Y_{\ell'_N m'_N}(\hat{\pi}'_N) \\
&\quad \times \delta_{[K_{N-1}][K'_{N-1}]} \delta_{K_{N-1}K'_{N-1}} \delta_{L_{N-1}L'_{N-1}} \delta_{M_{L_{N-1}} M'_{L_{N-1}}}\,,
\end{aligned}
\tag{5.148}
$$

where we have extracted the part dependent on the angular variables $\Omega^{(Q)}_{N-1}$ with the help of the Clebsch–Gordan coefficients. The second step regards the calculation of the integral in the angular variables $d\hat{\pi}_N\, d\hat{\pi}'_N$. As shown in detail in Ref. [107], in order to perform this integral, we use the technique described in Ref. [108], which leads to

$$
\begin{aligned}
I_2 &= \int d\hat{\pi}_N\, d\pi_N\, \pi_N^2\, d\hat{\pi}'_N\, d\pi'_N\, \pi'^2_N\, Y^*_{\ell_N m_N}(\hat{\pi}_N)\, V(\boldsymbol{\pi}_N, \boldsymbol{\pi}'_N)\, Y_{\ell'_N m'_N}(\hat{\pi}'_N) \\
&= \delta_{\ell_N \ell'_N} \delta_{m_N m'_N} \frac{8\pi^2}{2\ell_N + 1} \int dt\, d\pi_N\, \pi_N^2\, d\pi'_N\, \pi'^2_N \\
&\quad \times \sum_{m=-\ell_N}^{\ell_N} Y^*_{\ell_N m}(\hat{\pi}''_N)\, V(\pi_N, \pi'_N, t)\, Y_{\ell_N m}(\hat{\pi}'''_N) \qquad (5.149a) \\
&= \delta_{\ell_N \ell'_N} \delta_{m_N m'_N}\, 4\pi \int d\pi_N\ \pi_N^2\, d\pi'_N\, \pi'^2_N\, V_{\ell_N}(\pi_N, \pi'_N)\,. \qquad (5.149b)
\end{aligned}
$$

In performing the explicit calculation of the spherical harmonics functions appearing in Eq. (5.149a), we have used the following standard definition

$$
Y_{\ell m}(\theta, \phi) = (-1)^m \sqrt{\frac{2\ell + 1}{4\pi}} \sqrt{\frac{(\ell - m)!}{(\ell + m)!}} P_{\ell m}(\cos\theta) e^{im\phi}\,, \tag{5.150}
$$

where $P_{\ell m}(\cos\theta)$ are the associated Legendre polynomials. As a consequence, $Y_{\ell_N m}(\hat{\pi}''_N)$, where $\hat{\pi}''_N = (\theta''_N, \phi''_N) = (0, 0)$, is simply proportional to the delta function δ_{m0}; the calculation of $Y_{\ell_N m}(\hat{\pi}'''_N)$ in the direction $\hat{\pi}'''_N = (\theta'''_N, \phi'''_N) = (\arccos t, 0)$ gives rise to the factor $P_{\ell_N m}(t)$ instead. By combining these results, and by using the definition

$$
V_{\ell_N}(\pi_N, \pi'_N) = \frac{1}{2} \int dt\, V(\pi_N, \pi'_N, t) P_{\ell_N}(t)\,, \tag{5.151}
$$

with $P_{\ell_N}(t)$ the Legendre polynomial, the final result in Eq. (5.149b) is easily obtained.

The partial calculations carried out in Eqs. (5.148) and (5.149) lead to the

following expression for the two–body potential matrix elements

$$\begin{aligned}\langle\Psi_{m\mu}|V_{12}|\Psi_{m'\mu'}\rangle = &\sum_{\substack{m_N M_{L_{N-1}}\\ m'_N M'_{L_{N-1}}}} (\ell_N m_N L_{N-1} M_{L_{N-1}}|LM_L)(\ell'_N m'_N L'_{N-1} M'_{L_{N-1}}|LM_L)\\ &\times \delta_{[K_{N-1}][K'_{N-1}]}\delta_{K_{N-1}K'_{N-1}}\delta_{L_{N-1}L'_{N-1}}\delta_{M_{L_{N-1}}M'_{L_{N-1}}}\delta_{\ell_N\ell'_N}\delta_{m_N m'_N}\\ &\times \frac{1}{(2\pi)^3}\,\mathcal{N}_{n_N}^{K_N;\ell_N,K_{N-1}}\,\mathcal{N}_{n'_N}^{K'_N;\ell'_N,K'_{N-1}}\\ &\times \int d\varphi_N\,(\cos\varphi_N)^{3N-4}(\sin\varphi_N)^2\int dQ\,Q^{3N-1}\int dQ'\,Q'^2\sin\varphi'_N\\ &\times (\sin\varphi_N)^{\ell_N}\,(\cos\varphi_N)^{K_{N-1}}\,P_{n_N}^{\left(\ell_N+\frac{1}{2},K_{N-1}+\frac{3N-5}{2}\right)}(\cos 2\varphi_N)\\ &\times f_m(Q)\,4\pi\,V_{\ell_N}(p_{12},p'_{12})\,f_{m'}(Q')\\ &\times (\sin\varphi'_N)^{\ell'_N}\,(\cos\varphi'_N)^{K'_{N-1}}\,P_{n'_N}^{\left(\ell'_N+\frac{1}{2},K'_{N-1}+\frac{3N-5}{2}\right)}(\cos 2\varphi'_N)\,.\end{aligned} \tag{5.152}$$

By exploiting the delta functions in the equation above, and the validity of the relation $\sum_{m_N M_{L_{N-1}}} (\ell_N m_N L_{N-1} M_{L_{N-1}}|LM_L)\,(\ell_N m_N L_{N-1} M_{L_{N-1}}|LM_L) = 1$, it is not difficult to obtain

$$\begin{aligned}\langle\Psi_{m\mu}|V_{12}|\Psi_{m'\mu'}\rangle = &\,\delta_{[K_{N-1}][K'_{N-1}]}\,\mathcal{N}_{n_N}^{K_N;\ell_N,K_{N-1}}\,\mathcal{N}_{n'_N}^{K'_N;\ell_N,K_{N-1}}\\ &\times \frac{1}{(2\pi)^3}\int d\varphi_N\int dQ\,Q^{3N-1}\int dQ'\,Q'^2\\ &\times (\sin\varphi_N)^{\ell_N+2}\,(\cos\varphi_N)^{K_{N-1}+3N-4}\,P_{n_N}^{\left(\ell_N+\frac{1}{2},K_{N-1}+\frac{3N-5}{2}\right)}(\cos 2\varphi_N)\\ &\times f_m(Q)\,4\pi\,V_{\ell_N}(p_{12},p'_{12})\,f_{m'}(Q')\\ &\times (\sin\varphi'_N)^{\ell_N+1}\,(\cos\varphi'_N)^{K_{N-1}}\,P_{n'_N}^{\left(\ell_N+\frac{1}{2},K_{N-1}+\frac{3N-5}{2}\right)}(\cos 2\varphi'_N)\,,\end{aligned} \tag{5.153}$$

where, from Eqs. (5.142) and (5.122), we have the equivalence $p_{12} = C_{12}^{\pi} Q \sin\varphi_N$ and $p'_{12} = C_{12}^{\pi} Q' \sin\varphi'_N$. Moreover, the hyperangle φ'_N is still implicitly defined as in Eq. (5.145).

In our cluster EFT framework also charged particles are present. In this case, in addition to the two–body effective potential, we have to consider a Coulomb term as well. In momentum space, the Coulomb potential assumes the form

$$V_C(\boldsymbol{p}_{12}-\boldsymbol{p}'_{12}) = \frac{Z_\alpha^2 4\pi\alpha_{\rm em}}{(\boldsymbol{p}_{12}-\boldsymbol{p}'_{12})^2} = \frac{Z_\alpha^2 4\pi\alpha_{\rm em}}{(p_{12}^2+p_{12}'^2-2p_{12}p'_{12}t)}\,,\quad t=\hat{\pi}_N\cdot\hat{\pi}'_N\,. \tag{5.154}$$

Specifically, in the calculations we will consider the S–wave component, which is defined as

$$V_{C,0}\,(p_{12},p'_{12}) = \frac{1}{2}\int dt\,V_C\,(\boldsymbol{p}_{12}-\boldsymbol{p}'_{12})\,P_0(t)\,. \tag{5.155}$$

Of course, the matrix elements of this additional Coulomb term can also be calculated with the procedure shown above.

The three–body potential matrix elements

As derived in Section 4.5, the three–body interaction employed in this work is a hypercentral non–local potential, depending entirely on the hypermomentum as follows

$$V_3(Q,Q') = e^{-\left(\frac{Q}{\Lambda_3}\right)^2} \tilde{\lambda}_3 \, e^{-\left(\frac{Q'}{\Lambda_3}\right)^2} \tag{5.156}$$

where $\tilde{\lambda}_3$ is a constant and Λ_3 is a cut–off parameter. The matrix elements of this term can therefore be calculated in the following way

$$\begin{aligned} \langle \Psi_{m\mu} | V_3 | \Psi_{m'\mu'} \rangle = \delta_{\mu\mu'} \int dQ \, Q^{3N-1} \int dQ' \, Q'^{3N-1} \\ \times f_m(Q) \, e^{-\left(\frac{Q}{\Lambda_3}\right)^2} \lambda_3 \, e^{-\left(\frac{Q'}{\Lambda_3}\right)^2} f_{m'}(Q') \, , \end{aligned} \tag{5.157}$$

where the delta function $\delta_{\mu\mu'}$ is due to the orthonormality property of the functions $\mathcal{Y}_\mu^{JM\pi}(\Omega_N^{(Q)})$.

5.4 The Fourier transform of the basis

In Sections 5.1.3 and 5.3.2 we have defined a basis both in coordinate space, Eq. (5.61), and in momentum space, Eq. (5.129), with which we calculate the matrix elements of the nuclear Hamiltonian, in order to solve variationally the Schrödinger equation relative to the bound–state problem. We write again the bases here

$$\langle \vec{\boldsymbol{\eta}} \, | \, \Phi_\kappa \rangle = f_m(\rho) \, \mathcal{Y}_\mu^{JM\pi}(\Omega_N^{(\rho)}) \, , \tag{5.158}$$

$$\langle \vec{\boldsymbol{\pi}} \, | \, \Psi_\kappa \rangle = \mathcal{N} f_m(Q) \, \mathcal{Y}_\mu^{JM\pi}(\Omega_N^{(Q)}) \, , \tag{5.159}$$

remarking that both functions $f_m(\rho)$ and $f_m(Q)$ are constructed by means of a Laguerre polynomials basis.

As done in the previous works in Refs. [107] and [29], here we will mainly use the basis defined in Eq. (5.159) to diagonalize the Hamiltonian matrix. As already pointed out, the reason for this choice is the fact that the effective potentials employed are born in momentum space. Moreover, the Laguerre polynomials basis is a quite manageable set for performing calculations. Since, within this framework, we will also have to calculate matrix elements of operators that are defined in coordinate space, it is useful to construct a basis in coordinate space that is consistent with the choice (5.159). This point will be further developed in Section 5.4.1, by making an extensive use of the formalism presented in Ref. [109].

We also mention that, in order to solve the variational problem in momentum space, another strategy is possible. In fact, an alternative way to proceed is to define a proper basis in momentum space starting from the one in Eq. (5.158). In Section 5.4.2 we will briefly discuss also this approach, whose development started in the work that can be found in Ref. [110].

5.4.1 From the basis in momentum space to the basis in coordinate space

Our starting point is basis in momentum space defined in Eq. (5.159). We remark that the "hypermomental" functions $f_m(Q)$, given in Eq. (5.132), contain the Laguerre polynomials. The consistent basis in coordinate space can be constructed as follows

$$\langle \vec{\boldsymbol{\eta}} \,|\, \Psi_\kappa \rangle = \int \frac{d^{3N}\vec{\boldsymbol{\pi}}}{(2\pi)^{3N}} \langle \vec{\boldsymbol{\eta}} \,|\, \vec{\boldsymbol{\pi}} \rangle \langle \vec{\boldsymbol{\pi}} \,|\, \Psi_\kappa \rangle \ , \tag{5.160}$$

where $\vec{\boldsymbol{\eta}}$ and $\vec{\boldsymbol{\pi}}$ are shorthand notations for the vectors of the Jacobi coordinates $\vec{\boldsymbol{\eta}} = (\boldsymbol{\eta}_1, \ldots, \boldsymbol{\eta}_N)$ and Jacobi momenta $\vec{\boldsymbol{\pi}} = (\boldsymbol{\pi}_1, \ldots, \boldsymbol{\pi}_N)$, respectively, and the volume element is defined as $d^{3N}\vec{\boldsymbol{\pi}} = d^3\boldsymbol{\pi}_1 \ldots d^3\boldsymbol{\pi}_N$. The factor $\langle \vec{\boldsymbol{\eta}} \,|\, \vec{\boldsymbol{\pi}} \rangle$ can be rewritten by using the following expression for the plane wave expansion in the $3N$–dimensional space [111, 112]

$$\langle \vec{\boldsymbol{\eta}} \,|\, \vec{\boldsymbol{\pi}} \rangle = e^{i\vec{\boldsymbol{\pi}}\cdot\vec{\boldsymbol{\eta}}} = \frac{(2\pi)^{3N/2}}{(Q\rho)^{\frac{3N}{2}-1}} \sum_{[K]} i^K \, [\mathcal{Y}^{KLM_L}_{[K]}(\Omega^{(Q)}_N)]^* \mathcal{Y}^{KLM_L}_{[K]}(\Omega^{(\rho)}_N) J_{\bar{K}+\frac{1}{2}}(Q\rho) \, , \tag{5.161}$$

where the dot product is explicitly $\vec{\boldsymbol{\pi}} \cdot \vec{\boldsymbol{\eta}} \equiv \sum_{i=1}^N \boldsymbol{\pi}_i \cdot \boldsymbol{\eta}_i$ and the function $J_{\bar{K}+\frac{1}{2}}(Q\rho)$ is a Bessel function [45] with the definition $\bar{K} = K + \frac{3N-3}{2}$. Notice that, in the case $N = 1$, corresponding to $A = 2$, we have only one Jacobi coordinate $\boldsymbol{\eta}_1$ and one Jacobi momentum $\boldsymbol{\pi}_1$, with $\rho = \eta_1$ and $Q = \pi_1$, and Eq. (5.161) reproduces the usual expansion for a plane wave in three–dimensional space

$$e^{i\boldsymbol{\pi}_1\boldsymbol{\eta}_1} = 4\pi \sum_{\ell m} i^\ell Y^*_{\ell m}(\hat{\pi}_1) Y_{\ell m}(\hat{\eta}_1) j_\ell(\pi_1\eta_1) \, . \tag{5.162}$$

In this case the HH functions reduce to the spherical harmonics functions and, in the relation above, $j_\ell(\pi_1\eta_1)$ is the spherical Bessel function defined from the ordinary Bessel function as $j_\ell(x) = \sqrt{\frac{\pi}{2x}} J_{\ell+\frac{1}{2}}(x)$ [45]. By using explicitly Eqs. (5.159) and (5.161) in Eq. (5.160), and by exploiting the orthogonality property of the HH functions, we obtain the following result for the basis in coordinate space

$$\Psi_\kappa(\rho, \Omega^{(\rho)}_N) = g_{mK}(\rho) \mathcal{Y}^{JM\pi}_\mu(\Omega^{(\rho)}_N) \, , \tag{5.163}$$

where the functions $g_{mK}(\rho)$ are defined through the following integral

$$g_{mK}(\rho) = i^K \int dQ \, \frac{Q^{3N-1}}{(Q\rho)^{\frac{3N}{2}-1}} J_{\bar{K}+\frac{1}{2}}(Q\rho) f_m(Q) \, . \tag{5.164}$$

By looking at the bases defined consistently in momentum and in coordinate space, Eqs. (5.159) and (5.164), respectively, we can make two comments. The form of the HH, spin and isospin part is the same, $\mathcal{Y}^{JM\pi}_\mu(\Omega^{(Q)}_N) \to \mathcal{Y}^{JM\pi}_\mu(\Omega^{(\rho)}_N)$, with the replacement $\vec{\boldsymbol{\pi}} \to \vec{\boldsymbol{\eta}}$. Moreover, the hyperradial basis functions $g_{mK}(\rho)$, which are calculated essentially as a Fourier transform of the functions $f_m(Q)$, depend explicitly on the grand–angular momentum quantum number K of the HH function $\mathcal{Y}^{KLM_L}_{[K]}(\Omega^{(\rho)}_N)$ to which they are associated.

When the functions $f_m(Q)$ are constructed by means of the Laguerre polynomials as in Eq. (5.132), the integral (5.164) can be calculated analytically [109]. We conclude this section with the derivation of the complete expression for the functions $g_{mK}(\rho)$. As a first step, we write the generalized Laguerre polynomials by using the expansion [113]

$$L_m^{(3N-1)}\left(\frac{Q}{\beta}\right) = \sum_{n=0}^{m}(-1)^n \binom{m+3N-1}{m-n}\frac{1}{n!}\left(\frac{Q}{\beta}\right)^n , \tag{5.165}$$

which leads to

$$\begin{aligned} g_{mK}(\rho) = i^K \left(\frac{1}{\beta}\right)^{\frac{3N}{2}} \sqrt{\frac{m!}{(m+3N-1)!}} \sum_{n=0}^{m} \frac{(-1)^n}{n!} \binom{m+3N-1}{m-n} \frac{1}{\beta^n} \\ \times \int dQ \, \frac{Q^{3N-1+n}}{(Q\rho)^{\frac{3N}{2}-1}} J_{\bar{K}+\frac{1}{2}}(Q\rho)\, \mathrm{e}^{-\frac{Q}{2\beta}} . \end{aligned} \tag{5.166}$$

The result for the integration of a Bessel function combined with a power and an exponential [113]

$$\int dx\, J_\nu(\gamma x)\, x^{\mu-1} e^{-\alpha x} = (\alpha^2+\gamma^2)^{-\frac{\mu}{2}}\, \Gamma(\nu+\mu)\, P_{\mu-1}^{-\nu}\left[\alpha(\alpha^2+\gamma^2)^{-\frac{1}{2}}\right] , \tag{5.167}$$

where $P_b^a(z)$ are the associated Legendre functions, yields to the following expression

$$\begin{aligned} g_{mK}(\rho) = i^K \beta^{\frac{3N}{2}} \sqrt{\frac{m!}{(m+3N-1)!}} \sum_{n=0}^{m} \frac{(-1)^n}{n!} \binom{m+3N-1}{m-n} \\ \times \Gamma(K+3N+n) \, \frac{(2u)^{3N+n}}{(1-u^2)^{\frac{3N}{4}-\frac{1}{2}}} \, P_{\frac{3N}{2}+n}^{1-K-\frac{3N}{2}}(u) , \end{aligned} \tag{5.168}$$

with the definition $u \equiv [1+(2\beta Q)^2]^{-\frac{1}{2}}$. The associated Legendre functions can be written in terms of the Hypergeometric functions ${}_2F_1(A,B;C;z)$ as [113]

$$P_b^a(z) = \frac{1}{\Gamma(1-a)}\left(\frac{z+1}{z-1}\right)^{\frac{a}{2}} {}_2F_1\left(-b, b+1; 1-a; \frac{1-z}{2}\right) , \tag{5.169}$$

leading to the following final expression for the basis functions $g_{mK}(\rho)$

$$\begin{aligned} g_{mK}(\rho) = i^K \beta^{\frac{3N}{2}} \sqrt{\frac{m!}{(m+3N-1)!}} \sum_{n=0}^{m} \frac{(-1)^n}{n!} \binom{m+3N-1}{m-n} \\ \times \frac{\Gamma(K+3N+n)}{\Gamma(K+\frac{3N}{2})} \frac{(2u)^{3N+n}}{(1-u^2)^{\frac{3N}{4}-\frac{1}{2}}} \left(\frac{u+1}{u-1}\right)^{\frac{1}{2}-\frac{K}{2}-\frac{3N}{4}} \\ \times {}_2F_1\left(-\frac{3N}{2}-n, \frac{3N}{2}+n+1; K+\frac{3N}{2}; \frac{1-u}{2}\right) . \end{aligned} \tag{5.170}$$

5.4.2 From the basis in coordinate space to the basis in momentum space

A basis in momentum space which is consistent with the definition (5.158) can be constructed as

$$\langle \vec{\boldsymbol{\pi}} \,|\, \Phi_\kappa \rangle = \int d^{3N}\vec{\boldsymbol{\eta}}\, \langle \vec{\boldsymbol{\pi}} \,|\, \vec{\boldsymbol{\eta}} \rangle \, \langle \vec{\boldsymbol{\eta}} \,|\, \Phi_\kappa \rangle \ , \tag{5.171}$$

where $\langle \vec{\boldsymbol{\pi}} \,|\, \vec{\boldsymbol{\eta}} \rangle = e^{-i\vec{\boldsymbol{\pi}}\cdot\vec{\boldsymbol{\eta}}}$. By using the definition of $\langle \vec{\boldsymbol{\eta}} \,|\, \Phi_\kappa \rangle$ given in (5.158), together with the expansion of the plane wave in the $3N$–dimensional space, Eq. (5.161), we obtain the result

$$\Phi_\kappa(Q, \Omega_N^{(Q)}) = \mathcal{N} g_{mK}(Q) \mathcal{Y}_\mu^{JM\pi}(\Omega_N^{(Q)}) \, , \tag{5.172}$$

with $\mathcal{N} = (2\pi)^{\frac{3N}{2}}$. The functions $g_{mK}(Q)$ are explicitly

$$g_{mK}(Q) = (-i)^K \int d\rho \, \frac{\rho^{3N-1}}{(Q\rho)^{\frac{3N}{2}-1}} J_{\bar{K}+\frac{1}{2}}(Q\rho) f_m(\rho) \, , \tag{5.173}$$

where $\bar{K} = K + \frac{3N-3}{2}$ and the functions $f_m(\rho)$ are constructed from a Laguerre polynomials set as in Eq. (5.62). Notice that the functions $g_{mK}(Q)$ above differ from those defined in configuration space in Eq. (5.164) essentially by a phase factor.

Within this framework, the matrix elements of the norm and kinetic energy can be computed as well, and they are similar in form to the ones reported in Eq. (5.135). In fact we have

$$\langle \Phi_{m\mu} | \Phi_{m'\mu'} \rangle = N_{mK,m'K'} \, \delta_{\mu\mu'} \, , \qquad \langle \Phi_{m\mu} | T | \Phi_{m'\mu'} \rangle = T_{mK,m'K'} \, \delta_{\mu\mu'} \, , \tag{5.174}$$

where now the delta functions $\delta_{\mu\mu'}$ comes from the orthonormality property of the functions $\mathcal{Y}_\mu^{JM\pi}(\Omega_N^{(Q)})$ and $N_{mK,m'K'}$ and $T_{mK,m'K'}$ can be calculated as

$$N_{mK,m'K'} = \int dQ \, Q^{3N-1} \, g^*_{mK}(Q) \, g_{m'K'}(Q) \, , \tag{5.175}$$

$$T_{mK,m'K'} = \frac{\hbar^2}{2m_{\rm ref}} \int dQ \, Q^{3N+1} \, g^*_{mK}(Q) \, g_{m'K'}(Q) \, . \tag{5.176}$$

The matrix elements of a two–body central potential are

$$\begin{aligned} \langle \Phi_{m\mu} | V_{12} | \Phi_{m'\mu'} \rangle = \frac{1}{(2\pi)^3} \int d^3\boldsymbol{\pi}_1 \ldots d^3\boldsymbol{\pi}_{N-1} \, d^3\boldsymbol{\pi}_N \, d^3\boldsymbol{\pi}'_N \left[\mathcal{Y}^{KLM_L}_{[K]}(\Omega_N^{(Q)}) \right]^\dagger \\ \times g^*_{mK}(Q) V(\boldsymbol{p}_{12}, \boldsymbol{p}'_{12}) g_{m'K'}(Q) \, \mathcal{Y}^{KLM_L}_{[K']}(\Omega_N^{\prime(Q)}) \, , \end{aligned} \tag{5.177}$$

whose calculation can be developed by following the approach discussed in Section 5.3.3. Finally, for the three–body hypercentral potential we have

$$\begin{aligned} \langle \Phi_{m\mu} | V_3 | \Phi_{m'\mu'} \rangle = \delta_{\mu\mu'} \int dQ \, Q^{3N-1} \int dQ' \, Q'^{3N-1} \\ \times g^*_{mK}(Q) \, e^{-\left(\frac{Q}{\Lambda_3}\right)^2} \lambda_3 \, e^{-\left(\frac{Q'}{\Lambda_3}\right)^2} g_{m'K'}(Q) \, . \end{aligned} \tag{5.178}$$

Chapter 6

The Beryllium–9 photodisintegration reaction

6.1 The reaction cross section: detailed derivation

Our aim is to compute the reaction cross section of the ^{9}Be photodisintegration

$$\gamma + {}^9\mathrm{Be} \to \alpha + \alpha + n\,. \tag{6.1}$$

In order to evaluate the response function defined in Eq. (2.20), first we calculate the LIT by means of the method thoroughly described in Chapter 3, and then we perform an inversion.

6.1.1 The $E1$ transition operator

The operator of interest to us is the nuclear current operator J_λ, as defined in Eq. (2.38). In the multipole expansion we neglect the electric multipoles with $J > 1$, retaining only the first term $J = 1$. Moreover, in order to calculate $T^{el}_{1\lambda}(q)$, we apply the Siegert theorem (i.e. the continuity equation). Due to the fact that we are studying the ^{9}Be photodisintegration reaction in the low–energy regime of astrophysical relevance, our calculations can be performed in the limit of low–momentum transfer by the real photon. As a consequence, we are allowed to use only the Siegert operator $T^{el,S}_{1\lambda}(q)$ in the long–wavelength approximation, which has been derived in (2.55). Furthermore, in this work we neglect all the contributions due to the magnetic multipole operators. The lowest term in the expansion, $T^{mag}_{1\lambda}(q)$, is the subject of a different study. Based on these assumptions, the operator of interest is the following

$$J_\lambda(q) \simeq -\sqrt{6\pi}T^{el,S}_{1\lambda}(q) \simeq -i\sqrt{\frac{4\pi}{3}}\omega_{\boldsymbol{q}} d_\lambda\,, \tag{6.2}$$

where we have defined

$$d_\lambda = \int d^3\boldsymbol{x}\, x\rho(\boldsymbol{x})Y_{1\lambda}(\hat{x})\,. \tag{6.3}$$

Since we are working in a cluster framework, when we consider a system made up of A components, the nuclear charge operator assumes the general form

$$\rho(\boldsymbol{x}) = \sum_{i=1}^{A} Z_i \delta^3(\boldsymbol{x}_i - \boldsymbol{r}'_i)\,, \tag{6.4}$$

where Z_i is the electromagnetic charge of the particle in the position $\boldsymbol{r}'_i$, and the unit charge factor e has been extracted. Specifically, when dealing with ^{9}Be nucleus, the particles involved are neutrons and α–particles, so the charge Z_i is either zero or $Z_\alpha = 2$. By substituting the definition of the nuclear charge and performing the integral in Eq. (6.3) we obtain

$$d_\lambda = \sum_{i=1}^{A} Z_i r'_i Y_{1\lambda}(\hat{r}'_i)\,. \tag{6.5}$$

Notice that d_λ is proportional to the spherical component of the dipole operator $\boldsymbol{D}$, and in fact Eq. (6.2) can be written alternatively as

$$J_\lambda(q) \simeq -i\omega_{\boldsymbol{q}} D_\lambda\,. \tag{6.6}$$

In Eq. (6.5), the vectors $\boldsymbol{r}'_i$, $i = 1, \ldots, A$, are the position vectors defined with respect to the center–of–mass coordinate, $\boldsymbol{r}'_i = \boldsymbol{r}_i - \boldsymbol{R}_{\rm cm}$. If we consider the $A = 3$ case, the relations between the position vectors $\{\,\boldsymbol{r}_1, \boldsymbol{r}_2, \boldsymbol{r}_3\,\}$ and the Jacobi coordinates $\{\,\boldsymbol{\eta}_2, \boldsymbol{\eta}_1, \boldsymbol{\eta}_0\,\}$ are explicitly

$$\boldsymbol{r}_1 = -\sqrt{\frac{m_{\rm r} m_2}{M_2 m_1}}\boldsymbol{\eta}_2 - \sqrt{\frac{m_{\rm r} m_3}{M M_2}}\boldsymbol{\eta}_1 + \sqrt{\frac{m_{\rm r}}{M}}\boldsymbol{\eta}_0\,, \tag{6.7a}$$

$$\boldsymbol{r}_2 = \sqrt{\frac{m_{\rm r} m_1}{M_2 m_2}}\boldsymbol{\eta}_2 - \sqrt{\frac{m_{\rm r} m_3}{M M_2}}\boldsymbol{\eta}_1 + \sqrt{\frac{m_{\rm r}}{M}}\boldsymbol{\eta}_0\,, \tag{6.7b}$$

$$\boldsymbol{r}_3 = \sqrt{\frac{m_{\rm r} M_2}{M m_3}}\boldsymbol{\eta}_1 + \sqrt{\frac{m_{\rm r}}{M}}\boldsymbol{\eta}_0\,, \tag{6.7c}$$

where we have defined with M the total mass of the system, $M_2 = m_1 + m_2$ and $m_{\rm r}$ is a reference mass. The expressions above can be easily calculated starting from the general definition of the Jacobi coordinates in Eq. (5.3). Being $\boldsymbol{\eta}_0 = \sqrt{\frac{M}{m_{\rm r}}}\boldsymbol{R}_{\rm cm}$ [see Eq. (5.4)], it is straightforward that the coordinates $\boldsymbol{r}'_i$ can be obtained from Eqs. (6.7) by dropping each term proportional to $\boldsymbol{\eta}_0$. We therefore define

$$\boldsymbol{r}'_1 = -\mathcal{A}\boldsymbol{\eta}_2 - \mathcal{B}\boldsymbol{\eta}_1\,, \tag{6.8a}$$

$$\boldsymbol{r}'_2 = \mathcal{C}\boldsymbol{\eta}_2 - \mathcal{B}\boldsymbol{\eta}_1\,, \tag{6.8b}$$

$$\boldsymbol{r}'_3 = \mathcal{D}\boldsymbol{\eta}_1\,, \tag{6.8c}$$

where the values of the mass factors $\mathcal{A}, \mathcal{B}, \mathcal{C}$ and $\mathcal{D}$ can be easily deduced from Eqs. (6.7):

$$\mathcal{A} = \sqrt{\frac{m_{\rm r} m_2}{M_2 m_1}}\,, \qquad \mathcal{B} = \sqrt{\frac{m_{\rm r} m_3}{M M_2}}\,, \qquad \mathcal{C} = \sqrt{\frac{m_{\rm r} m_1}{M_2 m_2}}\,, \qquad \mathcal{D} = \sqrt{\frac{m_{\rm r} M_2}{M m_3}}\,. \tag{6.9}$$

As shown in detail in Appendix E.1, in the most general case in which $A = 3$, the above expressions of $\boldsymbol{r}'_i$ allow to rewrite the sum (6.5) in terms of the Jacobi vectors as follows

$$d_\lambda = (-Z_1\mathcal{A} + Z_2\mathcal{C})\,\eta_2\,Y_{1\lambda}(\hat{\eta}_2) + [-(Z_1 + Z_2)\,\mathcal{B} + Z_3\mathcal{D}]\,\eta_1\,Y_{1\lambda}(\hat{\eta}_1)\,. \tag{6.10}$$

Clearly, in this form, the operator d_λ depends on the choice of the ordering of the particles. In the reference permutation, when the positions (123) are occupied by the particles $(n\alpha\alpha)$, we have $Z_1 = 0$ and $Z_2 = Z_3 = Z_\alpha$, and the masses are explicitly $m_1 = m_n$ and $m_2 = m_3 = m_\alpha$. In this case the coefficients of Eq. (6.10) reduce to

$$Z_2\mathcal{C} = Z_\alpha \frac{\mu}{\sqrt{\mu+1}}\,, \qquad -Z_2\mathcal{B} + Z_3\mathcal{D} = Z_\alpha \mu \sqrt{\frac{\mu}{(\mu+2)(\mu+1)}}\,. \tag{6.11}$$

In the equations above we have set the reference mass equal to the nucleon mass, $m_\mathrm{r} = m_n$, and we have defined the dimensionless factor $\mu \equiv m_n/m_\alpha$. The final complete form of the operator is

$$d_\lambda^{(12=n\alpha)} = Z_\alpha \left(\frac{\mu}{\sqrt{\mu+1}} \eta_2\,Y_{1\lambda}(\hat{\eta}_2) + \mu \sqrt{\frac{\mu}{(\mu+2)(\mu+1)}} \eta_1\,Y_{1\lambda}(\hat{\eta}_1) \right). \tag{6.12}$$

From a practical point of view, the alternative ordering (123) = $(\alpha\alpha n)$ is quite convenient. By imposing $Z_1 = Z_2 = Z_\alpha$, $Z_3 = 0$ in addition to $m_1 = m_2 = m_\alpha$ and $m_3 = m_n$, we obtain for the coefficients of Eq. (6.10)

$$-Z_1\mathcal{A} + Z_2\mathcal{C} = 0\,, \qquad -(Z_1 + Z_2)\,\mathcal{B} = -2Z_\alpha \frac{\mu}{\sqrt{2(\mu+2)}}\,, \tag{6.13}$$

and therefore the operator d_λ only depends on the Jacobi vector $\boldsymbol{\eta}_1$ as follows

$$d_\lambda^{(12=\alpha\alpha)} = -2Z_\alpha \frac{\mu}{\sqrt{2(\mu+2)}} \eta_1\,Y_{1\lambda}(\hat{\eta}_1)\,. \tag{6.14}$$

6.1.2 Calculation of the LIT

By using explicitly the electric $E1$ operator defined in Eq. (6.2), the response function given in (2.20) becomes

$$R(\omega_{\boldsymbol{q}}) = \frac{\omega_{\boldsymbol{q}}^2}{2(2J_0+1)} \frac{4\pi}{3} \sum_{\lambda=\pm1} \sum_{M_0} \sum_{M_f} R_d(\omega_{\boldsymbol{q}})\,, \tag{6.15}$$

with $R_d(\omega_{\boldsymbol{q}})$ defined as

$$R_d(\omega_{\boldsymbol{q}}) = \sum\!\!\!\!\!\!\int_f \left| \langle \Psi_f | \hat{d}_\lambda | \Psi_0 \rangle \right|^2 \delta(E_f - E_0 - \omega_{\boldsymbol{q}})\,, \tag{6.16}$$

which we want to calculate by following an integral transform approach. We therefore proceed by focussing on the calculation of the LIT. Specifically, we use the

procedure shown in Section 3.3.1, i.e. the eigenvalue method, referring mainly to Eq. (3.23), which we rewrite here for convenience

$$L(\sigma_R, \sigma_I) = \sum_{l=1}^{N_\Lambda} \frac{|\langle \Psi_l | \hat{d}_\lambda | \Psi_0 \rangle|^2}{(E_l - E_0 - \sigma_R)^2 + \sigma_I^2} \,. \tag{6.17}$$

By exploiting the existing codes, also used in the previous works [29, 76, 107], the eigenvalue E_0 and the wave function relative to the ^{9}Be ground state are obtained by using a variational method in conjunction with a NSHH basis defined in momentum space (Section 5.3). Basically, the calculation is reduced to solving the eigenvalue problem shown in Eq. (5.134) for the state $J^\pi = 3/2^-$, from which one can calculate E_0 and the vector of the coefficients $\{ c_\kappa^0 \}$. The latter allows to construct easily the bound–state wave function by means of the basis defined in momentum space in Eq. (5.129):

$$\langle \vec{\boldsymbol{\pi}} \,|\, \Psi_0 \rangle = \sum_\kappa c_\kappa^0 \, \langle \vec{\boldsymbol{\pi}} \,|\, \Psi_\kappa \rangle = \mathcal{N} \sum_{m\mu} c_{m\mu}^0 \, f_m(Q) \, \mathcal{Y}_\mu^{JM\pi}(\Omega_N^{(Q)}) \,. \tag{6.18}$$

As already said in Section 3.3.1, the energies E_l and the states $|\Psi_l\rangle$ are such that $\hat{H} \, |\Psi_l\rangle = E_l \, |\Psi_l\rangle$, and therefore they can be calculated as well by solving an eigenvalue problem of the same type but characterized by different quantum numbers. Due to the selection rules imposed by the nature of the operator employed, i.e. the dipole operator, concerning the parity, the total orbital angular momentum and the total spin of the initial and final states, we must have

$$\pi_f = -\pi_i \,, \qquad\qquad \Delta L = 0, \pm 1 \,, \qquad\qquad \Delta S = 0 \,. \tag{6.19}$$

As a consequence, in order to obtain the eigenvalues E_l $(l = 1, \ldots, N_\Lambda)$ and the coefficients $\{ c_\kappa^l \}$, the allowed quantum numbers to give as an input in the diagonalization of the Hamiltonian are the following: $J^\pi = 1/2^+, 3/2^+, 5/2^+$. By analogy with Eq. (6.18), we write for each l eigenstate

$$\langle \vec{\boldsymbol{\pi}} \,|\, \Psi_l \rangle = \sum_\kappa c_\kappa^l \, \langle \vec{\boldsymbol{\pi}} \,|\, \Psi_\kappa \rangle = \mathcal{N} \sum_{m\mu} c_{m\mu}^l \, f_m(Q) \, \mathcal{Y}_\mu^{JM\pi}(\Omega_N^{(Q)}) \,. \tag{6.20}$$

Looking back at Eq. (6.17), since we have defined the rescaled dipole operator entirely in terms of the internal Jacobi coordinates $\{ \boldsymbol{\eta}_2, \boldsymbol{\eta}_1 \}$, the calculation of the matrix elements $\langle \Psi_l | \hat{d}_\lambda | \Psi_0 \rangle$ should be carried out in configuration space. By considering the case of a general operator $\hat{\mathcal{O}}$, we start by introducing some sets of complete states as follows

$$\begin{aligned} \langle \Psi_l | \, \hat{\mathcal{O}} \, | \Psi_0 \rangle = \int d^{3N}\vec{\boldsymbol{\eta}} \int d^{3N}\vec{\boldsymbol{\eta}}' \int \frac{d^{3N}\vec{\boldsymbol{\pi}}}{(2\pi)^{3N}} \int \frac{d^{3N}\vec{\boldsymbol{\pi}}'}{(2\pi)^{3N}} \\ \times \langle \Psi_l \,|\, \vec{\boldsymbol{\pi}}' \rangle \, \langle \vec{\boldsymbol{\pi}}' \,|\, \vec{\boldsymbol{\eta}}' \rangle \, \langle \vec{\boldsymbol{\eta}}' | \, \hat{\mathcal{O}} \, | \vec{\boldsymbol{\eta}} \, \rangle \, \langle \vec{\boldsymbol{\eta}} \;\, | \, \vec{\boldsymbol{\pi}} \, \rangle \, \langle \vec{\boldsymbol{\pi}} \,|\, \Psi_0 \rangle \,, \end{aligned} \tag{6.21}$$

where for the states in momentum space we have followed the convention (5.137). Since the dipole operator is local, we can restrict to the case

$$\langle \vec{\boldsymbol{\eta}}' | \, \hat{\mathcal{O}} \, | \vec{\boldsymbol{\eta}} \, \rangle = \mathcal{O}(\vec{\boldsymbol{\eta}}) \, \delta^{3N}(\vec{\boldsymbol{\eta}}' - \vec{\boldsymbol{\eta}}) \,. \tag{6.22}$$

Moreover, by using Eq. (6.18), we can write

$$\int \frac{d^{3N}\vec{\boldsymbol{\pi}}}{(2\pi)^{3N}} \langle \vec{\boldsymbol{\eta}} \,|\, \vec{\boldsymbol{\pi}} \rangle \langle \vec{\boldsymbol{\pi}} \,|\, \Psi_0 \rangle = \sum_{\kappa} c^0_{\kappa} \int \frac{d^{3N}\vec{\boldsymbol{\pi}}}{(2\pi)^{3N}} \langle \vec{\boldsymbol{\eta}} \,|\, \vec{\boldsymbol{\pi}} \rangle \langle \vec{\boldsymbol{\pi}} \,|\, \Psi_{\kappa} \rangle \tag{6.23a}$$

$$= \sum_{m\mu} c^0_{m\mu}\, g_{mK}(\rho)\, \mathcal{Y}^{JM\pi}_{\mu}(\Omega^{(\rho)}_N)\,, \tag{6.23b}$$

where in (6.23b), we have used the basis consistently defined in configuration space as in Eq. (5.163). Since we can write similar relations for each l eigenstate

$$\int \frac{d^{3N}\vec{\boldsymbol{\pi}}}{(2\pi)^{3N}} \langle \vec{\boldsymbol{\eta}} \,|\, \vec{\boldsymbol{\pi}} \rangle \langle \vec{\boldsymbol{\pi}} \,|\, \Psi_l \rangle = \sum_{m\mu} c^l_{m\mu}\, g_{mK}(\rho)\, \mathcal{Y}^{JM\pi}_{\mu}(\Omega^{(\rho)}_N)\,, \tag{6.24}$$

the explicit calculation of the matrix elements in Eq. (6.21) reduces to the following integral in configuration space

$$\begin{aligned} \langle \Psi_l | \,\hat{\mathcal{O}}\, | \Psi_0 \rangle = \int d\Omega^{(\rho)}_N\, d\rho\, \rho^{3N-1} \Big[\sum_{m'\mu'} c^l_{m'\mu'}\, g_{m'K'}(\rho)\, \mathcal{Y}^{J'M'\pi'}_{\mu'}(\Omega^{(\rho)}_N) \Big]^{\dagger} \\ \times\, \mathcal{O}(\rho, \Omega_N) \Big[\sum_{m\mu} c^0_{m\mu}\, g_{mK}(\rho)\, \mathcal{Y}^{JM\pi}_{\mu}(\Omega^{(\rho)}_N) \Big]\,. \end{aligned} \tag{6.25}$$

As shown in Section 5.4.1, the basis functions $g_{mK}(\rho)$ can be expressed either in terms of the associated Legendre functions $P^a_b(z)$, Eq. (5.168), or by means of the hypergeometric functions ${}_2F_1(A, B; C; z)$, Eq. (5.170) [109]. In the literature, a Fortran package is available to compute the Hypergeometric functions, which is based on Ref. [114] by Michel and Stoitsov. Unfortunately, as mentioned in the paper itself, numerical instabilities arise in the calculation for increasing values of the parameters A, B and C, which in our case corresponds especially to enlarging the dimension of the basis through the index m. This Fortran package was used in Ref. [110], where the limit $m_{\max} = 24$ was set, in order to ensure an accuracy of the calculated basis functions up to the sixth decimal place. We have tried to perform calculations in quadrupole precision; in this case the limit can be extended up to $m_{\max} = 30$ or $m_{\max} = 35$ but in most cases these values are not sufficient to obtain convergent results. Another attempt has been made, which arranges to calculate the functions ${}_2F_1(A, B; C; z)$ with Python libraries, leading again to numerical instabilities. As a consequence, in order to perform calculations, we employ another strategy, which consists in using the defining integral in Eq. (5.164). Basically, starting from Eq. (6.21), once the vectors of coefficients $\{\, c^0_{m\mu} \,\}$ and $\{\, c^l_{m\mu} \,\}$ have been determined by diagonalizing the Hamiltonian represented on a basis defined in momentum space, we proceed by summing over the index m as follows

$$\sum_{m\mu} c^{0,l}_{m\mu}\, g_{mK}(\rho)\, \mathcal{Y}^{JM\pi}_{\mu}(\Omega^{(\rho)}_N) = \sum_{\mu} G^{0,l}_{\mu}(\rho) \mathcal{Y}^{JM\pi}_{\mu}(\Omega^{(\rho)}_N)\,, \tag{6.26}$$

where we have defined the functions $G^{0,l}_{\mu}(\rho)$ as

$$G^{0,l}_{\mu}(\rho) = \sum_{m} c^{0,l}_{m\mu}\, g_{mK}(\rho)\,. \tag{6.27}$$

The summation above allows us to work with $G_\mu^{0,l}(\rho)$, which are rather smooth, avoiding the highly oscillatory behaviour of the basis functions $g_{mK}(\rho)$ for increasing m. Then, from the defining integral given in Eq. (5.164), we can write

$$G_\mu^{0,l}(\rho) = i^K \int dQ \, \frac{Q^{3N-1}}{(Q\rho)^{\frac{3N}{2}-1}} J_{\bar{K}+\frac{1}{2}}(Q\rho) F_\mu^{0,l}(Q) \,, \tag{6.28}$$

with

$$F_\mu^{0,l}(Q) = \sum_m c_{m\mu}^{0,l} \, f_m(Q) \,. \tag{6.29}$$

Due to the explicit form of the functions $f_m(Q)$, Eq. (5.132), the integrals in Eq. (6.28) can be calculated parametrically for a grid of fixed values of ρ, for instance, by using a Laguerre quadrature method. At this point, one is able to fully determine the matrix elements of the desired operator in Eq. (6.25).

The actual matrix elements to be calculated here are those obtained by specializing Eq. (6.25) for $N = 2$ ($A = 3$) and for the dipole operator $\hat{d}_\lambda$:

$$\begin{aligned} \langle \Psi_l | \hat{d}_\lambda | \Psi_0 \rangle = \int d\Omega_2^{(\rho)} \, d\rho \, \rho^5 \Big[\sum_{m'\mu'} c_{m'\mu'}^{l} \, g_{m'K'}(\rho) \, \mathcal{Y}_{\mu'}^{JM\pi}(\Omega_2^{(\rho)}) \Big]^\dagger \\ \times \, d_\lambda(\rho, \Omega_2) \Big[\sum_{m\mu} c_{m\mu}^{0} \, g_{mK}(\rho) \, \mathcal{Y}_{\mu}^{JM\pi}(\Omega_2^{(\rho)}) \Big] \,. \end{aligned} \tag{6.30}$$

The computation strategy proposed above, in which the direct calculation of the basis functions $g_{mK}(\rho)$ is avoided, can be applied as well. Since the explicit expression of the operator depends on the chosen ordering of the particles, the rotation coefficients should also be taken into account for the correct evaluation of the matrix elements. By following Eq. (5.92) we write

$$\Big\langle \Psi_l \Big| \hat{d}_\lambda^{(ij)} \Big| \Psi_0 \Big\rangle = \Big\langle \Psi_l \Big| \, [\mathcal{Q}^{(12,ij)}]^\dagger \, \hat{d}_\lambda^{(12=ij)} \, \mathcal{Q}^{(12,ij)} \Big| \Psi_0 \Big\rangle \,, \tag{6.31}$$

where one can choose to use in the calculation the operator represented in coordinate space either in the form $(ij) = (12) = (n\alpha)$, with $d_\lambda^{(12=n\alpha)}$ defined as in Eq. (6.12), or in the form $(ij) = (23) = (\alpha\alpha)$, with $d_\lambda^{(12=\alpha\alpha)}$ as in Eq. (6.14). Notice that for the case $(ij) = (13) = (n\alpha)$ the operator to use is again $d_\lambda^{(12=n\alpha)}$.

There exists another formulation for the dipole operator $\hat{d}_\lambda$, in which it is constructed as a sum over three terms, each depending on the distances $\boldsymbol{r}_{12} \equiv \boldsymbol{r}_2 - \boldsymbol{r}_1$, $\boldsymbol{r}_{23} \equiv \boldsymbol{r}_3 - \boldsymbol{r}_2$ and $\boldsymbol{r}_{13} \equiv \boldsymbol{r}_3 - \boldsymbol{r}_1$. In fact, starting from the reference ordering $(123) = (n\alpha\alpha)$, it can be demonstrated that

$$\boldsymbol{r}_2 + \boldsymbol{r}_3 = \frac{m_n}{m_n + m_\alpha} \boldsymbol{r}_{12} + \frac{m_n}{m_n + 2m_\alpha} \left(\frac{m_\alpha}{m_n + m_\alpha} \boldsymbol{r}_{23} + \frac{m_n}{m_n + m_\alpha} \boldsymbol{r}_{13} \right) . \tag{6.32}$$

Similarly to the construction of the potential operator, by using the rotation coefficients, each term can then be related to the Jacobi coordinate $\boldsymbol{\eta}_2$. In this way the complete expression for $\hat{d}_\lambda$ turns out to be

$$\Big\langle \Psi_l \Big| \hat{d}_\lambda \Big| \Psi_0 \Big\rangle = \sum_{i<j=1}^{3} \Big\langle \Psi_l \Big| \, [\mathcal{Q}^{(12,ij)}]^\dagger \hat{\mathcal{D}}_\lambda^{(12=ij)} \mathcal{Q}^{(12,ij)} \Big| \Psi_0 \Big\rangle \,, \tag{6.33}$$

with $\hat{\mathcal{D}}_\lambda^{(12=ij)}$ represented in configuration space as

$$\mathcal{D}_\lambda^{(12=ij)} = Z_\alpha \mathcal{M}_{ij}\, \eta_2\, Y_{1\lambda}(\hat{\eta}_2)\,. \tag{6.34}$$

The mass coefficients are expressed by means of the parameter $\mu = m_n/m_\alpha$ as

$$\mathcal{M}_{12} = \frac{\mu}{\sqrt{\mu+1}} \qquad \mathcal{M}_{23} = \frac{\mu\sqrt{2\mu}}{(\mu+1)(\mu+2)} \qquad \mathcal{M}_{13} = \frac{\mu^2}{\sqrt{\mu+1}(\mu+2)}\,. \tag{6.35}$$

Although all the expressions analysed for the calculation of the dipole matrix elements $\langle\Psi_l|\hat{d}_\lambda|\Psi_0\rangle$ are equivalent, from the point of view of the computational strategy discussed above, the most convenient calculation is the one presented in Eq. (6.31) with the form of the dipole operator as in Eq. (6.14). In the following we will derive the explicit expression for the matrix elements in this specific case. After the application of the rotation coefficients ($c_{m\mu}^{0,l} \to c_{m\mu}^{0,l(\alpha\alpha)}$), by following Eq. (6.30), the matrix elements to be calculated are explicitly

$$\langle m', J'M'|d_\lambda^{(12=\alpha\alpha)}|m, JM\rangle = -2Z_\alpha \frac{\mu}{\sqrt{2(\mu+2)}} \langle m', J'M'|\rho\cos\varphi_2\, Y_{1\lambda}(\hat{\eta}_1)|m, JM\rangle\ , \tag{6.36}$$

where we have used the relation $\eta_1 = \rho\cos\varphi_2$. The detailed calculation of the integral above can be found in Appendix F. Basically, it can be separated into a hyperradial (F.17a), a hyperspherical (F.17b) and an angular part (F.17c) as follows

$$\begin{aligned}\langle m', J'M'|d_\lambda^{(12=\alpha\alpha)}|m, JM\rangle = -2Z_\alpha \frac{\mu}{\sqrt{2(\mu+2)}} &\int d\rho\, \rho^6 g^*_{m'K'}(\rho) g_{mK}(\rho) \\ &\times \int d\varphi_2\, \mathcal{N}_{n_2'}^{K_2';\ell_2',\ell_1'} P_{n_2'}^{(\ell_2'+\frac{1}{2},\ell_1'+\frac{1}{2})}(\cos 2\varphi_2) \\ &\times (\sin\varphi_2)^{\ell_2'+\ell_2+2} (\cos\varphi_2)^{\ell_1'+\ell_1+3} \\ &\times \mathcal{N}_{n_2}^{K_2;\ell_2,\ell_1} P_{n_2}^{(\ell_2+\frac{1}{2},\ell_1+\frac{1}{2})}(\cos 2\varphi_2) \\ &\times (-1)^{J'-M'} \begin{pmatrix} J' & 1 & J \\ -M' & \lambda & M \end{pmatrix} \langle J'\|Y_1(\hat{\eta}_1)\|J\rangle\ ,\end{aligned} \tag{6.37}$$

where the reduced matrix element is [see (F.22)]

$$\begin{aligned}\left\langle J' \,\middle\|\, Y_1(\hat{\eta}_1) \,\middle\|\, J \right\rangle = \delta_{\ell_2',\ell_2}\, \delta_{\{S'\},\{S\}}\, (-1)^{L_2'+\ell_2+L_2+S+J} &\\ \times \widehat{L_2'}\, \widehat{J'}\, \widehat{L_2}\, \widehat{J} \begin{Bmatrix} \ell_1' & L_2' & \ell_2 \\ L_2 & \ell_1 & 1 \end{Bmatrix} \begin{Bmatrix} L_2' & J' & S \\ J & L_2 & 1 \end{Bmatrix} &\\ \times \sqrt{\frac{3}{4\pi}}\, \widehat{\ell_1'}\, \widehat{\ell_1} \begin{pmatrix} \ell_1' & 1 & \ell_1 \\ 0 & 0 & 0 \end{pmatrix}\,.&\end{aligned} \tag{6.38}$$

We have reported in Appendix F also the detailed derivation of the matrix elements $\langle m', J'M'|\rho\sin\varphi_2\, Y_{1\lambda}(\hat{\eta}_2)|m, JM\rangle$, which are useful when the alternative forms of the dipole operator, Eqs. (6.12) and (6.34), are used in the calculation.

Once the matrix elements $\langle\Psi_l|\hat{d}_\lambda|\Psi_0\rangle$ have been computed, it is not difficult to reconstruct the LIT as in Eq. (6.17). The response function $R_d(\omega_{\boldsymbol{q}})$ in Eq. (6.16) is then calculated by performing an inversion.

6.1.3 The photodisintegration cross section

We conclude this Section by deriving explicitly the expression of the photodisintegration reaction cross section, starting from the definition given in Eq. (2.19), with the response function as in Eq. (6.15) and (6.16). The cross section reads

$$\sigma(\omega_{\boldsymbol{q}}) = \frac{4\alpha\omega_{\boldsymbol{q}}}{2(2J_0+1)}\frac{4\pi^3}{3}\sum_{\lambda=\pm1}\sum_{M_0}\sum_{M_f}(-1)^{2J_f-2M_f} \times \begin{pmatrix} J_f & 1 & J_0 \\ -M_f & \lambda & M_0 \end{pmatrix}\begin{pmatrix} J_f & 1 & J_0 \\ -M_f & \lambda & M_0 \end{pmatrix} R_d^{\mathrm{red}}(\omega_{\boldsymbol{q}})\,, \tag{6.39}$$

where, since we have extracted the $3j$ symbol appearing in Eq. (6.37), the response $R_d^{\mathrm{red}}(\omega_{\boldsymbol{q}})$ contains the reduced dipole operator matrix elements $\langle\Psi_f\|\hat{d}\|\Psi_0\rangle$ squared. Due to the symmetry properties of the $3j$ symbols we can write [115]

$$\begin{pmatrix} J_f & 1 & J_0 \\ -M_f & \lambda & M_0 \end{pmatrix} = \begin{pmatrix} J_0 & J_f & 1 \\ M_0 & -M_f & \lambda \end{pmatrix}\,, \tag{6.40}$$

and this allows us to exploit the orthogonality relation [115]

$$\sum_{M_0}\sum_{M_f}(2j+1)\begin{pmatrix} J_0 & J_f & j \\ M_0 & -M_f & \lambda \end{pmatrix}\begin{pmatrix} J_0 & J_f & j' \\ M_0 & -M_f & \lambda' \end{pmatrix} = \delta_{jj'}\delta_{\lambda\lambda'}\,, \tag{6.41}$$

for $j = j' = 1$ and $\lambda = \lambda'$. Moreover, the sum over the orthogonal polarizations gives a factor 2, since the whole expression has become λ–independent. This leads to the following final result for the cross section

$$\sigma(\omega_{\boldsymbol{q}}) = \alpha\omega_{\boldsymbol{q}}\frac{4\pi^3}{9}R_d^{\mathrm{red}}(\omega_{\boldsymbol{q}})\,, \tag{6.42}$$

where we have inserted the value $J_0 = 3/2$ for the spin of ^{9}Be nucleus in its ground state.

6.2 Results

^{9}Be provides a Borromean nuclear system that is loosely bound, since it is characterized by a $J^\pi = 3/2^-$ ground state with binding energy $B_3 = 1.5736\,\mathrm{MeV}$ [73]. A scheme of the energy levels is shown in Fig. 6.1, where also the states $J^\pi = 1/2^+, 5/2^+, 3/2^+$ are visible, which are connected with the ground state through $E1$ transitions. According to Ref. [73], they correspond to the energies 1.684 MeV, 3.049 MeV and 4.704 MeV, respectively. The major contribution to the total low–energy cross section is due to the $1/2^+$ resonance, being $\approx 0.11\,\mathrm{MeV}$ above the three–body threshold; the $5/2^+$ and $3/2^+$ resonances occur at higher energies. In Fig. 6.1 also the first states with negative parity are shown, representing magnetic $M1$ transitions from the ground state. As already stated, they will not be included in the calculation of the final cross section. The $5/2^-$ resonance at 2.429 MeV [73] is very narrow; the other resonances, $1/2^-$ and $3/2^-$, have a small effect on the final low–energy cross section.

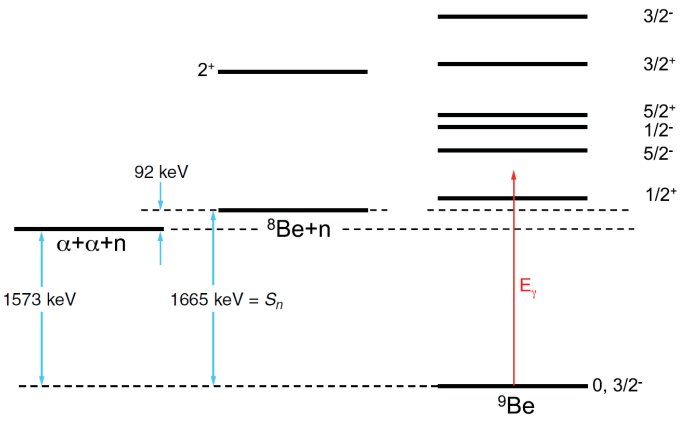

Figure 6.1: ^{9}Be level scheme taken from Ref. [5]. Energy threshold for three–body $\alpha + \alpha + n$ breakup occurs at incident photon energy 1.573 MeV. The threshold for the two–body breakup is also shown, arising at 1.665 MeV, which also corresponds to the neutron separation energy $S_n(^9\text{Be})$.

As discussed in Section 6.1.2, the calculation of the LIT assumes the knowledge of the bound state of the nuclear system under study. As a consequence, large part of this work is also devoted to ^{9}Be bound–state calculations. In the following Sections we will compute the photodisintegration cross section at Leading Order (LO) and beyond, by using different values of the EFT parameters and discussing how the results depend on the different inputs.

6.2.1 Calculations at Leading Order

The ^{9}Be ground state

We perform our calculations at LO by including the following interactions:

$$V_{LO} = V^S_{\alpha\alpha}(\Lambda^S_{\alpha\alpha}) + V^P_{\alpha n}(\Lambda^P_{\alpha n})\,, \tag{6.43}$$

namely an α–α S–wave effective potential as defined in Eq. (4.64), characterized by the cut–off parameter $\Lambda^S_{\alpha\alpha}$ of the Gaussian regulator function, in addition to an α–n effective potential in the partial wave P with cut–off $\Lambda^P_{\alpha n}$, in the form of Eq. (4.52).

The calculation of the ^{9}Be ground–state energy has been performed by using an existing Fortran code. The code, first developed for the work presented in Ref. [92], was later adapted to work with a HH basis defined in momentum space [107], including also the two–body α–α and α–n effective potentials already derived in Ref. [76]. Since we are diagonalising the Hamiltonian matrix represented on the basis (5.129) defined in momentum space, the matrix elements to be calculated are those reported in Section 5.3.3. Specifically, the matrix elements of the two–body effective potentials are computed by following the calculation derived in Eq. (5.153), and also the Coulomb potential between the two α–particles must be taken into account. Since the latter term is defined as in Eq. (5.155), it presents a logarithmic divergent character, as well as a highly oscillatory behaviour near the divergence. For this reason, as also pointed out in Ref. [29], a Gauss–Legendre quadrature integration is adopted, giving more accurate and stable results in comparison with the standard

Gauss–Laguerre method [45]. An alternative integration method has also been developed, whose details and associated tests can be found in Ref. [29]. The original Gauss–Legendre formula designed for the integration range $[-1,+1]$ [45] has been adapted to $[0,+\infty)$, in order to properly perform the integrations in Q and Q' of Eq. (5.153). The required change of variable is the following

$$x \to c \frac{\left(\frac{x+1}{2}\right)^a}{\left(1-\frac{x+1}{2}\right)^b}\,, \tag{6.44}$$

where a, b and c are real parameters. Then, the integration in the hyperangle φ_2 is carried out by means of a Gauss–Jacobi quadrature method [45].

We start by showing some convergence studies relative to the computation of the ground–state energy for the two–body cut–offs fixed to $\Lambda^S_{\alpha\alpha} = 190\,\mathrm{MeV}$ and $\Lambda^P_{\alpha n} = 300\,\mathrm{MeV}$. In Tab. 6.1 we have reported the calculated E_0 for different values of the dimension of the grids relative to the integration in the hypermomenta and in the hyperangle, N_Q ($N_{Q'} = N_Q$) and N_φ, respectively. This is done while keeping all the basis parameters fixed. Concerning the Laguerre basis relative to the "hypermomental" part, we have fixed the non–linear parameter β to the value $\beta = 0.05\,\mathrm{fm}^{-1}$, and we have considered a dimension $N_L = 30$; for the maximum grand–angular momentum, which is associated to the hyperspherical part of the basis, we have used $K^{\max} = 17$. Notice that, due to the characteristics of the potentials that we are integrating, the "hypermomental" and the hyperangular grids are deeply connected. With the parameters in Eq. (6.44) set to $a = b = 0.6$ and $c = 10$, for $N_Q, N_\varphi \approx 500$ we get an error in E_0 at the order of keV. The convergence is therefore rather slow. Due to the large number of integration points needed, the computational time of the original Fortran code is quite long. For this reason, in this work, we have opted for a first–level parallelization by using an OpenMP approach. Then, having fixed the dimension of the integration grids to $N_Q/N_\varphi = 550/500$, we have studied the variation of the energy by increasing the dimension of the Laguerre basis, from 20 to 40. In this case, as shown in Tab. 6.1, the results are stable up to the fifth digit for $N_L \geq 30$.

N_Q/N_φ	E_0	N_L	E_0
450/400	−1.948391	20	−1.948322
500/450	−1.955997	25	−1.948374
550/500	−1.962331	30	−1.948391
600/550	−1.967669	35	−1.948396
		40	−1.948398

Table 6.1: ^{9}Be ground state energies (in MeV) calculated for $K^{\max} = 17$ and $\beta = 0.05\,\mathrm{fm}^{-1}$ as a function of N_Q/N_φ, the number of points relative to the integration grids in the hypermomentum Q (Q') and in the hyperangle φ_2, respectively. On the right, the variation of E_0 by increasing N_L, the dimension of the Laguerre polynomials basis. The two–body potential cut–off parameters are fixed to $\Lambda^S_{\alpha\alpha} = 190\,\mathrm{MeV}$ and $\Lambda^P_{\alpha n} = 300\,\mathrm{MeV}$.

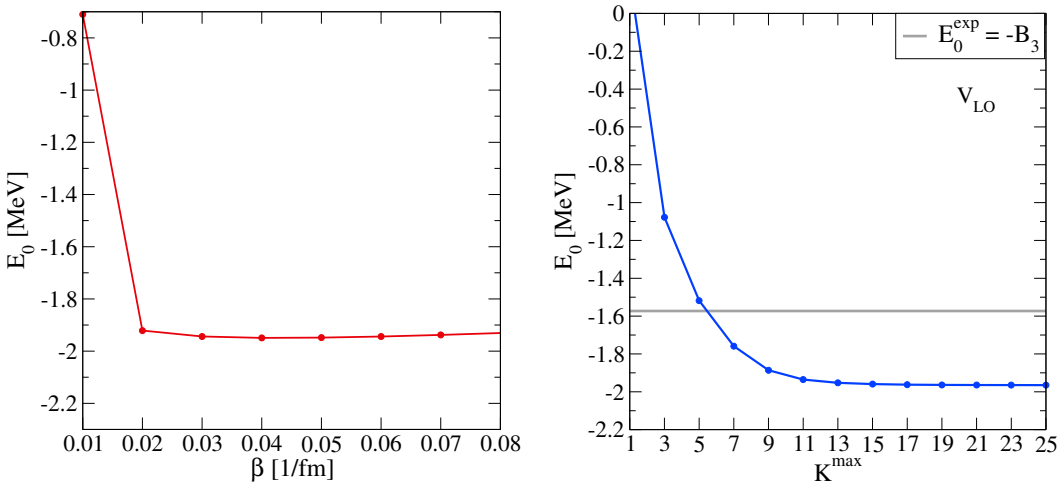

(a) (b)

Figure 6.2: ^{9}Be ground–state energy calculated with $N_L = 30$ as a function of the non–linear parameter β (a), and of $K^{\max}$ (b). In panel (a) the number of integration points is fixed to $N_Q/N_\varphi = 450/400$ and $K^{\max} = 17$. In panel (b) the results have been obtained with $N_Q/N_\varphi = 550/500$ and $\beta = 0.05$. In both cases the two–body potential cut–off parameters are fixed to $\Lambda^S_{\alpha\alpha} = 190\,\text{MeV}$ and $\Lambda^P_{\alpha n} = 300\,\text{MeV}$. The experimental three–body binding energy is $B_3 = 1.573\,\text{MeV}$ [73].

In Fig. 6.2a we have tested the stability of the results by varying the non–linear parameter β. It can be deduced that any value inside the range of stability $\beta = 0.03 - 0.06\,\text{fm}^{-1}$ can be employed to speed–up the convergence. Finally, we have studied the variation of the ground–state energy with respect to the maximum grand–angular momentum quantum number. The convergence pattern is shown in Fig. 6.2b. For $K^{\max} = 17, 19$ the error in the computed energy is of about a few keV units, while $K^{\max} = 23, 25$ ensures an accuracy up to the third or even fourth decimal place. The rather fast convergence in $K^{\max}$ to the value $E_0 = -1.965\,\text{MeV}$ is mainly due to the smoothness of the two–body effective potentials employed in the calculation. The typical values used to perform convergent calculations are therefore $\beta = 0.05\,\text{fm}^{-1}$, $N_Q/N_\varphi = 550/500$, $N_L = 30$ and $K^{\max} = 25$.

The square points in Fig. 6.3 show the calculated ^{9}Be ground state energy for fixed $\Lambda^S_{\alpha\alpha} = 190\,\text{MeV}$ and for three different values of the cut–off $\Lambda^P_{\alpha n}$ allowed by the Wigner bound $\Lambda^P_{\alpha n} < 330\,\text{MeV}$. On the right panel we have also put the results for E_0 computed with $\Lambda^P_{\alpha n} = 300\,\text{MeV}$ and for different values of $\Lambda^S_{\alpha\alpha}$, such that $\Lambda^S_{\alpha\alpha} < 230\,\text{MeV}$. As also discussed in Ref. [29], a variation of the cut–off $\Lambda^P_{\alpha n}$ gives rise to a broader range of values for the calculated E_0 ($\approx 1.8\,\text{MeV}$) with respect to the range originated by varying $\Lambda^S_{\alpha\alpha}$ ($\approx 0.7\,\text{MeV}$). However, the plotted behaviour is different: while by increasing $\Lambda^P_{\alpha n}$ at fixed $\Lambda^S_{\alpha\alpha} = 190\,\text{MeV}$ the results obtained show somehow a convergence for $\Lambda^P_{\alpha n} = 200 - 300\,\text{MeV}$, the energy E_0 obtained by varying $\Lambda^S_{\alpha\alpha}$ at fixed $\Lambda^P_{\alpha n} = 300\,\text{MeV}$ shows an oscillation. In any case, all the plotted results are theoretically allowed.

As explicitly shown in Fig. 6.3, the three–body ground–state energy depends on the choice of the two–body cut–off parameters $\Lambda^S_{\alpha\alpha}$ and $\Lambda^P_{\alpha n}$. In order to avoid such

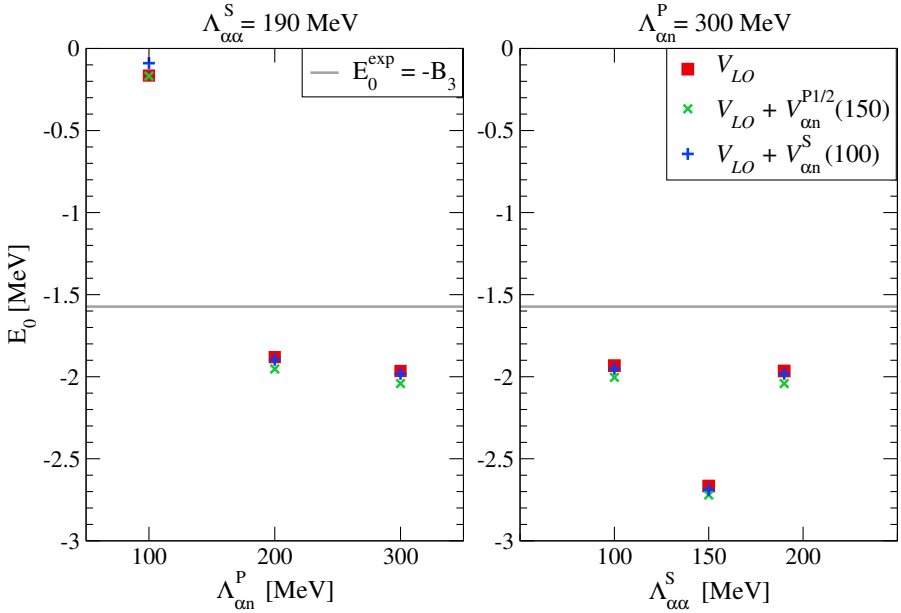

Figure 6.3: ^{9}Be ground–state energies calculated with fixed $\Lambda^S_{\alpha\alpha} = 190\,\text{MeV}$ for different values of the cut–off $\Lambda^P_{\alpha n}$ (left panel) and with fixed $\Lambda^P_{\alpha n} = 300\,\text{MeV}$ for different $\Lambda^S_{\alpha\alpha}$ (right panel). The green and blue symbols represent a correction to the LO calculation with $V_{LO} = V^S_{\alpha\alpha}(\Lambda^S_{\alpha\alpha}) + V^P_{\alpha n}(\Lambda^P_{\alpha n})$ (red squares) due to the additional terms $V^{P1/2}_{\alpha n}$ ($\Lambda^{P1/2}_{\alpha n} = 150\,\text{MeV}$) and $V^S_{\alpha n}$ ($\Lambda^S_{\alpha n} = 100\,\text{MeV}$), respectively (see Section 6.2.2). The experimental three–body binding energy is taken from Ref. [73] as $B_3 = 1.573\,\text{MeV}$.

a situation, we include in the calculation at LO also a three–body potential in the form of Eq. (5.156). This will allow us to fix $\Lambda^S_{\alpha\alpha}$ and $\Lambda^P_{\alpha n}$, while leaving the three–body parameters free. The matrix elements relative to the three–body potential can be evaluated as in Eq. (5.157) and the implementation of this interaction in the original Fortran code was first done in the work of Ref. [29]. With the notation V_{LO+3} we will therefore refer to the following potential:

$$V_{LO+3} = V^S_{\alpha\alpha}(\Lambda^S_{\alpha\alpha}) + V^P_{\alpha n}(\Lambda^P_{\alpha n}) + V_3(\Lambda_3, \lambda_3)\,. \tag{6.45}$$

Typically we will choose as two–body cut–offs $\Lambda^S_{\alpha\alpha} = 190\,\text{MeV}$ and $\Lambda^P_{\alpha n} = 300\,\text{MeV}$, being one of the pairs that best reproduce the α–α and α–n low–energy phase–shifts (see Figs. 4.5 and 4.7b). When doing bound–state calculations, once also Λ_3 has been fixed, the strength of the three–body force λ_3 is adjusted in order to ensure that the effective theory reproduces the correct energy of the ^{9}Be ground state. Fig. 6.4 shows the values of the constant $\lambda_3^{3/2^-}$ needed in order to obtain the energy $E_0 = -1.573\,\text{MeV}$ of the $3/2^-$ ground state by varying the three–body cut–off Λ_3 in the range of values from 100 to 600 MeV. Basically, by tuning the strength of the three–body potential, the dependence of the observable E_0 on the cut–offs associated to the two–body forces is cancelled, and the experimental energy of the ground state is reproduced for all the values of Λ_3. In Fig. 6.4 we have also plotted the behaviour of the dimensionless parameter $c_3^{3/2^-}$ by varying Λ_3 in the

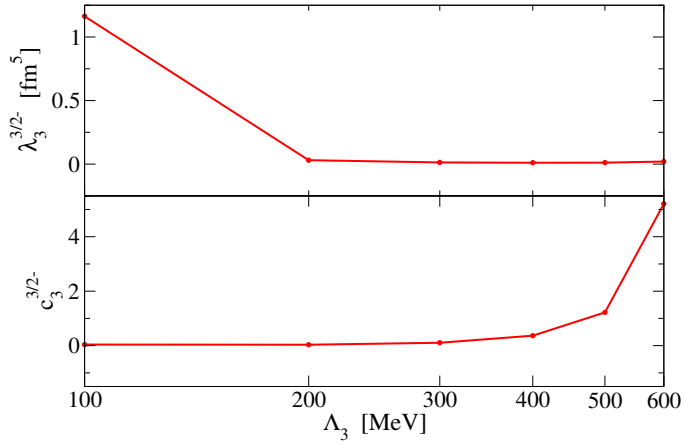

Figure 6.4: Values of $\lambda_3^{3/2^-}$ (upper panel) and of the dimensionless parameter $c_3^{3/2^-} = \lambda_3^{3/2-}\Lambda_3^5$ (lower panel) as a function of the three–body cut–off Λ_3. The strength $\lambda_3^{3/2^-}$ is tuned to reproduce the ^{9}Be experimental ground–state energy. The LO potential in Eq. (6.45) has been used in the calculations, with $\Lambda_{\alpha\alpha}^S = 190\,\text{MeV}$ and $\Lambda_{\alpha n}^P = 300\,\text{MeV}$.

same range of values. For purely dimensional reasons, we have defined $c_3 = \lambda_3\Lambda_3^5$. In principle, since other scales are present in the theory, one could have defined c_3 differently, for example by inserting a mass parameter in the relation, thus reducing the power relative to the dependence on Λ_3 ($\sim \Lambda_3^4$). This is in fact what Fig. 6.4 suggests. Finally, by fixing $\Lambda_3 = 300\,\text{MeV}$, we have studied the behaviour of the ground state energy E_0 as a function of the maximum grand–angular momentum $K^{\max}$. The convergence pattern has been plotted in Fig. 6.5 and, essentially, it is very similar to the one already shown in Fig 6.2b, which was obtained without the contribution of the three–body force.

The ^{9}Be photodisintegration cross section

By exploiting the results obtained for the ^{9}Be ground state, we compute the LIT associated to the $E1$ transition $3/2^- \to 1/2^+$, as in Eq. (6.17). In calculating the dipole matrix elements $\langle\Psi_l|\hat{d}_\lambda|\Psi_0\rangle$, due to the quite large degeneracy in the index l, we have performed a parallelization of the code on the loops involving this index by using an OpenMP approach. In order to solve the eigenvalue problem for the final state $J^\pi = 1/2^+$, we use the same Hamiltonian as the one employed for the ground state, including the potential V_{LO+3} in Eq. (6.45) with $\Lambda_{\alpha\alpha}^S = 190\,\text{MeV}$, $\Lambda_{\alpha n}^P = 300\,\text{MeV}$ and $\Lambda_3 = 300\,\text{MeV}$.

In Fig. 6.6, we show the calculated LIT $L(\sigma_R, \sigma_I)$, with fixed $\sigma_I = 0.2\,\text{MeV}$, for different values of the strength of the three–body potential $\lambda_3^{1/2^+}$. By using the same strength employed to calculate the ground state, i.e. $\lambda_3^{1/2^+} = \lambda_3^{3/2^-} = 0.013045\,\text{fm}^5$, we obtain a rather large resonance peak located above 2 MeV. The position of the latter is adjusted by varying the parameter towards negative values, until the experimental location $\approx 1.7\,\text{MeV}$ is reached. Notice that a $1/2^+$ bound state starts to appear already for $\lambda_3^{1/2^+} = -0.1140\,\text{fm}^5$, which is unphysical. This mechanism

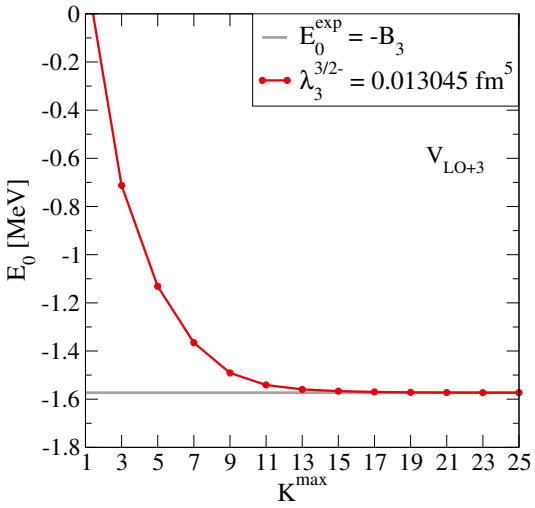

Figure 6.5: Convergence study of the ^{9}Be ground–state energy with respect to the maximum grand–angular momentum $K^{\max}$. E_0 is calculated at LO by including a three–body potential $[V^S_{\alpha\alpha}(190) + V^P_{\alpha n}(300) + V_3(300, 0.013045)$, see Eq. (6.45)]. We take $B_3 = 1.573\,\text{MeV}$ [73].

suggests that the three–body potential is state–dependent. Actually a similar result was obtained also in Refs. [18, 116]. In [116], for example, Odsuren, *et al.* have investigated the same ^{9}Be $1/2^+$ resonance by using the complex scaling method in a three–body cluster framework. Even though the potentials employed are of different type, and the three–body force is defined in coordinate space, $1/2^+$ calculations agree with the experimental data by choosing an appropriate strength for the three–body potential, which is different from the one used for the $3/2^-$ bound–state.

In Fig. 6.6, when computing the LIT, we have used a "hypermomental" (hyperradial) basis of dimension $N_L = 30$ with a non–linear parameter fixed to $\beta = 0.05$ and a maximum grand–angular momentum $K^{\max} = 26$. By taking as a starting point the result represented with the red solid line, i.e. the LIT with the resonance peak in the correct position at $\approx 1.7\,\text{MeV}$, we have carried out different calculations by varying β, $K^{\max}$ and N_L. The LIT for $\sigma_I = 0.2\,\text{MeV}$ is quite stable for β in the range of values from $0.03\,\text{fm}^{-1}$ to $0.06\,\text{fm}^{-1}$, as it can be deduced from Fig. 6.7. An increasing value of the grand–angular momentum quantum number K slightly affects the position and the width of the resonance peak, and convergent results can be obtained for $K^{\max} = 26$ as shown in Fig. 6.8a. A different behaviour can be noticed if one varies the dimension of the "hypermomental" (hyperradial) basis, as reported in Fig. 6.8b. The effect of an increasing N_L can be seen mainly outside the peak region at energies above $\approx 2.5\,\text{MeV}$, where the visible oscillations present at $N_L = 30$ are smoothed by taking $60 \leq N_L \leq 90$. Since a LIT with a smooth behaviour is preferable in order to obtain more accurate results during the inversion procedure, a value of at least $N_L = 60$ is recommended. The reason for such a highly oscillatory behaviour of the LIT, and therefore for such a slow rate of convergence, can be traced back to the small value chosen for σ_I, namely $0.2\,\text{MeV}$. This parameter is closely related to the width of the Lorentzian kernel used in defining the LIT itself. As also discussed in Section 3.2, the smaller is σ_I, the later the convergence

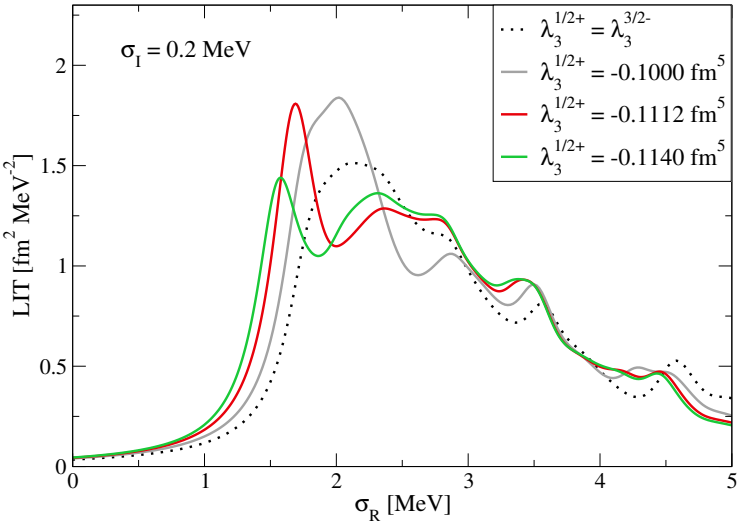

Figure 6.6: LIT relative to the $E1$ transition $3/2^- \to 1/2^+$ calculated for $\sigma_I = 0.2\,\text{MeV}$, $K^{\max} = 26$ and $N_L = 30$. The LO potential used is $V^S_{\alpha\alpha}(190) + V^P_{\alpha n}(300) + V_3(300, \lambda_3^{1/2^+})$ [see Eq. (6.45)], where the strength of the three–body force is varied to have a resonance peak located in the correct position.

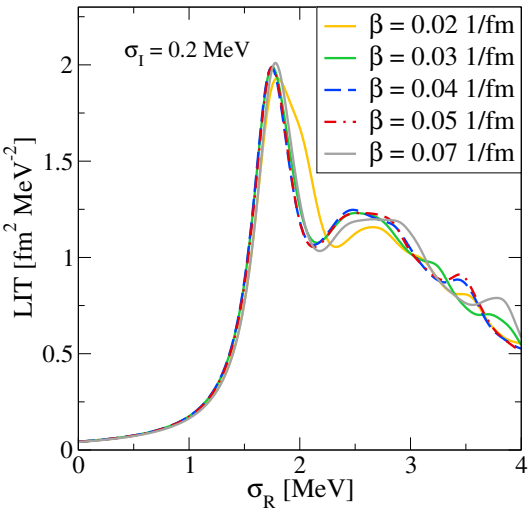

Figure 6.7: Same as Fig. 6.6 with the three–body strength fixed to $\lambda_3^{1/2^+} = 0.1112\,\text{fm}^5$. The LIT is calculated for different values of the non–linear parameter β relative to the "hypermomental" (hyperradial) basis employed.

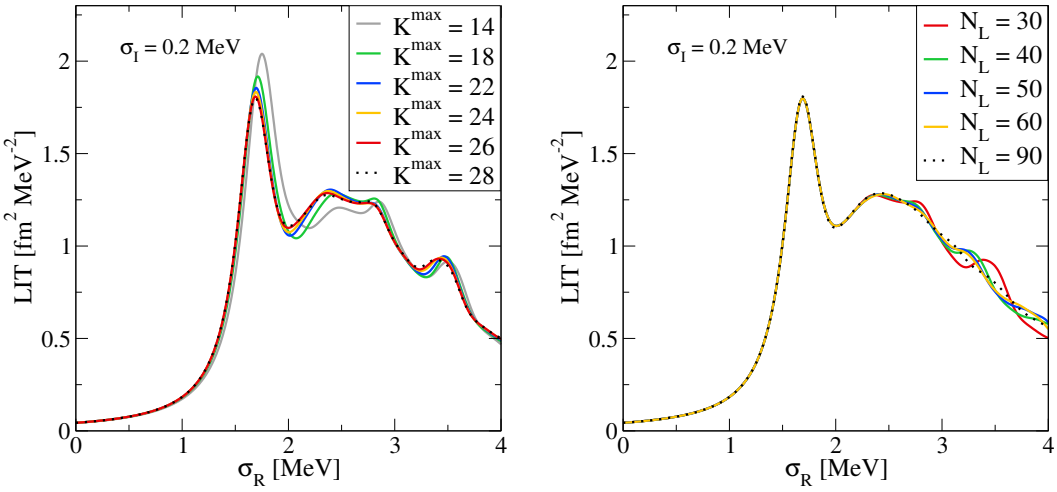

Figure 6.8: Same as Fig. 6.6 with fixed $\lambda_3^{1/2^+} = 0.1112\,\mathrm{fm}^5$. The convergence pattern of the LIT is shown both with respect to the maximum grand–angular momentum $K^{\max}$ ($N_L = 30$) (a) and with respect to the dimension of the "hypermomental" (hyperradial) basis N_L ($K^{\max} = 26$) (b).

is reached. However, in studying the narrow resonance associated to the ^{9}Be $1/2^+$ state, we are somehow forced to take $\sigma_I \lesssim 0.2\,\mathrm{MeV}$, because this is a value that is comparable with the experimental width of the peak. By taking $\sigma_I > 0.2\,\mathrm{MeV}$ the convergence will be faster but, at the same time, the information on the resonance peak is lost. This can be visualized in Fig. 6.9, where we have calculated the LIT for increasing σ_I. With respect to the case $\sigma_I = 0.2\,\mathrm{MeV}$, the resulting LITs are smaller in height; the peak starts to "blur" for $\sigma_I = 0.5\,\mathrm{MeV}$ while it completely disappears for $\sigma_I = 1\,\mathrm{MeV}$, not allowing to perform a good inversion.

Finally, we have calculated $L(\sigma_R, \sigma_I)$ for $\sigma_I = 0.2\,\mathrm{MeV}$ by varying the cut–off relative to the three–body potential, which so far has been kept fixed at $\Lambda_3 = 300\,\mathrm{MeV}$. The LIT for $\Lambda_3 = 400\,\mathrm{MeV}$ is in Fig. 6.10a, showing an increased height of about 8%. The results are therefore slightly dependent on the variation of Λ_3.

The LIT relative to the $E1$ transition $3/2^- \to 5/2^+$ is shown in Fig. 6.10b. In order to obtain this result, we have used again Eq. (6.17), with $J^\pi = 5/2^+$ as the final state. With a cut–off $\Lambda_3 = 400\,\mathrm{MeV}$ relative to the three–body force, the strength $\lambda_3^{5/2^+} = 0.0125\,\mathrm{fm}^5$ produces a resonance peak located at the experimental energy $\approx 3\,\mathrm{MeV}$. Furthermore, also in this case, we have used the value $\sigma_I = 0.2\,\mathrm{MeV}$, since the experimental width of the $5/2^+$ resonance is $\approx 0.2\,\mathrm{MeV}$. The result shown in Fig. 6.10b has been obtained with $K^{\max} = 26$ and $N_L = 40$. Due to the resonance position at $\approx 3\,\mathrm{MeV}$, on the basis of the results obtained for the $1/2^+$ state, we expect that these values do not assure a full convergence of the calculated LIT.

Starting from the fully convergent $1/2^+$ LIT results given Fig. 6.10a, we have performed an inversion to obtain the associated response functions [117]. Then, from Eq. (6.42), we have computed the ^{9}Be photodisintegration cross–section relative to the transition $3/2^- \to 1/2^+$, which is shown in Fig. 6.11. The results are plotted as a function of the incident photon energy ω. In the $1/2^+$ resonance region, our

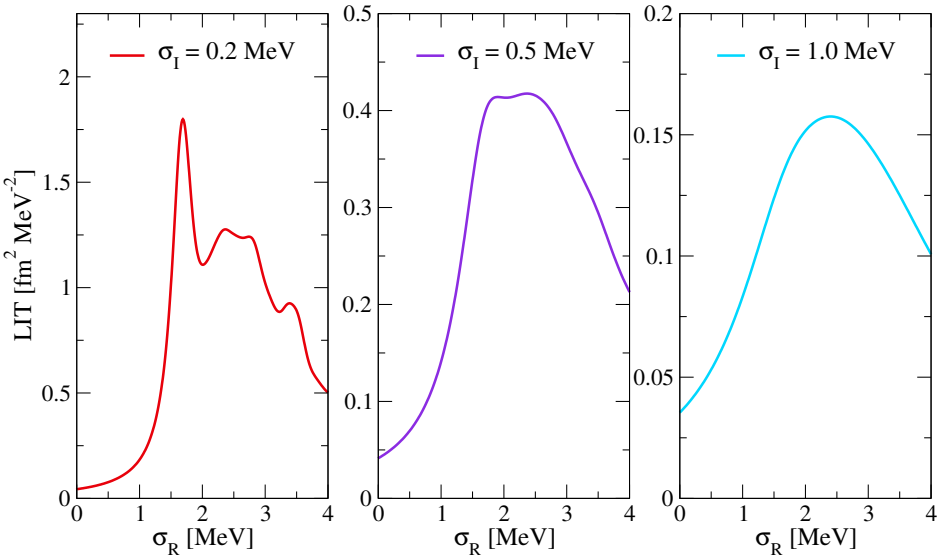

Figure 6.9: Same as Fig. 6.6 with fixed $\lambda_3^{1/2^+} = 0.1112\,\mathrm{fm}^5$, including other LITs calculated for different values of the parameter σ_I.

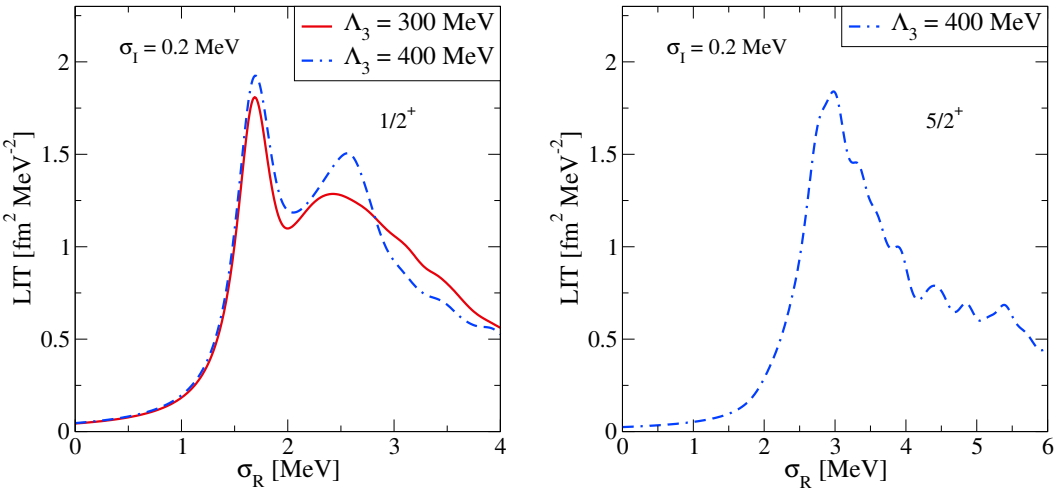

(a) (b)

Figure 6.10: (a) LIT relative to the transition $3/2^- \to 1/2^+$ calculated at convergence ($K^{\max} = 26$, $N_L = 90$) for two different values of the cut–off Λ_3. (b) LIT relative to the transition $3/2^- \to 5/2^+$ calculated for $\Lambda_3 = 400\,\mathrm{MeV}$ ($K^{\max} = 26$, $N_L = 40$). Both results have been obtained with the LO potential $V^S_{\alpha\alpha}(190) + V^P_{\alpha n}(300) + V_3(\Lambda_3, \lambda_3^{1/2^+})$ [see Eq. (6.45)] and for $\sigma_I = 0.2\,\mathrm{MeV}$.

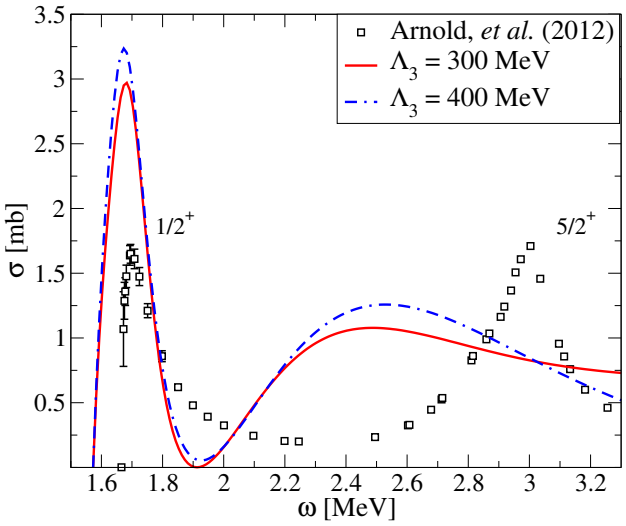

Figure 6.11: ^{9}Be photodisintegration cross section relative to the $E1$ transition $3/2^- \to 1/2^+$ as a function of the incident photon energy ω. The three–body energy threshold is located at 1.573 MeV. The results correspond to the LITs calculated in Fig. 6.10a for two different values of the three–body cut–off parameter. The set of experimental data is taken from Ref. [5].

calculated cross sections overestimate the experimental data of Ref. [5] by a factor of almost 2. In addition, the $1/2^+$ resonance has a high tail at energies above ≈ 2 MeV, which would also affect the cross section in the $5/2^+$ resonance region with a contribution of ≈ 1 mb. Although these final results are rather acceptable from a EFT point of view, as they slightly depend on a variation of the cut–off associated to the three–body interaction, we have decided to proceed by including in the calculation, not only the LO interactions in Eq. (6.43), but also other partial wave components of the effective two–body potentials. This study will be developed in the next Sections.

6.2.2 Calculations beyond Leading Order

Driven by the results obtained in the last Section, we have also performed calculations by adding other partial waves to the LO effective interactions of Eq. (6.43). In this Section we will use the following potentials

$$V_{LO} + V_{\alpha n}^{P1/2}(\Lambda_{\alpha n}^{P1/2}) \,, \tag{6.46}$$

$$V_{LO} + V_{\alpha n}^{S}(\Lambda_{\alpha n}^{S}) \,, \tag{6.47}$$

eventually adding also a three–body force term. We will often refer to these interaction as Next–to–Leading Order (NLO) potentials. In the equations above, $V_{\alpha n}^S$ is the effective α–n interaction in the partial wave S with associated cut–off $\Lambda_{\alpha n}^S$, as derived in Eq. (4.53), while $V_{\alpha n}^{P1/2}$ is the $P_{1/2}$–wave component, with cut–off $\Lambda_{\alpha n}^{P1/2}$, which we will consider in the form of Eq. (4.52). Our aim is to analyse the effect of these additional terms, first by calculating the ^{9}Be ground–state energy, and then the LIT.

The ^{9}Be ground state

We start by studying the case in which no three–body interaction is present in the model. We choose as cut–off parameters $\Lambda_{\alpha n}^{P1/2} = 150\,\text{MeV}$ and $\Lambda_{\alpha n}^{S} = 100\,\text{MeV}$, both allowed by each associated Wigner bound. The effect of the additional terms $V_{\alpha n}^{P1/2}$ and $V_{\alpha n}^{S}$ on the ^{9}Be ground–state energy is shown in Fig. 6.3, for different values of the cut–off $\Lambda_{\alpha n}^{P}$ at fixed $\Lambda_{\alpha\alpha}^{S}$, and vice versa. In most cases, E_0 is smaller with respect to the LO calculations: the $P_{1/2}$–wave induces a difference of about $\approx 70\,\text{keV}$, while the S–wave contribution is of $\approx 17\,\text{keV}$.

By adding the three–body potential term, i.e. by considering the NLO interactions

$$V_{LO+3} + V_{\alpha n}^{P1/2}(\Lambda_{\alpha n}^{P1/2})\,, \tag{6.48}$$

$$V_{LO+3} + V_{\alpha n}^{S}(\Lambda_{\alpha n}^{S})\,, \tag{6.49}$$

where V_{LO+3} is defined as in Eq. (6.45), the value of the strength $\lambda_3^{3/2^-}$ is adjusted in order to obtain the experimental ground state energy of ^{9}Be nucleus for each value of Λ_3. In Figs. 6.12a and 6.12b, we have studied the convergence of the calculated E_0 with respect to the grand–angular momentum $K^{\max}$. With the addition of the α–n effective interaction in the $P_{1/2}$–wave, the converge pattern is essentially the same as the one obtained at LO (see Fig 6.5), while the inclusion of the term $V_{\alpha n}^{S}$ seems to lead to a faster convergence in $K^{\max}$.

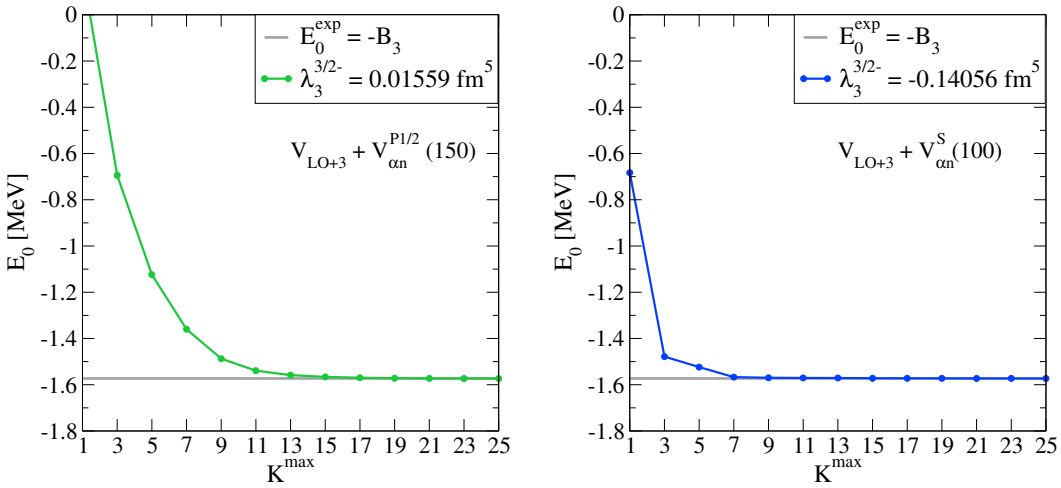

(a) (b)

Figure 6.12: Convergence study of ^{9}Be ground–state energy with respect to the maximum grand–angular momentum quantum number $K^{\max}$. E_0 is calculated by adding to V_{LO+3} $[V_{\alpha\alpha}^{S}(190) + V_{\alpha n}^{P}(300) + V_3(300, \lambda_3^{3/2^-})]$ either the α–n effective potential $V_{\alpha n}^{P1/2}(150)$ (a) or the interaction $V_{\alpha n}^{S}(100)$ (b). In both cases, the chosen strength of the three–body potential, $\lambda_3^{3/2^-}$, allows to obtain the experimental ground state energy $-1.573\,\text{MeV}$ [73].

The α–n S–wave effective potential

So far $\Lambda^S_{\alpha n} = 100\,\text{MeV}$ has been used in the calculations but the value of this parameter should be increased, in order to work with an α–n S–wave effective potential that better describes the experimental low–energy phase–shifts. This can be deduced, for example, by looking at Fig. 4.5. Unfortunately, already at $\Lambda^S_{\alpha n} = 200\,\text{MeV}$, a two–body bound–state of energy $e_0 = -5.615\,\text{MeV}$ appears, which is unphysical. In Tab. 6.2 we have collected the calculated energies of the existing bound–states by increasing the cut–off $\Lambda^S_{\alpha n}$ up to 525 MeV. All these values are theoretically allowed by the Wigner bound. Being a result of the T–matrix resummation procedure employed to determine the LECs of the effective potential $V^S_{\alpha n}$ (see Section 4.3), these bound–states are forbidden by the Pauli principle. In fact, a $\ell = 0$ state is not admitted for the neutron, since it is already fully occupied by the internal nucleons of the α–particles, which are not treated explicitly in the theory. Being forbidden, these bound–states must be projected out. This can be achieved [118] by adding to the effective potential $V^S_{\alpha n}$ the following "projection" term

$$V_{PR} = |\psi^S_{\alpha n}\rangle\, \Gamma\, \langle\psi^S_{\alpha n}|\ , \tag{6.50}$$

where Γ is a constant and $|\psi^S_{\alpha n}\rangle$ is the eigenstate relative to the deep bound–state with energy e_0. This method has been used also in Ref. [119] by Deltuva. There, it is applied to project out the forbidden states relative to the n–^{18}C potentials employed to study the low–energy n–^{19}C scattering in a three–body model. In momentum space the projection potential reads

$$V_{PR}(\boldsymbol{p}, \boldsymbol{p}') = \Gamma\, \Psi^{S*}_{\alpha n}(\boldsymbol{p})\, \Psi^S_{\alpha n}(\boldsymbol{p}')\,. \tag{6.51}$$

Being $\boldsymbol{p}$ ($\boldsymbol{p}'$) a relative momentum between the neutron and the α–particle, the matrix elements of the interaction above can be calculated as in Eq. (5.153), where the 2π–factors have been included in the constant Γ. The exact value of this parameter is not important, since, as also stated in Ref. [119], formally $\Gamma \to \infty$ but basically it is sufficient to use a value for which the three–body bound–state and scattering calculations turn out to be Γ–independent.

In the calculations we will mainly employ the effective potential $V^S_{\alpha n}$ with a fixed cut–off $\Lambda^S_{\alpha n} = 300\,\text{MeV}$, which has been also plotted in Fig. 6.13a. This

$\Lambda^S_{\alpha n}$	e_0
200	−5.615
250	−20.83
300	−12.25
400	−13.35
500	−13.85
525	−13.97

Table 6.2: Energies e_0 (MeV) of the α–n bound–states that exist in correspondence to some values of $\Lambda^S_{\alpha n}$ (MeV), the cut–off parameter relative to the α–n effective potential in the partial wave S.

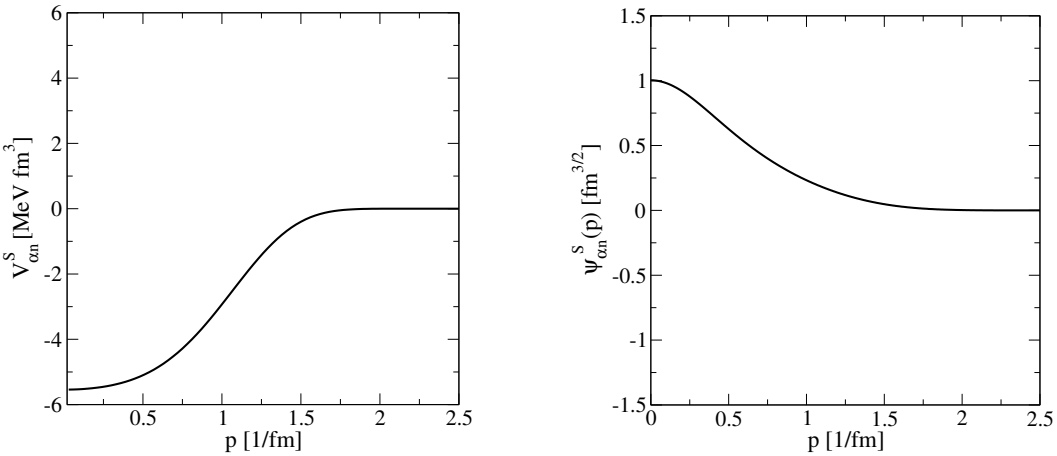

(a) (b)

Figure 6.13: α–n "diagonal" S–wave effective potential $V^S_{\alpha n}$ calculated with a cut–off fixed to the value $\Lambda^S_{\alpha n} = 300\,\text{MeV}$ (a) and the wave–function relative to the existing deeply bound–state with energy $E_0 = -12.25\,\text{MeV}$ (b).

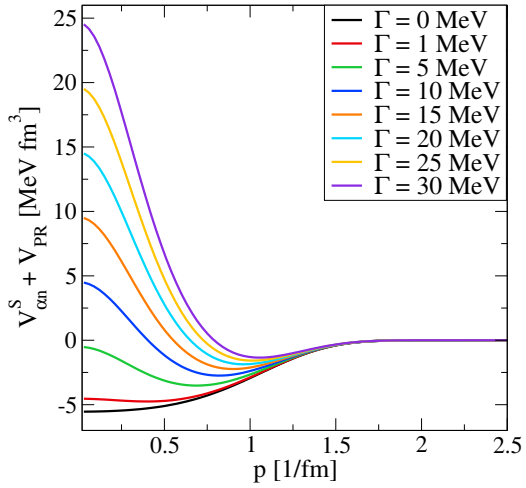

Figure 6.14: Effect of the addition of the "diagonal" projection potential term V_{PR} to the α–n S–wave "diagonal" effective interaction ($\Lambda^S_{\alpha n} = 300\,\text{MeV}$) for different values of the projection parameter Γ.

interaction produces a forbidden bound state with energy $e_0 = -12.25\,\text{MeV}$, whose wave function has been calculated [117] and is showed in Fig. 6.13b. The total interaction resulting from the sum of the effective potential and the projection term (6.51) is represented in Fig. 6.14, for different values of the parameter Γ. Essentially, by increasing Γ a repulsive core arises, which is supposed to project out the Pauli–forbidden two–body bound–state.

We have also studied the effect of the projection potential on the low–energy spectrum of the subsystem α–n. In Tab. 6.3 we have collected the first calculated eigenvalues by varying the projection parameter. As the latter increases, the forbidden bound–state becomes less bound until it disappears for values of Γ in the

Γ	e_0	e_1	e_2	e_3	e_4	e_5
0	−12.25	0.3149	1.266	2.871	5.168	8.212
1	−11.25	0.3149	1.266	2.871	5.168	8.212
5	−7.245	0.3149	1.266	2.871	5.168	8.212
10	−2.245	0.3149	1.266	2.871	5.168	8.212
15		0.3149	1.266	2.871	5.168	8.212
20		0.3149	1.266	2.871	5.168	8.212
50		0.3149	1.266	2.871	5.168	8.212
250		0.3149	1.266	2.871	5.168	8.212
2000		0.3149	1.266	2.871	5.168	8.212

Table 6.3: Discretized low–energy spectrum (MeV) for the channel $1/2^+$ relative to the subsystem α–n for different values of the projection parameter Γ (MeV).

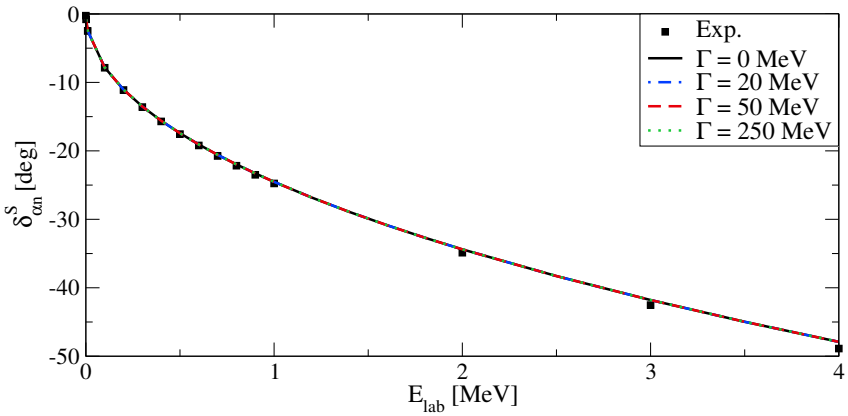

Figure 6.15: α–n S–wave low–energy phase–shifts calculated with the projection potential V_{PR} in addition to the two–body effective interaction $V^S_{\alpha n}(300)$, for different values of the projection parameter Γ. The experimental data are from Ref. [82].

range $\Gamma \geq 15\,\text{MeV}$; meanwhile, the rest of the discretized low–energy spectrum is completely unaffected. As a last check, we have calculated the α–n low–energy phase–shifts for different values of the parameter Γ. Also in this case, as Fig. 6.15 shows, no significant differences arise in the results when the projection potential is added and the constant Γ is varied.

The phase–shifts in Fig. 6.15 have been computed by using a method based on integral relations, which was first introduced in Refs. [120, 121] by Kievsky, *et al.*. Essentially, this technique provides a way to calculate scattering parameters, such as phase–shifts and mixing angles, making use of bound–state–like wave functions. A feasibility test of the method has been done in Ref. [94], for systems composed of $A = 2$ and 3 nucleons, in conjunction with a symmetrized HH method, and by employing both phenomenological and realistic NN potentials [122]. The results obtained here show that the method is also well suited to work with the two–body α–n system described by effective potentials defined in momentum space, such as those used in this work.

We conclude this Section by including some results regarding the effect of the

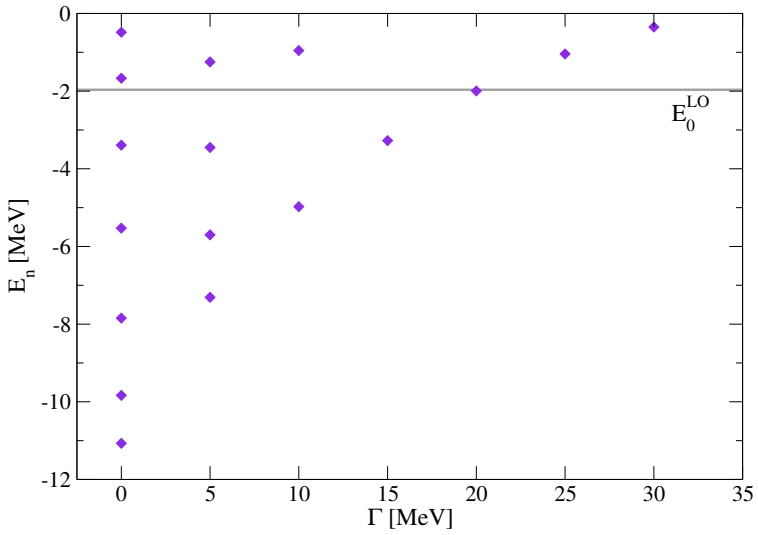

Figure 6.16: Negative eigenvalues for ^{9}Be obtained by diagonalizing the three–body Hamiltonian with the NLO potential $V_{LO} + V^S_{\alpha n}(300) + V_{PR}(\Gamma)$, with $V_{LO} = V^S_{\alpha\alpha}(190) + V^P_{\alpha n}(300)$, as a function of the projection parameter Γ. The values $K^{\max} = 25$ and $N_L = 30$ have been used in the calculation. $E_0^{LO} = -1.965\,\text{MeV}$ is the lowest eigenvalue obtained by using only the V_{LO} term.

additional projection potential term (6.51) in the three–body sector. By using the interaction in Eq. (6.47) including V_{PR},

$$V_{LO} + V^S_{\alpha n}(300) + V_{PR}(\Gamma)\,, \tag{6.52}$$

we have calculated the three–body discretized low–energy spectrum relative to the ^{9}Be system for $K^{\max} = 25$ and $N_L = 30$, and we have collected the results in Fig. 6.16. When the projection potential is missing, in diagonalizing the Hamiltonian matrix, 7 negative eigenvalues show up, in which the lower is at about 11 MeV. By increasing the value of the projection parameter Γ, the number of negative eigenvalues decreases until only one survives around 2 MeV, for Γ in the range from about 15 MeV to 30 MeV. Above this range, no negative eigenvalue exists. Notice that for $\Gamma \simeq 20\,\text{MeV}$ the lowest eigenvalue of the Hamiltonian approaches the value $E_0^{LO} = -1.965\,\text{MeV}$, which is the lowest eigenvalue obtained at LO (see Fig. 6.2b). By using a non–zero Γ, the absence of deeply bound three–body states is therefore ensured.

By including the three–body force in the calculation, namely by using the interaction

$$V_{LO+3} + V^S_{\alpha n}(300) + V_{PR}(\Gamma)\,, \tag{6.53}$$

with V_{LO+3} defined as in Eq. (6.45), we have studied the variation of the strength $\lambda_3^{3/2^-}$ for fixed $\Lambda_3 = 300\,\text{MeV}$, as a function of the projection parameter Γ. The results are plotted in Fig. 6.17. We recall here that, by tuning the constant $\lambda_3^{3/2^-}$, one manages to obtain the experimental ground–state energy of ^{9}Be for every value of the cut–off Λ_3 given in input. By including also the projection term V_{PR} in the theory, it is interesting to observe that, for fixed $\Lambda_3 = 300\,\text{MeV}$, the dependence

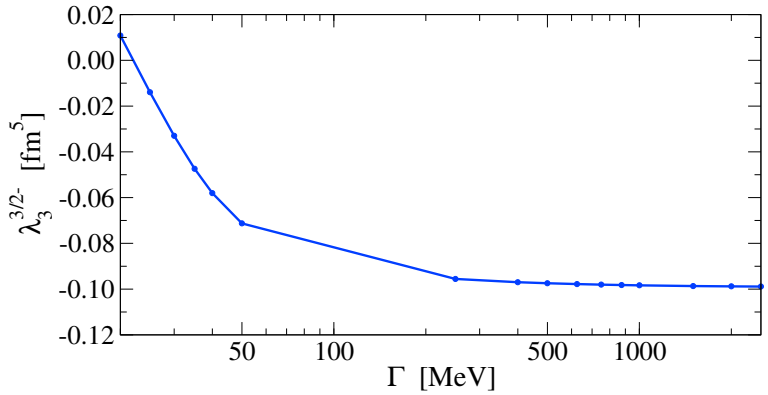

Figure 6.17: Strength of the three–body potential $\lambda_3^{3/2^-}$ as a function of the projection parameter Γ. $\lambda_3^{3/2^-}$ is tuned to reproduce the experimental ground state energy. The NLO potential used is $V_{LO+3} + V^S_{\alpha n}(300) + V_{PR}(\Gamma)$, where $V_{LO+3} = V^S_{\alpha\alpha}(190) + V^P_{\alpha n}(300) + V_3(\Lambda_3, \lambda_3^{3/2^-})$ and here $\Lambda_3 = 300\,\text{MeV}$.

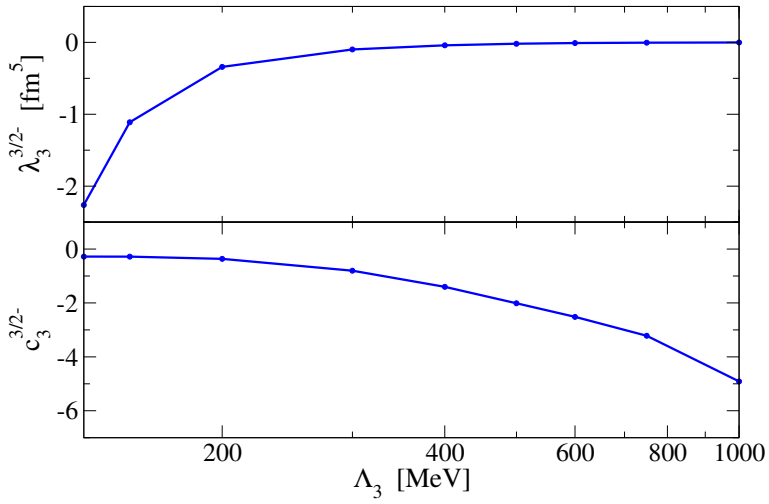

Figure 6.18: Values of $\lambda_3^{3/2^-}$ (upper panel) and of the dimensionless parameter $c_3^{3/2^-}$ (lower panel) as a function of three–body cut–off Λ_3. By tuning the strength $\lambda_3^{3/2^-}$ the experimental ground state energy is always reproduced. The NLO potential used is the same as Fig. 6.17 with $\Gamma = 2000\,\text{MeV}$.

of the strength $\lambda_3^{3/2^-}$ on Γ reaches a plateau in the region above $\Gamma \approx 500\,\text{MeV}$. A value of Γ taken in this region should therefore ensure that the three–body results are independent on Γ itself. Within this range, this constant can also no longer be considered as a free parameter. By fixing $\Gamma = 2000\,\text{MeV}$, we have then studied the behaviour of the strength of the three–body potential $\lambda_3^{3/2^-}$ by varying the cut–off Λ_3. The results are reported in Fig. 6.18, where the dependence of the dimensionless parameter $c_3^{3/2^-}$ on Λ_3 is also shown. Natural values of $c_3^{3/2^-}$ around unit arise for cut–offs $\Lambda_3 \sim 300 - 400\,\text{MeV}$. We point out again that c_3 is defined here as $c_3 = \lambda_3 \Lambda_3^5$.

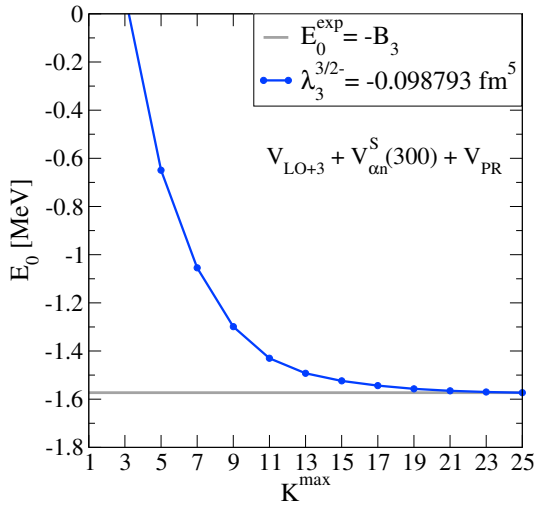

Figure 6.19: Convergence study of the ^{9}Be ground state energy with respect to the maximum grand–angular momentum quantum number $K^{\max}$. The NLO potential used is the same as Fig. 6.17 with $\Lambda_3 = 300\,\text{MeV}$ and $\Gamma = 2000\,\text{MeV}$. With the chosen strength $\lambda_3^{3/2^-}$ the experimental ground state energy [73] is reproduced.

With fixed $\Gamma = 2000\,\text{MeV}$ and $\Lambda_3 = 300\,\text{MeV}$, in Fig. 6.19 we have also studied the convergence of the ^{9}Be ground–state energy E_0 with respect to $K^{\max}$. Due to the presence of a more repulsive core, the convergence is slower in comparison with calculations done without the projection potential. However, by taking a maximum grand–angular momentum equal to 25, the error is still of the order of a few keV.

The ^{9}Be photodisintegration cross section

Here we will expose some results at NLO obtained by computing the LIT as in Eq. (6.17). We start by showing some calculations relative to the $E1$ transition $3/2^- \to 1/2^+$. In order to evaluate the total cross section of ^{9}Be photodisintegration, we will also discuss the cases $3/2^- \to 5/2^+$ and $3/2^- \to 3/2^+$.

$J^\pi = 1/2^+$ state

For the LIT results presented in Fig. 6.20, we have worked with the potentials given in Eqs. (6.48) and (6.49), comparing the NLO results with the ones already obtained at LO (see Fig. 6.6). The three–body force is included in the calculation. The addition of the $P_{1/2}$–wave α–n interaction leads to a slightly more pronounced peak located at $\approx 1.7\,\text{MeV}$, whose strength is equal to that obtained at LO, as expected. However, by adding the S–wave α–n effective potential, we obtain a peak with about half the strength of the LO result, leading to the conclusion that, in the $1/2^+$ case, this partial wave assumes an important role in our calculations. Moreover, with this additional interaction term, we are going in the right direction, since the cross section results obtained at LO overestimate the experimental data. In Fig. 6.20 we have employed a cut–off $\Lambda_{\alpha n}^S = 100\,\text{MeV}$ for the S–wave α–n effective potential. However, this gives rise to a high tail in the energy region $3 - 4\,\text{MeV}$, which, after

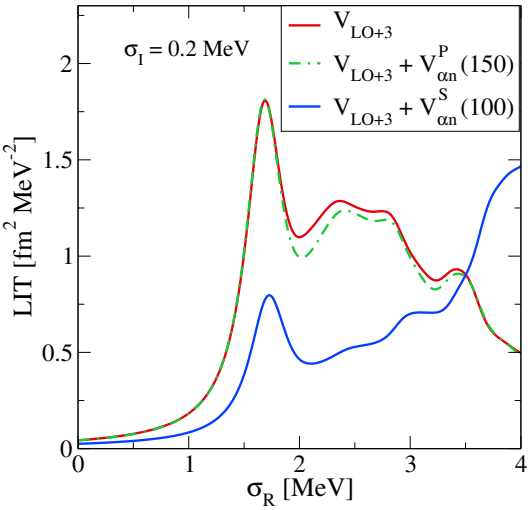

Figure 6.20: Correction to the LO result of Fig. 6.6 (red solid) by means of the additional interaction term $V_{\alpha n}^{P1/2}$, with a cut–off fixed to $\Lambda_{\alpha n}^{P} = 150\,\mathrm{MeV}$ (dashed dotted green), and of the term $V_{\alpha n}^{S}$, with $\Lambda_{\alpha n}^{S} = 100\,\mathrm{MeV}$ (solid blue line).

the inversion of the LIT, leads to an unphysical result for the cross section. As a consequence, we have chosen to use a larger cut–off parameter, $\Lambda_{\alpha n}^{S} = 300\,\mathrm{MeV}$, which also better reproduces the experimental low–energy phase–shifts. In this case, we are forced to add also a projection potential term (6.51), as discussed in Section 6.2.2. In the following, we will therefore analyse the results for the LIT obtained with the NLO potential of Eq. (6.53):

$$V_{LO+3} + V_{\alpha n}^{S}(300) + V_{PR}(\Gamma)\,. \tag{6.54}$$

The term V_{LO+3} will be kept fixed, $V_{LO+3} = V_{\alpha\alpha}^{S}(190) + V_{\alpha n}^{P}(300) + V_3(\Lambda_3, \lambda_3)$. We remark here again that, in order to solve the eigenvalue problem for the final state $J^\pi = 1/2^+$, we use the same Hamiltonian as the one employed for the ground state $J^\pi = 3/2^-$, with the exception of the strength λ_3. This parameter is in fact used to locate the resonance in the correct position.

In Figs. 6.21 we show the LIT calculated with $\sigma_I = 0.2\,\mathrm{MeV}$ by varying the values of the projection parameter Γ and with the cut–off of the three–body force fixed to $\Lambda_3 = 300\,\mathrm{MeV}$. The results are convergent for $\Gamma \approx 1000 - 2000\,\mathrm{MeV}$, and this is consistent with what was obtained for the bound–state calculations (see Fig. 6.17). As a consequence, by choosing a value in this range also the LITs should not depend on the projection parameter Γ.

The procedure of varying the three–body potential strength $\lambda_3^{1/2^+}$ in order to obtain a resonance peak located at the correct energy $\approx 1.70\,\mathrm{MeV}$ can be visualised in Figs. 6.22. We point out that by taking $\lambda_3^{1/2^+} = \lambda_3^{3/2^-}$, i.e. the same value used for the ground state, a $1/2^+$ bound–state is present. As a consequence, $\lambda_3^{1/2^+}$ must be changed towards less–attractive values. In Figs. 6.23 the convergence of the LIT with respect to the dimension of the "hypermomental" (hyperradial) basis is analysed. By taking, as an example, the values $\Gamma = 250\,\mathrm{MeV}$ and $\Gamma = 2000\,\mathrm{MeV}$ for the projection parameter, the LIT in the region up to about $\approx 2.5\,\mathrm{MeV}$ is

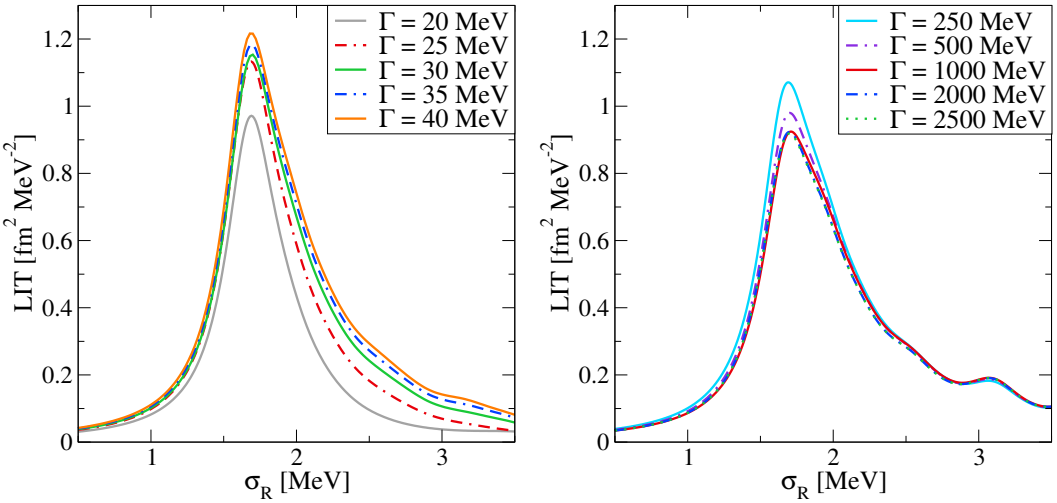

Figure 6.21: LIT calculated with the NLO potential of Eq. (6.54), with $\Lambda_3 = 300\,\text{MeV}$, by varying the projection potential Γ in the range $20 - 40\,\text{MeV}$ (a) and in the range $250 - 2500\,\text{MeV}$ (b).

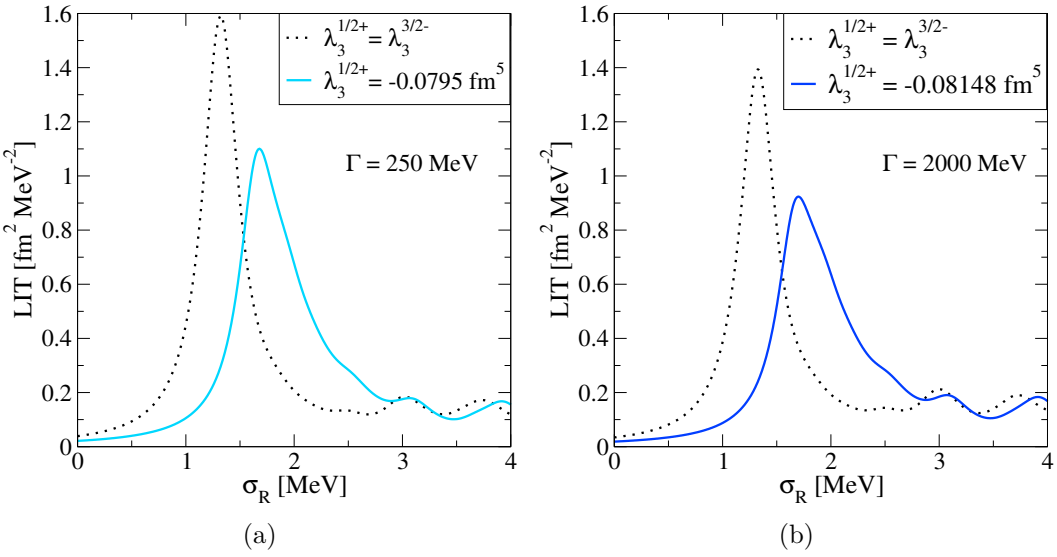

Figure 6.22: LIT calculated by using the NLO potential of Eq. (6.54), with $\Lambda_3 = 300\,\text{MeV}$ and $\Gamma = 250\,\text{MeV}$ (a) or $\Gamma = 2000\,\text{MeV}$ (b). The strength of the three–body potential $\lambda_3^{1/2^+}$ is adjusted to have a resonance peak located at the correct energy $\approx 1.70\,\text{MeV}$. In panel (a) $\lambda_3^{3/2^-} = -0.09554\,\text{fm}^5$, while in (b) we have used $\lambda_3^{3/2^-} = -0.098793\,\text{fm}^5$.

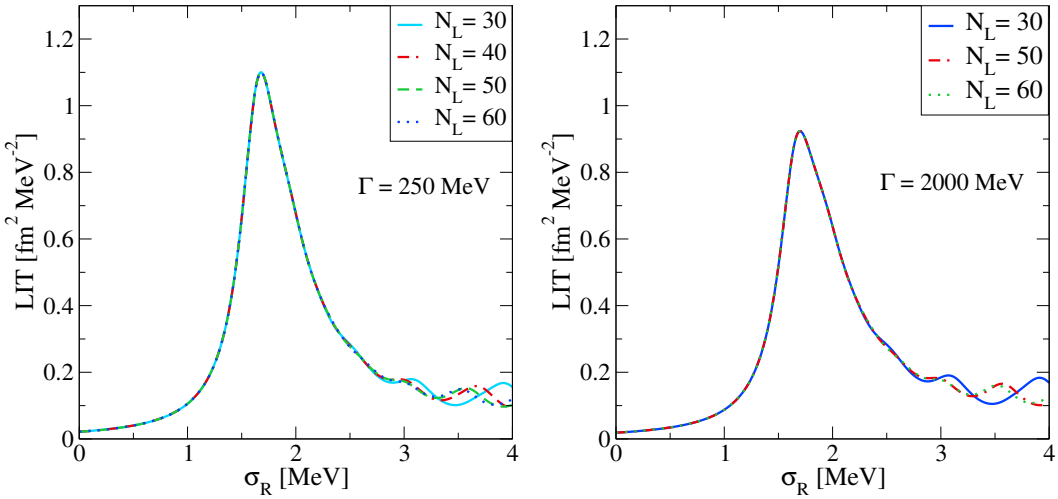

Figure 6.23: LIT calculated with the NLO potential of Eq. (6.54), with $\Lambda_3 = 300\,\text{MeV}$ and $\Gamma = 250\,\text{MeV}$ (a) or $\Gamma = 2000\,\text{MeV}$ (b). The chosen parameters of the HH basis are $\beta = 0.05\,\text{fm}^{-1}$, $K^{\max} = 26$. Moreover, the convergence in N_L is shown.

already convergent at $N_L = 30$. By increasing N_L the oscillations appearing above $\approx 2.5\,\text{MeV}$ tend to vanish. This is due to the fact that we are including more basis functions in the calculation.

So far the dipole matrix elements $\langle\Psi_l|\hat{d}_\lambda|\Psi_0\rangle$ that enter in the computation of the LIT (6.17) have been calculated in coordinate space, following Eq. (6.30). In performing the integral, instead of using the basis functions $g_{mK}(\rho)$ directly, we have applied the procedure discussed in Section 6.1.2, in which the functions $G^{0,l}_\mu(\rho)$ are computed by following Eq. (6.28). This has led to all the results shown in this Chapter. As already mentioned in Section 5.4, we could have followed another strategy. Essentially, by using this alternative procedure the dipole matrix elements $\langle\Psi_l|\hat{d}_\lambda|\Psi_0\rangle$ are computed in terms of basis functions constructed from a Laguerre polynomials basis in coordinate space. This alternative calculation provides a test of the results obtained in this Chapter. Since this entails also the use of a different Fortran code, we have included all the details in Appendix G, where the outcome of the test is also reported.

As already done for the LO calculation, we have also checked the behaviour of our results by varying the cut–off relative to the three–body potential. The LIT calculated for three different values of Λ_3 can be seen in Fig. 6.24. The shape of the resonance remains almost the same. The main difference lies in the tail of the LIT calculated with $\Lambda_3 = 200\,\text{MeV}$, which is rather high in comparison with the major peak. This "background" could lead to a considerable contribution also in the response function, and therefore in the final cross section. By focussing on the region of the main resonance peak, the LITs calculated with $\Lambda_3 = 200\,\text{MeV}$ and $\Lambda_3 = 400\,\text{MeV}$ are approximately 10% and 6% smaller compared to the LIT obtained with $\Lambda_3 = 300\,\text{MeV}$. Thus, our results slightly depend on Λ_3. In the following, we will perform an inversion of the $\Lambda_3 = 300\,\text{MeV}$ result. By excluding the calculation

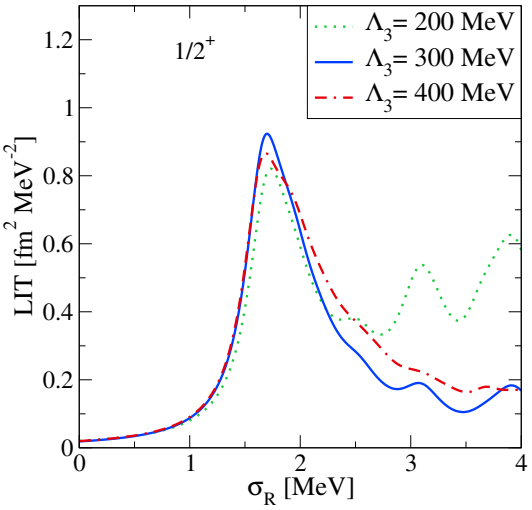

Figure 6.24: $1/2^+$ LIT calculated with the NLO potential of Eq. (6.54), with $\Gamma = 2000\,\text{MeV}$ and for different values of the cut–off Λ_3 relative to the three–body potential. σ_I is fixed to 0.2 MeV.

with the lower value of the three–body cut–off, it might be interesting to invert also the LIT obtained with $\Lambda_3 = 400\,\text{MeV}$, taking any difference in the final results as an error due to EFT model employed.

The response function obtained by inversion of the LIT in Fig. 6.24 with cut–off $\Lambda_3 = 300\,\text{MeV}$ can be seen in Fig. 6.25. The main characteristics of the inversion procedure have been already included in Section 3.4. Specifically, here we have employed the following set of basis functions [117]

$$\chi_1(x,\alpha_i) = \frac{1}{(x-\alpha_1)^2+\alpha_2^2}\left(1-e^{-x}\right)^{\alpha_3}, \tag{6.55a}$$

$$\chi_n(x,\alpha_i) = x^{\alpha_4}\exp\left\{-\frac{\alpha_5 x}{n-1}\right\}, \qquad n = 2,\ldots,N\,. \tag{6.55b}$$

In the $n = 1$ element, an explicit structure with a Lorentzian form has been introduced through the non–linear parameters α_1 and α_2. Moreover, with the additional factor the behaviour near the threshold is better under control through α_3. These parameters are treated as free during the inversion procedure. In Fig. 6.25 the results relative to an increasing number of basis functions, $N = 4, 8, 12$, are shown. In the lower panel also the ratio

$$r_N(\omega) = 100\cdot\frac{R^{(\bar{N})}(\omega) - R^{(N)}(\omega)}{R^{(\bar{N})}(\omega)}, \qquad \bar{N} = 12 \tag{6.56}$$

is represented, which is the percentage difference of each result $R^{(N)}(\omega)$ with respect to the one obtained with a basis of dimension $\bar{N} = 12$. The results are rather stable. The major source of error lies in the lower part of the peak region, around energy $\approx 1.68\,\text{MeV}$, where a percentage $\sim 18\%$ is found for $N = 4$, decreasing to $\sim 6\%$ for $N = 8$. In the latter case, an error of at most 3% is found in the tail. The difference between the response functions obtained with $N = 8$ and $N = 12$ is thus an estimate of the error due to the inversion procedure.

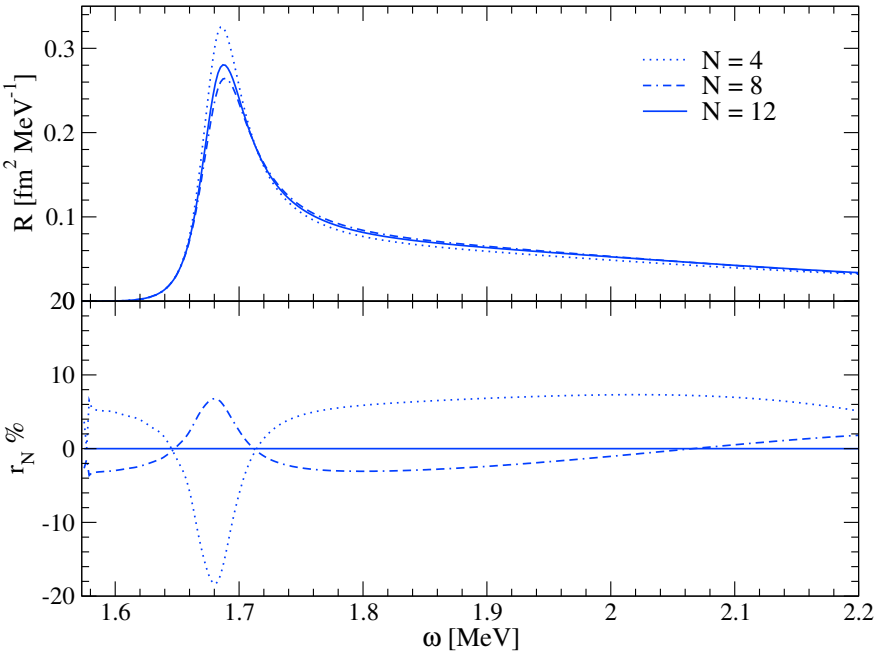

Figure 6.25: Calculated $1/2^+$ response function for an increasing number N of basis elements employed in the inversion procedure (upper panel). The associated percentage difference r_N, defined in Eq. (6.56), is also shown (lower panel).

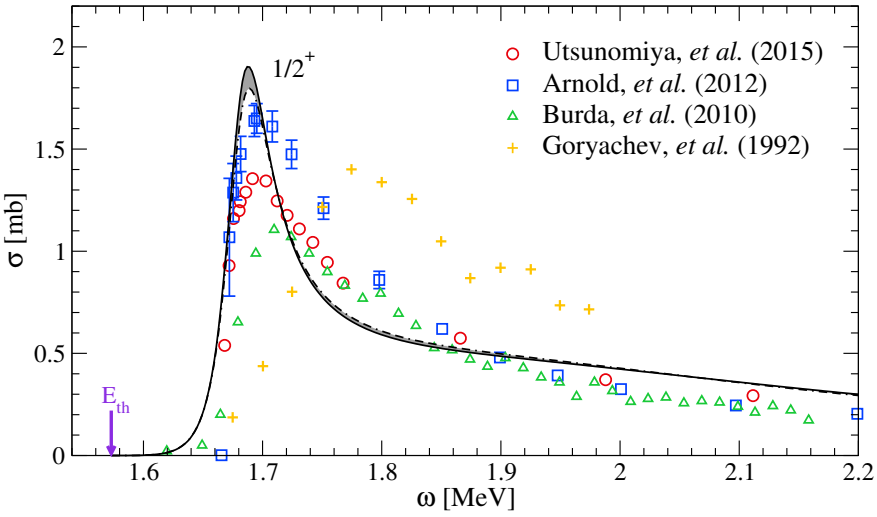

Figure 6.26: $1/2^+$ contribution to the ^{9}Be photodisintegration cross section in comparison with different sets of experimental data from Refs. [5, 8–10]. The shade represents the assumed error due to the inversion procedure. The three–body threshold energy corresponds to 1.573 MeV.

Finally, from the calculated response function, we have computed the cross section as a function of the photon energy by means of Eq. (6.42) obtaining the results in Fig. 6.26. The shade represents the assumed error due to the inversion procedure. By inspection of the plot, we can see that our results are in fair agreement

with the set of experimental data from Ref. [5] by Arnold, *et al.*. The calculated cross section σ shows a peak at energy $\sim 1.69\,\mathrm{MeV}$, which is the experimental location of the $1/2^+$ resonance. 1.85 mb can be taken as the maximum value of σ, with an estimated error ± 0.05 from the inversion procedure. The width is small if compared with the distribution of the experimental data points coming from the different measurements, leading to a underestimation in the energy region $\approx 1.74 - 1.84\,\mathrm{MeV}$. However, in the region above 2 MeV our result slightly overestimates all the experimental data. As already mentioned, it could be interesting to calculate the cross section by using a different value of the three–body cut–off relative to the EFT employed. In this way, also an estimate of the error due to the model can be obtained.

The total cross section

In order to be able to compare our theoretical results with the experimental data at higher energies, the contributions due to the $E1$ transitions $3/2^- \to 5/2^+$ and $3/2^- \to 3/2^+$ must be included in the calculation of the cross section. The associated resonances occur at energies $\approx 3\,\mathrm{MeV}$ and $\approx 4.7\,\mathrm{MeV}$, respectively.

By focussing first on the $5/2^+$ LIT calculations, we have reported in Fig. 6.27a the integral transforms obtained for $\sigma_I = 0.2\,\mathrm{MeV}$ by using a HH basis with $K^{\max} = 26$ and $N_L = 40$. Different values of the cut–off Λ_3 relative to the three–body potential has been employed. As usual, the strength $\lambda_3^{5/2^+}$ has been tuned to reproduce a resonance in the correct energy region. For $\Lambda_3 = 200\,\mathrm{MeV}$ we manage to obtain a resonance peak in the correct position, however also a $5/2^+$ bound state is present, which gives rise to the extremely high peak occurring at photon energy $\approx 1.5\,\mathrm{MeV}$ (see Fig. 6.27a). Probably, this value of the three–body cut–off is not large enough. Two peaks of almost the same size and width are produced by the cut–off values $\Lambda_3 = 300\,\mathrm{MeV}$ and $\Lambda_3 = 400\,\mathrm{MeV}$. However, the latter choice is preferable, as it gives rise to a more pronounced peak. As a consequence, we have decided to proceed by fixing $\Lambda_3 = 400\,\mathrm{MeV}$. In Fig. 6.27b the convergence in the basis parameter N_L is shown, with fixed $K^{\max} = 26$. As expected, in order to obtain convergent results for the state $5/2^+$, a large number of "hypermomental" (hyperradial) functions is needed. At least $N_L = 80$ should be taken, in order to obtain results as good as possible from the inversion procedure.

Concerning the $3/2^+$ resonance, since its experimental width is rather large compared to both $1/2^+$ and $5/2^+$ cases, a LIT calculated with $\sigma_I > 0.2\,\mathrm{MeV}$ can be taken for the inversion. A good choice is represented by $\sigma_I = 1.4\,\mathrm{MeV}$. For such a value, the HH basis parameters $K^{\max} = 26$ and $N_L = 30$ ensure convergent results.

In Fig. 6.28, we show the $5/2^+$ and $3/2^+$ LITs used to perform the final inversions as well as the associated response functions. We point out that, in the $5/2^+$ case, we have chosen a LIT calculated with $K^{\max} = 28$ and $N_L = 80$. By increasing $K^{\max}$ from 26 to 28, the $5/2^+$ LIT decreases of about 8% in the peak region, meaning that these parameters do not ensure full convergence. However a calculation with $K^{\max} = 30$ and $N_L = 80$ is computationally demanding, so for the moment we have chosen to use $K^{\max} = 28$, bearing in mind that any final result obtained can be improved.

The $5/2^+$ and $3/2^+$ contributions to the ^{9}Be photodisintegration cross section

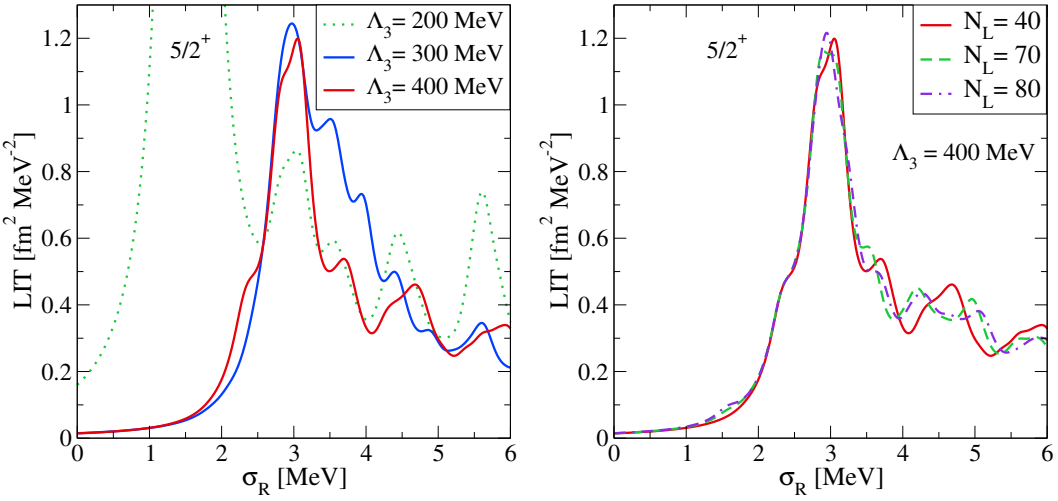

Figure 6.27: LIT relative to the $E1$ transition $3/2^- \to 5/2^+$ calculated by using the NLO potential of Eq. (6.54), with $\Gamma = 2000\,\mathrm{MeV}$. In panel (a) the LIT is calculated for different values of the cut–off Λ_3. The basis parameters used are $\beta = 0.05\,\mathrm{fm}^{-1}$, $N_L = 40$ and $K^{\max} = 26$. In panel (b) the convergence in N_L is shown at fixed $\Lambda_3 = 400\,\mathrm{MeV}$. σ_I is always $0.2\,\mathrm{MeV}$.

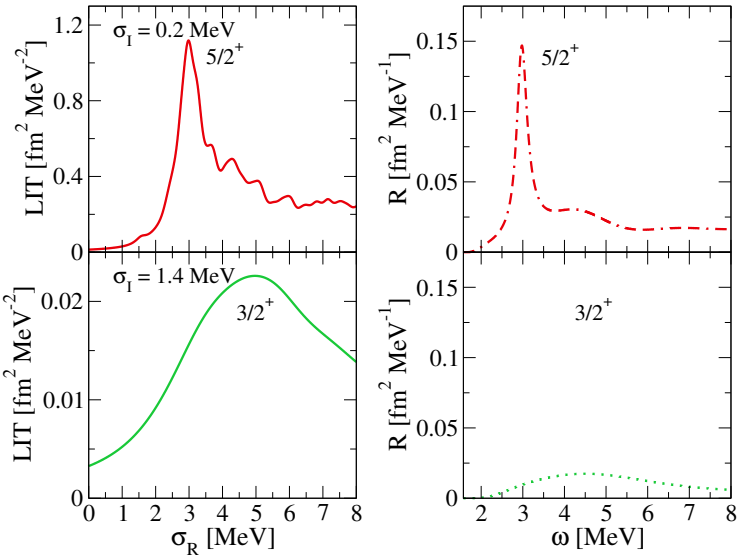

Figure 6.28: LITs relative to the $E1$ transitions $3/2^- \to 5/2^+$ (solid red) and $3/2^- \to 3/2^+$ (solid green) calculated at NLO with $\Lambda_3 = 400\,\mathrm{MeV}$, $K^{\max} = 28$, $N_L = 80$ and $\Lambda_3 = 300\,\mathrm{MeV}$, $K^{\max} = 26$, $N_L = 30$, respectively. The associated response functions obtained from an inversion procedure are shown on the right side as a function of the photon energy ω.

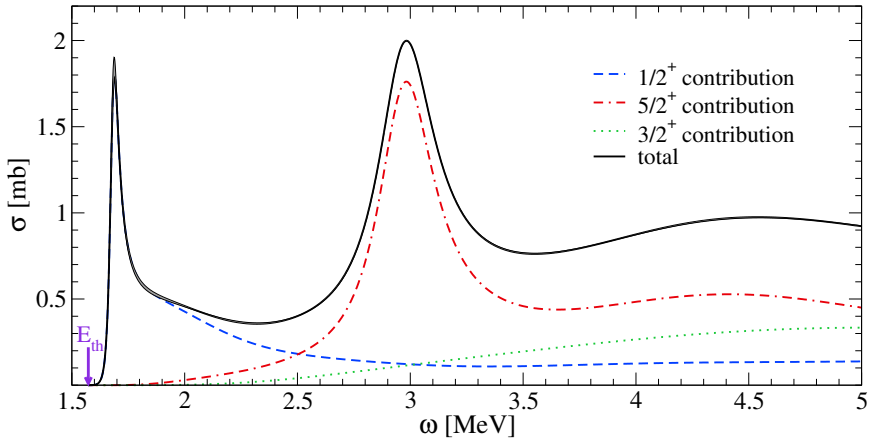

Figure 6.29: Individual contributions to the ^{9}Be photodisintegration cross section as a function of the photon energy. The sum is represented by the solid black line.

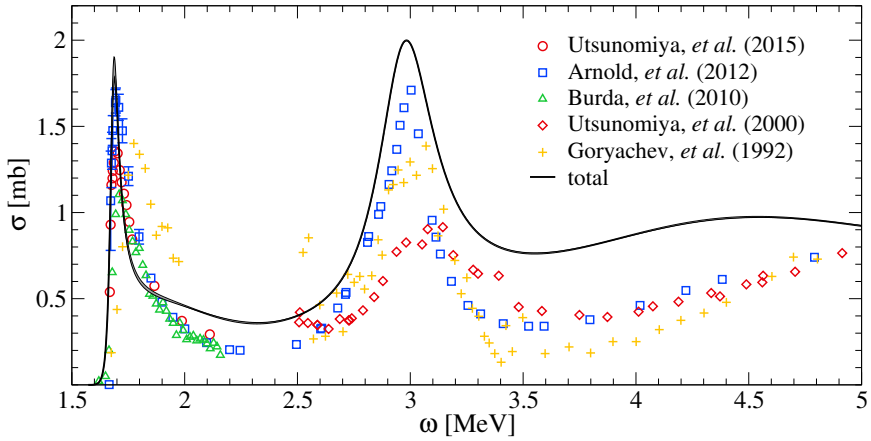

Figure 6.30: Total ^{9}Be photodisintegration cross section from our *ab initio* three–body calculation in comparison with different set of experimental data from Refs. [5, 7–10].

are represented in Fig. 6.29. Given the response functions, each contribution has been computed separately by using Eq. 6.42. In order to get the full picture, we have also added the calculated $1/2^+$ resonance. The total cross section can be obtained by summing the three individual contributions. Near the three–body threshold at 1.573 MeV and up to energy ≈ 2 MeV the entire cross section is given by the $1/2^+$ resonance. Then, the $5/2^+$ contribution begins to appear, peaking at ≈ 3 MeV. The resonance due to the $3/2^+$ state is broader, whose maximum contribution is ≈ 0.35 mb at higher energies around 5 MeV.

Finally, in Fig. 6.30 our cross section result is shown, in comparison with different set of experimental data. In the energy region around ≈ 3 MeV and above, an overestimation of the data is present. This could be ascribed entirely to the $5/2^+$ resonance. As already mentioned, the calculation relative to the $3/2^- \to 5/2^+$ transition can be improved, probably leading to a smaller height of the resonance peak.

6.2.3 Comparison of the results with the one–body current calculations

All the cross section results presented in Sections 6.2.1 and 6.2.2 have been obtained by using the Siegert operator $T^{el,S}_{1\lambda}(q;\tilde{\rho})$ derived in Eq. (2.55) in the long–wavelength approximation. As explained in Section 2.4, this allows to implicitly include in the calculation the contribution due to the one–body and the many–body currents. The one–body current operator has been derived in a covariant form in Ref. [29], where it has been also implemented in the calculation of the LITs associated to the ^{9}Be photodisintegration cross section. Since our effective potentials defined in momentum space have non–commuting terms with the nuclear charge [see Eq. (2.68)], we could expect non–vanishing many–body currents, which may contribute to the total cross section. By comparing the calculations carried out with the Siegert operator and with $\tilde{\boldsymbol{J}}^{[1]}$, i.e. the convection current, we should be able to quantify this contribution due to the many–body terms of the nuclear current.

An indication of the existence of such a contribution is given by the behaviour of the LIT calculated at LO with the matrix elements $\langle\Psi_l|\hat{J}^{[1]}_\lambda|\Psi_0\rangle$ by varying the three–body cut–off Λ_3. Unlike the results obtained by using the dipole matrix elements $\langle\Psi_l|\hat{d}_\lambda|\Psi_0\rangle$, which are rather stable by varying Λ_3 (see Figs. 6.10a and 6.11), the LIT calculated by using the one–body current strongly depends on Λ_3, as can be seen in Fig. 6.31a. A variation of Λ_3 from 300 MeV to 400 MeV gives rise to a cross section that almost doubles, as Fig. 6.31b shows. This could be seen as an effect due to the missing contribution of the many–body currents in the calculation. We remind that at LO only the α–n $P_{3/2}$–wave and α–α S_0–wave are present in the calculation, in addition to a three–body interaction.

We have calculated the LIT by using the one–body current matrix elements

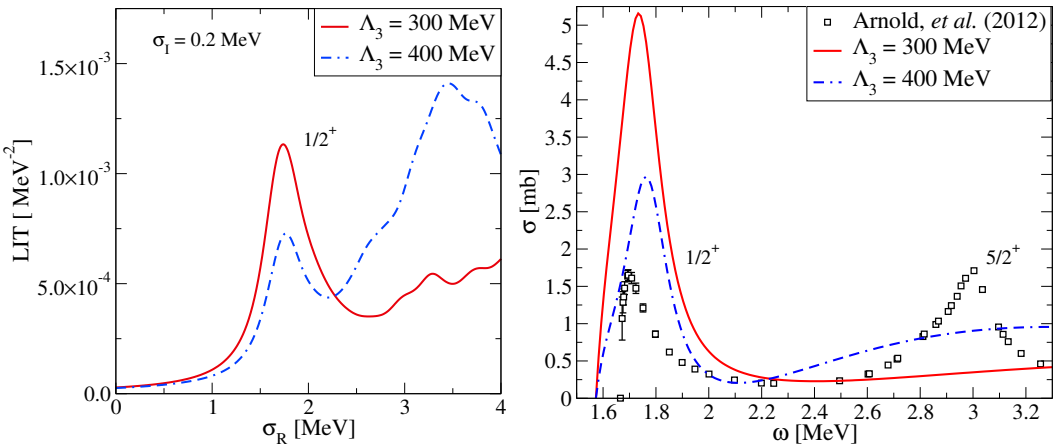

(a) (b)

Figure 6.31: (a) Same as Fig. 6.10a but the LIT is calculated at LO with the one–body current operator $\langle\Psi_l|\hat{J}^{[1]}_\lambda|\Psi_0\rangle$, i.e. the convection current. (b) ^{9}Be photodisintegration cross section relative to the $E1$ transition $3/2^- \to 1/2^+$ as a function of the incident photon energy. The results correspond to the LITs calculated in panel (a). The experimental data are taken from Ref. [5].

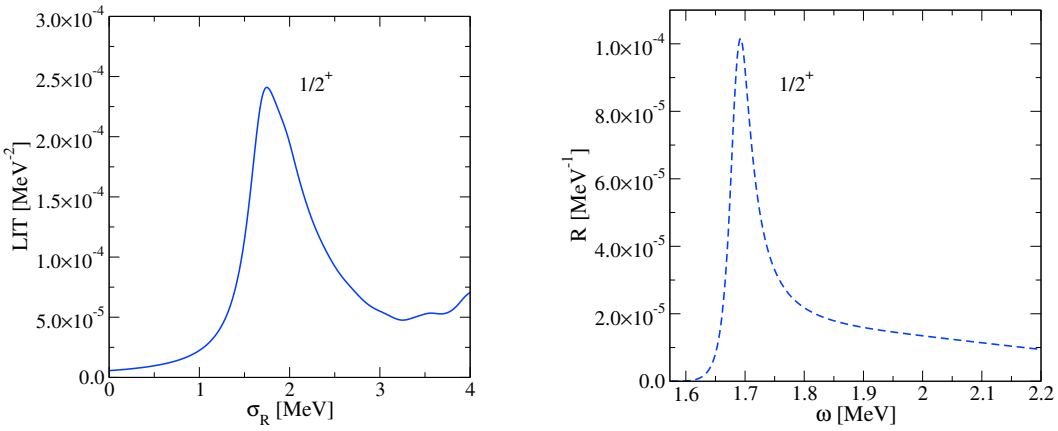

Figure 6.32: (a) Same as Fig. 6.24 but the $1/2^+$ LIT is calculated at NLO with the one–body current operator $\langle\Psi_l|\hat{J}^{[1]}_\lambda|\Psi_0\rangle$, i.e. the convection current, for $\Lambda_3 = 300\,\text{MeV}$. (b) Response function relative to the LIT shown in panel (a).

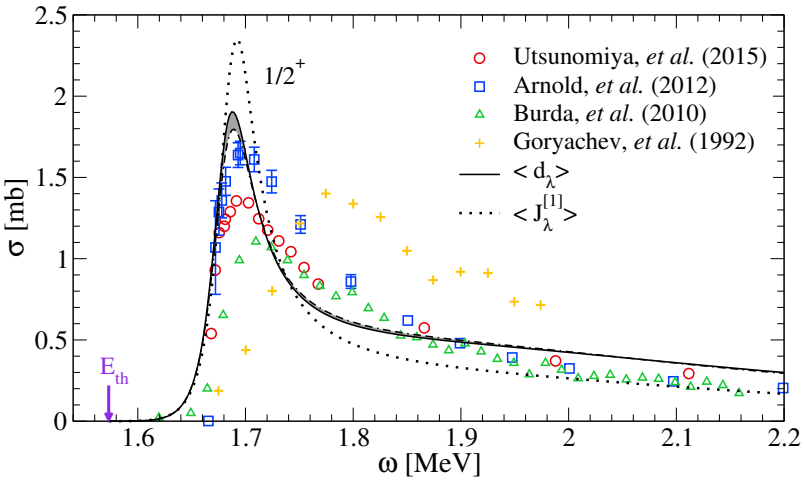

Figure 6.33: $1/2^+$ contribution to the ^{9}Be photodisintegration cross section calculated by using the the dipole operator (as in Fig. 6.26) and the one–body current operator. The three–body threshold energy corresponds to 1.573 MeV. The experimental data are from Refs. [5, 8–10].

also at NLO, i.e. by adding in the model an α–n $S_{1/2}$–wave effective potential as well as a projection term (see Section 6.2.2). The results relative to the transition $3/2^- \to 1/2^+$ are reported in Fig. 6.32a, whose associated response function can be seen in Fig. 6.32b. The calculated contribution to the cross section is shown in Fig. 6.33. To make the comparison easier, also the $1/2^+$ result obtained by means of the Siegert operator, i.e. with the dipole matrix elements $\langle\Psi_l|\hat{d}_\lambda|\Psi_0\rangle$, is shown. We remark that all the EFT parameters have been kept identical in both calculations. The calculated cross sections differ in the resonance peak region and in the tail, i.e. at higher energies. This can be ascribed to a non–vanishing contribution due the many–body currents.

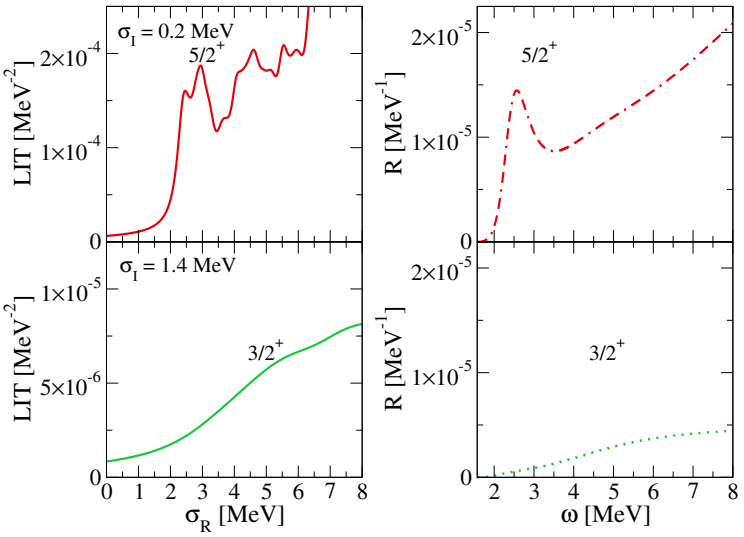

Figure 6.34: Same as Fig. 6.28 but the $5/2^+$ and $3/2^+$ LITs are calculated with the one–body current operator $\langle\Psi_l|\hat{J}^{[1]}_\lambda|\Psi_0\rangle$. The associated response functions are shown in the right panels.

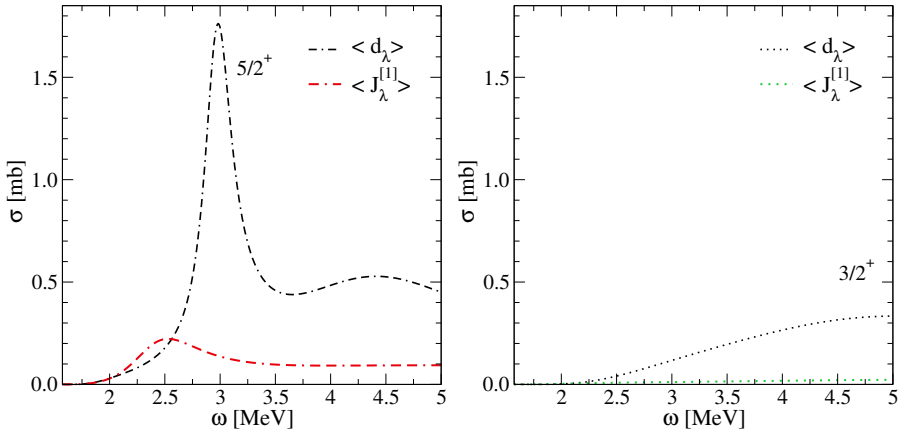

Figure 6.35: Comparison between the $5/2^+$ (a) and $3/2^+$ (b) contributions to the ^{9}Be photodisintegration cross section calculated by using the dipole operator and the one–body current operator. The results relative to the the dipole operator are those already shown in Fig. 6.29.

By means of the the one–body current operator, we have also calculated the LITs relative to the transitions $3/2^- \to 5/2^+$ and $3/2^- \to 3/2^+$. The results are summarized in Fig. 6.34, where also the associated response functions are shown. The cross section results have been put in Figs. 6.35a and 6.35b, highlighting the difference with respect to the calculations carried out by using the dipole matrix elements $\langle\Psi_l|\hat{d}_\lambda|\Psi_0\rangle$. Interestingly, the two results relative to the $5/2^+$ contribution are very different, as the cross section obtained from the calculations with $\langle\Psi_l|\hat{J}^{[1]}_\lambda|\Psi_0\rangle$ almost vanishes in the region around the resonance peak. This seems to indicate

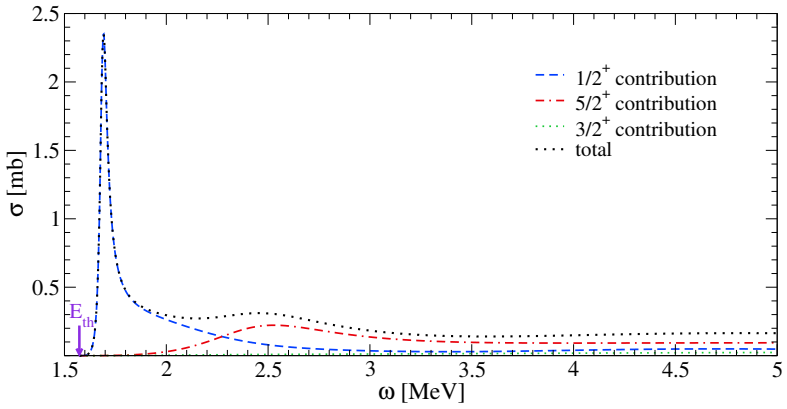

Figure 6.36: Individual contributions to the ^{9}Be photodisintegration cross section calculated by using the one–body current operator $\langle\Psi_l|\hat{J}^{[1]}_\lambda|\Psi_0\rangle$ as a function of the photon energy. The sum is represented by the dotted black line.

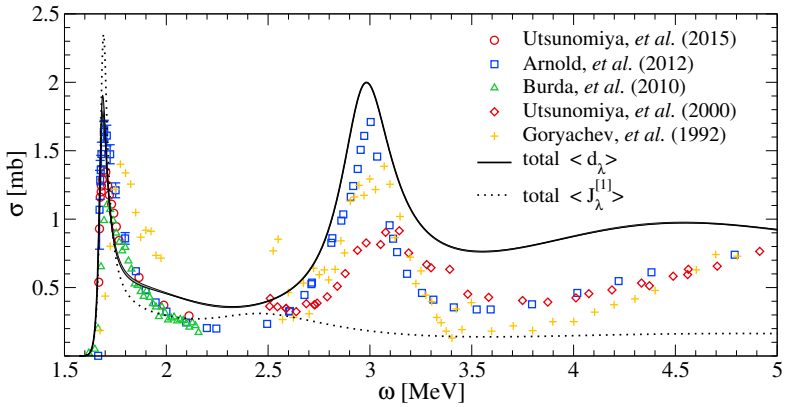

Figure 6.37: Comparison between the total ^{9}Be photodisintegration cross section calculated by using the one–body current and the Siegert operator. The results relative to the the Siegert operator are those already shown in Fig. 6.30. The experimental data are taken from Refs. [5, 7–10].

that the contribution of the many–body currents is higher in this case, with respect to the $1/2^+$ case. The $1/2^+$ resonance is mainly due to ^{8}Be, and therefore to the α–α S–wave effective interaction; in the $5/2^+$ resonance, the α–n $P_{3/2}$–wave should be dominant. By examining the form of these two effective potentials, the results appear to be consistent. With respect to the S–wave interaction, in the P–wave potential the additional factor $p\,p'$ is present. Being more momentum–dominated, this potential could generate a higher contribution in terms of many–body currents.

As done in the previous Section, in order to visualize the total cross section obtained by means of the one–body convection current operator, we have collected all the partial contributions in one plot, given in Fig. 6.36. Finally, in Fig. 6.37 the total cross section can be seen in comparison with the results obtained with the Siegert operator and the experimental data. As already mentioned, the major difference between the two theoretical calculations lies in the energy region ≈ 3 MeV.

Chapter 7

The Carbon–12 photodisintegration reaction

7.1 The reaction cross section: detailed derivation

In this Section we want to derive the cross section relative to the following reaction

$$\gamma + {}^{12}\mathrm{C} \to \alpha + \alpha + \alpha \,, \tag{7.1}$$

proceeding through the $J^\pi_n = 2^+_1$ bound state of ^{12}C nucleus to the 0^+_2 state in the continuum. In order to study this photodisintegration process, we will follow the analysis already carried out in Section 6.1 for the ^{9}Be, by specialising to the ^{12}C nucleus. The nuclear response function is evaluated by means of the LIT method discussed in Chapter 3.

7.1.1 The $E2$ transition operator

Since the process (7.1) is represented by an electric quadrupole transition to the continuum, the operator of interest is the $J = 2$ term in the multipole expansion of the nuclear current of Eq. (2.38), $T^{el}_{2\lambda}(q)$. We study the reaction in the low–energy limit, and therefore it is sufficient to consider the Siegert operator in the long–wavelength approximation given in Eq. (2.55)

$$J_\lambda(q) \simeq -\sqrt{10\pi} T^{el,S}_{2\lambda}(q) \simeq -\sqrt{\frac{\pi}{15}} \omega^2_{\boldsymbol{q}} u_\lambda \,. \tag{7.2}$$

The operator u_λ here is defined as

$$u_\lambda = \int d^3\boldsymbol{x}\, x^2 \rho(\boldsymbol{x}) Y_{2\lambda}(\hat{x}) = \sum_{i=1}^{3} Z_i (r'_i)^2 Y_{2\lambda}(\hat{r}'_i) \,, \tag{7.3}$$

where, in deriving the last expression, we have used the definition of the nuclear charge given in Eq. (6.4). The summation above runs over the three α–particles. The vectors $\boldsymbol{r}'_i$, being defined as the position of each α–particle with respect to the center–of–mass coordinate, are explicitly $\boldsymbol{r}'_i = \boldsymbol{r}_i - \boldsymbol{R}_{\rm cm}$. The relations (6.8) between

the vectors $\{\boldsymbol{r}'_1, \boldsymbol{r}'_2, \boldsymbol{r}'_3\}$ and the internal Jacobi coordinates $\{\boldsymbol{\eta}_1, \boldsymbol{\eta}_2\}$ remain valid, and they can be exploited to rewrite the operator u_λ, obtaining

$$u_\lambda = \left(Z_1\mathcal{A}^2 + Z_2\mathcal{C}^2\right)\eta_2^2\, Y_{2,\lambda}(\hat{\eta}_2) + \left[(Z_1+Z_2)\,\mathcal{B}^2 + Z_3\mathcal{D}^2\right]\eta_1^2\, Y_{2,\lambda}(\hat{\eta}_1) + \sqrt{\frac{10(4\pi)}{3}}\,(Z_1\mathcal{A}\mathcal{B} - Z_2\mathcal{C}\mathcal{B})\,\eta_2\eta_1 \sum_{\mu'=0,\pm1} \langle 1, \lambda-\mu', 1, \mu'|2,\lambda\rangle\, Y_{1,\lambda-\mu'}(\hat{\eta}_2) Y_{1,\mu'}(\hat{\eta}_1)\,, \tag{7.4}$$

where the mass coefficients $\mathcal{A}$, $\mathcal{B}$, $\mathcal{C}$ and $\mathcal{D}$ are defined as in Eq. (6.9). A detailed derivation of the expression above can be found in Appendix E.2. In the specific case of three α–particles, by imposing $Z_i = Z_\alpha$ and $m_i = m_\alpha$, for $i = 1, 2, 3$, since the following relations are valid

$$Z_1\mathcal{A}^2 + Z_2\mathcal{C}^2 = Z_\alpha \frac{m_\mathrm{r}}{m_\alpha}\,, \tag{7.5a}$$

$$(Z_1+Z_2)\,\mathcal{B}^2 + Z_3\mathcal{D}^2 = Z_\alpha \frac{m_\mathrm{r}}{m_\alpha}\,, \tag{7.5b}$$

$$Z_1\mathcal{A}\mathcal{B} - Z_2\mathcal{C}\mathcal{B} = 0\,, \tag{7.5c}$$

the term proportional to $\eta_2\eta_1$ vanishes, and the final form of the $E2$ operator u_λ is simply

$$u_\lambda = Z_\alpha \mu \left(\eta_2^2\, Y_{2\lambda}(\hat{\eta}_2) + \eta_1^2\, Y_{2\lambda}(\hat{\eta}_1)\right)\,. \tag{7.6}$$

Since our reference mass corresponds to the nucleon mass, in the equation above μ is the dimensionless parameter defined as $\mu = m_n/m_\alpha$.

7.1.2 Calculation of the LIT

Our aim is to calculate the cross section already derived in Eq. (2.19), with the response function defined as

$$R(\omega_{\boldsymbol{q}}) = \frac{\omega_{\boldsymbol{q}}^4}{2(2J_0+1)}\frac{\pi}{15}\sum_{\lambda=\pm1}\sum_{M_0}\sum_{M_f} R_u(\omega_{\boldsymbol{q}})\,, \tag{7.7}$$

where $R_u(\omega_{\boldsymbol{q}})$ is given explicitly by the following expression

$$R_u(\omega_{\boldsymbol{q}}) = \sum\!\!\!\!\!\!\int_f |\langle\Psi_f|\hat{u}_\lambda|\Psi_0\rangle|^2 \delta(E_f - E_0 - \omega_{\boldsymbol{q}})\,. \tag{7.8}$$

To avoid the direct calculation of the nuclear response function above, we use the LIT method discussed in Chapter 3. Specifically, the eigenvalue method of Section 3.3.1 provides the following expression for evaluating the LIT

$$L(\sigma_R, \sigma_I) = \sum_{l=1}^{N_\Lambda} \frac{|\langle\Psi_l|\hat{u}_\lambda|\Psi_0\rangle|^2}{(E_l - E_0 - \sigma_R)^2 + \sigma_I^2}\,, \tag{7.9}$$

where E_0 ($|\Psi_0\rangle$) is the eigenvalue (eigenstate) relative to the 2_1^+ bound state of ^{12}C, while E_l and $|\Psi_l\rangle$ are such that $\hat{H}\,|\Psi_l\rangle = E_l\,|\Psi_l\rangle$, and therefore they can be calculated as well by employing bound–state methods. By inverting the function

$L(\sigma_R, \sigma_I)$ above at a fixed value of the parameter σ_I, the nuclear response function of interest is recovered.

Essentially, the procedure to compute E_0 and E_l as well as the quadrupole matrix elements $\langle \Psi_l | \hat{u}_\lambda | \Psi_0 \rangle$ is the same as that discussed in Section 6.1.2 for the ^{9}Be case. We diagonalize the Hamiltonian matrix represented on a NSHH basis defined in momentum space [see Eq. (5.134)] by using different quantum numbers in input: for the initial bound state we insert $J^\pi = 2^+$, while for the final state we use $J^\pi = 0^+$, according to the electric quadrupole transition selection rules. The most general expression to evaluate the matrix elements of a local operator represented in configuration space, Eq. (6.25), can be specialized to the calculation of the quadrupole matrix elements for a system with $N = 2$ as follows

$$\begin{aligned} \langle \Psi_l | \hat{u}_\lambda | \Psi_0 \rangle = \int d\Omega_2^{(\rho)}\, d\rho\, \rho^5 \Big[\sum_{m'\mu'} c^l_{m'\mu'}\, g_{m'K'}(\rho)\, \mathcal{Y}^{J'M'\pi'}_{\mu'}(\Omega_N^{(\rho)}) \Big]^\dagger \\ \times\, u_\lambda(\rho, \Omega_2) \Big[\sum_{m\mu} c^0_{m\mu}\, g_{mK}(\rho)\, \mathcal{Y}^{JM\pi}_{\mu}(\Omega_2^{(\rho)}) \Big] . \end{aligned} \tag{7.10}$$

The expression for $u_\lambda(\rho, \Omega_2)$ in hyperspherical coordinates can be easily derived from Eq. (7.6) by using the relations $\eta_2 = \rho \sin\varphi_2$ and $\eta_1 = \rho\cos\varphi_2$, obtaining

$$u_\lambda(\rho, \Omega_2) = Z_\alpha \mu \left(\rho^2 \sin\varphi_2^2\, Y_{2\lambda}(\hat{\eta}_2) + \rho^2 \cos^2\varphi_2\, Y_{2\lambda}(\hat{\eta}_1) \right) . \tag{7.11}$$

By denoting the two contributions as $u^{(2)}_\lambda(\rho, \Omega_2)$ and $u^{(1)}_\lambda(\rho, \Omega_2)$, respectively, the matrix elements to be calculated are explicitly

$$\begin{aligned} \langle m', J'M' | \hat{u}^{(2)}_\lambda | m, JM \rangle = Z_\alpha \mu \int d\rho\, \rho^7 g^*_{m'K'}(\rho) g_{mK}(\rho) \\ \times \int d\varphi_2\, \mathcal{N}^{K'_2;\ell'_2,\ell'_1}_{n'_2} P^{(\ell'_2+\frac{1}{2},\ell'_1+\frac{1}{2})}_{n'_2}(\cos 2\varphi_2) \\ \times (\sin\varphi_2)^{\ell'_2+\ell_2+4} (\cos\varphi_2)^{\ell'_1+\ell_1+2} \\ \times \mathcal{N}^{K_2;\ell_2,\ell_1}_{n_2} P^{(\ell_2+\frac{1}{2},\ell_1+\frac{1}{2})}_{n_2}(\cos 2\varphi_2) \\ \times (-1)^{J'-M'} \begin{pmatrix} J' & 2 & J \\ -M' & \lambda & M \end{pmatrix} \langle J' \| Y_2(\hat{\eta}_2) \| J \rangle \ , \end{aligned} \tag{7.12}$$

where we have performed a separation into a hyperradial, a hyperspherical and an angular part, as explicitly shown also in Appendix F [Eqs. (F.6a), (F.6b) and (F.6c)]. The expression of the reduced matrix element is [see Eq. (F.15)]

$$\begin{aligned} \langle J' \,\|\, Y_2(\hat{\eta}_2) \,\|\, J \rangle = \delta_{\ell'_1,\ell_1}\, \delta_{\{S'\},\{S\}}\, (-1)^{\ell_1+\ell_2+S+J+1} \\ \times \widehat{L'_2}\, \widehat{J'}\, \widehat{L_2}\, \widehat{J} \begin{Bmatrix} \ell'_2 & L'_2 & \ell_1 \\ L_2 & \ell_2 & 2 \end{Bmatrix} \begin{Bmatrix} L'_2 & J' & S \\ J & L_2 & 2 \end{Bmatrix} \\ \times (-1)^{\ell'_2} \sqrt{\frac{5}{4\pi}}\, \widehat{\ell'_2}\, \widehat{\ell_2} \begin{pmatrix} \ell'_2 & 2 & \ell_2 \\ 0 & 0 & 0 \end{pmatrix} . \end{aligned} \tag{7.13}$$

By using once again the results reported in Appendix F, one can also calculate the

contribution to the matrix elements due to the second term in Eq. (7.11). We obtain

$$\begin{aligned}\langle m', J'M'|\hat{u}^{(1)}_{\lambda}|m, JM\rangle = Z_\alpha \mu \int d\rho\, \rho^7 g^*_{m'K'}(\rho) g_{mK}(\rho) \\ \times \int d\varphi_2\, \mathcal{N}^{K'_2;\ell'_2,\ell'_1}_{n'_2} P^{(\ell'_2+\frac{1}{2},\ell'_1+\frac{1}{2})}_{n'_2}(\cos 2\varphi_2) \\ \times (\sin\varphi_2)^{\ell'_2+\ell_2+2} (\cos\varphi_2)^{\ell'_1+\ell_1+4} \\ \times \mathcal{N}^{K_2;\ell_2,\ell_1}_{n_2} P^{(\ell_2+\frac{1}{2},\ell_1+\frac{1}{2})}_{n_2}(\cos 2\varphi_2) \\ \times (-1)^{J'-M'} \begin{pmatrix} J' & 2 & J \\ -M' & \lambda & M \end{pmatrix} \langle J' \| Y_2(\hat{\eta}_1) \| J\rangle \,,\end{aligned} \tag{7.14}$$

where the reduced matrix element is now of the form

$$\begin{aligned}\langle J' \,\|\, Y_2(\hat{\eta}_1) \,\|\, J\rangle = \delta_{\ell'_2,\ell_2}\, \delta_{\{S'\},\{S\}}\, (-1)^{L'_2+\ell_2+L_2+S+J+1} \\ \times \widehat{L'_2}\, \widehat{J'}\, \widehat{L_2}\, \widehat{J} \begin{Bmatrix} \ell'_1 & L'_2 & \ell_2 \\ L_2 & \ell_1 & 2 \end{Bmatrix} \begin{Bmatrix} L'_2 & J' & S \\ J & L_2 & 2 \end{Bmatrix} \\ \times \sqrt{\frac{5}{4\pi}}\, \widehat{\ell'_1}\, \widehat{\ell_1} \begin{pmatrix} \ell'_1 & 2 & \ell_1 \\ 0 & 0 & 0 \end{pmatrix} .\end{aligned} \tag{7.15}$$

7.1.3 The photodisintegration cross section

We conclude by writing the expression of the reaction cross section relative to the process (7.1) proceeding through the states $2^+_1 \to 0^+_2$. We use the definition given in Eq. (2.19) as well as the response function in Eqs. (7.7) and (7.8), obtaining

$$\begin{aligned}\sigma(\omega_{\boldsymbol{q}}) = \frac{4\alpha\omega^3_{\boldsymbol{q}}}{2(2J_0+1)} \frac{\pi^3}{15} \sum_{\lambda=\pm1} \sum_{M_0} \sum_{M_f} (-1)^{2J_f-2M_f} \\ \times \begin{pmatrix} J_f & 2 & J_0 \\ -M_f & \lambda & M_0 \end{pmatrix} \begin{pmatrix} J_f & 2 & J_0 \\ -M_f & \lambda & M_0 \end{pmatrix} R^{\mathrm{red}}_u(\omega_{\boldsymbol{q}}) \,,\end{aligned} \tag{7.16}$$

where the response $R^{\mathrm{red}}_u(\omega_{\boldsymbol{q}})$ contains the square of the reduced matrix elements $\langle \Psi_f \| \hat{d} \| \Psi_0 \rangle$. The Wigner $3j$ symbols comes from the expressions (7.12) and (7.14) derived in the last Section. By making use of the orthogonality relation in Eq. (6.41), together with the value $J_0 = 2$ relative to the initial bound state of ^{12}C nucleus, the final result for the cross section is

$$\sigma(\omega_{\boldsymbol{q}}) = \alpha\omega^3_{\boldsymbol{q}} \frac{4}{25} \frac{\pi^3}{15} R^{\mathrm{red}}_u(\omega_{\boldsymbol{q}}) \,. \tag{7.17}$$

7.2 Results

A scheme of the energy levels of ^{12}C nucleus is depicted in Fig. 7.1. From the three–α threshold, the energy of the ground state corresponds to $E^{\mathrm{exp}}(0^+_1) = -7.275\,\mathrm{MeV}$, the energy of the first excited bound state is $E^{\mathrm{exp}}(2^+_1) = -2.875\,\mathrm{MeV}$, while the Hoyle state is located at $E^{\mathrm{exp}}(0^+_2) = 0.379\,\mathrm{MeV}$ [123].

Since we are interested in the transition $2^+_1 \to 0^+_2$, we will start by studying the bound state 2^+_1, which also enters in the calculation of the LIT. Then, we will

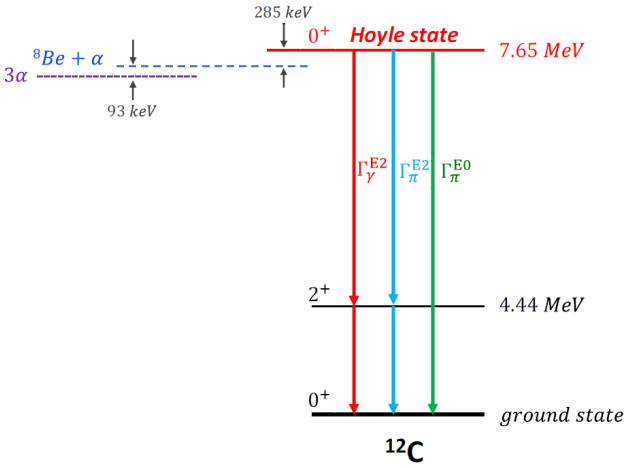

Figure 7.1: ^{12}C level scheme taken from Ref. [11]. At incident photon energy 7.275 MeV the three–body $\alpha+\alpha+\alpha$ breakup occurs. The $^8\mathrm{Be}+\alpha$ threshold is also shown. The possible electromagnetic transitions between the Hoyle state (0_2^+) and the ground state (0_1^+) and between the Hoyle state and the first excited bound state (2_1^+) are represented with different colours.

show some results about the calculation of the cross section relative to the ^{12}C photodisintegration.

7.2.1 Calculations at Leading Order

The $^{12}\mathrm{C}(2_1^+)$ bound state

In order to perform the calculation we use the LO α–α S–wave effective potential defined in Eq. (4.64), as well as a three–body potential in the form of Eq. (5.156)

$$V_{LO+3} = V^S_{\alpha\alpha}(\Lambda^S_{\alpha\alpha}) + V_3(\Lambda_3, \lambda_3)\,. \tag{7.18}$$

In the expression above $\Lambda^S_{\alpha\alpha}$ is the cut–off parameter relative to the two–body potential. In this Section we will always use $\Lambda^S_{\alpha\alpha} = 190$ MeV, one of the values for which the α–α low–energy phase–shifts are better reproduced (see Fig. 4.7b). The parameters Λ_3 and λ_3 are the cut–off and the strength of the three–body interaction, respectively.

A study of the ground state 0_1^+ has been carried out in Ref. [29]. For fixed $\Lambda^S_{\alpha\alpha} = 190$ MeV, if no three–body force is employed, the calculated energy of the ground state of the system results to be $E(0^+) = -0.91$ MeV. This bound state is shallow in comparison with the experimental value $E^{\mathrm{exp}}(0_1^+)$. By including a three–body interaction in the model, for every fixed cut–off Λ_3 inside the range allowed by the Wigner bound, the constant λ_3 is chosen so that the calculated energy corresponds to the experimental one. For example, with $\Lambda_3 = 130$ MeV and $\lambda_3^{0^+} = -8.422\,\mathrm{fm}^5$ the experimental energy $E^{\mathrm{exp}}(0_1^+)$ is obtained. With these values for Λ_3 and $\lambda_3^{0^+}$, a 2^+ bound state is found. However, its energy is different from the experimental one, $E^{\mathrm{exp}}(2_1^+)$. This suggests that also in this case the three–body force is state–dependent.

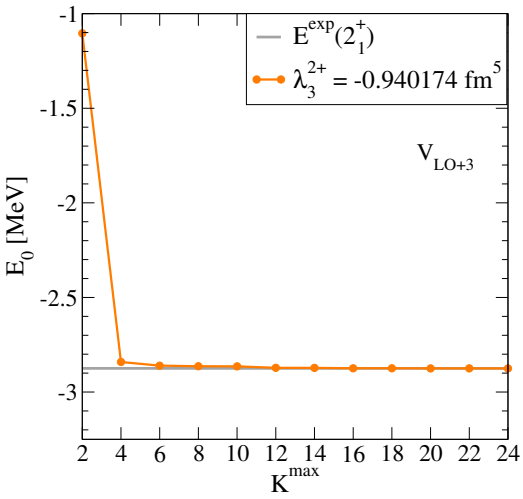

Figure 7.2: Convergence study relative to the ^{12}C(2^+_1) bound–state energy with respect to the maximum grand–angular momentum quantum number $K^{\max}$. The effective potential V_{LO+3} (7.18) is used, with $\Lambda_3 = 200\,\text{MeV}$ and $\lambda_3^{2^+} = -0.9401736\,\text{fm}^5$. With the chosen strength $\lambda_3^{2^+}$ the experimental energy $E^{\text{exp}}(2^+_1) = -2.875\,\text{MeV}$ [123] is reproduced.

By focussing on the study of the 2^+_1 state, we have found that a three–body force must be included in the calculation, otherwise no 2^+ bound states exist. The typical values of the parameters of the basis used to perform convergent calculations are in this case $\beta = 0.02\,\text{fm}^{-1}$, $N_Q/N_\varphi = 550/500$, $N_L = 30$ and $K^{\max} = 20$. The convergence pattern of the lowest eigenvalue with respect to the variation of the maximum grand–angular momentum $K^{\max}$ is shown in Fig. 7.2, for fixed $\Lambda_3 = 200\,\text{MeV}$ and $\lambda_3^{2^+} = -0.9401736\,\text{fm}^5$. As expected, the convergence is very fast, due to the smooth character of the α–α S–wave effective potential. The difference in the calculated energy between $K_{\max} = 18$ and $K_{\max} = 20$ is of ~ 0.5 keV. As a consequence, $K_{\max} = 20$ is a good value to take in our bound–state calculations.

We have also analysed the variation of the strength $\lambda_3^{2^+}$ as a function of the cut–off Λ_3 in the range of values from 70 to 400 MeV, obtaining the behaviour reported in Fig. 7.3. As a comparison, we have added in the plot also the variation of the strength $\lambda_3^{0^+}$ with Λ_3. As already explained, λ_3 is chosen so that the experimental energy of the bound state is reproduced for all the values of Λ_3. In Fig. 7.3 the behaviour of the combination $\lambda_3\Lambda_3^4$ is also reported. The result for $\Lambda_3 = 400\,\text{MeV}$ suggests that the scaling of λ_3 with the cut–off may involve a lower power.

The ^{12}C photodisintegration cross section

By making use of the results obtained for the 2^+_1 bound state, the LIT relative to the transition $2^+_1 \to 0^+_2$ can be computed by means of Eq. (7.9), which depends on the quadrupole matrix elements $\langle\Psi_l|\hat{u}_\lambda|\Psi_0\rangle$. In solving the eigenvalue problem for the final state 0^+_2, we use the same Hamiltonian as the one employed for the 2^+_1 bound state, with the exception of the strength λ_3 relative to the three–body term in Eq. (7.18).

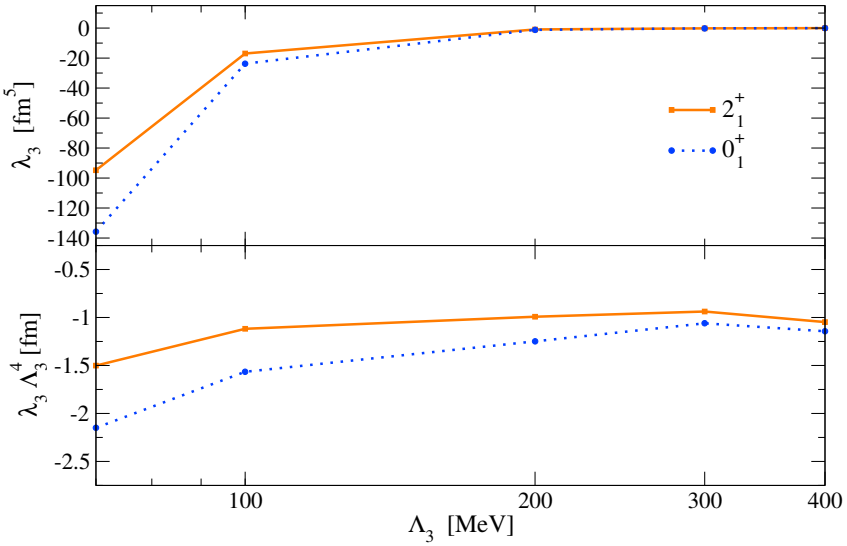

Figure 7.3: Values of the strengths λ_3^{2+}, λ_3^{0+} (upper panel) and of the relative combination $c_3 = \lambda_3 \Lambda_3^4$ (lower panel) as a function of the three–body cut–off Λ_3. The potential V_{LO+3} (7.18) has been used in the calculations. The constant λ_3^{2+} (λ_3^{0+}) is tuned so that the experimental energy $E^{\rm exp}(2_1^+) = -2.875\,{\rm MeV}$ [123] ($E^{\rm exp}(0_1^+) = -7.275\,{\rm MeV}$ [123]) is reproduced.

The calculated LIT can be seen in Fig. 7.4, for fixed $\sigma_I = 0.05\,{\rm MeV}$ and $K^{\rm max} = 20$, where also the convergence in N_L is visible. This parameter is related to the dimension of the "hypermomental" (hyperradial) basis employed. A few comments about Fig. 7.4 are here in order. For the moment, we have decided to restrict the LIT calculation to one single value of the three–body cut–off parameter, $\Lambda_3 = 200\,{\rm MeV}$. By varying the strength of the three–body force in a wide range of values, at least one 0^+ bound state is always present. As a consequence, we have chosen a value for $\lambda_3^{0^+}$ that produces a resonance peak in the expected location of the Hoyle state, at energy $\sim 3.255\,{\rm MeV}$. When $\lambda_3^{0^+} = -0.70918\,{\rm fm}^5$ is fixed, the calculated energy of the 0^+ bound state is $E(0^+) = -1.792\,{\rm MeV}$. By looking at Fig. 7.4, this 0^+ bound state can be associated to the high peak on the left occurring at around $\approx 1\,{\rm MeV}$. Moreover, it can also be identified with the ground state of the system, even though the calculated energy differs from the experimental value $E^{\rm exp}(0_1^+) = -7.275\,{\rm MeV}$ by a factor of about 4. A possible explanation is that our effective theory at LO is not able to reproduce the 0_1^+ and 0_2^+ states simultaneously. The description could be improved by including in the calculation an α–α effective potential in the partial wave $\ell = 2$. As a matter of fact, by using the effective potential in Eq. (7.18) most of the binding is due to the three–body interaction, since there are no bound states without this term. By including a D–wave in the two–body effective potential, the contribution of the three–body interaction would probably be reduced, leading to a better description of the whole system. In Fig. 7.4 we have chosen to use $K^{\rm max} = 20$, which is the same value employed for the 2^+ bound–state calculations. From a preliminary study, we have seen that this value gives convergent results concerning the peak on the left around $\approx 1\,{\rm MeV}$. On the other hand, with $K^{\rm max} = 20$ the resonance peak above 3 MeV is not fully convergent. As a consequence, there

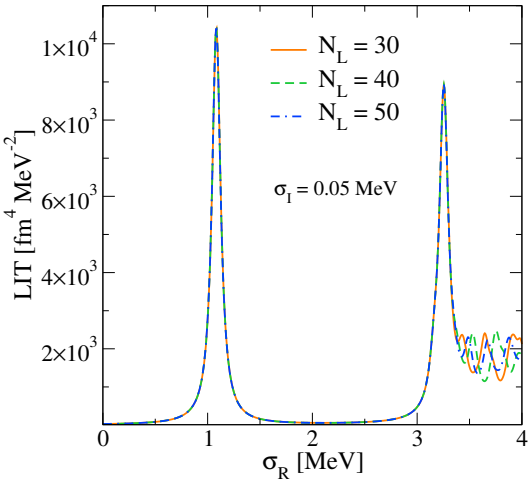

Figure 7.4: LIT relative to the quadrupole transition $2^+_1 \to 0^+_2$ for $\sigma_I = 0.05\,\text{MeV}$. The potential V_{LO+3} is used in the calculation with cut–off $\Lambda_3 = 200\,\text{MeV}$ and strength $\lambda_3 = -0.70918\,\text{fm}^5$. The value of the maximum grand–angular momentum is fixed at $K^{\max} = 20$, while the convergence by increasing the basis parameter N_L is shown.

is room for improvement. By increasing the dimension of the "hypermomental" (hyperradial) basis through the parameter N_L, the results are visibly convergent at $N_L = 50$ up to energies $\approx 3.4\,\text{MeV}$. However, since the experimental width of the state 0^+_2 in the continuum is extremely small, $\Gamma^{\text{exp}}(0^+_2) = 8.5\,\text{eV}$ [123], a value $N_L > 50$ is recommended, in order to perform an inversion as accurate as possible. Due to the small $\Gamma^{\text{exp}}(0^+_2)$, a value of the parameter σ_I lower than the one employed in Fig. 7.4 is also required. Figs. 7.5 show the same LIT calculated for $\sigma_I = 0.01\,\text{MeV}$ and $\sigma_I = 0.0001\,\text{MeV}$, respectively. As expected, other peaks emerge in addition to the principal ones, due to the fact that the resolution is higher.

Since a proper inversion procedure is not possible at this stage, by looking at Fig. 7.5b, we have tried to proceed by considering the highest peak located at energy 3.25617 MeV as a single "LIT state". By imposing for the width of the Lorentzian kernel the experimental value $\Gamma^{\text{exp}}(0^+_2) = 8.5\,\text{eV}$, we obtain the response function in Fig. 7.6a (solid line). Our result for the cross section calculated by means of Eq. (7.17) is shown in Fig. 7.6b (solid line). The maximum value of the cross section occurring at photon energy $\omega = 3.25617$ MeV is $\sigma = 8.26\,\text{fm}^2$.

In order to be able to make a first comparison of our results with other theoretical calculations, we have computed the response function also by assuming the width $\Gamma^{\text{th}}(0^+_2) = 15.8\,\text{eV}$, corresponding to the one reported in Ref. [33]. The obtained result is visible in Fig. 7.6a (dashed line), and the corresponding calculated cross section is in Fig. 7.6b (dashed line). In this case, at photon energy $\omega = 3.25617$ MeV the computed cross section corresponds to $\sigma = 5.69\,\text{fm}^2$. In Ref. [33] Suno *et al.* have calculated the reaction rates relative to the triple–α process with the transmission–free complex absorbing potential method by using a α–α local phenomenological potential, in addition to a three–body force. They have also computed the photodisintegration cross section from the $^{12}\text{C}(2^+_1)$ state to the 0^+_2 in the continuum.

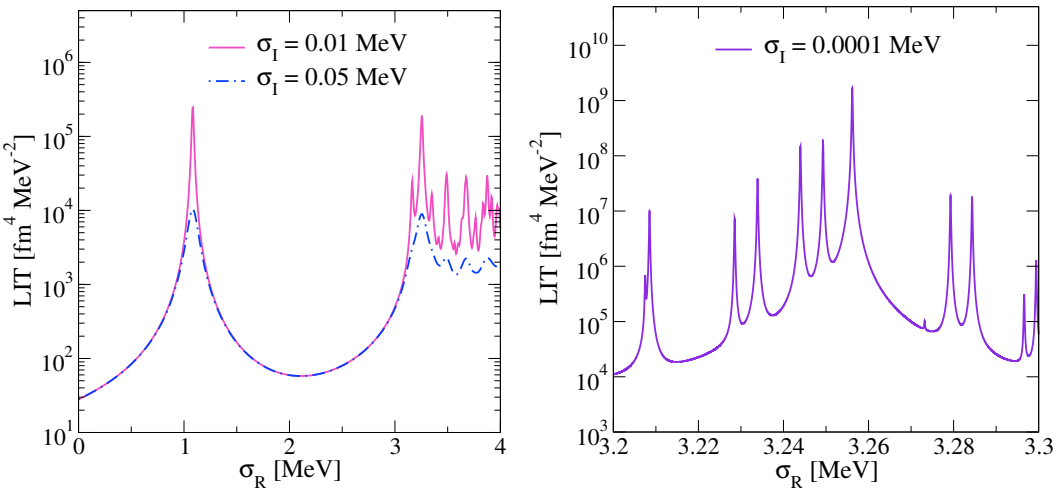

(a) (b)

Figure 7.5: Same as Fig. 7.4 but here the LIT is calculated also for $\sigma_I = 0.01\,\text{MeV}$ (a) and $\sigma_I = 0.0001\,\text{MeV}$ (b.)

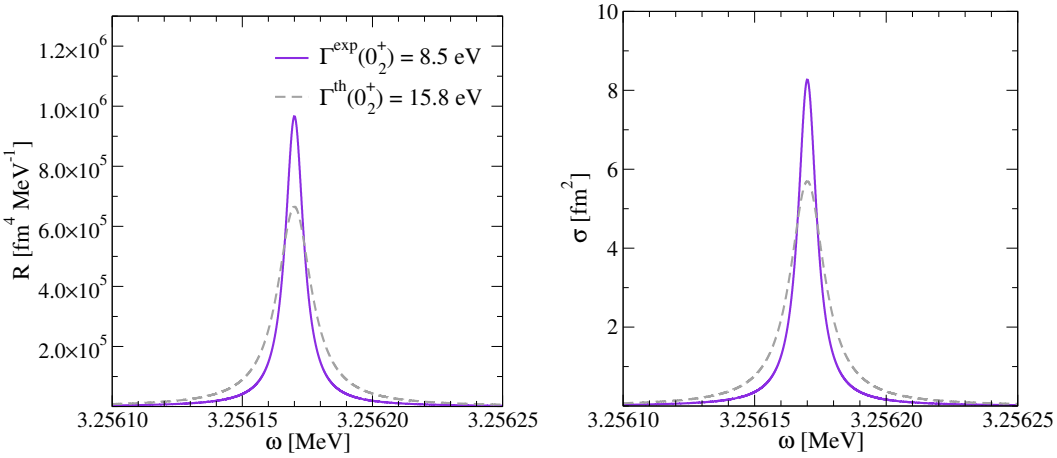

(a) (b)

Figure 7.6: (a) Response function obtained by imposing for the width of the Lorentzian kernel the experimental value $\Gamma^{\text{exp}}(0_2^+) = 8.5\,\text{eV}$ (solid line) and the value obtained in Ref. [33] $\Gamma^{\text{th}}(0_2^+) = 15.8\,\text{eV}$ (dashed line). (b) Calculated cross sections for the $E2$ transition $2_1^+ \to 0_2^+$. In both panels ω is the energy of the photon and the three–α threshold is located at 2.875 MeV.

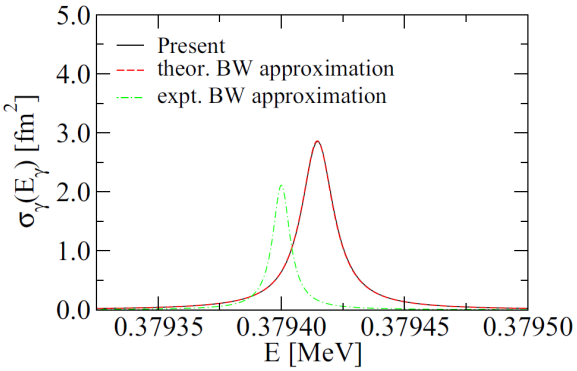

Figure 7.7: ^{12}C photodisintegration cross section through the states $2_1^+ \to 0_2^+$ as a function of the energy $E = E_\gamma + Q$ with $Q = -2.836\,\text{MeV}$ taken from Ref. [33]. A comparison with our results in Fig. 7.6b can be made. More details can be found in the text.

This is reported in Fig. 7.7, being denoted with the label "Present". By assuming a Breit–Wigner (BW) shape for the cross section near the Hoyle resonance, they have also derived the BW estimates by inserting as parameters both their theoretical results ($\Gamma^{\text{th}}(0_2^+) = 15.8\,\text{eV}$, among the others) and the experimental ones. These approximations are shown in Fig. 7.7, labelled with "theor. BW" and "expt. BW", respectively. At this point, a direct comparison between our calculations in Fig. 7.6b and the results in Fig. 7.7 can be done. The position of the resonance is almost the same, since our peak is located at energy 0.381 MeV above the three–α threshold. Concerning the height of the peaks, our results overestimate both theoretical and experimental BW approximations in Fig. 7.7. By considering our cross section obtained by assuming $\Gamma^{\text{exp}}(0_2^+) = 8.5\,\text{eV}$, the factor is ≈ 3.93, while in the other case our result is 1.98 times bigger. As anticipated, this could be possibly ascribed to the lack of a D–wave term in the effective α–α potential.

Finally, both our results for the ^{12}C photodisintegration cross section are represented in Fig. 7.8, where the photon energy ω is taken from the three–α threshold 2.875 MeV. The sharp peak that is characteristic of the Hoyle state is clearly visible.

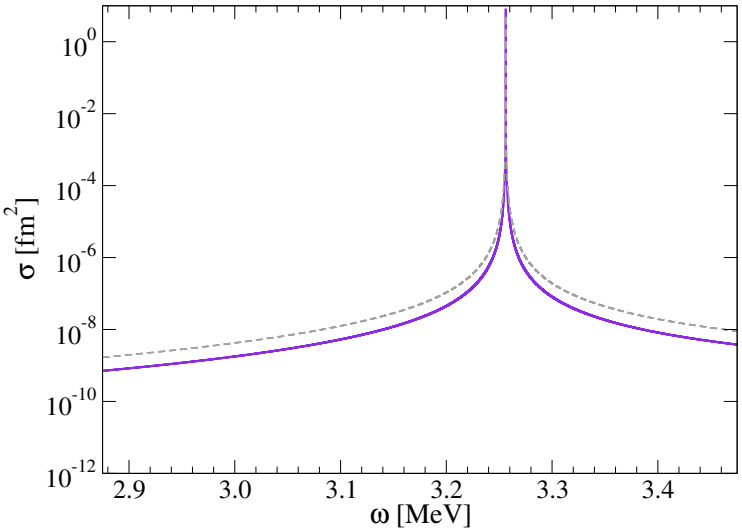

Figure 7.8: Same as Fig. 7.6b. Here the ^{12}C photodisintegration cross section proceeding through the states $2^+_1 \to 0^+_2$ is represented as a function of the photon energy taken in a range starting from the three–α threshold located at 2.875 MeV.

Chapter 8

Conclusions

In this Thesis we have presented the theoretical study of the following photodisintegration reactions

$$\gamma + {}^{9}\mathrm{Be} \to \alpha + \alpha + n\,, \qquad\qquad \gamma + {}^{12}\mathrm{C} \to \alpha + \alpha + \alpha\,, \tag{8.1}$$

in a fully three–body *ab initio* approach and in the regime of low energy. The inverse reactions relative to the two processes above are of astrophysical relevance, since, under certain astrophysical conditions, they are capable of bridging the mass gaps at $A = 5$ and $A = 8$.

Different theoretical calculations of ^{9}Be photodisintegration cross section can be found in the literature, where the nucleus is represented as a three–body system interacting through phenomenological potentials. Here, the separation of scales exhibited by ^{9}Be (the three–body binding is much smaller compared to the α–particle binding) is exploited, leading to a description of this nuclear system in terms of interactions derived from a halo/cluster EFT. This approach is based on a more solid theoretical background. ^{12}C is analysed on the same footing.

In Chapter 2, the photodisintegration reaction cross section has been derived in detail. A key quantity that determines this observable is represented by the Nuclear Current matrix element (NCme), which encodes all the information about the nuclear structure. At low energies, when the continuity equation is used explicitly, the transverse electric multipoles of the nuclear current operator can be related to the Coulomb multipoles of the nuclear charge. In this way, the exact form of the nuclear current is not needed in the calculations, since the NCme can be computed by using only the nuclear charge, i.e. by using the so–called Siegert operator. However, there is an alternative way to determine the NCme. Since the nuclear current can be decomposed as the sum of a one–body and many–body terms, one can take into account only the one–body current in order to compute the NCme. This has been done in Ref. [29]. By proceeding in this way, the contribution due to the many–body currents is lost. On the other hand, by using the Siegert operator, this is automatically included in the calculation. As a consequence, by comparing the results of the reaction cross section obtained from these two different calculations, the contribution due to the many–body currents can be quantified. Basically, this Thesis has been developed to move in this direction.

In Chapter 3 we have introduced the LIT method, which belongs to the more general context of calculating reactions cross sections by using integral transforms.

The direct calculation of the response function of inclusive processes involves the explicit wave functions belonging to the continuum spectrum of the nuclear system, and therefore it is not an easy task. By means of the LIT method, the problem is reformulated as a typical bound–state problem in terms of an integral transform. Then, the response function is recovered by means of an inversion procedure. The practical calculation of the LIT can be implemented in different ways. Here, we have mainly used the eigenvalue method, whose derivation has been presented in detail.

Chapter 4 contains a thorough derivation of the two–body α–n and α–α effective potentials within the context of halo/cluster EFT. These potentials are defined in momentum space as a series of contact terms, and they are regularized by the inclusion of a momentum–regulator function of Gaussian form. The LECs are determined by means of an implicit renormalization procedure: by requiring that the EFT reproduces the low–energy T–matrix ERE, the LECs are fixed on the experimental values of the scattering length and the effective range. For each of the two–body systems α–n and α–α, this is achieved by solving the Lippmann–Schwinger equation, i.e. in a non–perturbative way, using the multipole decomposition of the effective potential. With respect to the α–n system, the α–α case is more involved, as the Coulomb potential must be taken into account in addition to the strong force. In this case, the Coulomb–modified ERE is considered. Our effective potentials are therefore able to reproduce the low–energy phase–shifts of these systems. Due to the adopted power counting for ^{9}Be, the relevant partial waves to be considered at LO calculations are represented by the α–n $P_{3/2}$–wave and the α–α S_0–wave, both enhanced by the presence of a resonance in each two–body system. Concerning the α–n pair, also the non–enhanced waves $S_{1/2}$ and $P_{1/2}$ are taken into account as "NLO" contributions. In addition, a three–body force is introduced in the model, in order to cure the mild dependence of the three–body observables on the two–body cut–offs. The ^{12}C is described at LO by means of an α–α S_0–wave and a three–body interaction term.

The bound–state problem is solved by employing a variational method in conjunction with a NSHH basis. In Chapter 5, the NSHH method has been thoroughly analysed, giving a formulation both in coordinate and in momentum space. The main characteristic of this method is the expansion of the wave function over a basis with no symmetry imposed. Clearly, the dimension of the basis is larger but the symmetrization procedure typical of the HH method in its standard version for A identical particles is avoided, and this might well be advantageous for calculations involving systems with a number of components $A \geq 4$. In particular, this constitutes a suitable framework to study systems composed of non–identical particles.

The original contribution of this Thesis lies in Chapters 6 and 7. This entails the code implementation of the Siegert operator, in the long–wavelength approximation, in order to carry out photodisintegration cross section calculations. The effective potentials that we use are born in momentum space, and the basis on which we diagonalize the Hamiltonian to perform bound–state calculations is defined in the same space. On the other hand, the Siegert operator is defined in coordinate space. Consequently, much work has been devoted to implementing a suitable and consistent basis to calculate the matrix elements in coordinate space. The technique

employed is explained in Chapter 6. Since the effective interactions are non–local, the computational time for calculating the integrals of the potential matrix elements is quite long, so a first–level parallelization has been implemented in the existing code. In our cross sections calculations, we have used different values of the EFT parameters, discussing how the results depend on the different inputs, always in connection with the experimental data available in the literature. Among other results, we have also included the calculation of the nuclear binding energies, which however has been carried out by employing an existing code.

In Chapter 6 we have presented all the results relative to the calculation of the ^{9}Be photodisintegration cross section. In this work we have focused on $E1$ dipole transitions, which are dominant at low energies. The calculation of the magnetic transitions could be implemented as well. At LO we have mainly analysed the contribution to the cross section due to the $1/2^+$ resonance. Our results at LO show a clear overestimation of the experimental data. However, the EFT model employed is rather good, as we have verified the relatively small dependence on the cut–off associated to the three body force. No significant difference arises in the results when a α–n $P_{1/2}$–wave effective potential is added in the model. However, the α–n $S_{1/2}$ partial wave plays an important role in the calculation of the cross section. In fact, by considering also this contribution, the final results are more consistent with the experimental data. Effects of further partial waves are expected to be small. For some values of the cut–off relative to the α–n $S_{1/2}$ interaction, also a projection potential term is needed, as two–body deep bound states arise. The associated parameter has been fixed to a value inside a range of stability of the results, thus this procedure does not add new parameters in the theory. The NLO results of the cross section are in fair agreement with the experimental measurements by Arnold *et al.* [5]. The resonance due to the $1/2^+$ state shows a smaller width than the one seen in the experiment. However, our calculations slightly overestimate the data in the maximum of the peak. The LEC relative to the three–body force is fixed to have a resonance peak located in the correct position. This should not be seen as a loss of predictive power of the theory, since width and height are fairly reproduced. In the final calculation we have considered also the contributions due to the states $5/2^+$ and $3/2^+$. Also in the $5/2^+$ case there is an overestimation of the data around 3 MeV and above. However, this calculation can be improved by enlarging the dimension of the basis and new results will be added in the near future. It would be interesting to add also the cross section results obtained by using a different value of the three–body cut–off. In this way also an error due to the EFT can be evaluated. Moreover, since here a S–wave three–body potential has been used, the effect due to higher order terms could be explored.

By comparing our cross section results with those obtained by using the one–body convection current operator of Ref. [29], we can say that a non–negligible contribution of the many–body currents is present in the resonance associated to the $1/2^+$ state. However, concerning the $5/2^+$ case, the cross section calculated by using only the one–body current operator almost vanishes in the resonance peak region. This seems to indicate that the contribution of the many–body currents is higher in this case. This could be ascribed to the different potentials that contribute the most in creating the resonance peak associated to the $1/2^+$ and $5/2^+$ states. The first is mainly due to the ^{8}Be, therefore the α–α S_0–wave interaction plays the

major role. The latter is dominated by the α–n $P_{3/2}$–wave interaction. The two potentials differ by a relative factor pp'. Since the P–wave interaction is more–momentum dominated, a higher contribution in terms of many–body currents is generated in this case.

Our calculations of ^{12}C photodisintegration cross section, at a very early stage, can be found in Chapter 7. We have analysed the $E2$ quadrupole transition proceeding through the states $2_1^+ \rightarrow 0_2^+$. As a consequence, also $^{12}\mathrm{C}(2_1^+)$ binding energy calculations have been included in the Chapter. Our LO EFT is not able to reproduce simultaneously the $^{12}\mathrm{C}(0_1^+)$ ground state and the $^{12}\mathrm{C}(0_2^+)$ state in the continuum. In fact, by using the three–body LEC to locate the Hoyle state in the correct position, the 0_1^+ state results to be underbound. This indicates that probably a calculation beyond LO is necessary. Our first result for ^{12}C photodisintegration cross section, obtained by considering only one "LIT state" and by imposing the experimental width of the resonance during the inversion procedure, overestimates the experimental BW approximation by a factor 4. Our computation at LO involves a α–α S–wave interaction as well as a three–body force. Calculations can be refined possibly by including in the model a D–wave interaction. Improvements can also be made by enlarging the dimension of the basis in describing the Hoyle state. Also in this case a one–body current operator can be implemented to calculate the cross section, in order to make a comparison with the results obtained with the quadrupole operator. At LO, since only a S–wave interaction is present, we expect a small contribution due to the many–body currents. However this needs to be validated.

With a view to extending the formalism to the study of other nuclear clustering systems, even with $A > 3$ components, some improvements could be considered to start with: the inclusion of a n–n effective potential in the calculations, and the implementation of a three–body force that takes into account the particles permutations. At this point, with an adequate parallelization of the codes, also other nuclear reactions will become accessible for studies in the low–energy regime. An example is provided by the following process: $\gamma + {}^{16}\mathrm{O} \rightarrow \alpha + \alpha + \alpha + \alpha$. One of the most significant reactions in astrophysics is in fact $^{12}\mathrm{C}(\alpha,\gamma)^{16}\mathrm{O}$, and in this connection the study of the ^{16}O photodisintegration into four α–particles is of great interest. The final goal of this project could therefore be the study of the ^{16}O formation.

Appendix A

The vector spherical harmonics functions

In this Appendix we report some of the properties of the vector spherical harmonics functions, which are useful to derive the relations in Section 2.2. For the notations and the definitions, we will make large use of Ref. [44] as well as Ref. [43].

The vector spherical harmonics are defined as follows

$$\boldsymbol{Y}^{(\ell 1)}_{JM}(\hat{x}) = \sum_{m\lambda} C^{JM}_{\ell m,1\lambda} Y_{\ell m}(\hat{x}) \hat{\boldsymbol{\varepsilon}}_\lambda \,, \tag{A.1}$$

where $\hat{x}$ is the generic pair of spherical polar angles $\hat{x} = (\theta_x, \phi_x)$ and the coefficients $C^{JM}_{\ell m,1\lambda} = \langle \ell m 1\lambda | (\ell 1) JM \rangle$ are the Clebsch–Gordan coefficients. The functions $Y_{\ell m}(\hat{x})$ are the usual spherical harmonics and the unit vectors $\hat{\boldsymbol{\varepsilon}}_\lambda$, with $\lambda = 0, \pm 1$, are defined on a spherical basis as

$$\begin{aligned} \hat{\boldsymbol{\varepsilon}}_0 &= \hat{\boldsymbol{\varepsilon}}_z \,, \\ \hat{\boldsymbol{\varepsilon}}_{\pm 1} &= \mp \frac{1}{\sqrt{2}} (\hat{\boldsymbol{\varepsilon}}_x \pm i \hat{\boldsymbol{\varepsilon}}_y) \,. \end{aligned} \tag{A.2}$$

The complex conjugate vectors and the scalar products are

$$\hat{\boldsymbol{\varepsilon}}^*_\lambda = (-1)^\lambda \hat{\boldsymbol{\varepsilon}}_{-\lambda} \,, \qquad\qquad \hat{\boldsymbol{\varepsilon}}^*_\lambda \cdot \hat{\boldsymbol{\varepsilon}}_{\lambda'} = \delta_{\lambda\lambda'} \,. \tag{A.3}$$

The vector spherical harmonics are eigenfunctions of the total angular momentum operator $\boldsymbol{J}^2$ and of its projection on the z–axis J_z with eigenvalues $J(J+1)$ and M, respectively, and the following relation is valid

$$\boldsymbol{L} Y_{JM}(\hat{x}) = \sqrt{J(J+1)} \boldsymbol{Y}^{(J1)}_{JM}(\hat{x}) \,, \tag{A.4}$$

with $\boldsymbol{L}$ the orbital angular momentum operator. These functions have also the orthonormality property

$$\int d\hat{x}\, \boldsymbol{Y}^{(\ell 1)*}_{JM}(\hat{x})\, \boldsymbol{Y}^{(\ell' 1)}_{J'M'}(\hat{x}) = \delta_{JJ'} \delta_{MM'} \delta_{\ell\ell'} \,. \tag{A.5}$$

To simplify the notation, from now on we will drop one of the superscripts in definition of Eq. (A.1), $\boldsymbol{Y}^{(\ell)}_{JM}(\hat{x}) \equiv \boldsymbol{Y}^{(\ell 1)}_{JM}(\hat{x})$, and we will use these functions in momentum space.

The vector spherical harmonics can be generated by applying the unit vector $\hat{\boldsymbol{q}}$ as follows

$$\hat{\boldsymbol{q}}\, Y_{JM}(\hat{q}) = \sqrt{\frac{J}{2J+1}}\boldsymbol{Y}^{(J-1)}_{JM}(\hat{q}) - \sqrt{\frac{J+1}{2J+1}}\boldsymbol{Y}^{(J+1)}_{JM}(\hat{q})\,. \tag{A.6}$$

By applying the operator $\hat{\boldsymbol{q}}\times$, they can be expressed as a linear combination of vector spherical harmonics with the same J and M but different parity

$$\hat{\boldsymbol{q}} \times \boldsymbol{Y}^{(J+1)}_{JM}(\hat{q}) = i\sqrt{\frac{J}{2J+1}}\boldsymbol{Y}^{(J)}_{JM}(\hat{q})\,, \tag{A.7a}$$

$$\hat{\boldsymbol{q}} \times \boldsymbol{Y}^{(J)}_{JM}(\hat{q}) = i\sqrt{\frac{J+1}{2J+1}}\boldsymbol{Y}^{(J-1)}_{JM}(\hat{q}) + i\sqrt{\frac{J}{2J+1}}\boldsymbol{Y}^{(J+1)}_{JM}(\hat{q})\,, \tag{A.7b}$$

$$\hat{\boldsymbol{q}} \times \boldsymbol{Y}^{(J-1)}_{JM}(\hat{q}) = i\sqrt{\frac{J+1}{2J+1}}\boldsymbol{Y}^{(J)}_{JM}(\hat{q})\,. \tag{A.7c}$$

By combining Eqs. (A.6) and (A.7b) we obtain the relations

$$\boldsymbol{Y}^{(J-1)}_{JM}(\hat{q}) = \sqrt{\frac{J}{2J+1}}\hat{\boldsymbol{q}}\, Y_{JM}(\hat{q}) - i\sqrt{\frac{J+1}{2J+1}}\hat{\boldsymbol{q}} \times \boldsymbol{Y}^{(J)}_{JM}(\hat{q})\,, \tag{A.8a}$$

$$\boldsymbol{Y}^{(J+1)}_{JM}(\hat{q}) = -\sqrt{\frac{J+1}{2J+1}}\hat{\boldsymbol{q}}\, Y_{JM}(\hat{q}) - i\sqrt{\frac{J}{2J+1}}\hat{\boldsymbol{q}} \times \boldsymbol{Y}^{(J)}_{JM}(\hat{q})\,. \tag{A.8b}$$

By assuming that the unit vector $\hat{\boldsymbol{q}}$ is oriented along the z–axis, $\hat{\boldsymbol{q}} = \hat{\boldsymbol{\varepsilon}}_z = \hat{\boldsymbol{\varepsilon}}_0$, we also calculate the quantities $\hat{\boldsymbol{q}}\, Y^*_{JM}(\hat{q})$, $\hat{\boldsymbol{q}} \times \boldsymbol{Y}^{(J)*}_{JM}(\hat{q})$ and $\boldsymbol{Y}^{(J)*}_{JM}(\hat{q})$, which are used in the text. The first and the last are explicitly

$$\hat{\boldsymbol{q}}\, Y^*_{JM}(\hat{q}) = \sqrt{\frac{2J+1}{4\pi}}\hat{\boldsymbol{\varepsilon}}_0\,, \tag{A.9}$$

$$\boldsymbol{Y}^{(J)*}_{JM}(\hat{q}) = \sqrt{\frac{2J+1}{4\pi}}C^{JM}_{J0,1M}\hat{\boldsymbol{\varepsilon}}^*_M\,, \tag{A.10}$$

where we have used the definition of the vector spherical harmonics in Eq. (A.1) and the relation $Y_{\ell m}(\hat{\boldsymbol{\varepsilon}}_z) = \sqrt{\frac{2\ell+1}{4\pi}}\delta_{m0}$. Then $\hat{\boldsymbol{q}} \times \boldsymbol{Y}^{(J)*}_{JM}(\hat{q})$ can be calculated from Eq. (A.10) by taking into account that $\hat{\boldsymbol{\varepsilon}}_0 \times \hat{\boldsymbol{\varepsilon}}^*_M = iM\hat{\boldsymbol{\varepsilon}}^*_M$, and the final result is

$$\hat{\boldsymbol{q}} \times \boldsymbol{Y}^{(J)*}_{JM}(\hat{q}) = iM\sqrt{\frac{2J+1}{4\pi}}C^{JM}_{J0,1M}\hat{\boldsymbol{\varepsilon}}^*_M\,. \tag{A.11}$$

The Clebsch–Gordan coefficients in Eqs. (A.10) and (A.11) are $C^{JM}_{J0,1M} = -M/\sqrt{2}$.

In the rest of this Appendix we will derive Eqs. (2.28) and (2.29). We start from the expression of the electric and magnetic current operators in terms of the vector spherical harmonics, Eqs. (2.26) and (2.27), which we rewrite here for convenience

$$\tilde{\boldsymbol{J}}^{el}_{JM}(\boldsymbol{q}) = J^{J-1}_{JM}(q)\boldsymbol{Y}^{(J-1)*}_{JM}(\hat{q}) + J^{J+1}_{JM}(q)\boldsymbol{Y}^{(J+1)*}_{JM}(\hat{q}) \tag{A.12}$$

$$\tilde{\boldsymbol{J}}^{mag}_{JM}(\boldsymbol{q}) = J^{J}_{JM}(q)\boldsymbol{Y}^{(J)*}_{JM}(\hat{q})\,, \tag{A.13}$$

where the coefficients are defined explicitly as

$$J^{J-1}_{JM}(q) = \int d\hat{q}'\, \tilde{\boldsymbol{J}}(\boldsymbol{q}') \cdot \boldsymbol{Y}^{(J-1)}_{JM}(\hat{q}')\,, \tag{A.14a}$$

$$J^{J+1}_{JM}(q) = \int d\hat{q}'\, \tilde{\boldsymbol{J}}(\boldsymbol{q}') \cdot \boldsymbol{Y}^{(J+1)}_{JM}(\hat{q}')\,, \tag{A.14b}$$

and

$$J^{J}_{JM}(q) = \int d\hat{q}'\, \tilde{\boldsymbol{J}}(\boldsymbol{q}') \cdot \boldsymbol{Y}^{(J)}_{JM}(\hat{q}')\,. \tag{A.15}$$

By substituting Eqs. (A.8) in Eqs. (A.14) we obtain for the coefficients $J^{J\pm1}_{JM}(q)$

$$J^{J-1}_{JM}(q) = \int d\hat{q}'\, \tilde{\boldsymbol{J}}(\boldsymbol{q}') \cdot \left[\sqrt{\frac{J}{2J+1}}\hat{\boldsymbol{q}}'\, Y_{JM}(\hat{q}') - i\sqrt{\frac{J+1}{2J+1}}\hat{\boldsymbol{q}}' \times \boldsymbol{Y}^{(J)}_{JM}(\hat{q}') \right], \tag{A.16a}$$

$$J^{J+1}_{JM}(q) = \int d\hat{q}'\, \tilde{\boldsymbol{J}}(\boldsymbol{q}') \cdot \left[-\sqrt{\frac{J+1}{2J+1}}\hat{\boldsymbol{q}}'\, Y_{JM}(\hat{q}') - i\sqrt{\frac{J}{2J+1}}\hat{\boldsymbol{q}}' \times \boldsymbol{Y}^{(J)}_{JM}(\hat{q}') \right]. \tag{A.16b}$$

Then, from the expressions above and from Eqs. (A.8), the electric multipole operators in Eq. (A.12) become explicitly

$$\begin{aligned} \tilde{\boldsymbol{J}}^{el}_{JM}(\boldsymbol{q}) = \hat{\boldsymbol{q}}\, Y^*_{JM}(\hat{q}) \int d\hat{q}'\ \hat{\boldsymbol{q}}' \cdot \tilde{\boldsymbol{J}}(\boldsymbol{q}')\, Y_{JM}(\hat{q}') \\ + \hat{\boldsymbol{q}} \times \boldsymbol{Y}^{(J)*}_{JM}(\hat{q}) \int d\hat{q}' \left(\hat{\boldsymbol{q}}' \times \boldsymbol{Y}^{(J)}_{JM}(\hat{q}') \right) \cdot \tilde{\boldsymbol{J}}(\boldsymbol{q}')\,. \end{aligned} \tag{A.17}$$

By following the same reasoning, we can rewrite the magnetic multipole operators in Eq. (A.12) as

$$\tilde{\boldsymbol{J}}^{mag}_{JM}(\boldsymbol{q}) = \boldsymbol{Y}^{(J)*}_{JM}(\hat{q}) \int d\hat{q}'\, \tilde{\boldsymbol{J}}(\boldsymbol{q}') \cdot \boldsymbol{Y}^{(J)}_{JM}(\hat{q}')\,. \tag{A.18}$$

Appendix B

The Lanczos algorithm

The Lanczos method is essentially a technique used to tridiagonalize matrices [58]. When the Hamiltonian operator $\hat{H}$ is represented on a suitable basis, the Lanczos algorithm is often used to determine the lowest eigenvalue and eigenvector, i.e. the ground state. The algorithm can be also applied in the calculation of the LIT (see Section 3.3.2).

The idea is to construct a orthonormal basis of Lanczos vectors $|\phi_n\rangle$ with $n = 0, \ldots, N_{\text{Lanc}}$, in a recursive way. On this basis, the matrix Hamiltonian results to be tridiagonal, and therefore it can be diagonalized by making use of standard routines. If the dimension of the Hamiltonian matrix is $N \times N$, then the maximum number of possible Lanczos steps is $N_{\text{Lanc}}^{\max} = N - 1$. The advantage of the method lies in the fact that convergent results can be obtained already for $N_{\text{Lanc}} \ll N - 1$. As a consequence, calculations are computationally less demanding with respect to the full diagonalization of the Hamiltonian matrix. This method requires mainly the evaluation of matrix–vector products.

The starting vector, also known as pivot, is an arbitrary normalized vector $|\phi_0\rangle$. Then, $\hat{H}\,|\phi_0\rangle$ is used to construct the first vector $|\phi_1\rangle$ as follows

$$|\widetilde{\phi}_1\rangle = \hat{H}\,|\phi_0\rangle - a_0\,|\phi_0\rangle = b_1\,|\phi_1\rangle\,, \tag{B.1}$$

where $a_0 = \langle\phi_0|\hat{H}|\phi_0\rangle$ and $b_1^2 = \langle\widetilde{\phi}_1|\widetilde{\phi}_1\rangle$. In this way $|\phi_0\rangle$ and $|\phi_1\rangle$ are orthonormal. Then one proceeds to construct another vector by taking $\hat{H}\,|\phi_1\rangle$, by orthogonalizing with respect to the previous vectors, and then normalizing as follows

$$|\widetilde{\phi}_2\rangle = \hat{H}\,|\phi_1\rangle - a_1\,|\phi_1\rangle - b_1\,|\phi_0\rangle = b_2\,|\phi_2\rangle\ , \tag{B.2}$$

with $a_1 = \langle\phi_1|\hat{H}|\phi_1\rangle$ and $b_2^2 = \langle\widetilde{\phi}_2|\widetilde{\phi}_2\rangle$. As a consequence, the recursive formula to construct the Lanczos basis of vectors is the following

$$|\widetilde{\phi}_{i+1}\rangle = \hat{H}\,|\phi_i\rangle - a_i\,|\phi_i\rangle - b_i\,|\phi_{i-1}\rangle = b_{i+1}\,|\phi_{i+1}\rangle\ , \tag{B.3}$$

and the definition of the so–called Lanczos coefficients is

$$a_i = \langle\phi_i|\hat{H}|\phi_i\rangle\ , \qquad\qquad b_i^2 = \langle\widetilde{\phi}_i|\widetilde{\phi}_i\rangle \tag{B.4}$$

where, $i = 0, 1, 2, \ldots$ and $b_0 = 0$, $|\phi_{-1}\rangle = 0$. On this basis the Hamiltonian matrix is explicitly

$$H_{\mathrm{T}} = \begin{pmatrix} a_0 & b_1 & 0 & 0 & \ldots & 0 & 0 \\ b_1 & a_1 & b_2 & 0 & \ldots & 0 & 0 \\ 0 & b_2 & a_2 & b_3 & & 0 & 0 \\ 0 & 0 & b_3 & a_3 & & 0 & 0 \\ \vdots & \vdots & & & \ddots & & \vdots \\ 0 & 0 & 0 & 0 & & a_{N_{\mathrm{Lanc}}-1} & b_{N_{\mathrm{Lanc}}} \\ 0 & 0 & 0 & 0 & \ldots & b_{N_{\mathrm{Lanc}}} & a_{N_{\mathrm{Lanc}}} \end{pmatrix}, \tag{B.5}$$

where N_{Lanc} is the number of steps used. The eigenvalues of the tridiagonal matrix H_{T} are good approximations of the extreme eigenvalues of the Hamiltonian matrix, and they converge already with a number of steps $N_{\mathrm{Lanc}} \ll N - 1$. We point out that after a certain number of Lanczos steps, the Lanczos vectors loose their orthogonality property, and this could lead to results that are not so accurate. For this reason, an additional re–orthogonalization process is often needed [59].

Appendix C

Lippmann–Schwinger equation

In this Appendix we write the detailed derivation of the Lippmann–Schwinger equations (4.19) and (4.61) used as a starting point for the calculation of the coefficients of the two–body α–n and α–α effective potentials. More details about the formalism can be found in Refs. [25, 83, 124, 125].

C.1 General formalism

In relative coordinates, the system composed of two particles with reduced mass μ is described by the free Hamiltonian $\hat{H}_0 = \frac{\hat{p}^2}{2\mu}$ and the Schrödinger equation $\hat{H}_0 |\boldsymbol{p}\rangle = E |\boldsymbol{p}\rangle$, where the energy is $E = \frac{p^2}{2\mu}$. The set of eigenstates $|\boldsymbol{p}\rangle$ is a complete and orthogonal set, satisfying the following relations

$$\Omega \int \frac{d^3\boldsymbol{p}}{(2\pi)^3} |\boldsymbol{p}\rangle \langle \boldsymbol{p}| = 1 \,, \qquad \langle \boldsymbol{p}|\boldsymbol{p}'\rangle = \frac{(2\pi)^3}{\Omega} \delta^3(\boldsymbol{p} - \boldsymbol{p}') \,, \tag{C.1}$$

representing also a complete set of plane wave solutions $\langle \boldsymbol{r}|\boldsymbol{p}\rangle = e^{i\boldsymbol{p}\boldsymbol{r}}/\sqrt{\Omega}$. In the text the convention for which $\Omega = 1$ is used. The free Green's function relative to the system is defined as [125]

$$\hat{G}_0^{(\pm)}(E) = \frac{1}{E - \hat{H}_0 \pm i\varepsilon} \,. \tag{C.2}$$

By inserting a complete set of states $|\boldsymbol{q}\rangle$, we have

$$\hat{G}_0^{(+)}(E) = \Omega \int \frac{d^3\boldsymbol{q}}{(2\pi)^3} \frac{|\boldsymbol{q}\rangle \langle \boldsymbol{q}|}{E - \frac{q^2}{2\mu} + i\varepsilon} \,, \tag{C.3}$$

which allows us to write for the free Green's function matrix element

$$\langle \boldsymbol{p}|\hat{G}_0^{(+)}(E)|\boldsymbol{p}'\rangle = \frac{(2\pi)^3}{\Omega} \frac{\delta^3(\boldsymbol{p} - \boldsymbol{p}')}{E - \frac{q^2}{2\mu} + i\varepsilon} \,. \tag{C.4}$$

When we add a potential to the free Hamiltonian, the full Hamiltonian is $\hat{H} = \hat{H}_0 + \hat{V}$, and the solutions of the Schrödinger equation $(\hat{H} - E)|\psi\rangle = 0$ can be expressed formally as

$$|\psi_{\boldsymbol{p}}^{(\pm)}\rangle = |\boldsymbol{p}\rangle + \hat{G}_0^{(\pm)} \hat{V} |\psi_{\boldsymbol{p}}^{(\pm)}\rangle \,, \tag{C.5}$$

where the prescription $(\pm)$ reflects their asymptotic behaviour (incoming or outgoing). The full Green's function is now

$$\hat{G}^{(\pm)}(E) = \frac{1}{E - \hat{H} \pm i\varepsilon} \,. \tag{C.6}$$

Notice that by using the relation $\hat{G}_0^{(\pm)} = \hat{G}^{(\pm)} - \hat{G}^{(\pm)}\hat{V}\hat{G}_0^{(\pm)}$ between the free and the full Green's functions defined in Eqs. (C.2) and (C.6), respectively, we can rewrite the solutions in Eq. (C.5) in terms of the free–solutions $|\boldsymbol{p}\rangle$ as follows

$$|\psi_{\boldsymbol{p}}^{(\pm)}\rangle = \left(1 + \hat{G}^{(\pm)}\hat{V}\right)|\boldsymbol{p}\rangle \,. \tag{C.7}$$

Another useful equivalence is $\hat{G}^{(\pm)} = \hat{G}_0^{(\pm)} + \hat{G}_0^{(\pm)}\hat{V}\hat{G}^{(\pm)}$, whose iterative solution for $\hat{G}^{(\pm)}$ leads to the expansion $\hat{G}^{(\pm)} = \sum_{n=0}^{\infty}(\hat{G}_0^{(\pm)}\hat{V})^n\hat{G}_0^{(\pm)}$ and consequently to

$$|\psi_{\boldsymbol{p}}^{(\pm)}\rangle = \left[1 + \sum_{n=1}^{\infty}(\hat{G}_0^{(\pm)}\hat{V})^n\right]|\boldsymbol{p}\rangle \,. \tag{C.8}$$

From the definition of the operator $\hat{T}$, $(\hat{T}\,|\boldsymbol{p}\rangle = \hat{V}\,|\psi_{\boldsymbol{p}}^{(+)}\rangle)$, by making use of Eq. (C.5), we can write

$$\hat{T} = \hat{V} + \hat{V}\hat{G}_0^{(+)}\hat{T} \,, \tag{C.9}$$

which is the Lippmann–Schwinger equation for $\hat{T}$ in operator form. By inserting different complete sets of states $|\boldsymbol{p}\rangle$ and using Eq. (C.4), we can write explicitly for the T–matrix element

$$\langle \boldsymbol{p}|\hat{T}(E)|\boldsymbol{p}'\rangle = \langle \boldsymbol{p}|\hat{V}|\boldsymbol{p}'\rangle + \Omega\int \frac{d^3\boldsymbol{q}}{(2\pi)^3}\,\langle \boldsymbol{p}|\hat{V}|\boldsymbol{q}\rangle\,\frac{1}{E - \frac{\boldsymbol{q}^2}{2\mu} + i\varepsilon}\,\langle \boldsymbol{q}|\hat{T}(E)|\boldsymbol{p}'\rangle \,. \tag{C.10}$$

The formalism presented above can be applied when the interaction between the two particles of the system is given only by the strong interaction $\hat{V} = \hat{V}_{\mathrm{S}}$. When both the Coulomb potential $\hat{V}_{\mathrm{C}}$ and the strong short–range potential $\hat{V}_{\mathrm{S}}$ are present, we have to proceed in a different way.

C.2 Coulomb and strong potential

We start by considering the repulsive Coulomb potential $\hat{V}_C = Z_1 Z_2 \alpha_{\mathrm{em}}/r$ acting between the two particles of the system whose electromagnetic charges are Z_1 and Z_2, $\alpha_{\mathrm{em}} = \frac{e^2}{4\pi}$ being the fine–structure constant [25, 83]. In this case the Hamiltonian is $\hat{H} = \hat{H}_0 + \hat{V}_C$ and the Green's function can be written following Eq. (C.6) as

$$\hat{G}_C^{(\pm)}(E) = \frac{1}{E - \hat{H} \pm i\varepsilon} \,. \tag{C.11}$$

As in Eq. (C.7), we write the incoming and outgoing solutions of the Schrödinger equation $(\hat{H} - E)\,|\psi\rangle = 0$, i.e. the Coulomb wave functions, in the form

$$|\psi_{\boldsymbol{p}}^{(\pm)}\rangle = \left(1 + \hat{G}_C^{(\pm)}\hat{V}_C\right)|\boldsymbol{p}\rangle \,, \tag{C.12}$$

where the prescription $(\pm)$ depends again on the chosen boundary conditions at infinity. The solutions are normalized as in (C.1), and therefore, by analogy with Eq. (C.3), we can write

$$\hat{G}_C^{(+)}(E) = \Omega \int \frac{d^3\boldsymbol{q}}{(2\pi)^3} \frac{|\psi_{\boldsymbol{q}}^{(\pm)}\rangle \langle \psi_{\boldsymbol{q}}^{(\pm)}|}{E - \frac{\boldsymbol{q}^2}{2\mu} + i\varepsilon} \,. \tag{C.13}$$

These solutions can also be calculated by solving the Schrödinger equation and in coordinate space they are

$$\psi_{\boldsymbol{p}}^{(\pm)}(\boldsymbol{r}) = \langle \boldsymbol{r}|\psi_{\boldsymbol{p}}^{(\pm)}\rangle = e^{-\frac{\pi}{2}\eta}\Gamma(1 \pm i\eta) M(\mp i\eta, 1; \pm ipr - i\boldsymbol{pr}) e^{i\boldsymbol{pr}} \,, \tag{C.14}$$

where $\Gamma(z)$ and $M(a, b; z)$ are the Gamma function and the confluent hypergeometric function, respectively, [45] and $\eta = \eta(p)$ is the Sommerfeld parameter, defined as

$$\eta = Z_1 Z_2 \frac{\alpha_{\rm em}\mu}{p} \,. \tag{C.15}$$

The Coulomb wave functions have the following properties [25]:

$$\psi_{\boldsymbol{p}}^{(\pm)*}(0)\psi_{\boldsymbol{p}}^{(\pm)}(0) = e^{-\pi\eta}\Gamma(1 \mp i\eta)\Gamma(1 \pm i\eta) = \frac{2\pi\eta}{e^{2\pi\eta} - 1} \equiv C_\eta^2 \,, \tag{C.16}$$

$$\psi_{\boldsymbol{p}}^{(\mp)*}(0)\psi_{\boldsymbol{p}}^{(\pm)}(0) = e^{-\pi\eta}[\Gamma(1 \pm i\eta)]^2 = C_\eta^2 e^{\pm 2i\sigma_0} \,, \tag{C.17}$$

where we have introduced the Sommerfeld factor $C_\eta = C_{\eta(p)}$ and the Coulomb phase-shift $\sigma_0 = \sigma_0(p)$ for the $\ell = 0$ partial wave. The latter is defined in general as

$$\sigma_\ell = \arg\, \Gamma(\ell + 1 + i\eta) = \frac{1}{2i} \ln \left[\frac{\Gamma(\ell + 1 + i\eta)}{\Gamma(\ell + 1 - i\eta)} \right] \,. \tag{C.18}$$

By making an expansion of the Coulomb wave functions in partial waves, we write

$$\psi_{\boldsymbol{p}}^{(\pm)}(\boldsymbol{r}) = \sum_{\ell=0}^{\infty} i^\ell (2\ell + 1) R_\ell^{(\pm)}(pr) P_\ell(\cos\theta) \,, \tag{C.19}$$

and the $\ell = 0$ term is explicitly

$$R_0^{(\pm)}(pr) = C_{\eta(p)} e^{\pm i\sigma_0} M(1 + i\eta, 2; -2ipr) e^{ipr} \,. \tag{C.20}$$

With the identity $M(a, b; z) = M(b - a, b; -z)$, it can be demonstrated that the ingoing and outgoing solutions differ only by the phase factor $e^{\pm i\sigma_0}$ [83].

When we add the strong interaction $\hat{V}_S$ in the system we must consider the complete Hamiltonian $\hat{H} = \hat{H}_0 + \hat{V}_C + \hat{V}_S$ and the Green's function

$$\hat{G}_{SC}^{(\pm)}(E) = \frac{1}{E - \hat{H} \pm i\varepsilon} \,. \tag{C.21}$$

By following the formalism developed above, we can construct the solutions of the Schrödinger equation $(\hat{H} - E)\,|\Psi\rangle = 0$ in terms of the free–solutions $|\boldsymbol{p}\rangle$

$$|\Psi_{\boldsymbol{p}}^{(\pm)}\rangle = \left(1 + \hat{G}_{SC}^{(\pm)}(\hat{V}_C + \hat{V}_S)\right) |\boldsymbol{p}\rangle \,, \tag{C.22}$$

as well as those in terms of the Coulomb wave functions $|\psi_{\boldsymbol{p}}^{(\pm)}\rangle$

$$|\Psi_{\boldsymbol{p}}^{(\pm)}\rangle = |\psi_{\boldsymbol{p}}^{(\pm)}\rangle + \hat{G}_C^{(\pm)}\hat{V}_S\,|\Psi_{\boldsymbol{p}}^{(\pm)}\rangle\ . \tag{C.23}$$

Finally, it can be demonstrated that the matrix element of the operator $\hat{T}$, formally defined as

$$\hat{T} = (\hat{V}_C + \hat{V}_S)[1 + \hat{G}_{SC}^{(+)}(\hat{V}_C + \hat{V}_S)]\,, \tag{C.24}$$

can be expressed as a sum of two terms

$$\langle \boldsymbol{p}|\hat{T}|\boldsymbol{p}'\rangle = \langle \boldsymbol{p}|\hat{T}_C|\boldsymbol{p}'\rangle + \langle \boldsymbol{p}|\hat{T}_{SC}|\boldsymbol{p}'\rangle = \langle \boldsymbol{p}|\hat{V}_C|\psi_{\boldsymbol{p}'}^{(+)}\rangle + \langle \psi_{\boldsymbol{p}}^{(-)}|\hat{V}_S|\Psi_{\boldsymbol{p}'}^{(+)}\rangle\ , \tag{C.25}$$

$\langle \boldsymbol{p}|\hat{T}_C|\boldsymbol{p}'\rangle$ being the pure Coulomb term and $\langle \boldsymbol{p}|\hat{T}_{SC}|\boldsymbol{p}'\rangle$ the strong term modified by the Coulomb corrections. By making use of Eqs. (C.23) and (C.13), the Coulomb–distorted strong term can be written as follows

$$\langle \boldsymbol{p}|\hat{T}_{\mathrm{SC}}(E)|\boldsymbol{p}'\rangle = \langle \psi_{\boldsymbol{p}}^{(-)}|\,\hat{V}_{\mathrm{S}}\,|\psi_{\boldsymbol{p}'}^{(+)}\rangle + \Omega\int \frac{d^3\boldsymbol{q}}{(2\pi)^3}\,\langle \psi_{\boldsymbol{p}}^{(-)}|\,\hat{V}_{\mathrm{S}}\,|\psi_{\boldsymbol{q}}^{(-)}\rangle\,\frac{\langle \boldsymbol{q}|\hat{T}_{\mathrm{SC}}(E)|\boldsymbol{p}'\rangle}{E - \frac{\boldsymbol{q}^2}{2\mu} + i\varepsilon}\,. \tag{C.26}$$

Appendix D

Orthogonal polynomials

D.1 Jacobi polynomials

The Jacobi polynomials $P_n^{(a,b)}(x)$ of order $n = 0, 1, 2, \ldots$ are the solution of the following linear homogeneous differential equation of second order [45]

$$(1-x^2)[P_n^{(a,b)}]'' + [b-a-x(b+a+2)][P_n^{(a,b)}]' + n(n+b+a+1)P_n^{(a,b)} = 0\,, \quad \text{(D.1)}$$

with $a, b > -1$ and $-1 \leq x \leq 1$. The symbols $[P_n^{(a,b)}]'$ and $[P_n^{(a,b)}]''$ denote the derivatives with respect to the argument: $\frac{d}{dx}P_n^{(a,b)}(x)$ and $\frac{d^2}{dx^2}P_n^{(a,b)}(x)$, respectively. Note that the first two coefficients of Eq. (D.1) do not depend on the parameter n.

The Jacobi polynomials are a system of orthogonal polynomials in the interval $[-1, 1]$ and they satisfy the relation

$$\int_{-1}^{1} dx\,(1+x)^b(1-x)^a P_n^{(a,b)}(x)P_m^{(a,b)}(x) = \delta_{nm}\,h_n\,, \quad \text{(D.2)}$$

where $(1+x)^b(1-x)^a = w(x)$ is a weight function and the normalization coefficient h_n is explicitly

$$h_n = \frac{2^{b+a+1}}{2n+b+a+1}\frac{\Gamma(n+b+1)\Gamma(n+a+1)}{n!\,\Gamma(n+b+a+1)}\,. \quad \text{(D.3)}$$

D.2 Generalized Laguerre polynomials

The generalized Laguerre polynomials $L_n^{(\alpha)}(x)$ are the solution of the differential equation of second order [45]

$$x[L_n^{(\alpha)}(x)]'' + (\alpha+1-x)[L_n^{(\alpha)}(x)]' + nL_n^{(\alpha)}(x) = 0 \quad \text{(D.4)}$$

with $n = 0, 1, 2, \ldots$ and $\alpha > -1$. The notation $[L_n^{(\alpha)}(x)]' \equiv \frac{d}{dx}L_n^{(\alpha)}(x)$ and $[L_n^{(\alpha)}(x)]'' \equiv \frac{d^2}{dx^2}L_n^{(\alpha)}(x)$ is adopted.

The generalized Laguerre polynomials are a system of orthogonal polynomials in the interval $[0, \infty)$ with respect to the weight function $w(x) = e^{-x}x^\alpha$, i.e.

$$\int_0^\infty dx\,x^\alpha e^{-x} L_n^{(\alpha)}(x)L_m^{(\alpha)}(x) = \delta_{nm}\frac{(n+\alpha)!}{n!} \quad \text{(D.5)}$$

Appendix E

Derivation of the $E1$ and $E2$ transition operators

E.1 The electric dipole transition operator

We want to rewrite the rescaled dipole operator d_λ, which is defined in Eq. (6.5) as a sum of A terms. For $A = 3$ the operator is

$$d_\lambda = \sum_{i=1}^{3} Z_i r'_i Y_{1\lambda}(\hat{r}'_i)\,, \tag{E.1}$$

where each position vector $\boldsymbol{r}'_i$ is a linear combination of the internal Jacobi coordinates $\{\,\boldsymbol{\eta}_2, \boldsymbol{\eta}_1\,\}$, as explicitly written in Eq. (6.8). To this aim we make use of the following general relation [126]

$$\begin{aligned} v^\ell\, Y_{\ell m}(\hat{v}) = \sum_{\lambda'\mu'} \sqrt{\frac{4\pi(2\ell+1)!}{(2\lambda'+1)!(2\ell-2\lambda'+1)!}}\, \langle \ell-\lambda', m-\mu', \lambda', \mu' | \ell, m\rangle \\ \times a^{\ell-\lambda'}\, Y_{\ell-\lambda', m-\mu'}(\hat{a})\, b^{\lambda'}\, Y_{\lambda',\mu'}(\hat{b})\,, \end{aligned} \tag{E.2}$$

which is valid when the vector $\boldsymbol{v}$ can be written as $\boldsymbol{v} = \boldsymbol{a} + \boldsymbol{b}$. Specifically, we will consider the case in which $\ell = 1$ and $m = \lambda$. To rewrite the term $r'_1 Y_{1\lambda}(\hat{r'_1})$ we use Eq. (E.2) with

$$\boldsymbol{v} = \boldsymbol{r}'_1\,, \qquad \boldsymbol{a} = -\mathcal{A}\boldsymbol{\eta}_2\,, \qquad \boldsymbol{b} = -\mathcal{B}\boldsymbol{\eta}_1\,, \tag{E.3}$$

while for $r'_2 Y_{1\lambda}(\hat{r'_2})$ we impose

$$\boldsymbol{v} = \boldsymbol{r}'_2\,, \qquad \boldsymbol{a} = \mathcal{C}\boldsymbol{\eta}_2\,, \qquad \boldsymbol{b} = -\mathcal{B}\boldsymbol{\eta}_1\,. \tag{E.4}$$

These choices follow directly from Eqs. (6.8). The operator d_λ is then

$$\begin{aligned} d_\lambda = \sum_{\lambda'\mu'} \sqrt{\frac{6(4\pi)}{(2\lambda'+1)!(3-2\lambda')!}}\, \langle 1-\lambda', \lambda-\mu', \lambda', \mu' | 1, \lambda\rangle \\ \times \left[Z_1 (-\mathcal{A})^{1-\lambda'} (-\mathcal{B})^{\lambda'} + Z_2 \mathcal{C}^{1-\lambda'} (-\mathcal{B})^{\lambda'} \right] \\ \times \eta_2^{1-\lambda'}\, Y_{1-\lambda', \lambda-\mu'}(\hat{\eta}_2)\, \eta_1^{\lambda'}\, Y_{\lambda',\mu'}(\hat{\eta}_1) + Z_3 \mathcal{D}\, \eta_1 Y_{1,\lambda}(\hat{\eta}_1)\,, \end{aligned} \tag{E.5}$$

where the index λ' runs from 0 to ℓ, while $\mu' = -\lambda', \ldots, \lambda'$. By calculating explicitly the sum for $\lambda' = 0$ ($\mu' = 0$) and for $\lambda' = 1$ ($\mu' = 0, \pm 1$), we obtain

$$\begin{aligned} d_\lambda = {} & \sqrt{4\pi}\,(-Z_1\mathcal{A} + Z_2\mathcal{C})\,\eta_2\,Y_{1,\lambda}(\hat{\eta}_2)\,Y_{0,0}(\hat{\eta}_1) + Z_3\mathcal{D}\,\eta_1 Y_{1,\lambda}(\hat{\eta}_1) \\ & + \sqrt{4\pi} \sum_{\mu'=0,\pm1} \langle 0, \lambda-\mu', 1, \mu' | 1, \lambda\rangle\,[-(Z_1+Z_2)\mathcal{B}]\,\eta_1\,Y_{0,\lambda-\mu'}(\hat{\eta}_2)\,Y_{1,\mu'}(\hat{\eta}_1)\,. \end{aligned} \tag{E.6}$$

Then, we get the final result

$$d_\lambda = (-Z_1\mathcal{A} + Z_2\mathcal{C})\,\eta_2\,Y_{1,\lambda}(\hat{\eta}_2) + [-(Z_1+Z_2)\mathcal{B} + Z_3\mathcal{D}]\,\eta_1 Y_{1,\lambda}(\hat{\eta}_1)\,, \tag{E.7}$$

where we have used the properties of the Clebsch–Gordan coefficients that appear in the sum of Eq. (E.6), in addition to the identities $Y_{0,0}(\hat{\eta}_1) = Y_{0,0}(\hat{\eta}_2) = 1/\sqrt{4\pi}$. The most general definitions of the mass factors $\mathcal{A}$, $\mathcal{B}$, $\mathcal{C}$ and $\mathcal{D}$ that can be deduced from Eqs. (6.7) and (6.8) are

$$\mathcal{A} = \sqrt{\frac{m_{\rm r} m_2}{M_2 m_1}}\,, \qquad \mathcal{B} = \sqrt{\frac{m_{\rm r} m_3}{M M_2}}\,, \qquad \mathcal{C} = \sqrt{\frac{m_{\rm r} m_1}{M_2 m_2}}\,, \qquad \mathcal{D} = \sqrt{\frac{m_{\rm r} M_2}{M m_3}}\,. \tag{E.8}$$

From these expressions, the coefficients in Eq. (E.7), relative to the dependence of the operator on the Jacobi vectors $\boldsymbol{\eta}_2$ and $\boldsymbol{\eta}_1$, are explicitly

$$-Z_1\mathcal{A} + Z_2\mathcal{C} = -\sqrt{\frac{m_{\rm r}}{M_2}}\left(Z_1\sqrt{\frac{m_2}{m_1}} - Z_2\sqrt{\frac{m_1}{m_2}}\right)\,, \tag{E.9a}$$

$$-(Z_1+Z_2)\,\mathcal{B} + Z_3\mathcal{D} = -(Z_1+Z_2)\sqrt{\frac{m_{\rm r} m_3}{M M_2}} + Z_3\sqrt{\frac{m_{\rm r} M_2}{M m_3}}\,. \tag{E.9b}$$

E.2 The electric quadrupole transition operator

In this Section we will explicitly derive the $E2$ operator written in Eq. (7.4), by starting from the following expression

$$u_\lambda = \sum_{i=1}^{3} Z_i (r_i')^2 Y_{2\lambda}(\hat{r}_i')\,, \tag{E.10}$$

where the vectors $\{\boldsymbol{r}_1', \boldsymbol{r}_2', \boldsymbol{r}_3'\}$ are related to the set of Jacobi vectors $\{\boldsymbol{\eta}_2, \boldsymbol{\eta}_1\}$ through the relations in Eq. (6.8). To this aim we employ Eq. (E.2) with $\ell = 2$ and $m = \lambda$, which leads to the following result

$$\begin{aligned} u_\lambda = {} & \sum_{\lambda'\mu'} \sqrt{\frac{5!(4\pi)}{(2\lambda'+1)!(5-2\lambda')!}}\,\langle 2-\lambda', \lambda-\mu', \lambda', \mu' | 2, \lambda\rangle \\ & \times \left[Z_1(-\mathcal{A})^{2-\lambda'}(-\mathcal{B})^{\lambda'} + Z_2(\mathcal{C})^{2-\lambda'}(-\mathcal{B})^{\lambda'}\right] \\ & \times \eta_2^{2-\lambda'}\,Y_{2-\lambda',\lambda-\mu'}(\hat{\eta}_2)\,\eta_1^{\lambda'}\,Y_{\lambda',\mu'}(\hat{\eta}_1) + Z_3\mathcal{D}^2\,\eta_1^2 Y_{2,\lambda}(\hat{\eta}_1)\,. \end{aligned} \tag{E.11}$$

Starting from the expression above, if we perform the explicit calculations for the values $\lambda' = 0, 1, 2$ and $\mu' = -\lambda', \ldots, \lambda'$, then we obtain

$$\begin{aligned} u_\lambda = {} & \sqrt{4\pi}\left(Z_1\mathcal{A}^2 + Z_2\mathcal{C}^2\right)\eta_2^2\, Y_{2,\lambda}(\hat{\eta}_2)\, Y_{0,0}(\hat{\eta}_1) + Z_3\mathcal{D}^2\,\eta_1^2 Y_{2,\lambda}(\hat{\eta}_1) \\ & + \sqrt{\frac{5!(4\pi)}{3!3!}} \sum_{\mu'=0,\pm1} \langle 1, \lambda-\mu', 1, \mu' | 2, \lambda\rangle \left(Z_1\mathcal{A}\mathcal{B} - Z_2\mathcal{C}\mathcal{B}\right)\eta_2\, Y_{1,\lambda-\mu'}(\hat{\eta}_2)\,\eta_1\, Y_{1,\mu'}(\hat{\eta}_1) \\ & + \sqrt{4\pi} \sum_{\mu'=0,\pm1,\pm2} \langle 0, \lambda-\mu', 2, \mu' | 2, \lambda\rangle \left[\left(Z_1 + Z_2\right)\mathcal{B}^2\right] Y_{0,\lambda-\mu'}(\hat{\eta}_2)\,\eta_1^2\, Y_{2,\mu'}(\hat{\eta}_1)\,, \end{aligned} \tag{E.12}$$

where the mass coefficients $\mathcal{A}$, $\mathcal{B}$, $\mathcal{C}$ and $\mathcal{D}$ are defined in Eq. (E.8), and the symbols $\langle 1, \lambda-\mu', 1, \mu' | 2, \lambda\rangle$ and $\langle 0, \lambda-\mu', 2, \mu' | 2, \lambda\rangle$ denote the Clebsch–Gordan coefficients. By exploiting the properties of the latter, and by using $Y_{0,0}(\hat{\eta}_1) = Y_{0,0}(\hat{\eta}_2) = 1/\sqrt{4\pi}$ we get

$$\begin{aligned} u_\lambda = {} & \left(Z_1\mathcal{A}^2 + Z_2\mathcal{C}^2\right)\eta_2^2\, Y_{2,\lambda}(\hat{\eta}_2) + \left[\left(Z_1 + Z_2\right)\mathcal{B}^2 + Z_3\mathcal{D}^2\right]\eta_1^2\, Y_{2,\lambda}(\hat{\eta}_1) \\ & + \sqrt{\frac{10(4\pi)}{3}}\left(Z_1\mathcal{A}\mathcal{B} - Z_2\mathcal{C}\mathcal{B}\right)\eta_2\eta_1 \sum_{\mu'=0,\pm1} \langle 1, \lambda-\mu', 1, \mu' | 2, \lambda\rangle\, Y_{1,\lambda-\mu'}(\hat{\eta}_2) Y_{1,\mu'}(\hat{\eta}_1)\,, \end{aligned} \tag{E.13}$$

whose coefficients can be calculated explicitly by means of the definitions in Eq. (E.8), obtaining

$$Z_1\mathcal{A}^2 + Z_2\mathcal{C}^2 = \frac{m_\mathrm{r}}{M_2}\left(Z_1\frac{m_2}{m_1} + Z_2\frac{m_1}{m_2}\right)\,, \tag{E.14a}$$

$$\left(Z_1 + Z_2\right)\mathcal{B}^2 + Z_3\mathcal{D}^2 = \left(Z_1 + Z_2\right)\frac{m_\mathrm{r} m_3}{M_2 M} + Z_3\frac{m_\mathrm{r} M_2}{M m_3}\,, \tag{E.14b}$$

$$Z_1\mathcal{A}\mathcal{B} - Z_2\mathcal{C}\mathcal{B} = \frac{m_\mathrm{r}}{M_2}\sqrt{\frac{m_3}{M}}\frac{Z_1 m_2 - Z_2 m_1}{\sqrt{m_1 m_2}}\,, \tag{E.14c}$$

where M is the total mass of the system and M_2 is defined as $M_2 = m_1 + m_2$.

Appendix F

Detailed calculation of some matrix elements

In this Appendix we calculate explicitly the integrals in Eqs. (6.30) and (7.10), where the operators $\hat{d}_\lambda$ and $\hat{u}_\lambda$, in configuration space, are constructed as a combination of terms proportional to $\eta_1\, Y_{1\lambda}(\hat{\eta}_1)$ and $\eta_2\, Y_{1\lambda}(\hat{\eta}_2)$ or $\eta_1^2\, Y_{2\lambda}(\hat{\eta}_1)$ and $\eta_2^2\, Y_{2\lambda}(\hat{\eta}_2)$. In the most general case, the basis functions $\mathcal{Y}_\mu^{JM\pi}(\Omega_2^{(\rho)})$ are [see Eq. (5.55)]

$$\mathcal{Y}^{JM\pi}_{[K][S][T]KLST}(\Omega_N^{(\rho)}) = \left[\mathcal{Y}^{KL}_{[K]}(\Omega_N^{(\rho)})\chi^{S}_{[S]}\right]_{JM} \xi^{TM_T}_{[T]}\,, \tag{F.1}$$

with the HH term defined as in Eq. (5.47), which we rewrite here as

$$\mathcal{Y}^{KLM_L}_{[K]}(\Omega_N^{(\rho)}) = \left[\{L_{N-1}\},\ell_N\right]_{LM_L} {}^N\mathcal{P}^{\ell_N,K_{N-1}}_{n_N}(\varphi_N) \prod_{j=2}^{N-1} {}^j\mathcal{P}^{\ell_j,K_{j-1}}_{n_j}(\varphi_j)\,. \tag{F.2}$$

The expression of the basis functions that we will use is the following:

$$\left[\left[\{L_{N-1}\},\ell_N\right]_L\{S\}\right]_{JM} {}^N\mathcal{P}^{K_{N-1},\ell_N}_{n_N}(\varphi_N) \prod_{j=2}^{N-1} {}^j\mathcal{P}^{K_{j-1},\ell_j}_{n_j}(\varphi_j)\,. \tag{F.3}$$

Basically, since $\eta_2 = \rho\sin\varphi_2$ and $\eta_1 = \rho\cos\varphi_2$, the whole calculation is reduced to the computation of the following matrix elements

$$\langle m', J'M'|\rho^a\,(\sin\varphi_2)^b(\cos\varphi_2)^c\, Y_{\alpha\lambda}(\hat{\eta}_2)|m, JM\rangle\ , \tag{F.4}$$

$$\langle m', J'M'|\rho^a\,(\sin\varphi_2)^b(\cos\varphi_2)^c\, Y_{\alpha\lambda}(\hat{\eta}_1)|m, JM\rangle\ . \tag{F.5}$$

First we focus on the calculation of the integral (F.4) in configuration space. The derivation that follows is valid for a generic value of $N \equiv A-1$. By using the volume element defined in Eqs. (5.16) and (5.17), the integral easily separates into

a hyperradial, a hyperspherical and an angular part

$$\langle m', J'M'|\rho^a\,(\sin\varphi_N)^b(\cos\varphi_N)^c\,Y_{\alpha\lambda}(\hat{\eta}_N)|m, JM\rangle =$$

$$= \int d\rho\,\rho^{3N-1+a} g^*_{m'K'}(\rho) g_{mK}(\rho) \tag{F.6a}$$

$$\times\,\delta_{\{n'_{N-1}\},\{n_{N-1}\}} \int d\varphi_N\,\mathcal{N}^{K'_N;\ell'_N,K'_{N-1}}_{n'_N} P^{(\ell'_N+\frac{1}{2},K'_{N-1}+\frac{3N-5}{2})}_{n'_N}(\cos 2\varphi_N)$$

$$\times\,(\sin\varphi_N)^{\ell'_N+\ell_N+2+b}(\cos\varphi_N)^{K'_{N-1}+K_{N-1}+3N-4+c}$$

$$\times\,\mathcal{N}^{K_N;\ell_N,K_{N-1}}_{n_N} P^{(\ell_N+\frac{1}{2},K_{N-1}+\frac{3N-5}{2})}_{n_N}(\cos 2\varphi_N) \tag{F.6b}$$

$$\times\,\left\langle J'M' \,\middle|\, Y_{\alpha\lambda}(\hat{\eta}_N) \,\middle|\, JM \right\rangle . \tag{F.6c}$$

Notice that in the equation above we have already performed the hyperspherical integrals in the variables $d\varphi_j$, with $j = 2, \ldots, N-1$, giving rise to the delta functions. In order to calculate the last angular integral (F.6c), which is explicitly

$$\begin{aligned}&\left\langle J'M' \,\middle|\, Y_{\alpha\lambda}(\hat{\eta}_N) \,\middle|\, JM \right\rangle \\ &\equiv \left\langle \left[\{L'_{N-1}\}, \ell'_N\right]_{L'}\{S'\}\right]_{J'M'} \middle| Y_{\alpha\lambda}(\hat{\eta}_N) \middle| \left[\left[\{L_{N-1}\}, \ell_N\right]_L\{S\}\right]_{JM}\right\rangle ,\end{aligned} \tag{F.7}$$

the basis must be manipulated further, specifically as

$$\left|\left[\left[\{L_{N-1}\}, \ell_N\right]_L\{S\}\right]_{JM}\right\rangle \to \left|\left[\ell_N\,[\{L_{N-1}\}, \{S\}]_j\right]_{JM}\right\rangle . \tag{F.8}$$

In order to achieve this, as a first step, we bring the single orbital angular momentum ℓ_N to the first position, and this operation gives rise to a phase factor $(-1)^{L_{N-1}+\ell_N-L}$. Then, we perform the L–S recoupling by making use of the general relation [115]

$$\left|\left[[j_1, j_2]_{j_{12}} j_3\right]_{JM}\right\rangle = (-1)^{j_1+j_2+j_3+j} \sum_{j_{23}} \widehat{j_{12}}\,\widehat{j_{23}} \begin{Bmatrix} j_1 & j_2 & j_{12} \\ j_3 & J & j_{23} \end{Bmatrix} \left|\left[j_1 [j_2, j_3]_{j_{23}}\right]_{JM}\right\rangle , \tag{F.9}$$

obtaining the following result

$$\begin{aligned}\left\langle J'M' \,\middle|\, Y_{\alpha\lambda}(\hat{\eta}_N) \,\middle|\, JM \right\rangle &= (-1)^{2L'_{N-1}+2\ell'_N-L'_N+S'+J'}(-1)^{2L_{N-1}+2\ell_N-L_N+S+J} \\ &\times \sum_{j'j} \widehat{L'_N}\,\widehat{j'}\,\widehat{L_N}\,\widehat{j} \begin{Bmatrix} \ell'_N & L'_{N-1} & L'_N \\ S' & J' & j' \end{Bmatrix} \begin{Bmatrix} \ell_N & L_{N-1} & L_N \\ S & J & j \end{Bmatrix} \\ &\times \left\langle \left[\ell'_N\,[\{L'_{N-1}\}, \{S'\}]_{j'}\right]_{J'M'} \middle| Y_{\alpha\lambda}(\hat{\eta}_N) \middle| \left[\ell_N\,[\{L_{N-1}\}, \{S\}]_j\right]_{JM}\right\rangle ,\end{aligned} \tag{F.10}$$

where the curl brackets denote the Wigner $6j$ symbols. Here and henceforth, the hat symbol on a generic quantum number $\widehat{J}$ stands for the expression $\widehat{J} \equiv \sqrt{2J+1}$. Now we are allowed to employ the following expression [115]

$$\begin{aligned}\left\langle [j'_1, j'_2]_{J'M'} \middle| \hat{P}_{\alpha\beta}(1) \middle| [j_1, j_2]_{JM}\right\rangle &= (-1)^{J'-M'} \begin{pmatrix} J' & \alpha & J \\ -M' & \beta & M \end{pmatrix} \delta_{j'_2 j_2}(-1)^{j'_1+j'_2+J+\alpha} \\ &\times \widehat{J'}\,\widehat{J} \begin{Bmatrix} j_1 & j'_2 & J \\ J' & \alpha & j'_1 \end{Bmatrix} \left\langle j'_1 \middle\| \hat{P}_\alpha(1) \middle\| j_1 \right\rangle ,\end{aligned} \tag{F.11}$$

which is valid whenever a generic operator $\hat{P}_{\alpha\beta}(1)$ acts only on the subsystem 1. By rewriting Eq. (F.10) as

$$\langle J'M' \,|\, Y_{\alpha\lambda}(\hat{\eta}_N) \,|\, JM \rangle = (-1)^{J'-M'} \begin{pmatrix} J' & \alpha & J \\ -M' & \lambda & M \end{pmatrix} \langle J' \,\|\, Y_\alpha(\hat{\eta}_N) \,\|\, J \rangle \ , \tag{F.12}$$

the complete expression of the reduced matrix elements results to be

$$\begin{aligned} \langle J' \,\|\, Y_\alpha(\hat{\eta}_N) \,\|\, J \rangle &= (-1)^{2L'_{N-1}+2\ell'_N-L'_N+S'+J'} (-1)^{2L_{N-1}+2\ell_N-L_N+S+J} \\ &\times \sum_{j'j} \widehat{L'_N}\,\hat{j}'\,\widehat{L_N}\,\hat{j} \begin{Bmatrix} \ell'_N & L'_{N-1} & L'_N \\ S' & J' & j' \end{Bmatrix} \begin{Bmatrix} \ell_N & L_{N-1} & L_N \\ S & J & j \end{Bmatrix} \\ &\times \delta_{j'j}\,\delta_{\{L'_{N-1}\},\{L_{N-1}\}}\,\delta_{\{S'\},\{S\}}\,(-1)^{J+\ell'_N+j-\alpha} \\ &\times \hat{J}'\,\hat{J} \begin{Bmatrix} \ell_N & j & J \\ J' & \alpha & \ell'_N \end{Bmatrix} \langle \ell'_N \| Y_\alpha(\hat{\eta}_N) \| \ell_N \rangle \ . \end{aligned} \tag{F.13}$$

By exploiting the delta function $\delta_{j'j}$ the summations over j and j' simplify, and one can apply the following general property of the $6j$ symbols [115]

$$\begin{aligned} \sum_x (-1)^{a+b+c+d+e+f+p+q+r+x} (2x+1) \begin{Bmatrix} a & b & x \\ c & d & p \end{Bmatrix} \begin{Bmatrix} c & d & x \\ e & f & q \end{Bmatrix} \begin{Bmatrix} e & f & x \\ b & a & r \end{Bmatrix} \\ = \begin{Bmatrix} p & q & r \\ e & a & d \end{Bmatrix} \begin{Bmatrix} p & q & r \\ f & b & c \end{Bmatrix} , \end{aligned} \tag{F.14}$$

obtaining the final result

$$\begin{aligned} \langle J' \,\|\, Y_\alpha(\hat{\eta}_N) \,\|\, J \rangle &= \delta_{\{L'_{N-1}\},\{L_{N-1}\}}\,\delta_{\{S'\},\{S\}}\,(-1)^{L_{N-1}+\ell_N+S+J+\alpha+1} \\ &\times \widehat{L'_N}\,\hat{J}'\,\widehat{L_N}\,\hat{J} \begin{Bmatrix} \ell'_N & L'_N & L_{N-1} \\ L_N & \ell_N & \alpha \end{Bmatrix} \begin{Bmatrix} L'_N & J' & S \\ J & L_N & \alpha \end{Bmatrix} \\ &\times \langle \ell'_N \| Y_\alpha(\hat{\eta}_N) \| \ell_N \rangle \ . \end{aligned} \tag{F.15}$$

The reduced matrix element of the spherical harmonics $Y_{\alpha\lambda}(\hat{\eta}_N)$ is explicitly [115]

$$\langle \ell'_N \| Y_\alpha(\hat{\eta}_N) \| \ell_N \rangle = (-1)^{\ell'_N}\,\widehat{\ell'_N}\,\frac{\widehat{\alpha}}{\sqrt{4\pi}}\,\widehat{\ell_N} \begin{pmatrix} \ell'_N & \alpha & \ell_N \\ 0 & 0 & 0 \end{pmatrix} . \tag{F.16}$$

For the computation of the integral in Eq. (F.5) in configuration space one can follow a very similar procedure. The whole integral factorizes again into a hyperradial, a hyperspherical and an angular term

$$\langle m', J'M' | \rho^a\,(\sin\varphi_2)^b (\cos\varphi_2)^c\, Y_{\alpha\lambda}(\hat{\eta}_1) | m, JM \rangle =$$

$$= \int d\rho\, \rho^{5+a} g^*_{m'K'}(\rho) g_{mK}(\rho) \tag{F.17a}$$

$$\times \int d\varphi_2\, \mathcal{N}^{K'_2;\ell'_2,K'_1}_{n'_2} P^{(\ell'_2+\frac{1}{2},K'_1+\frac{1}{2})}_{n'_2}(\cos 2\varphi_2)$$

$$\times (\sin\varphi_2)^{\ell'_2+\ell_2+2+b} (\cos\varphi_2)^{K'_1+K_1+2+c} \mathcal{N}^{K_2;\ell_2,K_1}_{n_2} P^{(\ell_2+\frac{1}{2},K_1+\frac{1}{2})}_{n_2}(\cos 2\varphi_2) \tag{F.17b}$$

$$\times \langle J'M' \,|\, Y_{\alpha\lambda}(\hat{\eta}_1) \,|\, JM \rangle \ , \tag{F.17c}$$

with $K_1 \equiv \ell_1$. The angular integral in (F.17c) is now explicitly

$$\langle J'M' \,|\, Y_{\alpha\lambda}(\hat{\eta}_1) \,|\, JM \rangle \equiv \left\langle \left[[\ell_1', \ell_2']_{L'} \{S'\} \right]_{J'M'} \middle| Y_{\alpha\lambda}(\hat{\eta}_1) \middle| \left[[\ell_1, \ell_2]_L \{S\} \right]_{JM} \right\rangle . \tag{F.18}$$

By applying the recoupling relation in Eq. (F.9), we obtain

$$\begin{aligned} \langle J'M' \,|\, Y_{\alpha\lambda}(\hat{\eta}_1) \,|\, JM \rangle = (-1)^{\ell_1'+\ell_2'+S'+J'} (-1)^{\ell_1+\ell_2+S+J} \\ \times \sum_{j'j} \widehat{L_2'}\, \hat{j}'\, \widehat{L_2}\, \hat{j} \begin{Bmatrix} \ell_1' & \ell_2' & L_2' \\ S' & J' & j' \end{Bmatrix} \begin{Bmatrix} \ell_1 & \ell_2 & L_2 \\ S & J & j \end{Bmatrix} \\ \times \left\langle \left[\ell_1' [\ell_2', \{S'\}]_{j'} \right]_{J'M'} \middle| Y_{\alpha\lambda}(\hat{\eta}_1) \middle| \left[\ell_1 [\ell_2, \{S\}]_j \right]_{JM} \right\rangle . \end{aligned} \tag{F.19}$$

Since the spherical harmonic $Y_{\alpha\lambda}(\hat{\eta}_1)$ only acts on the subsystem 1, Eq. (F.11) yields to the result

$$\langle J'M' \,|\, Y_{\alpha\lambda}(\hat{\eta}_1) \,|\, JM \rangle = (-1)^{J'-M'} \begin{pmatrix} J' & \alpha & J \\ -M' & \lambda & M \end{pmatrix} \langle J' \,\|\, Y_\alpha(\hat{\eta}_1) \,\|\, J \rangle , \tag{F.20}$$

where the explicit expression of the reduced matrix element is

$$\begin{aligned} \langle J' \,\|\, Y_\alpha(\hat{\eta}_1) \,\|\, J \rangle = (-1)^{\ell_1'+\ell_2'+S'+J'} (-1)^{\ell_1+\ell_2+S+J} \\ \times \sum_{j'j} \widehat{L_2'}\, \hat{j}'\, \widehat{L_2}\, \hat{j} \begin{Bmatrix} \ell_1' & \ell_2' & L_2' \\ S' & J' & j' \end{Bmatrix} \begin{Bmatrix} \ell_1 & \ell_2 & L_2 \\ S & J & j \end{Bmatrix} \\ \times \delta_{j'j}\, \delta_{\ell_2',\ell_2}\, \delta_{\{S'\},\{S\}}\, (-1)^{J+\ell_1'+j-\alpha} \\ \times \hat{J}'\, \hat{J} \begin{Bmatrix} \ell_1 & j & J \\ J' & \alpha & \ell_1' \end{Bmatrix} \langle \ell_1' \| Y_\alpha(\hat{\eta}_1) \| \ell_1 \rangle . \end{aligned} \tag{F.21}$$

Finally, by using Eq. (F.14) we get the final result

$$\begin{aligned} \langle J' \,\|\, Y_\alpha(\hat{\eta}_1) \,\|\, J \rangle = \delta_{\ell_2',\ell_2}\, \delta_{\{S'\},\{S\}}\, (-1)^{L_2'+\ell_1'+L_2+\ell_2+S+J+\alpha+1} \\ \times \widehat{L_2'}\, \hat{J}'\, \widehat{L_2}\, \hat{J} \begin{Bmatrix} \ell_1' & L_2' & \ell_2 \\ L_2 & \ell_1 & \alpha \end{Bmatrix} \begin{Bmatrix} L_2' & J' & S \\ J & L_2 & a \end{Bmatrix} \\ \times \langle \ell_1' \| Y_\alpha(\hat{\eta}_1) \| \ell_1 \rangle , \end{aligned} \tag{F.22}$$

where the reduced matrix element is defined as [115]

$$\langle \ell_1' \| Y_\alpha(\hat{\eta}_1) \| \ell_1 \rangle = (-1)^{\ell_1'}\, \hat{\ell}_1'\, \frac{\hat{\alpha}}{\sqrt{4\pi}}\, \hat{\ell}_1 \begin{pmatrix} \ell_1' & \alpha & \ell_1 \\ 0 & 0 & 0 \end{pmatrix} . \tag{F.23}$$

Appendix G

LIT calculation: test

The dipole matrix elements that enter in the computation of the LIT (6.17) have been calculated in coordinate space following Eq. (6.30). In performing the integral, instead of using the basis functions $g_{mK}(\rho)$ directly, we have applied the procedure discussed in Section 6.1.2, in which the functions $G^{0,l}_{\mu}(\rho)$ are computed by following Eq. (6.28). This has led to all the results shown in Section 6.2. As already mentioned in Section 5.4, we could have followed another strategy. If one diagonalizes the Hamiltonian matrix represented on a basis in momentum space as the one defined in Eq. (5.172), which uses the functions $g_{mK}(Q)$, then it is allowed to use in coordinate space the basis (5.158) defined in terms of $f_m(\rho)$. In this way, the dipole matrix elements $\langle \Psi_l | \hat{d}_\lambda | \Psi_0 \rangle$ can be calculated as follows

$$\begin{aligned} \langle \Psi_l | \hat{d}_\lambda | \Psi_0 \rangle = \int d\Omega_2^{(\rho)}\, d\rho\, \rho^5 \Big[\sum_{m'\mu'} c^{l}_{m'\mu'}\, f_m(\rho)\, \mathcal{Y}^{JM\pi}_{\mu'}(\Omega_2^{(\rho)}) \Big]^\dagger \\ \times\, d_\lambda(\rho, \Omega_2) \Big[\sum_{m\mu} c^{0}_{m\mu}\, f_m(\rho)\, \mathcal{Y}^{JM\pi}_{\mu}(\Omega_2^{(\rho)}) \Big] , \end{aligned} \tag{G.1}$$

where the basis functions $f_m(\rho)$ are constructed by means of a Laguerre polynomials basis. A Fortran code that makes use of the functions $g_{mK}(Q)$ to find the eigenvalues and eigenvectors of the Hamiltonian has started to be developed in Ref. [110]. There these functions are calculated by means of a Fortran package [114], and the limiting value 24 was imposed on the index m to avoid instabilities in calculating $g_{mK}(Q)$. As already mentioned in Section 6.1.2, by doing calculations in quadrupole precision, this limiting value can be increased. Therefore, we have applied some modifications to the original Fortran code in order to be able to run with $m^{\max} = 30$, as well as an OpenMP parallelization to reduce the computational time. We have also introduced the three–body force, by implementing the integrals necessary to calculate the relative matrix elements, as in Section 5.4.2. Since, within this framework, the dipole matrix elements $\langle \Psi_l | \hat{d}_\lambda | \Psi_0 \rangle$ can be calculated as in Eq. (G.1), this has provided a way to test the results presented in Section 6.2

Regarding the Fortran code that works with the $g_{mK}(Q)$ basis, by choosing the parameters in Eq. (6.44) as $a = b = 0.6$ and $c = 0.8$, the typical values needed to perform convergent bound–state calculations are $\beta = 1.4\,\mathrm{fm}^{-1}$, $N_Q/N_\varphi = 550/500$, $N_L = 30$ and $K^{\max} = 25$. We have then implemented the computation of the dipole matrix elements as in (G.1). As anticipated, in order to perform the test,

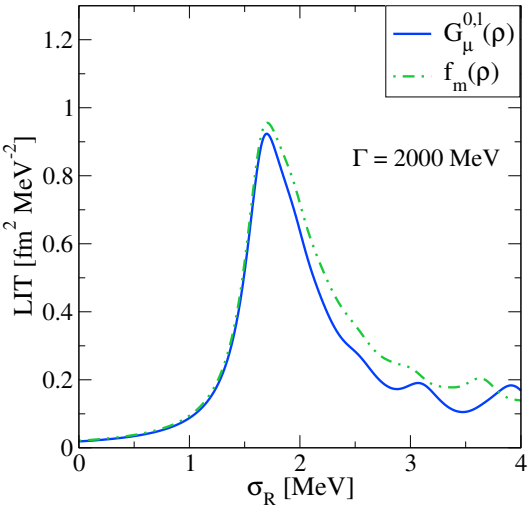

Figure G.1: LIT computed by using Eq. (6.30) and the functions $G_\mu^{0,l}(\rho)$ in (6.28) (solid blue) or Eq. (G.1) with $f_m(\rho)$ (dot–dashed green line) to evaluate the dipole matrix elements $\langle\Psi_l|\hat{d}_\lambda|\Psi_0\rangle$.

we must compare these results with those obtained by calculating $\langle\Psi_l|\hat{d}_\lambda|\Psi_0\rangle$ with the functions $G_\mu^{0,l}(\rho)$ of Eq. (6.28). In both cases, we have employed the interaction potential in Eq. (6.54) by setting the parameters to the same values: $\Lambda_3 = 300\,\text{MeV}$, $\Gamma = 2000\,\text{MeV}$, as well as the values of the strength of the three–body potentials (see 6.22b). By focussing on the $1/2^+$ resonance, the outcome of this test is shown in Fig. G.1. The results are in agreement, since the two calculated LIT have the same shape and almost the same strength, with a slight difference in the height of the tail. This could be ascribed to the different rate of convergence, since two different set of bases have been used.

Within this framework, we have also carried out two other types of checks. The first concerns the moment of order zero relative to the response function, which is formally defined as

$$m_0 = \int d\omega R(\omega)\,. \tag{G.2}$$

By using the definition of the response function (6.16), it can be demonstrated that m_0 can be calculated with the following expressions

$$m_0 = \sum_{l=0}^{N_\Lambda} \left|\langle\Psi_l|\hat{d}_\lambda|\Psi_0\rangle\right|^2 = \langle\Psi_0|\hat{d}_\lambda^\dagger\hat{d}_\lambda|\Psi_0\rangle\ , \tag{G.3}$$

where in the second equivalence we have exploited the completeness of the basis $|\Psi_l\rangle$. We have that $\langle\Psi_0|\hat{d}_\lambda^\dagger\hat{d}_\lambda|\Psi_0\rangle|_{f_m(\rho)} = 0.18663284\,\text{fm}^2$, while m_0 calculated from the summation over l of the dipole matrix elements $\langle\Psi_l|\hat{d}_\lambda|\Psi_0\rangle|_{f_m(\rho)}$ is $0.18663284\,\text{fm}^2$, which is in full agreement. By using $\langle\Psi_l|\hat{d}_\lambda|\Psi_0\rangle|_{G_\mu^{0,l}(\rho)}$ the summation over l gives $0.16648564\,\text{fm}^2$. However, this smaller value is consistent with the results shown in Fig. G.1.

As a second check, we have also exploited the behaviour of the LIT in the limit $\sigma_R \to \infty$ as follows

$$L(\sigma_R, \sigma_I) \to \int d\omega \, \frac{R(\omega)}{\sigma_R^2} \,, \tag{G.4}$$

leading to the relation

$$\sigma_R^2 \, L(\sigma_R, \sigma_I) \to m_0 \,. \tag{G.5}$$

With σ_I fixed to 0.2 MeV, we have evaluated the expression above separately for the LIT calculated with the functions $G_\mu^{0,l}(\rho)$ and $f_m(\rho)$, and we have collected the results in Tab. G.1. For $\sigma_R = 10^8$ MeV both calculations are in full agreement with the relative m_0 with a precision at the fifth digit.

σ_R	$\sigma_R^2 \, L(\sigma_R)\big\vert_{G_\mu^{0,l}(\rho)}$	$\sigma_R^2 \, L(\sigma_R)\big\vert_{f_m(\rho)}$
10^1	5.1551628	9.4621599
10^2	1.0312183	6.7717493
10^3	0.15610013	0.42814407
10^4	0.19039451	0.25308260
10^5	0.16804176	0.18822082
10^6	0.16663583	0.18678598
10^7	0.16650061	0.18664810
10^8	0.16648714	0.18663436
10^9	0.16648579	0.18663299
10^{10}	0.16648566	0.18663285

Table G.1: Evaluation of the expression $\sigma_R^2 \, L(\sigma_R, \sigma_I)$ (fm^2) for increasing σ_R (MeV) by using the functions $G_\mu^{0,l}(\rho)$ or $f_m(\rho)$ to calculate the dipole matrix elements in the LIT $L(\sigma_R, \sigma_I)$. σ_I is fixed at 0.2 MeV. More details can be found in the text.

Bibliography

[1] A. Aprahamian, K. Langanke, and M. Wiescher, "Nuclear structure aspects in nuclear astrophysics", Progress in Particle and Nuclear Physics **54**, 535–613 (2005) DOI: 10.1016/j.ppnp.2004.09.002.

[2] H. Oberhummer, A. Csótó, and H. Schlattl, "Bridging the mass gaps at $A = 5$ and $A = 8$ in nucleosynthesis", Nuclear Physics A **689**, European Few-Body Problems in Physics, 269–279 (2001) DOI: 10.1016/S0375-9474(01)00841-7.

[3] K. Sumiyoshi, H. Utsunomiya, S. Goko, and T. Kajino, "Astrophysical reaction rate for $\alpha(\alpha n, \gamma)^9$Be by photodisintegration", Nuclear Physics A **709**, 467–486 (2002) DOI: 10.1016/S0375-9474(02)01058-8.

[4] T. Sasaqui, T. Kajino, G. J. Mathews, K. Otsuki, and T. Nakamura, "Sensitivity of r–process nucleosynthesis to light–element nuclear reactions", The Astrophysical Journal **634**, 1173 (2005) DOI: 10.1086/497061.

[5] C. W. Arnold, T. B. Clegg, C. Iliadis, H. J. Karwowski, G. C. Rich, J. R. Tompkins, and C. R. Howell, "Cross–section measurement of ^{9}Be$(\gamma, n)^8$Be and implications for $\alpha + \alpha + n \rightarrow {}^9$Be in the r process", Phys. Rev. C **85**, 044605 (2012) DOI: 10.1103/PhysRevC.85.044605.

[6] M. Fujishiro, T. Tabata, K. Okamoto, and T. Tsujimoto, "Cross section of the reaction ^{9}Be(γ, n) near threshold", Canadian Journal of Physics **60**, 1672–1677 (1982) DOI: 10.1139/p82-224.

[7] H. Utsunomiya, Y. Yonezawa, H. Akimune, T. Yamagata, M. Ohta, M. Fujishiro, H. Toyokawa, and H. Ohgaki, "Photodisintegration of ^{9}Be with laser–induced Compton backscattered γ rays", Phys. Rev. C **63**, 018801 (2000) DOI: 10.1103/PhysRevC.63.018801.

[8] O. Burda, P. von Neumann–Cosel, A. Richter, C. Forssén, and B. A. Brown, "Resonance parameters of the first $1/2^+$ state in ^{9}Be and astrophysical implications", Phys. Rev. C **82**, 015808 (2010) DOI: 10.1103/PhysRevC.82.015808.

[9] H. Utsunomiya, S. Katayama, I. Gheorghe, S. Imai, H. Yamaguchi, D. Kahl, Y. Sakaguchi, T. Shima, K. Takahisa, and S. Miyamoto, "Photodisintegration of ^{9}Be through the $1/2^+$ state and cluster dipole resonance", Phys. Rev. C **92**, 064323 (2015) DOI: 10.1103/PhysRevC.92.064323.

[10] A. M. Goryachev, G. N. Zalesnyy, and I. V. Pozdnev, Izv. Ross. Akad. Nauk, Ser. Fiz. **56**, 159 (1992).

[11] I. Lombardo and D. Dell'Aquila, "Clusters in light nuclei: history and recent developments", La Rivista del Nuovo Cimento **46**, 521–618 (2023) DOI: 10.1007/s40766-023-00047-4.

[12] M. Freer, H. Horiuchi, Y. Kanada–En'yo, D. Lee, and U.-G. Meißner, "Microscopic clustering in light nuclei", Rev. Mod. Phys. **90**, 035004 (2018) DOI: 10.1103/RevModPhys.90.035004.

[13] S. Ali and A. Bodmer, "Phenomenological α–α potentials", Nuclear Physics **80**, 99–112 (1966) DOI: 10.1016/0029-5582(66)90829-7.

[14] K. Ikeda, N. Takigawa, and H. Horiuchi, "The systematic structure–change into the molecule–like structures in the self–conjugate $4n$ nuclei", Progress of Theoretical Physics Supplement **E68**, 464–475 (1968) DOI: 10.1143/PTPS.E68.464.

[15] M. Freer and H. Fynbo, "The Hoyle state in ^{12}C", Progress in Particle and Nuclear Physics **78**, 1–23 (2014) DOI: 10.1016/j.ppnp.2014.06.001.

[16] W. von Oertzen, "Two–center molecular states in ^{9}B, ^{9}Be, ^{10}Be, and ^{10}B", Zeitschrift für Physik A Hadrons and Nuclei **354**, 37–43 (1996) DOI: 10.1007/s002180050010.

[17] V. Efros, H. Oberhummer, A. Pushkin, and I. Thompson, "Low–energy photodisintegration of ^{9}Be and $\alpha + \alpha + \alpha \rightarrow {}^{9}\mathrm{Be} + \gamma$ reactions at astrophysical conditions", The European Physical Journal A - Hadrons and Nuclei **1**, 447–453 (1998) DOI: 10.1007/s100500050079.

[18] J. Casal, M. Rodríguez–Gallardo, J. M. Arias, and I. J. Thompson, "Astrophysical reaction rate for ^{9}Be formation within a three–body approach", Phys. Rev. C **90**, 044304 (2014) DOI: 10.1103/PhysRevC.90.044304.

[19] Y. Kikuchi, M. Odsuren, T. Myo, and K. Katō, "Photodisintegration cross section of ^{9}Be up to 16 MeV in the $\alpha+\alpha+n$ three–body model", Phys. Rev. C **93**, 054605 (2016) DOI: 10.1103/PhysRevC.93.054605.

[20] H.-W. Hammer, C. Ji, and D. R. Phillips, "Effective field theory description of halo nuclei", Journal of Physics G: Nuclear and Particle Physics **44**, 103002 (2017) DOI: 10.1088/1361-6471/aa83db.

[21] S. Weinberg, "Nuclear forces from chiral lagrangians", Physics Letters B **251**, 288–292 (1990) DOI: 10.1016/0370-2693(90)90938-3.

[22] H.-W. Hammer, S. König, and U. van Kolck, "Nuclear effective field theory: status and perspectives", Rev. Mod. Phys. **92**, 025004 (2020) DOI: 10.1103/RevModPhys.92.025004.

[23] C. Bertulani, H.-W. Hammer, and U. van Kolck, "Effective field theory for halo nuclei: shallow p–wave states", Nuclear Physics A **712**, 37–58 (2002) DOI: 10.1016/S0375-9474(02)01270-8.

[24] P. Bedaque, H.-W. Hammer, and U. van Kolck, "Narrow resonances in effective field theory", Physics Letters B **569**, 159–167 (2003) DOI: 10.1016/j.physletb.2003.07.049.

[25] R. Higa, H.-W. Hammer, and U. van Kolck, "$\alpha\alpha$ Scattering in halo effective field theory", Nuclear Physics A **809**, 171–188 (2008) DOI: 10.1016/j.nuclphysa.2008.06.003.

[26] S. Bacca and S. Pastore, "Electromagnetic reactions on light nuclei", Journal of Physics G: Nuclear and Particle Physics **41**, 123002 (2014) DOI: 10.1088/0954-3899/41/12/123002.

[27] V. D. Efros, W. Leidemann, G. Orlandini, and N. Barnea, "The Lorentz Integral Transform (LIT) method and its applications to perturbation–induced reactions", Journal of Physics G: Nuclear and Particle Physics **34**, R459 (2007) DOI: 10.1088/0954-3899/34/12/R02.

[28] S. Deflorian, N. Barnea, W. Leidemann, and G. Orlandini, "Nonsymmetrized Hyperspherical Harmonics with realistic NN potentials", Few-Body Systems **54**, 1879–1887 (2013) DOI: 10.1007/s00601-013-0717-y.

[29] E. Filandri, "Effective field theory description of α cluster nuclei: the ^{9}Be ground state and ^{9}Be photodisintegration", PhD thesis (Università di Trento, 2022), DOI: https://dx.doi.org/10.15168/11572_338316.

[30] H. Arenhövel, "Electroweak processes in few–nucleon systems", Few–Body Systems **26**, 43–98 (1999) DOI: 10.1007/s006010050105.

[31] A. J. F. Siegert, "Note on the interaction between nuclei and electromagnetic radiation", Phys. Rev. **52**, 787–789 (1937) DOI: 10.1103/PhysRev.52.787.

[32] F. Hoyle, "On nuclear reactions occuring in very hot stars. I. The synthesis of elements from Carbon to Nickel.", Astrophysical Journal Supplement **1**, 121 (1954).

[33] H. Suno, Y. Suzuki, and P. Descouvemont, "Precise calculation of the triple–α reaction rates using the transmission–free complex absorbing potential method", Phys. Rev. C **94**, 054607 (2016) DOI: 10.1103/PhysRevC.94.054607.

[34] C. Angulo, M. Arnould, M. Rayet, P. Descouvemont, D. Baye, C. Leclercq-Willain, A. Coc, S. Barhoumi, P. Aguer, C. Rolfs, R. Kunz, J. Hammer, A. Mayer, T. Paradellis, S. Kossionides, C. Chronidou, K. Spyrou, S. Degl'Innocenti, G. Fiorentini, B. Ricci, S. Zavatarelli, C. Providencia, H. Wolters, J. Soares, C. Grama, J. Rahighi, A. Shotter, and M. Lamehi Rachti, "A compilation of charged–particle induced thermonuclear reaction rates", Nuclear Physics A **656**, 3–183 (1999) DOI: 10.1016/S0375-9474(99)00030-5.

[35] K. Ogata, M. Kan, and M. Kamimura, "Quantum three–body calculation of the nonresonant triple–α reaction rate at low emperatures", Progress of Theoretical Physics **122**, 1055–1064 (2009) DOI: 10.1143/PTP.122.1055.

[36] E. Garrido, R. de Diego, D. V. Fedorov, and A. S. Jensen, "Direct and sequential radiative three–body reaction rates at low temperatures", The European Physical Journal A **47**, 102 (2011) DOI: 10.1140/epja/i2011-11102-8.

[37] N. B. Nguyen, F. M. Nunes, and I. J. Thompson, "Investigation of the triple–α reaction in a full three–body approach", Phys. Rev. C **87**, 054615 (2013) DOI: 10.1103/PhysRevC.87.054615.

[38] S. Ishikawa, "Three–body calculations of the triple–α reaction", Phys. Rev. C **87**, 055804 (2013) DOI: 10.1103/PhysRevC.87.055804.

[39] T. de Forest Jr. and J. Walecka, "Electron scattering and nuclear structure", Advances in Physics **15**, 1–109 (1966) DOI: 10.1080/00018736600101254.

[40] S. Bacca, "Study of electromagnetic reactions on light nuclei with the Lorentz Integral Transform method", PhD thesis (Johannes Gutenberg–Universität Mainz, 2005), DOI: 10.25358/openscience-1901.

[41] M. Miorelli, "Electromagnetic properties of medium–mass nuclei from coupled–cluster theory", PhD thesis (University of British Columbia, Vancouver, 2017), DOI: http://dx.doi.org/10.14288/1.0362379.

[42] J. Walecka, *Theoretical Nuclear and Subnuclear Physics*, 2nd ed. (Imperial College Press, 2004).

[43] J. Golak, H. Kamada, H. Witała, W. Glöckle, J. Kuroś–Zołnierczuk, R. Skibiński, V. V. Kotlyar, K. Sagara, and H. Akiyoshi, "Faddeev calculations of proton–deuteron radiative capture with exchange currents", Phys. Rev. C **62**, 054005 (2000) DOI: 10.1103/PhysRevC.62.054005.

[44] A. R. Edmonds, *Angular Momentum in Quantum Mechanics*, Investigations in physics (Princeton University Press, 1957).

[45] M. Abramovitz and I. A. Stegun, *Handbook of Mathematical Functions* (Dover Publications, New York, 1972).

[46] J. L. Friar and S. Fallieros, "Gauge–invariant nuclear Compton amplitude manifesting low–energy theorems", Phys. Rev. C **34**, 2029–2042 (1986) DOI: 10.1103/PhysRevC.34.2029.

[47] J. Golak, R. Skibiński, W. Glöckle, H. Kamada, A. Nogga, H. Witała, V. Efros, W. Leidemann, G. Orlandini, and E. Tomusiak, "Benchmark calculation of the three–nucleon photodisintegration", Nuclear Physics A **707**, 365–378 (2002) DOI: 10.1016/S0375-9474(02)00989-2.

[48] J. Carlson and R. Schiavilla, "Structure and dynamics of few–nucleon systems", Rev. Mod. Phys. **70**, 743–841 (1998) DOI: 10.1103/RevModPhys.70.743.

[49] H. Arenhövel, "Exchange currents in electric transitions and the rôle of Siegert's theorem: a case study in deuteron photodisintegration", Zeitschrift für Physik A Atoms and Nuclei **302**, 25–30 (1981) DOI: 10.1007/BF01425099.

[50] V. D. Efros, W. Leidemann, and G. Orlandini, "Response functions from integral transforms with a Lorentz kernel", Physics Letters B **338**, 130–133 (1994) DOI: 10.1016/0370-2693(94)91355-2.

[51] V. D. Efros, W. Leidemann, and G. Orlandini, "Electromagnetic few–body response functions with the Lorentz Integral Transform method", Few–Body Systems **26**, 251–269 (1999) DOI: 10.1007/s006010050118.

[52] V. D. Efros, "Computation of inclusive transition spectra and reaction cross sections without use of the continuum wave functions", Sov. J. Nucl. Phys. **41**, 949 (1985).

[53] L. D. Faddeev, "Scattering theory for a three–particle system", Soviet Physics JETP **12**, 1014–1019 (1961).

[54] O. Yakubovsky, Soviet Journal of Nuclear Physics **5**, 937–951 (1967).

[55] V. D. Efros, W. Leidemann, and G. Orlandini, "Electron scattering response functions from their Stieltjes transforms", Few–Body Systems **14**, 151–170 (1993) DOI: 10.1007/BF01080714.

[56] N. Barnea, V. D. Efros, W. Leidemann, and G. Orlandini, "The Lorentz Integral Transform and its inversion", Few–Body Systems **47**, 201–206 (2010) DOI: 10.1007/s00601-009-0081-0.

[57] W. Leidemann, "Energy resolution with the Lorentz Integral Transform", Phys. Rev. C **91**, 054001 (2015) DOI: 10.1103/PhysRevC.91.054001.

[58] C. Lanczos, "An iteration method for the solution of the eigenvalue problem of linear differential and integral operators", J. Research Nat. Bur. Standards **45**, 255–282 (1950).

[59] M. A. Marchisio, N. Barnea, W. Leidemann, and G. Orlandini, "Efficient method for Lorentz integral transforms of reaction cross sections", Few–Body Systems **33**, 259–276 (2003) DOI: 10.1007/s00601-003-0017-z.

[60] A. N. Tikhonov and V. Y. Arsenin, *Solutions of ill–posed problems* (V. H. Winston & Sons, Washington, D.C.: John Wiley & Sons, New York, 1977).

[61] S. Bacca, N. Barnea, W. Leidemann, and G. Orlandini, "Isoscalar monopole resonance of the alpha particle: a prism to nuclear Hamiltonians", Phys. Rev. Lett. **110**, 042503 (2013) DOI: 10.1103/PhysRevLett.110.042503.

[62] W. Leidemann, "Calculation of a narrow resonance with the LIT method", Few–Body Systems **42**, 139–151 (2008) DOI: 10.1007/s00601-008-0199-5.

[63] G. P. Lepage, "How to renormalize the Schrödinger equation", in *Nuclear Physics: Proceedings of the VIII Jorge André Swieca Summer School, 1997*, edited by C. A. Bertulani, M. E. Bracco, B. V. Carlson, and M. Nielsen (World Scientific, Singapore, 1998), DOI: 10.1142/9789814529358.

[64] U. van Kolck, "Effective field theory of short–range forces", Nuclear Physics A **645**, 273–302 (1999) DOI: 10.1016/S0375-9474(98)00612-5.

[65] J. B. Habashi, S. Fleming, S. Sen, and U. van Kolck, "Effective field theory for two–body systems with shallow S–wave resonances", Annals of Physics **422**, 168283 (2020) DOI: 10.1016/j.aop.2020.168283.

[66] S. Beane, T. Cohen, and D. Phillips, "The potential of effective field theory in NN scattering", Nuclear Physics A **632**, 445–469 (1998) DOI: 10.1016/S0375-9474(98)00007-4.

[67] D. R. Phillips, S. R. Beane, and T. D. Cohen, "Nonperturbative regularization and renormalization: simple examples from nonrelativistic quantum mechanics", Annals of Physics **263**, 255–275 (1998) DOI: 10.1006/aphy.1997.5771.

[68] D. B. Kaplan, "More effective field theory for non–relativistic scattering", Nuclear Physics B **494**, 471–483 (1997) DOI: 10.1016/S0550-3213(97)00178-8.

[69] H. A. Bethe, "Theory of the effective range in nuclear scattering", Phys. Rev. **76**, 38–50 (1949) DOI: 10.1103/PhysRev.76.38.

[70] R. A. Arndt, D. D. Long, and L. Roper, "Nucleon–alpha elastic scattering analyses: (I). Low–energy n–α and p–α analyses", Nuclear Physics A **209**, 429–446 (1973) DOI: 10.1016/0375-9474(73)90837-3.

[71] D. Tilley, C. Cheves, J. Godwin, G. Hale, H. Hofmann, J. Kelley, C. Sheu, and H. Weller, "Energy levels of light nuclei A=5, 6, 7", Nuclear Physics A **708**, 3–163 (2002) DOI: 10.1016/S0375-9474(02)00597-3.

[72] C. Ji, C. Elster, and D. R. Phillips, "^{6}He Nucleus in halo effective field theory", Phys. Rev. C **90**, 044004 (2014) DOI: 10.1103/PhysRevC.90.044004.

[73] D. Tilley, J. Kelley, J. Godwin, D. Millener, J. Purcell, C. Sheu, and H. Weller, "Energy levels of light nuclei A=8, 9, 10", Nuclear Physics A **745**, 155–362 (2004) DOI: 10.1016/j.nuclphysa.2004.09.059.

[74] S. A. Afzal, A. A. Z. Ahmad, and S. Ali, "Systematic survey of the $\alpha - \alpha$ interaction", Rev. Mod. Phys. **41**, 247–273 (1969) DOI: 10.1103/RevModPhys.41.247.

[75] C. Ji, Private communication (2023).

[76] C. A. Manzata, "Ground state and photodisintegration of Beryllium–9 in cluster Effective Field Theory" (Università di Trento, 2016).

[77] E. P. Wigner, "Lower limit for the energy derivative of the scattering phase shift", Phys. Rev. **98**, 145–147 (1955) DOI: 10.1103/PhysRev.98.145.

[78] H.-W. Hammer and D. Lee, "Causality and the effective range expansion", Annals of Physics **325**, 2212–2233 (2010) DOI: 10.1016/j.aop.2010.06.006.

[79] S. Beck, B. Bazak, and N. Barnea, "Removing the Wigner bound in non–perturbative effective field theory", Physics Letters B **806**, 135485 (2020) DOI: 10.1016/j.physletb.2020.135485.

[80] G. L. Morgan and R. L. Walter, "Neutron–Helium interaction. II. Angular distributions and phase shifts from 0.2 to 7.0 MeV", Phys. Rev. **168**, 1114–1130 (1968) DOI: 10.1103/PhysRev.168.1114.

[81] D. R. Phillips and T. D. Cohen, "How short is too short? Constraining zero–range interactions in nucleon–nucleon scattering", Physics Letters B **390**, 7–12 (1997) DOI: 10.1016/S0370-2693(96)01411-6.

[82] G. M. Hale, Private communication (2021).

[83] X. Kong and F. Ravndal, "Coulomb effects in low energy proton–proton scattering", Nuclear Physics A **665**, 137–163 (2000) DOI: 10.1016/S0375-9474(99)00406-6.

[84] V. Eremenko, N. Upadhyay, I. Thompson, C. Elster, F. Nunes, G. Arbanas, J. Escher, and L. Hlophe, "Coulomb wave functions in momentum space", Computer Physics Communications **187**, 195–203 (2015) DOI: 10.1016/j.cpc.2014.10.002.

[85] E. Filandri, P. Andreatta, C. A. Manzata, C. Ji, W. Leidemann, and G. Orlandini, "Beryllium–9 in cluster effective field theory", SciPost Phys. Proc., 034 (2020) DOI: 10.21468/SciPostPhysProc.3.034.

[86] V. Efimov, "Energy levels arising from resonant two–body forces in a three–body system", Physics Letters B **33**, 563–564 (1970) DOI: 10.1016/0370-2693(70)90349-7.

[87] P. F. Bedaque, H.-W. Hammer, and U. van Kolck, "Renormalization of the three–body system with short–range interactions", Phys. Rev. Lett. **82**, 463–467 (1999) DOI: 10.1103/PhysRevLett.82.463.

[88] L. E. Marcucci, J. Dohet-Eraly, L. Girlanda, A. Gnech, A. Kievsky, and M. Viviani, "The Hyperspherical Harmonics method: a tool for testing and improving nuclear interaction models", Frontiers in Physics **8**, 1–21 (2020) DOI: 10.3389/fphy.2020.00069.

[89] M. Gattobigio, A. Kievsky, M. Viviani, and P. Barletta, "Harmonic Hyperspherical basis for identical particles without permutational symmetry", Phys. Rev. A **79**, 032513 (2009) DOI: 10.1103/PhysRevA.79.032513.

[90] S. Rosati, "The Hyperspherical Harmonics method: a review and some recent developments", in A. Fabrocini, S. Fantoni, and E. Krotscheck, *Introduction to modern methods of quantum many–body theory and their applications*, Vol. 7, Series on Advances in Quantum Many-Body Theory (World Scientific, London, Singapore, Hong Kong, 2002), pp. 339–378, DOI: 10.1142/9789812777072_0009.

[91] N. Y. Vilenkin, G. I. Kuznetsov, and Y. A. Smorodinskii, Sov. J. Nucl. Phys. **2**, 645 (1966).

[92] F. Ferrari Ruffino, "Non–Symmetrized Hyperspherical Harmonics method applied to light hypernuclei", PhD thesis (Università di Trento, 2017), URL: https://hdl.handle.net/11572/368323.

[93] A. Kievsky, S. Rosati, M. Viviani, L. E. Marcucci, and L. Girlanda, "A high–precision variational approach to three– and four–nucleon bound and zero–energy scattering states", Journal of Physics G: Nuclear and Particle Physics **35**, 063101 (2008) DOI: 10.1088/0954-3899/35/6/063101.

[94] Y. Capitani, "Theoretical description of few–nucleon scattering states in terms of integral relations" (Università di Pisa, 2020), URL: https://etd.adm.unipi.it/t/etd-06252020-190237.

[95] W. Leidemann and G. Orlandini, "Modern ab initio approaches and applications in few–nucleon physics with $A \geq 4$", Progress in Particle and Nuclear Physics **68**, 158–214 (2013) DOI: 10.1016/j.ppnp.2012.09.001.

[96] N. Barnea, "Exact solution of the Schrödinger and Faddeev equations for few body systems", PhD thesis (Hebrew University, Jerusalem, 1997).

[97] N. Barnea, W. Leidemann, and G. Orlandini, "Ground state wave functions in the hyperspherical formalism for nuclei with $A > 4$", Nuclear Physics A **650**, 427–442 (1999) DOI: 10.1016/S0375-9474(99)00113-X.

[98] S. Bacca, H. Arenhövel, N. Barnea, W. Leidemann, and G. Orlandini, "Ab initio calculation of ^{7}Li photodisintegration", Physics Letters B **603**, 159–164 (2004) DOI: 10.1016/j.physletb.2004.10.025.

[99] A. Gnech, M. Viviani, and L. E. Marcucci, "Calculation of the ^{6}Li ground state within the hyperspherical harmonic basis", Phys. Rev. C **102**, 014001 (2020) DOI: 10.1103/PhysRevC.102.014001.

[100] M. Gattobigio, A. Kievsky, and M. Viviani, "Nonsymmetrized hyperspherical harmonic basis for an A–body system", Phys. Rev. C **83**, 024001 (2011) DOI: 10.1103/PhysRevC.83.024001.

[101] F. Ferrari Ruffino, D. Lonardoni, N. Barnea, S. Deflorian, W. Leidemann, G. Orlandini, and F. Pederiva, "Benchmark results for few–body hypernuclei", Few-Body Systems **58**, 113 (2017) DOI: 10.1007/s00601-017-1273-7.

[102] J. Raynal and J. Revai, "Transformation coefficients in the hyperspherical approach to the three–body problem", Il Nuovo Cimento A (1965-1970) **68**, 612–622 (1970) DOI: 10.1007/BF02756127.

[103] V. Aquilanti and S. Cavalli, "Coordinates for molecular dynamics: orthogonal local systems", The Journal of Chemical Physics **85**, 1355–1361 (1986) DOI: 10.1063/1.451223.

[104] M. S. Kil'dyushov, Sov. J. Nucl. Phys. **15**, 113 (1972).

[105] A. Messiah, *Quantum mechanics*, Quantum Mechanics (North-Holland Publishing Company, 1962).

[106] A. Novoselsky and J. Katriel, "Symmetry analysis of many–body wave functions, with applications to the nuclear shell model", Phys. Rev. C **51**, 412–415 (1995) DOI: 10.1103/PhysRevC.51.412.

[107] P. Andreatta, "Beryllium–9 in Cluster Effective Field Theory", PhD thesis (Università di Trento, 2019), URL: http://eprints-phd.biblio.unitn.it/3725/.

[108] V. D. Efros, "Elimination of rotational degrees of freedom in expansion methods for three nucleons", Few-Body Systems **32**, 169–181 (2002) DOI: 10.1007/s00601-002-0116-2.

[109] M. Viviani, L. E. Marcucci, S. Rosati, A. Kievsky, and L. Girlanda, "Variational calculation on $A = 3$ and 4 nuclei with non–local potentials", Few-Body Systems **39**, 159–176 (2006) DOI: 10.1007/s00601-006-0158-y.

[110] F. Bonaiti, "Application of the Lorentz Integral Transform method to ^{9}Be photodisintegration in a cluster effective model" (Università di Trento, 2019).

[111] J. Ballot and M. Fabre de la Ripelle, "Application of the hyperspherical formalism to the trinucleon bound state problems", Annals of Physics **127**, 62–125 (1980) DOI: 10.1016/0003-4916(80)90150-5.

[112] J. Avery, *Hyperspherical harmonics, Applications in quantum theory* (Springer Dordrecht: Kluwer Academic Publishers 1989, 1989), DOI: 10.1007/978-94-009-2323-2.

[113] I. S. Gradshteyn and I. M. Ryzhik, *Table of integrals, series, and products*, edited by A. Jeffrey and D. Zwillinger, 7th ed. (Academic Press, 2007).

[114] N. Michel and M. Stoitsov, "Fast computation of the Gauss hypergeometric function with all its parameters complex with application to the Pöschl–Teller–Ginocchio potential wave functions", Computer Physics Communications **178**, 535–551 (2008) DOI: 10.1016/j.cpc.2007.11.007.

[115] D. A. Varshalovich, A. N. Moskalev, and V. K. Khersonskii, *Quantum Theory of Angular Momentum* (World Scientific Publishing Company, Singapore, 1988).

[116] M. Odsuren, K. Katō, Y. Kikuchi, M. Aikawa, and T. Myo, "A resonance problem on the low–lying resonant state in the ^{9}Be system", Journal of Physics: Conference Series **569**, 012072 (2014) DOI: 10.1088/1742-6596/569/1/012072.

[117] W. Leidemann, Private communication (2023).

[118] I. J. Thompson, B. V. Danilin, V. D. Efros, J. S. Vaagen, J. M. Bang, and M. V. Zhukov, "Pauli blocking in three–body models of halo nuclei", Phys. Rev. C **61**, 024318 (2000) DOI: 10.1103/PhysRevC.61.024318.

[119] A. Deltuva, "Neutron–^{19}C scattering: towards including realistic interactions", Physics Letters B **772**, 657–662 (2017) DOI: 10.1016/j.physletb.2017.07.036.

[120] A. Kievsky, M. Viviani, P. Barletta, C. Romero-Redondo, and E. Garrido, "Variational description of continuum states in terms of integral relations", Phys. Rev. C **81**, 034002 (2010) DOI: 10.1103/PhysRevC.81.034002.

[121] A. Kievsky, M. Viviani, and L. E. Marcucci, "Theoretical description of three– and four–nucleon scattering states using bound–state–like wave functions", Phys. Rev. C **85**, 014001 (2012) DOI: 10.1103/PhysRevC.85.014001.

[122] Y. Capitani and L. E. Marcucci, In preparation (2024).

[123] F. Ajzenberg-Selove, "Energy levels of light nuclei $A = 11 - 12$", Nuclear Physics A **506**, 1–158 (1990) DOI: 10.1016/0375-9474(90)90271-M.

[124] M. L. Goldberger and K. M. Watson, *Collision Theory* (John Wiley, New York, 1964).

[125] L. S. Rodberg and R. M. Thaler, *Introduction to the Quantum Theory of Scattering* (Academic Press, New York and London, 1967).

[126] D. M. Brink and G. R. Satchler, *Angular momentum* (Clarendon Press, Oxford, 1968).